Modular engineering of self-division in synthetic cells

Dissertation der Fakultät für Biologie
der Ludwig–Maximilians–Universität München

María Reverte López

München, 2025

Modular engineering of self-division in synthetic cells

Dissertation
der Fakultät für Biologie
der Ludwig–Maximilians–Universität
München

vorgelegt von
María Reverte López
aus Talavera de la Reina, Spain

München, 2025

Diese Dissertation wurde angefertigt
unter der Leitung von Prof. Dr. Petra Schwille
im Bereich von Max-Planck-Institut für Biochemie
an der Ludwig-Maximilians-Universität München

Dissertation zur Erlangung des Doktorgrades der
Naturwissenschaften Doctor rerum naturalium (Dr. rer. nat.)

Erstgutachter/in:	Prof. Dr. Heinrich Leonhardt
Zweitgutachter/in:	Prof. Dr. Petra Schwille
Tag der Abgabe:	02.04.2025
Tag der mündlichen Prüfung:	06.08.2025

Eidesstattliche Erklärung

Ich versichere hiermit an Eides statt, dass meine Dissertation selbstständig und ohne unerlaubte Hilfsmittel angefertigt worden ist.
Die vorliegende Dissertation wurde weder ganz noch teilweise bei einer anderen Prüfungskommission vorgelegt.
Ich habe noch zu keine früheren Zeitpunkt versucht, eine Dissertation einzureichen oder an einer Doktorprüfung teilzunehmen.

München, den 31.03.2025

María Reverte López

Para Nando y Lulu

Kings and lords come and go and leave
nothing but statues in a desert, while
a couple of youngsters tinkering in a
workshop change the way the world works.

—Terry Pratchett, *The Truth*

Table of Contents

List of Figures

List of Abbreviations

2PP	two-photon polymerization
ABP	actin binding protein
AFM	atomic force microscopy
A-mix	actin mix
APTES	(3-aminopropyl)triethoxysilane
AR	aspect ratio
BSA	bovine serum albumin
cDICE	continuous droplet interface crossing encapsulation
DLW	direct laser writing
E.coli	Escherichia coli
ELCs	essential light chains
GUV	giant unilamellar vesicle
JCVI	J. Craig Venter Institute
LB	Langmuir-Blodgett
Ld	liquid-disordered
Lo	liquid-ordered
LS	Langmuir-Schäfer
LUV	large unilamellar vesicle
MHC-II	myosin II heavy chains
MTS	membrane targeting sequence
NM II	non-muscle myosin II
PDMS	polydimethylsiloxane
PEG	polyethylene glycol

PH	pleckstrin-homology
PIP	phosphatidylinositol phosphate
PIP3	phosphatidylinositol (3,4,5)-triphosphate
RLCs	regulatory light chains
ROI	region of interest
RT	room temperature
SEM	scanning electron microscopy
SLB	supported lipid bilayer
SUV	small unilamellar vesicle
TEG	triethylene glycol
TIRFM	total internal reflection fluorescence microscopy
w/o	water-in-oil
Z-ring	FtsZ division ring

Abstract

Bottom-up synthetic biology is an interdisciplinary area of research working towards one grand goal: building an artificial cell from scratch. To achieve such feat, this discipline employs a forward-engineering strategy based on mimicking life's fundamental principles. Accordingly, researchers from diverse backgrounds apply a modular assembly approach, recapitulating essential cellular processes into independent operating modules within giant unilamellar vesicles (GUVs) as *in vitro* minimal cell models. Each of these synthetic modules, composed of molecular building blocks, confers the lipid-based vesicles with specific functions, enabling the construction of minimal cellular systems through their combinatorial integration. However, one of the major challenges posed by this building strategy is the efficient integration of various modules within vesicles to yield a functioning reconstituted system exhibiting the desired properties. Without thorough module characterization and careful adjustment of design variables, our reconstituted minimal cells can display non-functional attributes and behaviours due to incompatibilities. Despite these challenges, a critical endeavour in the field of synthetic biology is the development of a minimal division machinery to confer artificial cells with the ability to split into two identical daughter cells. One of the approaches working towards this goal focuses on assembling a eukaryotic-inspired synthetic division machinery in the form of a contractile actomyosin ring. Although preliminary studies employing a minimal set of proteins have shown promising results, *in vitro* reconstituted actomyosin rings fail to effectively transmit their contractile forces to the vesicle membrane due to a lack of spatiotemporal control. In animal cells, precise equatorial positioning of actomyosin rings is crucial for cleavage furrow formation and symmetric division. Nevertheless, recapitulating this highly regulated and convoluted process *in vitro* within GUVs is currently unattainable. A simpler mechanism for achieving mid-cell positioning of *in vitro* actomyosin rings has yet to be established.

To address this challenge, we have further characterized and exploited a bacterial protein system as a positioning module: the *Escherichia coli* MinDE system. This reaction-diffusion system self-organizes on membranes through ATP-driven attachment-detachment cycles, forming dynamic and quasi-stationary patterns. While its *in vivo* role involves inhibiting the formation of the bacterial division ring at the cell poles via their lateral (pole-to-pole) oscillations, the MinDE system has shown an unexpected new function *in vitro*: the spatiotemporal control of diffusible, membrane-bound cargo via diffusiophoretic transport. Consequently, to characterize its positioning capabilities and exploit them for other

biotechnological applications, we first evaluated the MinDE system as a versatile patterning tool for complex 3D structures like microrobots and microcarriers for drug delivery. Employing two-photon lithography, we 3D-printed microswimmer-like robotic structures and demonstrated that Min proteins can spatiotemporal control biomolecules of varying nature on their lipid-coated surfaces. In addition, we showed that the patterning capabilities of Min proteins extend to free-standing membranes and achieved the quasi-stationary positioning of cargo on the inner leaflet of vesicular microcarrier systems. After demonstrating the robustness of the MinDE system as a synthetic positioning module, we then leveraged it to tackle our primary challenge: the spatiotemporal control of actomyosin rings at the equator of GUVs for the synthetic division of these minimal cell models. Through the *in vitro* co-reconstitution of the actomyosin contraction module with the MinDE system under optimized encapsulation conditions, we demonstrated that integrating both modules yields the effective MinDE-driven positioning of actomyosin rings at mid-cell, which generated the sustained equatorial deformation of vesicles. Intriguingly, we also showed that the synergistic effect of Min oscillations and contractile actomyosin networks leads to the emergence of unexpected behaviours, such as the formation of dynamic bleb-like outward protrusions in vesicles and the remodelling of phase-separated lipid domains.

Taken together, the experimental research presented in this thesis provides strong evidence that the MinDE system can be employed as a robust positioning module not only for the eukaryotic-based division of synthetic cells, but also for other biomedically relevant applications such as the functionalization of microfabricated devices and microcarrier systems. Moreover, this work offers new insights into the synergistic effects arising from the integration of well-defined functional modules, as well as the mechanistic aspects of the MinDE system that remain unclear and will require further scrutiny and characterization. Hence, by demonstrating the successful *in vitro* integration of synthetic modules, this thesis advances synthetic biology efforts towards the long-term goal of building an artificial cell capable of autonomous self-division.

List of Publications

Publications Included in this Thesis

P1 **M. Reverte-López***, S. Gavrilovic*, A. Merino-Salomón*, H. Eto, A. Yagüe Relimpio, G. Rivas, and P. Schwille. Protein-Based Patterning to Spatially Functionalize Biomimetic Membranes. Small Methods, 7(12):2300173, June 2023. (see section 3.1)

P2 **M. Reverte-López**, N. Kanwa, Y. Qutbuddin, V. Belousova, M. Jasnin, and P. Schwille. Self-organized spatial targeting of contractile actomyosin rings for synthetic cell division. Nature Communications, 15(1):10415, Nov. 2024. (see section 3.2)

---

* *These authors contributed equally to this work*

Other Publications

M. Fu, T. Burkart, I. Maryshev, H. G. Franquelim, A. Merino-Salomón, **M. Reverte-López**, E. Frey, and P. Schwille. Mechanochemical feedback loop drives persistent motion of liposomes. Nature Physics, 19(8):1211–1218, Aug. 2023.

Declaration of Contributions

P1 Protein-Based Patterning to Spatially Functionalize Biomimetic Membranes.

Co-first author

M.R.-L., S.G., and A.M.-S. contributed equally to this work. **M.R.-L.**, S.G., A.M.-S., and P.S. conceived the study. **M.R.-L.**, S.G., A.M.-S., and H.E. performed the patterning experiments. **M.R.-L.** and H.E. designed geometries and **M.R.-L.** printed the 3D microstructures. S.G. performed SEM imaging and DNA origami validation. A.M.-S. and A.Y-R. performed encapsulation in lipid vesicles. G.R. provided technical advice on crowding conditions. **M.R.-L.** wrote the original draft. **M.R.-L.**, S.G., A.M.-S., and P.S. revised the manuscript and figures. All authors discussed the results and revised the manuscript.

P2 Self-Organized Spatial Targeting of Contractile Actomyosin Rings for Synthetic Cell Division.

First author

M.R.-L. and P.S. conceived the study. **M.R.-L.** designed and performed encapsulation experiments, analysed data, and interpreted results. N.K and **M.R.-L.** designed and carried out phase-separation experiments. **M.R.-L.** and Y.Q analysed blebbing vesicles. V.B. assisted with the supplementary experiments. M.J. provided technical advice on protein conditions for encapsulation. **M.R.-L.** and P.S. wrote the manuscript and all authors revised and approved the final version of the manuscript.

We hereby confirm the contributions to the aforementioned publications.

Dr. Adrián Merino Salomón (Co-first author)	Svetozar Gavrilovic (Co-first author)
María Reverte López	Prof. Dr. Petra Schwille
Prof. Dr. Heinrich Leonhardt	

Munich, 25.03.2025

1 Introduction

1.1 Synthetic Biology: the science of making

It is within our hardwired nature to create. Whether as a form of artistic expression or to improve the collective survival, humans design, develop, and optimize. Our remarkable creativity and divergent thinking have brought us to where we are today as a species, and will undoubtedly be essential to face the technological, medical, and environmental challenges of the future.

To tackle these future challenges, there are several fields of scientific research with potential to contribute with innovative solutions. Among them, synthetic biology stands out as a promising discipline capable of bringing transformative ideas and, ultimately, provide effective advanced strategies for the next decades [1].

First coined by Barbara Hobom in 1980, synthetic biology was introduced as a term to define bacteria that had been genetically modified via recombinant DNA technology [2]. In the early 2000s, however, the debate over the term's precise scope led to the reconceptualization of the field's goals and the evaluation of its many facets [3]. Particularly, after the first synthetic biology conference held at MIT in 2004, the community broadened its horizons while acknowledging the diverse aims of its members. While some researchers continued applying the "biomimetic chemistry" or biotechnology-based approach from the field's early years (working on the construction of synthetic regulatory gene networks and the synthesis of artificial enzymes), the discipline started adhering to an engineering perspective which quickly gained momentum [4, 5, 6]. With a strong motivation to build, the bioengineering community set up a clear and ongoing goal for synthetic biology: to implement a large-scale modular approach to build artificial ("synthetic") systems mimicking living biological ones. In short, synthetic biology aims to assemble a minimal cell-like unit, a grand challenge that could not only contribute with varying biomedical applications, but also shed light on some of the fundamental questions about the intricacies of living matter.

Since then, synthetic biology has been defined as the "science of making" [7], a highly multidisciplinary study area nurtured by researchers from diverse backgrounds (biologists, chemists, physicists, and engineers among others) who bring their expertise and working

principles from their respective disciplines. Given its ambitious mission, many scientific initiatives and alliances have been launched globally [8]. From the seminal International Genetically Engineered Machine (iGEM) competition [9] to other European-based initiatives such as the European Synthetic Cell Initiative (SynCellEU) [10] and the European Association of Synthetic Biology Students and Postdocs (EUSynBioS) [11], these organizations approach the field's challenges from different viewpoints, each focusing on specific goals [12].

Although the field initially met some scepticism over its ability to deliver "real-world applications" [13], new technologies and commercial products have been developed through the application of synthetic biology tools [14, 15]. These technological achievements, beyond offering an optimistic view of the long journey ahead, confirm the impact this scientific discipline will have in answering fundamental questions and responding to future needs and opportunities.

1.1.1 The top-down and bottom-up strategies to synthetic life

Contemporary synthetic biology has become an international scientific endeavour with one main mission: the construction of a cell-like mimic [8]. Precisely defining which characteristic functions of living cells we must mimic is, however, no easy task. Life encompasses many different types of living assemblies with varying complexities. Consequently, researchers are focusing their efforts on recapitulating only the essential cellular functions in minimal artificial systems. The current field consensus is that, to sustain life, an artificial cell must comprise the following cellular processes: (1) compartmentalization, (2) metabolism, (3) biosynthesis, (4) energy supply, (5) stimuli-responsiveness, (6) replication of genetic information, and (7) self-reproduction [16, 17, 18]. Furthermore, to be fully considered a living entity, this self-assembled and self-sustaining system must eventually follow Darwinian evolution, adapting to its environment and acquiring new functionalities [19, 20, 21]. To approach the construction of such an artificial cell, the synthetic biology community is following two methodological lines of research: the top-down and bottom-up approaches.

On the one hand, the top-down approach pioneered by the J. Craig Venter Institute (JCVI) envisions a synthetic system as a biological entity reduced to its simplest form via the genetic manipulation of existing cells, stripping down their genome until solely their core essential and quasi-essential genes remain [22, 20]. Thanks to the advancements in high-throughput DNA engineering technologies, Hutchison, Gibson, and colleagues at the JCVI conducted genome erosion on *Mycoplasma mycoides* and transplanted this genome to a *Mycoplasma capricolum* cell [23, 24, 25]. The result, after several iterations, was JCVI-syn3.0, a self-replicating synthetic organism with only 473 genes [26]. The successful implementation of this approach has led to many fruitful applications where microbial engineering has enabled the production of advanced biofuels and drug precursors [27, 28].

Although this reductionist approach has provided important insights into the essential genomic information a synthetic cell would carry, one-third of the JCVI-syn3.0's genome has unknown function [29]. Like a black box, this synthetic organism consists of genes with uncharacterised purpose, posing an important bottleneck for those working in the top-down approach.

On the other hand, the bottom-up approach follows the minimization strategy from the opposite direction. As the term indicates, this strategy aims to construct artificial cells from scratch by the assembly of isolated components. Starting from minimal operating units taken from biological or synthetic sources (like proteins, DNA, polymers, etc.), the idea is to assemble them into functional entities, parts, and modules which, upon integration, yield complex yet fully characterized artificial cells [30, 16].

The bottom-up approach presents several advantages over its top-down counterpart. Partly inspired by the achievements and frameworks from fields such as origin of life research and synthetic chemistry, the characteristic bottom-up methodology allows researchers to garner the predictability and full control required to construct artificial systems. Building and studying a set of synthetic toolboxes provides the possibility to optimize their parts, prevent redundancy, and avoid unwanted crosstalk [31, 16, 32]. Most importantly, it allows for the stepwise increase in complexity [33]. The simple organic or inorganic synthetic molecules constituting their parts can be combined and repurposed, creating hybrid systems with tailored functions and processes which may not necessarily be observed in nature [18, 34]. Moreover, as a result of the systematic study of potential synthetic molecular toolkits, our understanding of biological processes advances while we unveil new questions about their working components [35, 36].

Although the bottom-up strategy bypasses some of the bottlenecks from the top-down approach, its working principles make the assembly of artificial cells a slow and complex process [37]. Hence, researchers consider necessary the combination of both methodologies. More precisely, we could strategically apply some of the genetic knowledge retrieved from JCVI-syn3.0 and consider this minimal organism as a module blueprint for a bottom-up assembled cell [19].

Nonetheless, many studies have already shown the wide range of foreseeable applications to which bottom-up synthetic biology could contribute [36]. In biomedicine, bottom-up artificial cells could be used as biomedical tools for the synthesis and delivery of drugs, or as biosensors for diagnostics [38, 39, 40, 41]. Furthermore, in addition to replacing cellular functions, customized synthetic systems could act as biocatalysts or intelligent biomaterials [42, 43], expanding their relevance within bioremediation and environmental efforts [44, 45].

1.1.2 Modular assembly of biological functions to build a cell from scratch

One fundamental feature that sets synthetic biology (especially its bottom-up approach) apart from other disciplines is the implementation of standard engineering principles to achieve the forward-engineering of biological systems [46, 4, 47]. While adhering to a rational design strategy, researchers in the field adopt engineering principles such as decoupling via modularity, standardization of parts, and abstraction of complexity [4, 48]. As a result, the most suitable workflow for this approach is the engineering cycle, a framework that consists of four steps: (i) design our synthetic systems based on purpose and constraints, (ii) build them by integrating standard biological parts or bio-bricks, (iii) test their functionality through quality assurance, and (iv) learn from the outcome to optimize the product before restarting the cycle [49, 50].

For those working in the bottom-up approach, these principles constitute the foundation of its modular design rationale [51]. As described above (see section 1.1.1), to design and build a customizable artificial cell, bottom-up synthetic biology follows the divide-and-conquer paradigm [52]. Due to the extraordinary complexity of biological systems, the idea is to decouple their essential cellular processes and reconstitute each of them independently as self-contained module units [4]. A synthetic module is therefore defined by its discrete and standardized function and comprises a series of elemental molecular building blocks of either natural or artificial origin (proteins, lipids, nucleotides, synthetic polymers, etc.) [53, 54, 31]. Building a cell thus becomes a plug-and-play process in which modules act like interlocking Lego bricks assembling and enriching the artificial cell with varying functions (Figure 1.1) [51].

Nonetheless, nature is no stranger to modularity. Functional modules are a crucial level of biological organization resulting from the cell's design principles, which favour robustness, efficiency, and adaptability [53, 55, 56]. These principles, managed and regulated by evolution, have given rise to discrete modules consisting of interacting biomolecules that provide specific functions to cells (e.g., signal transduction, DNA replication, protein synthesis, glycolysis, etc.) [42]. Given the successful modular organization of living cells, it is therefore reasonable to consider the mimicking strategy of bottom-up synthetic biology a feasible approach. However, due to the complexity of the task at hand, the need for collaboration within the bottom-up community is evident. Consequently, research labs focus on reconstituting particular functional modules with the set of building blocks of their preference [31, 33]. Of particular interest is the Registry of Standard Biological Parts, a growing synthetic library with a documented collection of genetic parts for their use as biobricks to build an artificial cell [57].

Although the process might seem straightforward, the modular design of an artificial cell poses a challenge. One can partition cellular functions into modules for the sake of reducing complexity, but the separate construction of these modules in labs around the

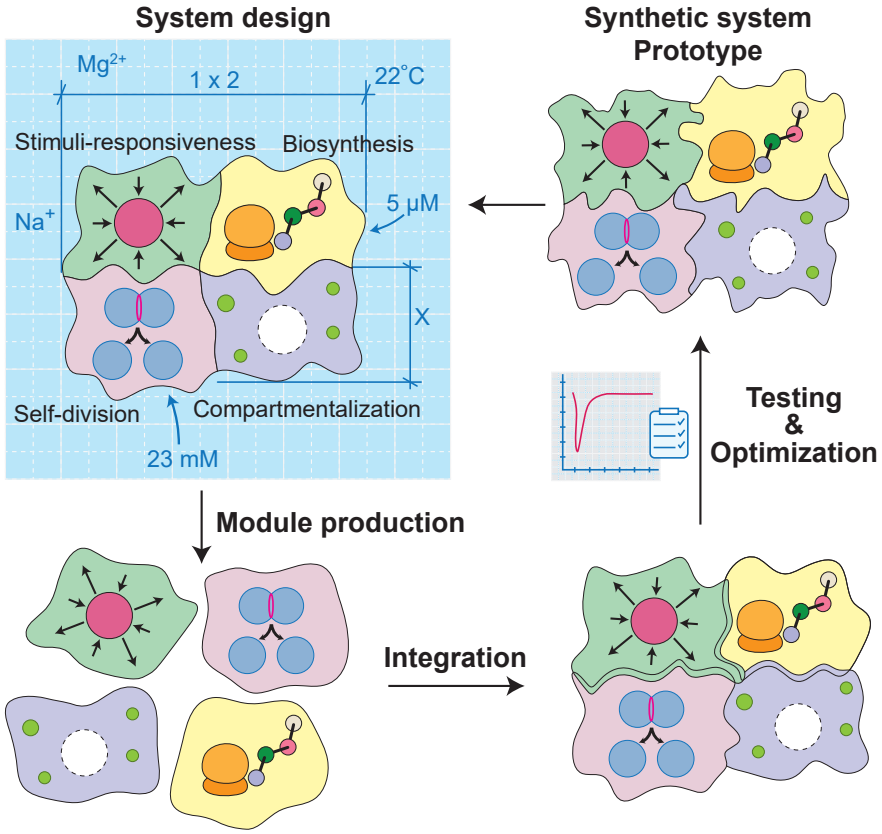

Figure 1.1. Modular assembly of synthetic cells: the engineering cycle. In the bottom-up approach of synthetic biology, artificial systems are built via the engineering principles of rational design. To construct a tailored synthetic system with specific capabilities, the first step consists of its design, where a set of essential functions is defined. Each of these functions is then reconstituted into autonomous modules (e.g., stimuli-responsiveness, biosynthesis, self-division, compartmentalization), comprising a set of optimized toolkits (DNA, proteins, etc.) that have been studied in detail to determine their working principles and design variables. Integration and assembly of these modules together require further testing and optimization to ensure that all functioning modules exhibit the expected behaviour and desired effects. Although this final prototype might differ from the initial design in experimental conditions and components, this iterative building process generates valuable resources and knowledge that nurture the next cycle.

world constitutes a problem once integration is sought. Therefore, it is crucial to consider compatibility when designing any functional module. One way to address this issue involves the meticulous and exhaustive characterization of the biomolecules comprising the modules to identify their design variables [58, 16]. These variables (e.g., buffer composition, concentration, geometry, etc.), responsible for the correct functioning of a particular molecular toolkit, determine the specific conditions and constraints of a synthetic functional unit. Knowing how to tune these design variables while attempting to combine

different modules may then enable their seamless integration into customizable artificial cells.

ln short, through the application of engineering principles, cellular processes could be reconstituted into synthetic modules regardless of their complexity. To this end, if we aim to confer our synthetic cells with functions like the ability to divide symmetrically into two identical daughter cells, we must start by considering which modules would be necessary to achieve this feat. To simplify this design step, a convenient key strategy that synthetic biologists can rely on is mimicry. A close look at different prokaryotic and eukaryotic division strategies and some tentative functional modules may already provide valuable hints. Given that single-cell organisms are partially isolated systems, we would first need a *compartment* which separates the content of our synthetic cell from the outside and confines its components and reactions within a set volume. Once we have isolated our cell from the outer environment, we could take inspiration from eukaryotic cellular division and assemble a *contractile division ring*. To ensure the partitioning of the cell's volume into two equally-sized shapes, additional modules would then be required to maintain the *position* of the ring precisely at the centre of our artificial cell while contraction occurs. According to this analysis, to equip our artificial cells with self-division capabilities, three modules would then be necessary to provide three functions: compartmentalization, positioning, and contractility.

To gain a deeper understanding of the tools required for the assembly of these three modules, in the next subsection a precise definition of the concept of *in vitro* reconstitution will be introduced. The rest of this introductory chapter will then focus on describing in more detail the elemental premises and recent breakthroughs behind the development of compartmentalization (see section 1.2), contractile (see section 1.3), and positioning modules (see section 1.4) for synthetic cells.

1.1.3 *In vitro* reconstitution of synthetic toolkits

Besides his remarkable contributions to the field of theoretical physics, Richard Feynman bestowed synthetic biologists with one of their core tenets. Extensively quoted by those in the bottom-up approach, his dictum: "That which I cannot create I do not understand" offers an evident hint. Experimental work on living cells is not enough to unravel their convoluted working mechanisms; venturing into mimicking their processes will [59].

However, making the leap from cell studies to experiments in test tubes is not a newfound idea. Indeed, the start of biochemistry as a discipline is regarded by many after the *in glass* (*in vitro*) experiments on fermentation by Maria Manàsseina and Eduard Buchner (between 1872 and 1897) which showed that it was possible to reproduce this metabolic process in the absence of living yeast, simply by employing a cell-free extract [60, 61]. These experiments were then followed by more complex reconstitutions like the ones performed

in the 1940s by Szent-Györgyi and Straub to study the physiology of muscle contraction [62, 63, 64]. Isolating actin and myosin from muscle tissue and reconstituting these two proteins together *in vitro* showed that, upon the addition of ATP and magnesium, this preparation resulted in the contraction of the actomyosin threads with a tension similar to that observed in living muscle [65, 66].

After the pioneering *in vitro* reconstitution assays on actin filaments by Oosawa and colleagues [67], the technological advancements brought by the field of fluorescent microscopy and the development of novel devices and techniques for these assays allowed the rapid progress of cytoskeletal reconstitutions. For example, the physical and mechanistic properties of cell motility were revealed thanks to improved purification techniques and the use of polystyrene microspheres, a novel substrate at the time that was intended for the study of force generation in cytoskeletal polymers [59]. The combination of a simple cocktail of purified actin and other actin-binding proteins (Arp2/3 complex, actin depolymerizing factor, and capping protein) on bacterium *Listeria monocytogenes*, as well as polysterene microspheres, generated the actin-based motility of these two substrates, thereby enabling the careful analysis of the mechanism behind actin filament nucleation and branching [68, 69].

Additionally, the numerous new avenues of research introduced by the development of total internal reflection fluorescence microscopy (TIRFM) allowed researchers to study cytoskeletal proteins at a new spatiotemporal resolution [70, 71]. To adapt to these new imaging techniques, *in vitro* assays continued to evolve by employing stabilizing, crowding, and binding agents, which facilitated the confinement and immobilization of actin filaments onto the surface of glass cover slips for image collection [72, 73]. In short, thanks to these *in vitro* reconstitutions, the investigation of filament polymerization dynamics advanced significantly, enabling researchers to validate molecular models that hypothesized about the kinetics and topology of actin filament assembly [30].

Performing *in vitro* reconstitutions thus constitutes a powerful reductionist approach for characterizing the biomolecules that comprise the set of toolkits needed to build artificial cells. From these experimental model systems, it is possible to discover the boundary conditions and design variables that determine the correct functioning of a synthetic cellular module (e.g., salt concentrations, temperature, net charge, geometry, etc.) [74]. Most importantly, the unnatural combination of biomolecules not only may shed light on their working principles and interactions inside the cell, but it could also uncover new functions and unknown properties not observed *in vivo* [75]. Furthermore, it provides synthetic biologists the tools to identify redundancies in molecular toolkits and potential cross-talks between their biomolecular building blocks. Therefore, the idea of a constructionist biology is a promising alternative strategy for building an artificial cell under controlled conditions while also addressing many of the open questions that drive biological research.

Finally, as a method to experimentally validate and assemble synthetic modules, *in*

vitro reconstitutions are accompanied by the development of technologies carried out by the many diverse scientists working in synthetic biology. From new micropatterning and 3D-printing techniques to enhanced microfluidic chips for sample preparation, the methods employed for the bottom-up reconstitution of synthetic cells continue to steadily grow [76, 59, 33]. Concurrently, with the advent of an era where artificial intelligence and computational models offer promising opportunities for synthetic biology, *in silico* mathematical models will continue to be a complementary tool with remarkable potential to guide and validate *in vitro* reconstitution experiments [52, 51].

1.2 Compartmentalization of artificial cells via lipid-based synthetic membrane systems

No matter how primitive or complex, one fundamental characteristic of every cell is its encapsulation by a compartment-defining barrier. Despite its crucial role in defining our concept of cells as distinct minimal units of life, the discovery of the cellular membrane as life's boundary was the result of a long and convoluted history of contributions to the field of cell membrane research [77, 78].

Considered nonessential secondary structures during most of the 19th century, and often mistaken for the cell walls of plant or fungi organisms, membranes were not widely accepted as part of the cell architecture until the early 20th century [79]. Thanks to Overton's studies on cell permeability and other experiments involving electrical measurements and cell microinjections [80, 81, 82], the field eventually distinguished cellular membranes from cellulose cell walls and started putting together an initial hypothesis regarding its phospholipid-based composition [80]. However, it was not until the direct observation of cell membranes with electron microscopy in the 1950s that their distinctive "railroad track" structure was revealed and their existence was corroborated and characterized [83, 84, 77].

Since then, cell membranes have been unmistakeably considered essential for life. The identity inferred from the separation between the exterior and the cell's microenvironment, the up-concentration of molecules facilitating the initiation of reactions, and the sequestration of genetic informational structures are all made possible because of this three-dimensional phospholipid barrier [85, 78].

Although some consider other membrane-less structures like hydrogels or coacervates (liquid-liquid phase separated droplets) as artificial cells-like mimics [86, 34], the most biologically relevant approach to build synthetic life is to confine the biobricks of an artificial cell within a biomimetic membrane that serves as a delimiting barrier. This not only would allow us to control the interaction of the synthetic cells with their environment, but it would also enable the reconstitution and study of many membrane-dependent cellular

processes by examining the transient interaction of biomolecules with this layer.

1.2.1 Cellular membranes

Life thrives in all sorts of adverse conditions due to the ubiquitous presence of membrane barriers confining cells into isolated microenvironments. As a structure encapsulating the biochemical content and reactions of cells, the cellular membrane is a chemically—and physically—complex fluid barrier [87]. It consists of a self-assembled phospholipid bilayer film of varying thickness with a heterogeneous chemical composition. On the one hand, amphiphilic lipid molecules rapidly diffuse within the membrane, featuring different hydrophilic polar head groups and hydrophobic acyl chains that allow them to be classified into a myriad of types [88]. On the other hand, in addition to carbohydrate chains, proteins embedded in the bilayer matrix or peripherally associated with the membrane are critical components of the cell membrane (e.g., ion channels, pumps, receptors, etc.) [89, 87, 77].

The prevailing organization of lipid membranes confers many essential functions to living cells. Besides acting as a selective barrier where molecule exchange can exclusively happen through specialized transport proteins, the lipid membrane is a dielectric insulating boundary (enabling the storage of electrical and chemical potential energy) and a fluid structure, key for changes in cellular shape. Additionally, its surface is a catalytic matrix where many reactions between transiently-bound cytosolic biomolecules take place. From vesicle trafficking to cytokinesis, it is therefore evident that the membrane is involved in a plethora of fundamental processes for the cell via the transient polar contact of biomolecules with its surface [87]

Importantly, as highlighted by Stachowiak and Kirchhausen, the only constant for cell membranes is change [90]. Due to its diverse chemical makeup, the membrane is under constant remodelling and presents characteristic mechanical properties such as curvature, elasticity, compressibility, etc. [91]. In particular, specific lipids and their interactions are behind some of its bulk properties and structure [92]. Moreover, since the seminal work published by Singer and Nicholson [93], our understanding of the biological membrane structure remains rooted in the Fluid-Mosaic model proposed in 1972, which has since evolved to include satisfactory explanations for recently discovered membrane structures [94]. Notably, in addition to the asymmetric distribution of lipids, carbohydrates, and proteins between the two leaflets, membranes exhibit lateral asymmetry. Arising from the electrostatic interactions and hydrophobic effect of its mixture of biomolecules, self-assembled domains (rafts) partition within the bilayer, resulting in phase-separated regions enriched in certain lipids or proteins [95].

1.2.2 Synthetic membrane model systems

Since the first artificially prepared lipid bilayers in the 1960s [96], the reconstitution of cellular membranes *in vitro* through the development of various biomimetic model systems has become crucial for two main purposes. First, to elucidate the properties conferred by each specific type of phospholipid and their effect on membrane structure and raft formation. Second, to provide a platform where we can mimic the conditions required for membrane-associated proteins to interact and orchestrate membrane-based physiological events (e.g., clathrin-mediated endocytosis, signal transduction, cell migration, etc.) [97, 98]. To this end, *in vitro* membrane models constitute a set of reliable platforms where lipid and protein composition, geometry, size, and mechanical properties can be carefully controlled.

According to their origin, composition, and shape, model membranes can be classified into different categories [99, 100]. In the case of lipid-based biomimetic membranes, a top-down approach can be applied and lipids can be directly extracted from cells and employed to form biomimetic membranes that closely resemble the compositional complexity of living cells. Alternatively, a bottom-up approach utilizes synthetic phospholipid molecules analogous to natural lipids, which enable the homogeneous and customizable assembly of artificial membranes through their mixing [99, 98]. In addition, with the advancements coming from the field of polymer chemistry, hybrid lipid-polymer systems and non-native membranes assembled from polymeric molecules have emerged as alternative membrane model platforms where polymer chains are employed as main biobricks. Some examples include polymersomes generated from block-copolymers, proteinosomes, and dendrimersomes [101, 102, 103]. The single or multi-layered films created by these polymer materials allow for the optimization of these models in some biomedically-relevant properties like biocompatibility and cargo release, turning them into prospective candidates for therapeutic applications [104].

Based on their shape and configuration, model membranes can be sorted into two categories: membranes on surfaces and membranes in solution. Depending on the experimental techniques employed for their formation, surface-based or bulk synthetic models can be reconstituted in monolayer (a single phospholipid film with one lipid molecule thickness) or bilayer (with inner and outer lipid leaflets) form. From solid-supported lipid bilayers to nanodiscs and liposomes in solution, biomimetic membranes can thus be selected according to the objective of the study and the biophysical methods available for their characterization [105].

Due to the pivotal role of lipid-assembled supported bilayers and giant vesicles for the work presented in this thesis, the following sections will describe these two models in detail with special emphasis on the utilization of photolithography techniques for generating bilayers on the surface of complex 3D geometries, as well as the use of vesicles as minimal cell models.

1.2.2.1 Supported lipid bilayers on flat surfaces

Membrane models created on surfaces include solid-supported lipid bilayers, suspended (free-standing) membranes on porous surfaces, and other variations such as tethered or cushioned supported lipid bilayers (Figure 1.2) [99, 97]. One of the most commonly used membrane models is the supported lipid bilayer (SLB). It consists of a flat phospholipid bilayer deposited onto the surface of a solid supporting material, with the polar heads of each bilayer leaflet exposed either to the material or the bulk solvent. To create an SLB, hydrophilic materials like borosilicate glass, mica, or silica are normally employed. However, polymers such as polydimethylsiloxane (PDMS), metals or other functionalized materials can also be employed [106].

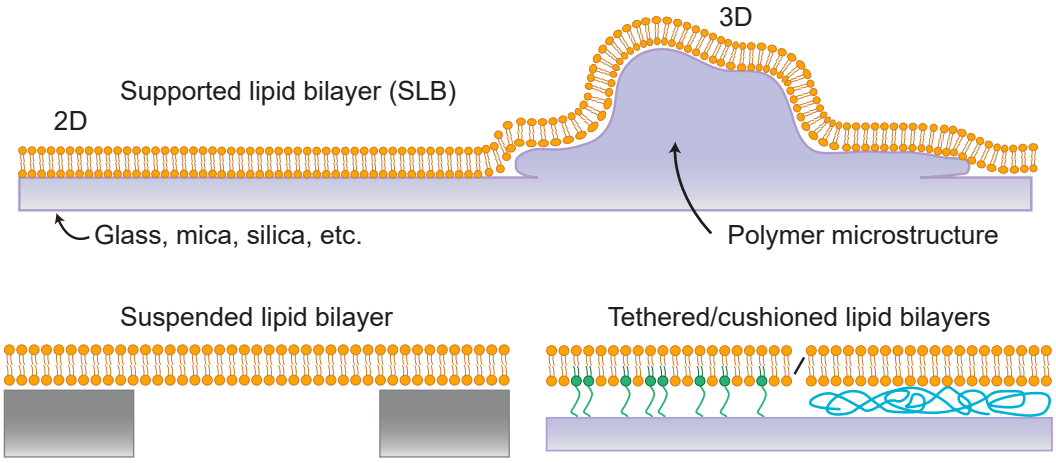

Figure 1.2. Synthetic membrane model systems: surface-assisted lipid bilayers. Schematic representation of commonly used lipid-based model membrane systems for *in vitro* reconstitution experiments. Solid-supported lipid bilayers in 2D can be formed on surfaces such as glass or mica, while 3D SLBs can be assembled on polymerized photoresist structures (top panel). In both cases, one lipid leaflet is in direct contact with the surface. However, lipid bilayers can also be decoupled from the underlying support to study protein incorporation and membrane interactions. This is the case for pore-suspended lipid bilayer, which allow accessibility to both lipid leaflets and enhance lipid diffusion (bottom left), and tethered/cushioned lipid bilayers, which offer long-term stability and a reduction in membrane-surface interaction, respectively (bottom right).

Besides Langmuir-type approaches (Langmuir-Blodgett or Langmuir-Schäfer deposition, LB/LS), a reliable and simple way to produce SLBs consists on the fusion of vesicles over the support. Developed in the 1980s [107], this vesicle deposition procedure relies on electrostatic interactions between the hydrophilic surface and charged lipid vesicles which leads to the adsorption, spreading, and fusion of the vesicles on the surface and, as a consequence, the self-assembly of a planar, fluid lipid bilayer. Moreover, the ionic strength and pH of the buffer solution can affect the optimization of the vesicle deposition procedure.

For instance, divalent ions like calcium and magnesium appear to interact directly with lipids and surfaces, promoting the rupture of vesicles and their adsorption [108, 109].

Although vesicle deposition is a relatively straightforward procedure and allows for the utilization of complex heterogeneous lipid mixtures for bilayer generation, it presents some limitations. The fusion of liposomes to form the bilayer makes it susceptible to membrane defects, and it only allows the formation of symmetric membranes; for the generation of asymmetric supported bilayers, LB/LS approaches are required [98, 108]. Furthermore, although the surface support makes SLBs more robust than liposomes and offers excellent accessibility to biophysical characterization techniques like AFM and TIRFM [99], this surface directly influences the properties of the membrane. Indeed, lipid mobility, lipid redistribution between the two leaflets, domain growth in phase-separated bilayers, and leaflet coupling may vary depending on both the lipid composition and the roughness and nature of the supporting material [110, 108, 111]. Nevertheless, to bypass these effects and allow the unrestricted diffusion of lipids, functionalized surfaces with polymer brushes can be employed as a "cushion" below the bilayer [112]. Tethering lipid bilayers to surfaces, however, produces the opposite effects with anchoring molecules such as DNA oligomers or thiolipids restricting lipid movement [113].

1.2.2.2 Biomimetic lipid membranes on 3D geometries

Planar supported bilayers on glass coverslips and cleaved mica can span chambers several millimetres in size, making the membrane a robust 2D nanomaterial in which many lipid-protein interactions can be studied via their *in vitro* reconstitution [106]. However, due to a lack of information along the Z axis, their use for the characterization of biomolecular interactions in complex three-dimensional shapes similar to those found in cells is not possible [76]. Adding this third dimension is particularly important for the study of many cellular processes such as protein organization, enzyme activation, and membrane fusion, where geometry has a direct effect on biomolecular properties, and curvature or shape are determining factors that dictate protein behaviour. [114, 115, 116].

To achieve SLBs with a particular geometry, a myriad of different approaches can be taken. On the one hand, silica nanoparticles or even nanodiamonds can be used as spherical substrates for their coating with lipid bilayers in a diverse set of biomedical applications [117, 118]. On the other hand, micropatterned structures fabricated via photolithography and soft lithography allow the formation of highly diffusible membranes on PDMS microfluidic chips, closed/open microwells made from different polymers, or micron-length grooves [119], thereby enabling the study of protein self-assembly and function on these artificial biomimetic 3D surfaces [120, 121, 122, 123, 124, 125, 126, 127, 128].

Most recently, due to the surge in more advanced 3D-printing techniques, it is now possible to fabricate and functionalize 3D-printed structures with lipid bilayers on their

surface. This is the case of two-photon polymerization (2PP) lithography, also known as direct laser writing (DLW). This novel additive manufacturing technique employs a photosensitive liquid material (a photoresist consisting of a mixture of photoinitiator and monomeric matrix molecules) to create micro/nano structures based on the 2PP approach (Figure 1.3a) [129, 130]. By focusing femtosecond-laser pulses on very small focal volumes within the photoresist, two photons are simultaneously absorbed at the laser focal area, leading to the cross-linking of the photoresist. More precisely, while the first photon excites the photoinitiator molecule to an intermediate virtual state, before decay to its ground state occurs, a second photon is absorbed and further excites the photoresist, triggering its polymerization into a 3D ellipsoidal volume (voxel). As the probability of two-photon absorption falls off dramatically away from the laser focal volume where laser intensity is at its maximum (outside this volume the spatial and temporal density of photons is insufficient), crosslinking of structures in the sub-micron resolution becomes possible [131, 130, 132, 133]. The rational design of structures and the scanning of the UV laser beam through these designs thus allow the sequential polymerization of voxel volumes in three dimensions, enabling the fabrication of solid architectures which can be used in a variety of biophysical and medical applications as biosensors, microrobots, etc. [119].

To coat 3D-printed structures with supported lipid bilayers, the surface of the polymerized photoresist can be further functionalized to facilitate membrane adherence. The type of post-functionalization applied depends on the polymer employed to print the structures and the composition of the lipid mixture. Due to their biorelevant properties like biocompatibility, low autofluorescence, and good light transmittance, Ormocomp (a silicate-based organic-inorganic hybrid polymer), pentaerythritol triacrylate (PETA), trimethylolpropane ethoxylate triacrylate (TPETA), hydrogels, and protein-based inks are suitable materials for the microfabrication of structures intended for biological applications [134, 135, 136, 137]. Once the surface chemistry of the 3D structure is optimized, SLBs are subsequently formed in a similar fashion to their flat counterparts. For instance, to render Ormocomp-printed structures susceptible to SLB coating, a silanization treatment with (3-aminopropyl)triethoxysilane (APTES) can be performed (Figure 1.3b) [135]. Since Ormocomp is a polymer with an organic-inorganic backbone, the printed structures are first exposed to argon plasma to generate reactive functional groups on their surface. Once surface activation is obtained, the organosilane APTES is used to anchor terminal, positively-charged amine groups to the surface. These positive charges are then exploited to create an SLB with negatively charged lipid vesicles, which rupture upon their electrostatic interaction with the surface.

In conclusion, coating 3D-printed microstructures with SLBs opens new avenues of research in which proteins, receptors, or other target biomolecules can be strategically arranged and displayed on the surface of microrobots such as microswimmers, microdevices, and biochemical assays. Therefore, this powerful biomimetic model system holds a promising future in membrane and biomedical research. In this regard, this 3D membrane model system is employed in this thesis to study the patterning capabilities of a protein sys-

tem and characterize its binding and organization on the surface of printed microswimmers.

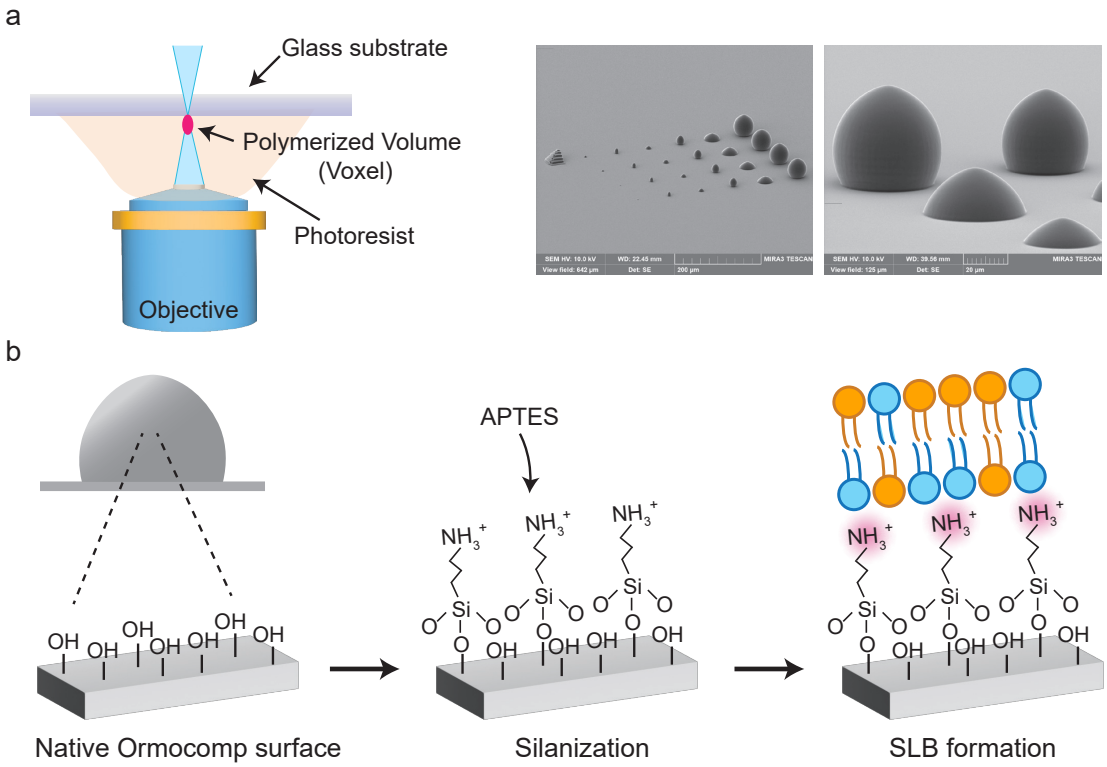

Figure 1.3. 3D-printing of microstructures via two-photon direct laser writing and their surface functionalization for lipid membrane coating. **a)** Schematic illustration of 2PP-DLW in dip-in laser lithography (DiLL) mode. The objective, immersed in the photoresists and moving downwards, focuses near infrared femtosecond-laser pulses to polymerize a small voxel volume (magenta) via the absorption of two photons at the laser focal point. By adjusting printing parameters like laser power, scanning speed, and the hatching and slicing of the designed geometries, microstructures can be fabricated on top of glass surfaces. Scanning electron microscopy (SEM) images of domes and pyramid microstructures printed in DiLL mode with Ormocomp. **b)** Graphical scheme depicting the functionalization steps to coat 3D-printed microstructures with lipid bilayers. After treatment with Argon plasma, Ormocomp structures are treated with APTES to endow surfaces with positive amine charges (silanization). The electrostatic interaction between the amine groups and liposomes containing negatively charged lipids induce vesicle bursting and membrane fusion, yielding the complete coating of 3D surfaces with lipid bilayers.

1.2.2.3 Vesicular systems as minimal cell models

Liposomes, also referred to as vesicles, are spherical membrane model systems consisting of a lipid bilayer confining an aqueous-filled volume from the exterior aqueous environment.

Although reports on lipid suspensions date back to the late 19th century, the first liposome preparations can be attributed to Bangham and colleagues in 1965, when their fluid-filled nature was fully understood [138].

Liposomes can be classified according to lamellarity (number of lipid bilayers) and size (Figure 1.4). On the basis of lamellarity, vesicles can be classified as unilamellar if one single lipid bilayer of 3-5 nm thickness encloses its inner aqueous solution, or as multilamellar vesicles (MLV) if they have several bilayers arranged in a multilayer configuration. Depending on their size, unilamellar vesicles are further sorted into: (1) small unilamellar vesicles (SUV), which have diameters in the range of 20–100 nm, (2) large unilamellar vesicles (LUV) with diameters between 100 nm and 1 μm, and (3) giant unilamellar vesicles with diameters of approximately 1–200 μm [139, 98].

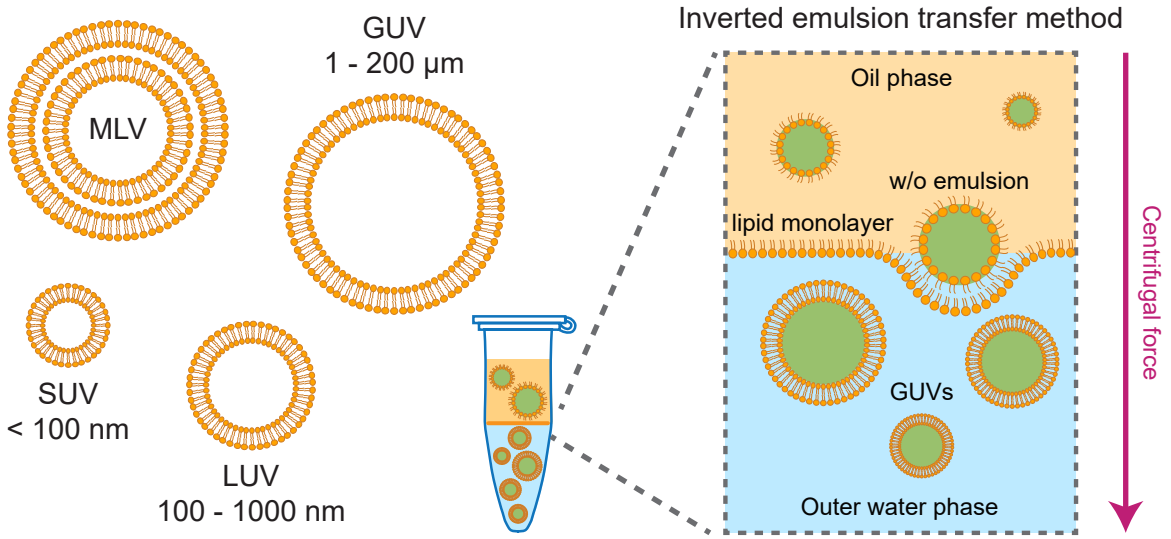

Figure 1.4. Synthetic membrane model systems: liposomes and the inverted emulsion method for GUV production. Classification of vesicles according to size (SUVs, LUVs and GUVs) and lamellarity (single or multilamellar vesicles). One commonly used method for the production of GUVs with encapsulated material is the inverted emulsion transfer. First, a water-in-oil (w/o) emulsion is prepared with an inner aqueous solution mix comprising the target molecules to be encapsulated and a lipid-containing oil mix. Centrifugation of this emulsion though a lipid monolayer prepared over an outer aqueous solution yields the production of GUVs enclosing the molecules of interest.

Different methods have been developed to generate liposomes with specific size, membrane properties, yield, or polydispersity. For instance, while SUVs can be obtained from the sonication of a suspension of MLVs retrieved from the hydration of a thin lipid film, LUVs are mainly prepared by extruding the hydrated lipid solution through a polycarbonate membrane to rupture the MLVs and induce their assembly into large unilamellar vesicles. Although MLVs are more stable than unilamellar vesicles, their heterogeneous

composition and the inaccessibility of biomolecules to their inner bilayers make them unsuitable models for quantitative biophysical studies. Conversely, since SUVs and LUVs are robust and well-defined, they are the standard models used in analytical studies (e.g., binding assays) to quantitatively measure protein-lipid interactions or curvature effects [99, 97, 105]. Moreover, they are used in a wide range of diagnostics and therapeutic applications, particularly as intracellular drug delivery systems [140, 141].

For the field of synthetic biology, however, GUVs with a diameter of 2-20 μm are the most suitable liposome model system [142]. With sizes close to those of living cells, these giant vesicles can be used as scaffolds where cellular processes can be reconstituted both on their surface and within their lumen. The coating and encapsulation of reactive biomolecules in GUVs thus allow to perform complex reconstitution experiments, protein-membrane interaction assays, or membrane remodelling studies which, due to the size of these vesicles, can be investigated using light microscopy techniques [143, 144, 145, 100]. Of particular interest is the production of phase-separated GUVs, in which macroscopic domain architecture and membrane properties can be effectively analysed [146, 147]. In addition, since their shape can be manipulated (e.g, via micropipette or capillary aspiration techniques), GUVs are an ideal model for mechanical studies on membrane-shaping proteins [148, 149].

There are several preparation methods available to produce GUVs. The earliest reported method is the gentle hydration or swelling. In this method, lipids are deposited as dried films on the surface of a substrate like glass, and the addition of an aqueous solution induces the slow swelling of the membrane into vesicles [150]. First introduced by Angelova and Dimitrov, electroformation later emerged as an alternative and much faster method for producing GUVs [151]. To accelerate the vesicle swelling process, lipid films are deposited onto two electrodes inside a fluid-filled chamber, and a uniform AC electric field is applied to assist on their rehydration [99, 152]. Although electroformation is a fast and reproducible method to generate monodisperse GUVs, it requires the use of aqueous solutions with low or physiologically relevant salt concentrations and lipid mixtures with low charge content [153, 154, 105]. Most importantly, both electroformation and swelling present major drawbacks for the encapsulation of proteins and other biomolecules. While swelling requires long incubation times and hinders the encapsulation of large macromolecules inside the forming vesicles, the salt conditions for electroformation limit the use of protein buffers and yield a non-homogeneous distribution of proteins inside vesicle [155, 142].

Bypassing past methods' technical limitations, the inverted emulsion transfer method has become a powerful approach for producing GUVs with encapsulated biomolecules [156]. This method is typically carried out in two steps. First, a water-in-oil (w/o) emulsion is created by adding an aqueous phase containing the biomolecules for encapsulation in a lipid-saturated oil phase, followed by tapping or vortexing the mixture. In this emulsion, droplets filled with our biomolecules of interest are confined by a lipid monolayer at the water/oil interface. In a second step, a two-phase system is prepared by carefully pouring

a lipid-saturated oil layer over an aqueous phase, forming a flat lipid monolayer at the interface. To generate the vesicles, the initially prepared w/o emulsion is then layered over the two-phase system and centrifuged. The centrifugal force allows the w/o droplets to cross through the lipid monolayer at the oil/water interface, resulting in the collection of unilamellar vesicles in the lower aqueous phase [157, 155, 158].

For bottom-up reconstitution purposes, the inverted emulsion method presents many advantages. Not only it is a very simple method that requires no specialized equipment, but it also enables the high-throughput generation of unilamellar vesicles with customizable characteristics. More precisely, GUVs with lipid bilayer asymmetry can be produced and large macrocomplexes can be encapsulated in their lumen with high efficiency [157]. However, the generation of vesicles with a wide size distribution and the contamination with remnants of oil at the membrane are disadvantages that have motivated others to improve this method with microfluidic-based techniques [155, 142, 159, 160]. In particular, microfluidic jetting and continuous droplet interface crossing encapsulation (cDICE) have drawn the attention of the synthetic biology field, as they enable precise control of vesicle size, membrane properties, and unilamellarity [161, 162, 163]. However, the need for specialized microfluidic equipment and expertise, together with the long preparation process these experimental setups require, make these methods a technical challenge for many research groups, which often opt for more straightforward methods [157, 158].

In conclusion, giant vesicles are an essential biomimetic membrane system for synthetic biology. At present, GUVs constitute the minimal cell model of the field and the scaffold in which cellular processes can be studied. Notably, from the reconstitution of complex biochemical reactions within their lumen, we are gaining tremendous knowledge about cytoskeletal, membrane-remodelling, and division proteins, which ultimately can be used in the construction of artificial cells with protein-based functional modules.

Hence, based on the above considerations, this thesis will use GUVs as minimal cell models. More specifically, these giant vesicles will allow to confine the synthetic building blocks of several functional modules into a well-defined compartment and analyse their dynamics and interplay for further biochemical characterization.

1.3 A synthetic division module for minimal cells

Omnis cellula e cellula, the Latin epigram coined by François-Vincent Raspail, formulates one of the fundamental tenets of cell biology [164]. Cells, the elemental units of life, divide to conquer. Cellular replication is therefore one of the hallmarks of life.

Due to genetic redundancy, division is a highly conserved and robust cellular process. In both prokaryotic and eukaryotic cells, it is tightly regulated and carried out by mul-

tiprotein machineries with varying mechanistic principles. While rod-shape bacteria like *Escherichia coli* (*E.coli*) employ more than 30 proteins for the regulation and assembly of its divisome, eukaryotic cells possess more complex division machineries with up to 130 genes required for cytokinesis [165, 166]. To achieve division, the first step a cell must undergo is growth. It needs to duplicate its genome and synthesize all the biological material intended to be distributed to the daughter cells. Following genome segregation, the membrane undergoes deformation and abscission. Symmetric or asymmetric division thus yield cells with equal genetic and cytosolic content or different molecular composition relative to the mother cell, respectively [167].

As a key function and prerequisite for life, self-division is one of the many essential functionalities that an artificial cell must possess to sustain its identity over several generations. Consequently, recapitulating division through the assembly of a set of defined modules has become one of the major goals in synthetic biology. To this end, several approaches have been devised to divide cell-like biomimetic models such as GUVs: (i) mechanical, based on physical stimuli generated by surface tension or other external forces, and (ii) chemical, which rely on triggered molecular reactions [168]. Remarkably, many of these strategies have already shown the successful division of liposomes. For instance, osmotic differences between the interior and exterior of phase-separated GUVs can lead to their division into two daughter cells with uniquely different membrane compositions [169]. Moreover, approaches aimed at altering membrane curvature successfully exploited temperature, pH, nanoparticles, or light irradiation to trigger changes in surface area and spontaneous curvature, ultimately leading to division of liposomes [170, 171, 172, 173].

However, these approaches preclude meeting one of the key requirements for the construction of a self-sustaining artificial cell: division should not depend on external mechanical or chemical actuated triggers; active cell division should be the resulting outcome of a concert of well-orchestrated coupled reactions within synthetic cells [20, 168]. Thus, to achieve this goal, a promising alternative to synthetic division is to mimic the strategies utilized by prokaryotic, eukaryotic, or archaeal cells, and assemble a protein-based divisome. In this approach, proteins would be the main responsible for generating the mechanical forces and membrane curvatures required to complete GUV scission and ensure the continuity of our artificial cells.

Two main mechanisms of cellular division are currently being recapitulated *in vitro* for their potential use in synthetic cells. On the one hand, the prokaryotic approach utilizes the bacterial *E.coli* division machinery to build the Z-ring, a mid-cell macromolecular structure primarily assembled by the protein FtsZ [174, 175]. This tubulin homolog, responsible for the scaffolding of the Z-ring on the inner bacterial membrane, polymerizes and recruits proteins such as FtsA, ZipA, and the Zap proteins for the maturation of the divisome and the initiation of the division process [176]. Although the precise mechanistic details of bacterial division remain obscure, current hypotheses point at the cooperative action of these proteins and the cell wall synthesis at the septum as responsible for generating the

constriction forces in bacterial division [177, 178]. For additional insights into the *in vivo* bacterial division machinery, see section 1.4.2.

Nevertheless, the efforts to build a prokaryotic-based synthetic divisome have yielded significant advancements. While Erickson managed to reconstitute a FtsZ-FtsA ring capable of vesicle division [179], Kohyama and colleagues achieved the complete *in vitro* reconstitution of the bacterial divisome using five proteins [143]. However, employing FtsZ as the main contractile element for the assembly of a division ring presents several drawbacks. Firstly, it is still under investigation whether FtsZ can generate the contractile forces necessary for vesicle abscission [180, 177]. Secondly, besides the scrutiny on its force-generating capabilities, the size scale of the FtsZ ring and its curvature may be incompatible with the complete abscission of giant vesicles [181, 182]. Finally, Erickson reported a division success rate of only 1.3%—far from obtaining a reliable mechanism for synthetic division [179].

On the other hand, an alternative strategy involves the assembly of a eukaryotic-inspired synthetic division machinery [183]. More precisely, in this approach the main aim is either the assembly of a cortical network or the engineering of a contractile cytokinetic ring, both mainly composed of actin and myosin. Although eukaryotic division is a highly complex and tightly regulated process encompassing many proteins [166], the goal is to recreate it with a minimal set of proteins which can recapitulate a simplified mechanism of constriction. Thus, an actin-based synthetic division machinery represents a promising alternative for the challenge at hand: build a division module that enables the self-replication of membrane-enclosed artificial cells.

1.3.1 The actin cytoskeleton and its modulating proteins

The cytoskeleton of animal cells is a highly dynamic scaffolding structure located beneath the plasma membrane which undergoes fast and coordinated remodelling to endow the cells with functions like motility, shape deformation, polarization, adhesion, and division. Composed of intermediate filaments, microtubules and actin filaments, the latter are the main cytoskeletal component responsible for the assembly of this filamentous network through interactions with many cortical proteins [184, 185, 186].

Highly conserved throughout all kingdoms of life and present in all eukaryotes, actin is one of the most abundant proteins on Earth. In particular, the eukaryotic actin protein consists of 375 amino acids (∼42 kDa) that fold into a flat, three-dimensional conformation with a deep medial cleft [187, 188]. In species like humans, several genes encode for different actin isoforms which exhibit high sequence similarity but present compartment- and tissue-specific functions and localizations. Four isoforms are expressed in striated and smooth muscle (α_{skeletal}-actin, α_{cardiac}-actin, α_{smooth}-actin, and γ_{smooth}-actin), while two isoforms are ubiquitously expressed in the cytoplasm (β_{cyto}-actin and γ_{cyto}-actin) [189, 190]. This functional versatility and robustness arise from the tendency of actin monomers (g-actin)

to self-assemble into semi-flexible thin filaments (f-actin) by the binding of ATP molecules to their medial cleft in the presence of divalent cations (Mg^{2+} or Ca^{2+}) [191, 187]. The resulting actin filament can be described as a two-stranded right-handed polar helix with differing monomer association/disassociation rates at each end; more specifically, net addition of monomers occurs at the barbed (+) end and net loss at the pointed (−) end, a process known as treadmilling [192, 188]. To regulate the assembly and disassembly of actin filaments, cells rely on a plethora of actin-binding proteins (ABP) (Figure 1.5a). These proteins regulate both monomeric and filamentous actin by promoting nucleotide exchange, phosphate disassociation, or filament disassembly. Among their functions, some maintain the pool of available actin monomers (e.g., profilin), nucleate the formation of new filaments (Arp2/3 complex, formins), promote elongation (formins, Ena/VASP) or sever filaments (cofilin, gelsolin), cap filament ends to terminate elongation (capping protein) or crosslink filaments into bundles (fimbrin, fascin, α-actinin) as well as disordered networks (filamin). Additionally, some anchor filaments to the plasma membrane (ezrin-radixin-moesin protein family, talin), or generate cortical tension via contractility through motor domains (myosins) [186, 188, 193].

The myosin superfamily of motor proteins comprises cytoskeletal molecular motors involved in short-range transport along actin filaments via ATPase activity [194, 195]. First identified in muscle, the class II myosin genes encode a hexameric protein (∼550 kDa) consisting of two heavy chains (MHC-II), two essential light chains (ELCs), and two regulatory light chains (RLCs) (Figure 1.5b) [196, 197, 198]. While the N-terminal motor domains of each MHC-II harbor the actin and ATP binding sites for the generation of force through chemical energy, the organization of the myosin monomer relies on the association of the two MHC-II into an α-helical coiled-coil. The interactions between these coiled-coils ultimately lead to the formation of small bipolar filaments, also known as "mini-filaments", consisting of approximately ∼28 myosin monomers [199, 198]. In muscle cells, the association of these bipolar filaments with f-actin through their motor domain in sarcomeric configuration generates tension and contractile force via the sliding filament mechanism (Figure 1.5c) [200]. However, in non-muscle cells, the mechanisms of contraction responsible for cellular functions such as cytokinesis are far more complex (Figure 1.5d) [201, 195].

1.3.2 The actomyosin contractile ring in eukaryotic cytokinesis

As the cell enters mitosis, the actin cytoskeleton undergoes major morphological changes. Although different cell types across kingdoms employ particular strategies for their self-division, the cytoskeleton is a crucial structure for organisms like animals, fungi, and amoeba, which rely on an actomyosin-based cytokinetic contractile machinery comprised of more than 100 proteins [202, 203, 204]. While model organisms such as *Dictyostelium* and *Caenorhabditis elegans* (*C.elegans*) divide through a dispersed actin meshwork, yeast and animal cells assemble a discrete ring made of randomly oriented actin filaments and myosin (Figure 1.6a) [205, 206]. For cytokinesis to effectively progress, these organisms

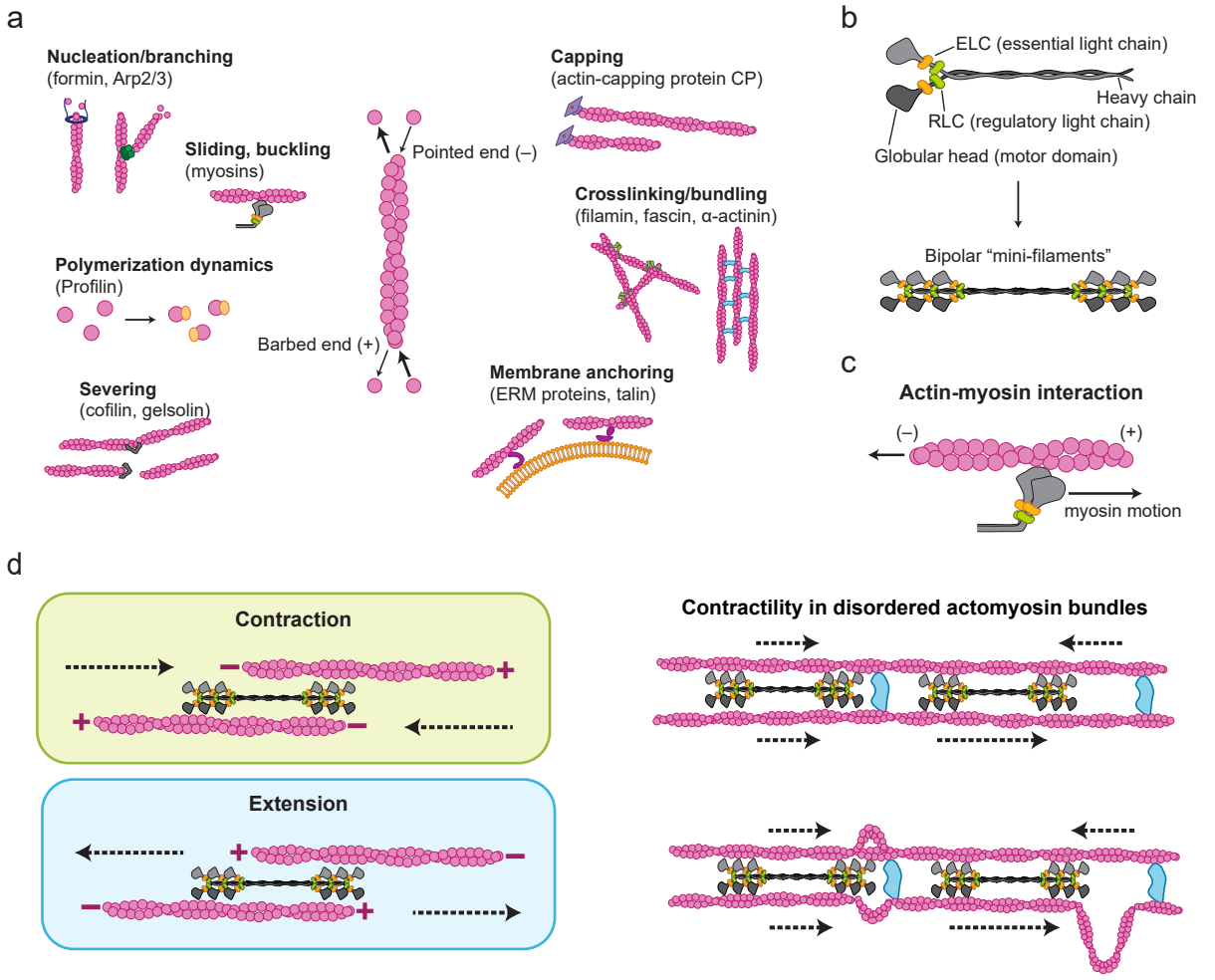

Figure 1.5. Overview of actin and its interaction with ABPs. a) Actin binding proteins (ABPs) can be classified in seven groups based on their cellular function. **b)** Schematic illustration of the non-muscle myosin II (NM II) domain structure. This hexameric protein consists of two heavy chains (dark and light grey), which contain the actin and ATP binding sites at their N-terminal motor domains, two essential light chains (ELC, orange), as well as two regulatory light chains (RLC, green). Upon RLC phosphorylation, myosin monomers assemble into bipolar "mini-filaments". **c)** Interaction between actin and myosin motor domains. The motion of myosin II towards the f-actin barbed end via the ATP-mediated swinging of its motor domain results in the contraction of sarcomeres in a mechanism known as the sliding-filament theory. **d)** Based on the polarity of actin filaments, the interaction between myosin II and f-actin may result in contraction or extension of the overlapping assembly (left panel). In non-sarcomeric and disordered actomyosin bundles, myosin II generates compressive and tensile stresses. Depending on the localization of crosslinkers with respect to myosin II and f-actin, these internal stresses induce the buckling and severing of f-actin, yielding bundle shortening (right panel).

follow several steps: (i) division site specification, (ii) actomyosin ring assembly at the cleavage furrow, (iii) ring constriction, (iv) ring disassembly and membrane scission (Figure 1.6b) [205].

In animal cells, the mitotic spindle is the main source of positional information for cleavage furrow formation, as well as the responsible machinery for contractile ring assembly and activation, since it determines the accumulation site of its two master regulators, the chromosomal passenger complex and the centralspindlin complex [207, 208]. Indeed, these two mitotic complexes are responsible for the recruitment and activation of critical downstream signalling proteins at a position midway between spindle poles. The main actuator in this signalling cascade is RhoA, a small GTPase protein of the Ras superfamily. The activation and accumulation of RhoA at an equatorial cortical zone by the spindle trigger the assembly of the contractile ring and determine the future cleavage site [209, 210, 208]. To assemble the ring, RhoA-GTP activates formins, which initiate new actin polymerization by nucleating f-actin at the cortical site, as well as anchor filaments at their barbed ends to the plasma membrane [211, 212]. In addition, RhoA-GTP indirectly activates myosin II via the phosphorylation of its RLCs, thereby triggering their assembly into bipolar filaments and allowing their interaction with actin filaments [213, 199]. The alignment of actin filaments of both polarities and their interdigitation with myosin II bipolar filaments result in a ring-like structure which is scaffolded and associated with the membrane by septin filaments after their recruitment by anillin, an actin crosslinker [214, 215, 216]. However, what is the precise macromolecular organization of the cytokinetic proteins comprising the contractile ring is one of the major questions which the field has not yet managed to resolve [217, 203]. Moreover, the wide variety of cytokinetic mechanisms observed in eukaryotic cells adds an additional layer of complexity to this question.

For instance, in the fission yeast *Schizosaccharomyces pombe* (*S. pombe*) the contractile ring arises from protein-clustered nodes around the cleavage furrow which anchor both formins and myosin heads projecting away from the membrane [218, 219]. When the formin-nucleated actin filaments bind to the myosins head from adjacent nodes, the myosin filaments presumably pull f-actin away in a disordered manner buckling the filaments and creating tension all around the ring cross section via a search, capture, and pull mechanism [220]. Consequently, nodes would reduce their interdistance, eventually yielding the condensation of these punctate structures [221]. Moreover, 2D and 3D simulation models show that rapid turnover of proteins and the disassembly of nodes at the ring are required to continue the constriction process [203].

Conversely, initial observations of the contractile ring in animal cells led to hypotheses suggesting a sarcomeric organization of the actomyosin filaments and a sliding filament mechanism for tension generation [224]. However, after electron microscopy images showed no discernible sarcomere-like structure of actomyosin filaments, further studies discarded this model and focused on analysing in detail the three-dimensional architecture of the ring [225, 226]. Using a combination of high-resolution and super-resolution light mi-

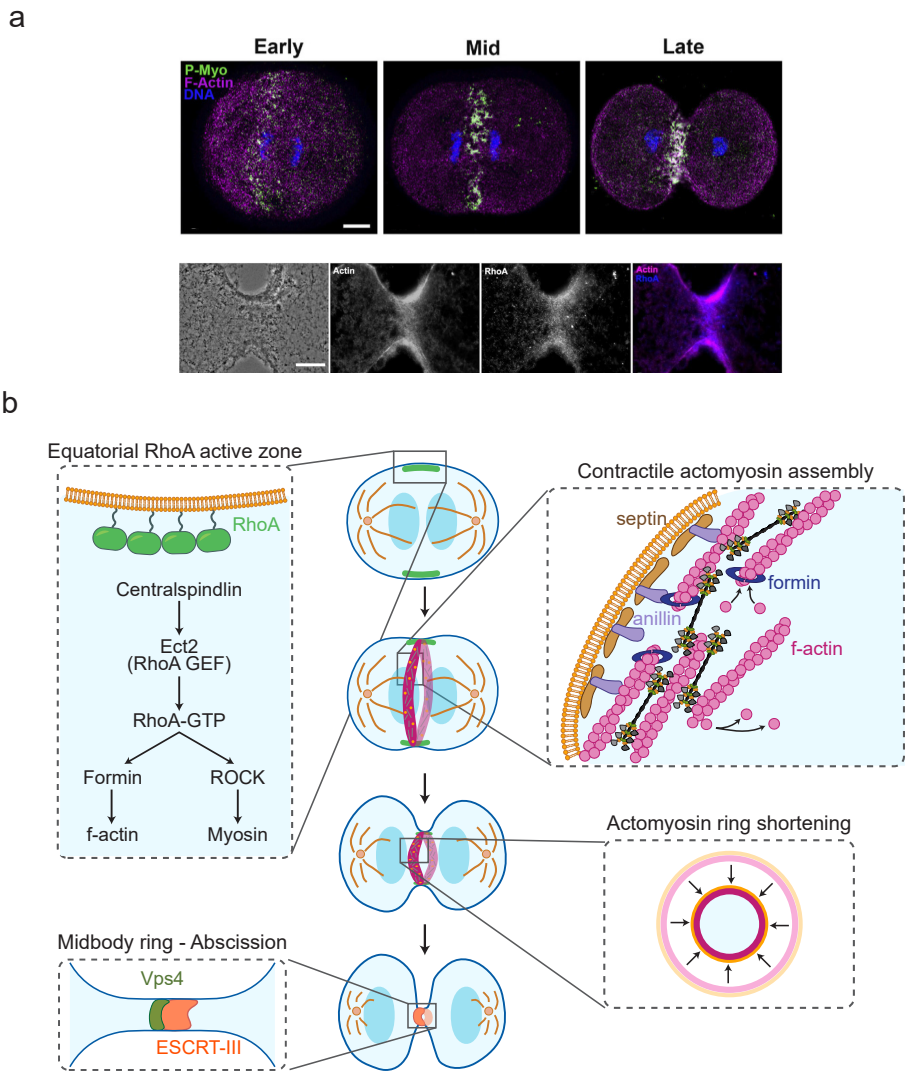

Figure 1.6. Cytokinesis in animal cells. a) Confocal imaging of sea urchin embryos immunofluorescently (IMF) stained for myosin II (P-Myo) depicting early, mid, and late-stage contractile rings (top panel). Wide-field imaging of immunofluorescently labelled cleavage cortices (actin in magenta and RhoA in blue). Phase contrast image is on the left (bottom panel). Scales bars are 10 μm. Top panel images adapted and reprinted from [222] under a CC BY 4.0 license (https://creativecommons.org/licenses/by/4.0/). Bottom panel images adapted and reprinted from [223] under a CC BY-NC-SA 3.0 license (http://creativecommons.org/licenses/by-nc-sa/3.0). **b)** Schematic of the animal cytokinesis process. First, RhoA activation triggers the assembly and localization of the actomyosin contractile ring at mid-cell. Subsequently, circumferential constriction of the ring leads to the symmetric deformation of the cell, culminating with the formation of the midbody ring and the abscission of the membrane into two daughter cells.

croscopy techniques, experiments performed on dividing HeLa cells showed the formation of a higher-order myosin assembly where filaments organized in stacks localized at the cleavage furrow—a possible contractile unit comprising the cytokinetic ring of these cells [227]. In parallel, Henson and colleagues utilized super-resolution light microscopy and platinum replica transmission electron microscopy (TEM) on dividing sea urchin embryos and reported two important observations [223]. Firstly, in the early stages of division, regularly spaced myosin clusters, reminiscent of fission yeast nodes, localized at the furrow band. As division progresses, however, myosin II bipolar filaments align end-to-end forming tight bundle-like bands. In addition, they described the presence of a thick mat of anisotropic, unbranched actin filaments oriented parallel to the plane of division. Based on these observations, the authors hypothesized that the interaction of these myosin bundles with actin can generate the contractile tension required for ring constriction via a sliding filament-based purse-string mechanism [228, 229]. Nonetheless, although these studies shed light on the architecture and contractile mechanism of the ring in animal cells, many others have reported on the presence of proteins such as α-actinin, F-BAR proteins, fimbrin, tropomyosin, etc., accumulating at the cleavage furrow via undetermined mechanisms [230, 231]. Their role and whether they are essential, however, is still unknown.

Once the magnitude of the strain rate increases due to myosin-induced constriction, the ring begins to shorten and decreases dramatically in diameter. To achieve constriction, some studies and models point at the fast turn over of the molecules at the furrow and the disassociation/association of components that continuously self-assemble into the ring structure [232, 203, 214, 231]. For many, this depolymerization of crosslinked f-actin is not only required for the remodelling of the ring shape but also for driving constriction, as this mechanism might also generate additional tension [233, 234]. Eventually, as the actomyosin ring closes, the spindle midzone undergoes remodelling and maturation, and to organize the intracellular bridge between the two daughter cells the midbody forms. The contractile ring transitions into a midbody ring, with anillin and septin becoming essential proteins to anchor this ring to the plasma membrane and prevent cytokinesis failure [235]. Finally, for the final abscission step, the membrane-associated ESCRT-III complex and the ATPase Vps4 play significant roles in separating the two daughter cells thanks to the contractile spiral structures assembled by ESCRT-III which catalyse the scission of the membrane [236, 237, 206].

1.3.3 Reconstitution of the eukaryotic division machinery *in vitro*

The *in vitro* reconstitution of macromolecular actin architectures inside giant vesicles has a long history of successful examples in the cytoskeletal field [238, 239, 240, 241]. More than three decades ago, the poor understanding of the interactions between actin, its ABPs, and the membrane propelled a series of elegant experiments on both the external surface and inside of vesicles, aiming to describe the molecular mechanisms and mechanical properties of the meshwork emerging from these interactions [242, 243]. Although Limozin and Sack-

mann, together with Honda *et al.*, showed that encapsulation of actin filaments and bundles inside the lumen of vesicles was possible via the electroformation and swelling method, respectively [244, 245], anchoring and assembling a minimal actin cortex on the inner leaflet of GUVs turned out to be a more complex feat [246]. However, with the development of inverted emulsion methods, the reconstitution of a wide range of membrane-associated cytoskeletal structures, such as networks and bundles, became possible and membrane protrusions, blebs, and inward deformations were recapitulated [247, 248, 249, 250].

Many of the advanced cytoskeletal reconstitutions from recent years stem from the synthetic biology field, especially from those working on the assembly of a eukaryotic-inspired cytokinetic module. As described at the beginning of section 1.3, work towards this major goal encompasses the *in vitro* reconstitution of actin-based contractile machineries to develop an optimized mechanism for autonomous division of GUVs. The efforts to achieve a cytokinetic division module can be classified into two distinct routes based on the actin architectures they rely on to achieve contraction [183].

On the one hand, the naturalistic route follows a cell-inspired strategy and aims at achieving division with a contractile cortex-like network anchored to the vesicle membrane. This cortex, composed mainly of disordered actin filaments and myosin motors, would self-assemble and remodel at the GUV equator, constricting the membrane through myosin-induced filament buckling and protein turnover [251]. For those working on this route, many key aspects concerning the composition, spatial organization, and dynamics of this actin network have to be finely tuned to achieve this goal. For instance, for the anchoring of the cortex to the membrane, several strategies employing biotinylated lipids with biotin-actin, nickelated lipids with His-tagged proteins, or PIP2-N-WASP links have shown successful binding of actin cortices to the membrane [252, 253, 254, 241, 255]. However, as described by Carvalho *et al.*, the weak or strong attachment of these cortices affects the morphology of network contraction inside liposomes [253]. Strong binding to the membrane is therefore needed since inward contraction and detachment from the bilayer occur when anchoring is too weak. In addition, their observations highlight the important role of protein nucleators (e.g., Arp2/3 complex), crosslinkers (fascin, anillin), and other ABPs for cortex reconstitution. Indeed, together with membrane anchoring, the network connectivity has a direct effect on the degree of cortex remodelling and the shape deformations it can induce on membranes [256, 249, 247]. Thus, an optimal ratio of [actin]:[motors]:[anchor]:[crosslinker] will be required to allow the generation of an active interconnected network, prevent rupture or dissociation of the actin shell, and achieve an efficient transmission of cortical stress by myosin at the vesicle midbody [257, 253, 250]. Nonetheless, the resulting actomyosin network could function not only as a contractile module, but also as a mechanoprotective and shape-changing scaffolding apparatus to confer synthetic cell with many other functions [183].

On the other hand, the engineering route aims at the generation of an isolated contractile ring bound to the membrane for the constriction and division of synthetic cells (Figure

1.7). Although challenging, building actin-based rings employing ABPs dates back to the late 1990s, when Honda *et al.* showed that crosslinkers like fascin or filamin can form actin bundles and render a ring configuration inside liposomes [245]. Contrary to other strategies where macromolecular crowders and cations are utilized to induce network and ring formation [258], recent approaches focus on using actin crosslinkers or combinations of them to study their interplay and optimize ring assembly and dynamics [248, 259, 142]. In this regard, the arrangement and orientation of actin filaments within the ring, as well as bundle bending stiffness, are key aspects worthy of consideration [260]. The current use of myosin as motor protein to endow the rings with contractile power requires careful design of the ring's macromolecular composition and bundle architecture due to the varying responses different actomyosin structures have to myosin-induced forces [261, 262, 263]. Thus, to promote a controlled but full contraction of actomyosin rings, the biochemical composition and spatial organization of f-actin are crucial parameters.

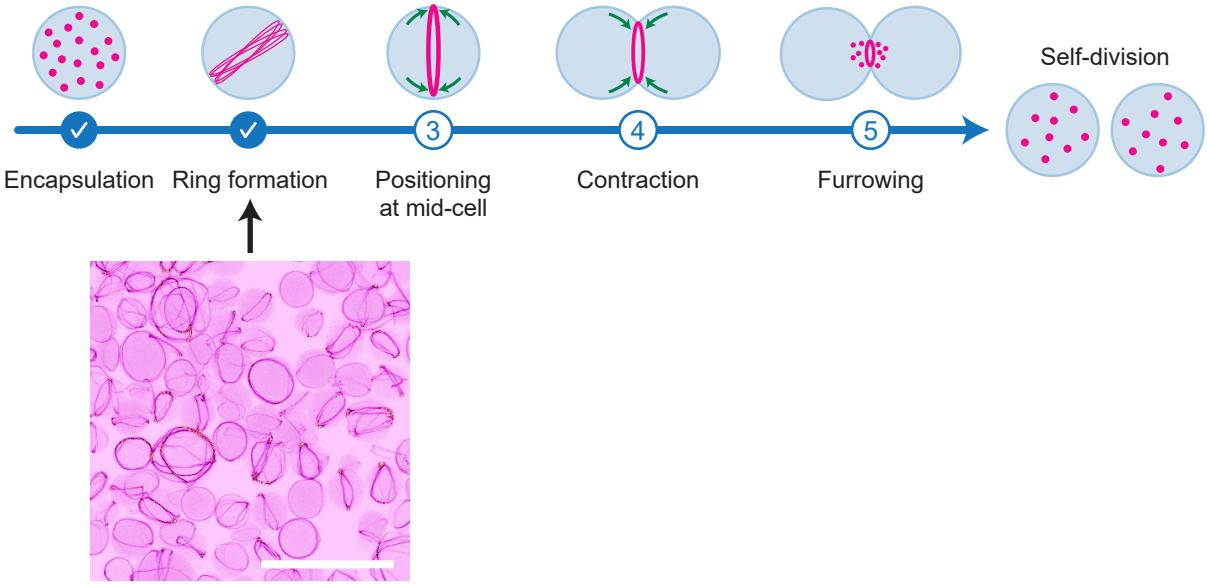

Figure 1.7. The engineering route for actomyosin-driven synthetic division of artificial cell. Schematic representation of the steps required to achieve a eukaryotic-based synthetic division of minimal cells. After encapsulation of proteins like actin, myosin, membrane linkers, bundlers, etc., a membrane-bound ring needs to assemble inside the vesicle. After localization of the ring at mid-cell, equatorial contraction of the ring by motor proteins leads to the furrowing and deformation of the membrane until division occurs. 3D projection image of a confocal microscopy stack depicting the formation of actin rings (fascin as actin bundler) inside vesicles employing the inverted emulsion transfer method for GUV production. Scale bar is 50 μm.

Remarkably, the reconstitution of contractile actomyosin rings has reached important milestones in the last 10 years. In their seminal work, Miyazaki and colleagues first showed

in water-in-oil droplets that cell-size spherical confinement facilitates the spontaneous formation of ring-shaped actin bundles [264]. More precisely, droplets with a radius equal to or smaller than the persistence length of f-actin enabled actin filaments to behave like elastic rods, thereby inducing the bundling of filaments into a ring-like structure at the inner periphery to minimize their bending energy [265, 266]. Besides confinement, the addition of myosin also promoted ring formation by the remodelling of the filamentous network. However, upon incorporation of an effective myosin concentration, this motor disorganized the ring and full contraction into a luminal actomyosin cluster occurred before ring disassembly. Interestingly, under these conditions, actin disassembly or depolymerization was not required to reach full contraction of the rings; the volume of the rings remained constant and their width increased as contraction progressed.

More recently, significant advances in the encapsulation of contractile rings inside vesicles have brought the field one step closer towards synthetic division. Litschel *et al.* employed a modified cDICE method to encapsulate actin with many different actin crosslinkers like fascin, α-actinin, talin, and vinculin [267]. Interestingly, rings anchored via biotin-neutravidin bonds, and formed by actin bundled with talin and vinculin, contracted when myosin was included in the inner encapsulation mix. The progressive myosin-induced contraction led to transient membrane deformations and the generation of fully contracted actomyosin clusters on the sides of vesicles. Similarly, by fine-tuning the stoichiometry of active and passive actin crosslinkers, Bashirzadeh and colleagues captured the time evolution of actomyosin ring formation and membrane contraction at the ring locus, providing valuable insights into ring assembly and the crosslinker effect on bundle contraction [263].

Moreover, studies performed with septins and anillin in bulk showed the potential these two crosslinker proteins hold for the *in vitro* reconstitution of contractile actin rings [268, 269]. Albeit encapsulation experiments are still needed, bulk volume assays already demonstrated that these two crosslinkers promote actin ring formation. In the case of anillin, however, a much more dramatic effect was observed. As Kučera and co-workers reported, this passive crosslinker not only formed anillo-actin rings in solution, but also generated contractile forces of entropic origin which yielded the myosin-independent constriction of these rings [269], suggesting that other non-myosin based contractile strategies could also be employed for synthetic division.

Nevertheless, for both strategies (naturalistic and ring-based) to succeed, there is an aspect of self-division that is imperative to address: the controlled symmetry breaking between the poles and the furrow [183, 255]. For a contractile actomyosin cortex or ring to yield two symmetric synthetic cells, tensile stresses must be targeted at the cleavage furrow. In the case of a cell-spanning cortex, to prevent detachment/peeling of the meshwork from the membrane and its accumulation at the poles [253], actomyosin flows need to align the actin filaments parallel to the division plane, forming a contractile band at the equator while furrowing takes place. Similarly, for the controlled contraction of isolated rings at mid-vesicle, a mechanism must be devised to localize the ring as it contracts to

avoid slippage and clustering on the sides of the vesicle [267]. As previously mentioned (see section 1.3.2), a highly complex machinery involving the mitotic spindle is responsible for the spatiotemporal regulation of the assembly and contraction of the cytokinetic ring. At present, *in vitro* reconstitution of this machinery is beyond our technical capabilities; it would require the encapsulation of many proteins and the recapitulation of reactions which need to unfold in a timely manner. Therefore, many strategies have been proposed to provide synthetic cells with a positional module for actomyosin-based contraction: mechanical confinement with microfluidic traps, local light activation of latent myosin II with blebbistatin, curvature-inducing or sensing molecules, external biochemical cues, etc. [270, 271, 272, 273, 274]. Conversely, the reconstitution of a simpler self-organized protein mechanism endowing synthetic cells with the capability of spatiotemporally regulating molecules constitutes a promising approach. The autonomy and self-sufficiency of the minimal cells would be assured, and the joint assembly of discrete protein machineries would compel their optimization into synergic modules.

1.4 Spatiotemporal organization of molecules via protein patterns

Many of the macromolecular structures introduced in previous sections (e.g., the mitotic spindle or the actomyosin cytoskeleton) share some common characteristics: they robustly perform their functions, adapt, and present a dynamic yet stable configuration. The reason cells are capable of building such complex and optimized structures stems from a fundamental hallmark of biological systems: self-organization. As one of the core building principles within cells, self-organization demonstrates the power of molecular interactions. Indeed, self-organization arises from the interplay of lower-order system components such as attraction, repulsion, and positive/negative feedbacks. These nonlinear interactions, which require the supply of an energy source like ATP or GTP, organize the molecules in higher degrees of complexity and, as a result of their collective behaviour in steady state, emergent properties and functions which cannot be directly predicted from their individual properties arise [275, 276]. Thus, as open systems far from thermodynamic equilibrium, cells are able to generate order from an initial homogeneous state via the dissipation of energy. Although energy dependency is a limiting factor for the endurance of self-organized structures, the emergence of an overall order in time and space endows cells with features such as the spontaneous formation of patterns, bi-stable switches, and the non-linear coupling of reactions [277, 278].

1.4.1 Self-organized reaction-diffusion systems

The formation of patterns as a spatiotemporal organization strategy has long fascinated cell and developmental biologists. Present across all biological length scales, patterns con-

stitute an organizational property observed in a plethora of fascinating phenomena like the collective behaviour of organisms or the pigmented shapes and forms in animal fur and skin [279]. Despite the complexity of biomolecular networks and their interacting subunits, several simple mathematical models have been proposed to describe the mechanisms by which self-organized patterns emerge in living systems. One particular work instrumental to our understanding of pattern formation is *The chemical basis of morphogenesis* by Alan Turing [280]. In 1952, this mathematician described spatiotemporal patterns using a simple system composed of two interacting substances which can diffuse in space and present different diffusion rates. Initially, the system is at equilibrium, with a near-uniform concentration distribution of its components. However, random disturbances trigger diffusion-driven instabilities, leading to pattern formation. Thus, in this reaction-diffusion model, the onset of pattern formation is unstable steady states (termed Turing instabilities), which emerge solely from the interplay between the chemical reactions of the interacting species and their lateral molecular diffusion [281, 282]. Varying the diffusion and reaction parameters of the formalized mathematical model gives rise to periodic patterns which in one and two dimensions take the form of traveling waves or stationary structures including stripes, spots, hexagons, labyrinths, etc.—which remarkably respond to small disturbances and self-regenerate [283, 284, 285].

Turing's reaction-diffusion model, especially his concept of instabilities, has been paramount in describing both chemical and biological pattern-forming systems. For instance, in chemistry, Turing's model accurately predicts and captures most of the qualitative features of the patterns formed in a chemical oscillating reaction termed the Belousov-Zhabotinsky reaction [286, 287]. Similarly, the general principles underpinning Turing's model, and its particular cases like the Gierer-Meinhardt system, have been applied to align these theoretical models to biological phenomena [288, 289]. Indeed, as Turing predicted, steady-state patterns can also underlie self-organization processes in living cells. Computer simulations of Turing's model recapitulated the expression patterns of signalling molecules involved in vertebrate digit patterning and other tissue-organization processes for limb development [290, 291], as well as calcium fluxes mediating the excitation-contraction coupling in cardiac cells [292].

Importantly, reaction-diffusion pattern formation accounts for the spatiotemporal regulation of many fundamental cellular processes. More precisely, in eukaryotic and prokaryotic cells, nanometre-scale protein machineries consume energy to interact,—i.e., self-organize—via reaction-diffusion mechanisms, resulting in protein patterns which play vital roles in the regulation of intracellular processes [293, 282]. For instance, polarity sorting in budding yeast *Saccharomyces cerevisiae* is spatially coordinated by the reaction-diffusion Cdc42 system [294]. Through a series of interconnected regulatory feedback loops and the different diffusion rates of its constituents, the Cdc42 system induces spontaneous symmetry breaking and bud formation, thereby enabling the asymmetric division of the cell [295, 296].

1.4.2 The reaction-diffusion MinDE protein system

In *E.coli* bacteria, correct placement of the divisome machinery at the cell's centre is essential to ensure symmetric division into two identical daughter cells, each containing a complete copy of the replicated chromosome. As previously described (see section 1.3), the Z-ring is a macromolecular structure scaffolded by the FtsZ protein, which recruits the rest of the required constituents to form the septum and initiate cell division. The spatiotemporal localization of the divisome machinery is mediated by one positive (TER linkage) and two negative regulatory systems. The two inhibitory machineries that direct the assembly of this ring to the mid-cell region are the nucleoid occlusion and the MinCDE system. While the nucleoid occlusion prevents contraction of the Z-ring over the unsegregated nucleoid, the MinCDE system precludes ring formation at the cell poles [297, 298, 299].

The mechanism by which the MinCDE system reliably achieves spatiotemporal regulation of the Z-ring is one of the most striking examples of self-organized pattern formation. To understand how this system self-organizes into patterns, one must take a careful look at the molecular basis of its mechanism—i.e., the properties and dynamics of its protein interactions. First identified by the mutation of the genetic locus *minB*, which yielded anucleated minicells via asymmetric division [300, 301], de Boear and colleagues later elucidated and described the proteins encoded in this system: MinD, its cognate activating protein MinE, and the ultimate effector of the system MinC [302, 303].

MinD is an ATPase from the P-loop NTPases superfamily [304]. Composed of 270 amino acids, this protein contains four main motifs [305, 306]. The Walker A or P-loop motif, together with the Walker B or switch II region, binds the ATP molecule and complex the Mg^{2+} ion, enabling dimerization. The switch I region mediates the binding and activation of MinC in conjunction with the switch II residues. Finally, the membrane targeting sequence (MTS), an amphipathic helix at its C-terminal, presents weak membrane affinity when the protein is at its monomeric form, but effectively enables membrane binding when several MTS motifs are in close proximity [307, 308]. As a result, the binding of the nucleotide to MinD acts as a switch for both its oligomerization and localization (Figure 1.8a). While the ATP-bound state induces the dimerization and binding of the protein to the membrane, in the ADP-bound state the protein is at monomeric and soluble form at the cytoplasm [305, 309]. MinD membrane binding is a highly cooperative process. As addressed in experimental studies and simulations, local increase in MinD density on the membrane augments its residence time and recruits further protein from the cytoplasm [310, 311, 312]. However, for membrane detachment, MinD needs to interact with the second key player of the system, MinE. Indeed, MinD has an intrinsically low ATPase activity, which translates into an inefficient ATP hydrolysis and subsequent detachment from the membrane. Therefore, once MinE triggers its enzymatic activity, MinD is able to return to its monomeric and soluble form [313].

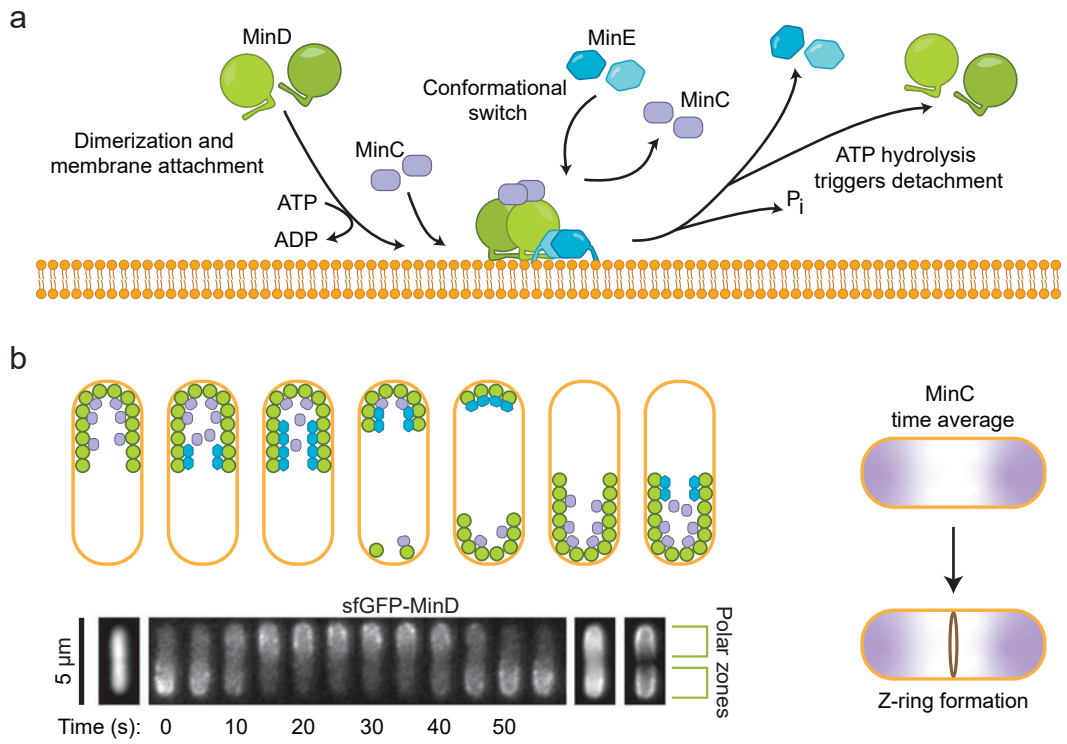

Figure 1.8. The reaction-diffusion MinCDE system in *E.coli*. **a)** Scheme depicting the molecular mechanism behind MinDE oscillations on a lipid bilayer. **b)** Graphical representation of the Min pole-to-pole oscillations *in vivo* (top panel) and fluorescence images of an *E.coli* cell expressing sfGFP-MinD over time (bottom panel). Time-average intensity and standard deviation show the formation of two polar zones with high MinD density. Images adapted with permission from [314], Copyright Springer Nature (2015). The MinC time-averaged concentration at the poles allows Z-ring formation only at the centre of the cell (right panel).

As the ATPase-activating protein of MinD, MinE is a small protein of 88 amino acids comprising two main functional domains. On the one side, the anti-MinCD domain at the N-terminal presents two motifs: an MTS composed of an amphipathic helix which enables its interaction with the membrane and inserts into the lipid bilayer, and a MinD contact helix crucial for the formation of the MinD-MinE complex and the stimulation of MinD ATPase activity [315]. On the other side, the topological specificity domain mediates the formation of MinE homodimers and is also required to fully stimulate the ATPase activity of MinD [316, 305]. Importantly, MinE has two distinct conformational states. In the closed state, the MTS motif of the MinE dimer is concealed in its hydrophobic core, which supports the free diffusion of the protein in the cytoplasm. When MinE encounters an ATP-bound MinD on the membrane, the MinE dimer adopts an open conformation that exposes the MTS and its contact helix, enabling its interaction with the MinD dimer [317]. Although this results in an asymmetric MinD-MinE complex (MinE is bound to only one

of the MinD subunits), it triggers hydrolysis of both ATP molecules in the MinD dimer, most likely due to a MinE-induced conformational change [318]. The localization of MinE after MinD detachment from the membrane remains obscure. While some studies showed a potential persistence binding of MinE to the membrane, the possible mechanisms by which MinE dimers interact with others membrane-bound MinD molecules or switches to its latent/closed state are still under debate [319, 305].

The third and final component of the system is MinC, the effector element. While it does not participate in the pattern formation mechanism, this protein is key to prevent aberrant septum formation. MinC contains two domains which bestow the protein with FtsZ inhibitory activity, preventing FtsZ from polymerizing and forming the Z-ring [320, 321]. In its dimeric form, MinC binds to ATP-bound MinD at the membrane [322]. However, since the surface region where MinC binds MinD overlaps with MinE's binding site, competition for complex formation at the same binding site results in MinE displacing MinC from membrane-bound MinD [323].

With the molecular intricacies and interactions already described, how does exactly the MinCDE system achieve Z-ring positioning at mid-cell? The answer lies in a fascinating protein oscillation from one pole of the cell to the other, resulting in a time-averaged concentration gradient of MinD-MinC localized only on both sides of the cell (Figure 1.8b) [303]. With the centre free from MinC-mediated FtsZ inhibitory activity, the Z-ring forms at the equator and symmetric division takes place [320, 324]. These rapid oscillations at the membrane, akin to an intracellular tennis match, are orchestrated by MinD and MinE. While MinC effectively functions as a passive passenger being carried by the oscillations, this dynamic protein pattern emerges solely from the self-organization of MinD and MinE via a reaction-diffusion mechanism at the membrane.

To initiate one oscillation cycle at a cell pole, MinD first binds ATP, which causes its dimerization and attachment to the membrane. MinD's cooperative binding then recruits more protein at the bilayer, leading to a reduction in their lateral diffusion and promoting high-order inter-dimer interactions [310, 309, 311]. Once membrane-bound, MinC associates with MinD in a 1:1 ratio [325]. Concurrently, homodimeric MinE remains in its latent, close state in solution until it senses a MinD dimer at the membrane, which triggers its conformational switch into a reactive state. The open conformation of MinE exposes the MTS and MinD contact helix, leading to its binding to MinD. If the MinD dimer is complexed with MinC, MinE promotes MinC detachment and displaces the protein into the cytoplasm [326]. In the MinD-MinE complex, MinE then stimulates MinD's ATPase activity, causing nucleotide hydrolysis on both subunits. Consequently, with MinD in its ADP-bound form, MinD monomerization and membrane-detachment follows [318]. Although the subsequent interaction and residence time of MinE at the membrane is still under scrutiny, it is however clear that MinD undergoes nucleotide exchange in the cytoplasm to restore its membrane-bound state and establishes a concentration gradient across the cell [282, 305]. The diffusion of MinD and its accumulation at the opposite pole subse-

quently re-starts the cycle, establishing a robust pole-to-pole protein oscillation inside the cell. This self-organized pattern, arising from a reaction-diffusion mechanism and responsive to cellular morphological changes, therefore regulates the spatiotemporal localization of the Z-ring [327].

In short, in the reaction-diffusion MinDE system, symmetry breaking at one pole first occurs when local disturbances, in the form of increased local MinD concentration, induce an enhanced recruitment of these dimers at the membrane (due to cooperative binding) causing the start of an oscillation. The protein pattern formation mechanism thus arises from membrane interactions and redistribution of MinD and MinE across the cell [282].

1.4.3 *In vitro* reconstitution of the MinDE system: uncovering hidden functions

The lipid membrane is the catalytic environment of several intracellular reaction-diffusion mechanisms, in particular the MinDE system. Given its crucial role in the formation of protein-patterns, the reconstitution of lipid bilayers in diverse model systems represented a turning point for the study of the MinDE system. Pioneering the MinDE reconstitution on flat membranes, Loose and colleagues were the first to successfully reconstitute the MinDE system on SLBs and describe its resulting pattern on two-dimensional (2D) membranes: a dynamic travelling and spiral wave (Figure 1.9a) [328]. In the search for a thorough description of the pattern-forming mechanism, a myriad of other studies have followed since. In chambers with flat SLBs and large bulk volumes, an in-depth investigation of the parameters affecting the MinDE oscillations was performed, and factors such as lipid composition, membrane fluidity, MinDE protein ratios, salt concentrations, flow, and temperature were shown to have a direct influence on pattern dynamics (wavelength, oscillation period, and wave velocity) [329, 123, 330, 331, 122]. For instance, while a higher diffusion coefficient of proteins at the membrane (due to increased fluidity) augments both the wavelength and the velocity of MinDE waves, an increase in anionic lipid content induces the decrease of both of these parameters [332, 329]. Importantly, by employing a MinE variant closer to the native protein, Glock *et al.* first showed that the MinDE reaction-diffusion mechanism on 2D flat SLBs can also yield quasi-stationary Turing-like patterns [333]. Meshes, spots, inverse spots, labyrinth-like patterns, and intermediate modes can thus emerge at the membrane depending on the MinD-MinE concentration incorporated into the chambers (Figure 1.9a).

Subsequently, with the implementation of photolithography techniques enabling the construction of patterned 2D SLBs and membrane-coated 3D microcompartments, several remarkable properties of the MinDE system were uncovered. Of particular significance is the reconstitution of MinDE oscillation on open *in vivo*-like compartments and surfaces with varying shapes and sizes [121, 335, 126]. Not only did these studies show that it was possible to recapitulate bacterial pole-to-pole oscillations and equatorial FtsZ localization *in vitro*, they also uncovered the geometry-sensing properties of the MinDE system. Indeed,

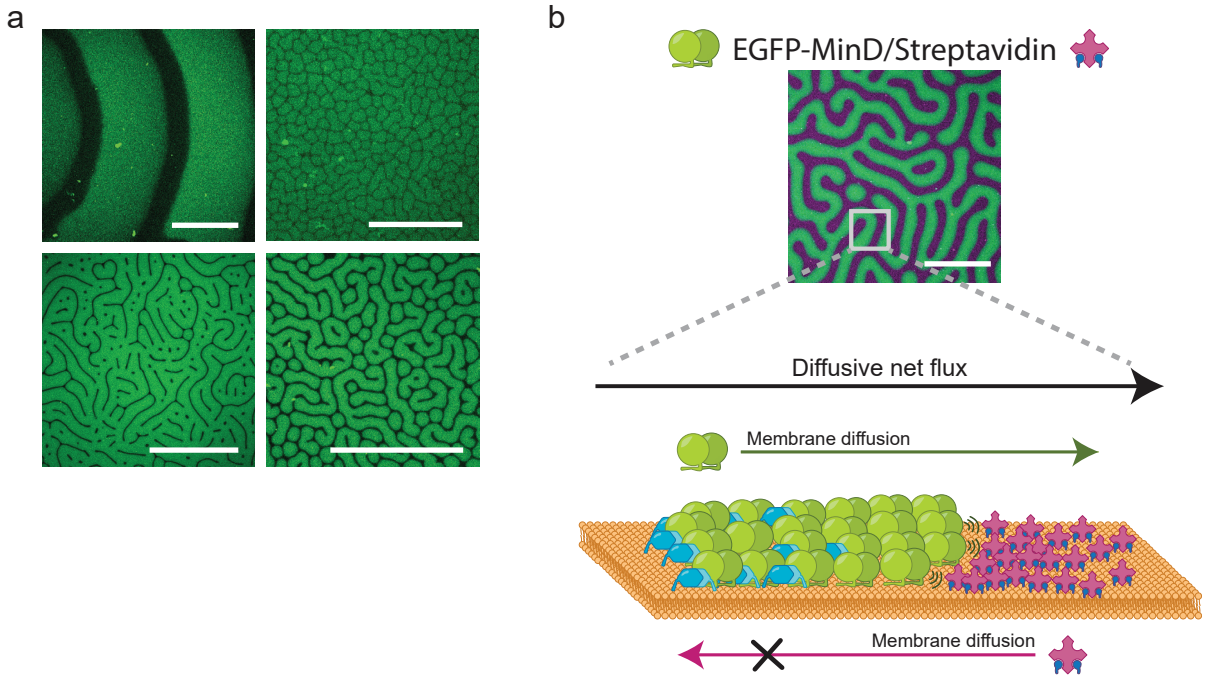

Figure 1.9. MinDE-driven diffusiophoretic transport of membrane-bound molecules. a) MinDE self-organization on SLBs generates wave-like dynamic patterns (top left) or quasi-stationary Turing patterns: mesh (top right), labyrinth (bottom right), and intermediate patterns that are a mix of two, e.g., inverse spots and labyrinth (bottom left). Scale bars are 100 μm. **b)** MinDE-driven transport of membrane-bound molecules via diffusiophoresis. Confocal image demonstrating the 2D patterning of streptavidin (cargo molecule) by Min proteins on an SLB. The mesoscopic friction arising from the non-specific interaction of MinDE and cargo fluxes induces the directed net transport and accumulation of cargo molecules in areas of low Min protein density. Scale bar is 50 μm. Scheme adapted from [334] under a CC BY 4.0 license (https://creativecommons.org/licenses/by/4.0/).

MinDE patterns adapt and show different oscillation modes based on surface topology and confined volume shape. To explore this intrinsic feature and investigate the spatiotemporal properties of MinDE patterns, several assays were subsequently performed employing closed microfluidic chambers [122], chambers with varying bulk volumes [120, 336], cell-sculpting PDMS microchambers [314], and 3D-printed microstructures [135]. From these studies, a plethora of dynamic modes as well as the geometrical selection rules behind MinDE oscillations were elucidated, and fundamental parameters such as lateral concentration gradients, bulk-surface coupling, and pattern multistability were described in the context of the MinDE reaction-diffusion mechanism [305, 337].

Moreover, encapsulation of the MinDE system inside lipid vesicles revealed that Min proteins can sustain different modes of oscillation at the inner leaflet of the GUVs: travelling waves, pulsing patterns, pole-to-pole oscillations, or trigger waves [338]. Alternatively,

when encapsulated inside deflated vesicles, MinDE binding to the membrane resulted in periodic vesicle deformations in concert with MinDE oscillations. More precisely, only when deflated vesicles exhibited pulsing patterns, periodic budding and subsequent bud fusion could be observed, alongside vesicle shape changes. This is the case of dumbbell-type vesicles, which split into two compartments after Min proteins relocated to their lumen, and then fused upon Min protein reattachment. In addition, advancements in the field of cell-free protein synthesis—particularly the encapsulation of these *in vitro* expression systems inside vesicles—have enabled the successful cell-free production of Min proteins inside GUVs. In this regard, not only were MinDE oscillations recapitulated, but also the membrane deformations observed in deflated vesicles subjected to osmotic shocks [143, 339].

Finally, pivotal experiments performed by Ramm *et al.* showed, once again, the instrumental role *in vitro* reconstitutions have in unveiling surprising "hidden" MinDE functions [340, 334]. Employing both flat surfaces and open microcompartments, these studies demonstrated the spatiotemporal regulation of peripheral and lipid-anchored proteins, as well as cholesterol-anchored DNA origami, in anti-correlated patterns via MinDE oscillations. This striking phenomenon, arising from both dynamic and quasi-stationary MinDE patterns, involves one particular type of phoretic transport: diffusiophoresis [341]. More precisely, the MinDE-mediated regulation of cargo molecules on the membrane emerges from the net diffusive flux generated by MinDE concentration gradients at the lipid bilayer (Figure 1.9b). MinDE proteins interact with cargo molecules in a non-specific manner, and the resulting net diffusive flux establishes a frictional force that guides the localization of these molecules towards areas of low MinDE density [334, 337]. Although its relevance in *in vivo* protein dynamics requires further investigation, these studies revealed a new mechanism that could be exploited for the spatiotemporal regulation of molecules on membranes—a particularly sought-after function for building a synthetic positioning module.

Taken together, the use of model membrane systems has enabled the reconstitution of the MinDE protein system under a plethora of controlled conditions. Recapitulating MinDE protein patterns not only has consolidated this protein system as a paradigmatic model to study reaction-diffusion mediated pattern formation, but also has enabled the in-depth characterization of the molecular basis behind MinD-MinE self-organization and the elucidation of unknown functions with potential to unlock newfound applications.

2 Objectives

The engineering of an actomyosin-based contractile module for synthetic division of minimal cells has shown remarkable advancements in the last decade. Past *in vitro* reconstitution of actin rings and their myosin-driven contraction inside water-in-oil droplets and vesicular systems have laid the groundwork for the assembly of such a module [264, 267, 263]. However, these reconstitutions have also exhibited an unequivocal shortcoming: the controlled positioning of contractile forces at the equator of synthetic cells. At present, the field lacks an effective strategy to overcome slippage of contractile rings and attain mid-cell localization of myosin-driven forces [267, 183]. Extensive attempts relying on external mechanical forces and careful revision of the eukaryotic-based division strategy have evidenced the importance of incorporating a positioning module into vesicular minimal cell models [270, 342]. To address this missing puzzle piece and prevent an impasse in the engineering of an actomyosin-based synthetic division module, in this thesis I set out to investigate the MinDE system as a suitable protein-based positioning module that could be assembled with the actomyosin contractile one. Thus, the ultimate goal of this thesis is to achieve the successful integration of both synthetic modules to attain spatiotemporal control of actomyosin rings and advance one step further in our endeavour to divide artificial cells.

To assemble and combine both modules together while retaining their functionality and integrity, I established a set of specific aims in a two-phase research approach. In the first phase of my research, I focused on studying the MinDE system. MinDE positioning of cargo molecules has been extensively characterized in open supported 2D lipid bilayers, open microcompartments, and *in vivo* [340, 334]. Although MinDE wave-like patterns have been studied employing 3D-printed architectures [135], the MinDE-driven positioning of complex biomolecules via diffusiophoretic transport has not been tested (and exploited) on the surface of intricate 3D geometries and free-standing membranes (GUVs). Therefore, I first set out to demonstrate the robustness of the MinDE protein system as a synthetic positioning module in these membrane model systems. Based on this goal, the objectives for this first phase of the thesis work were the following:

- Reconstitute dynamic and quasi-stationary Turing patterns on 3D surfaces obtained from the 2PP of a biocompatible hybrid photopolymer.
- Achieve the spatiotemporal control of a wide variety of unrelated membrane-bound

cargo molecules on 3D-printed microstructures and study the effect of cargo properties on MinDE patterning to test its mechanistic versatility.

- Exploit the diffusiophoretic capabilities of the MinDE system and demonstrate its potential application as a synthetic positioning/patterning module for the functionalization of microcarriers and cell mimics.

After this first research phase consolidated the MinDE system as a powerful and versatile synthetic module for positioning of complex biomolecules, this thesis work subsequently delved into the experimental challenges that co-reconstitution of modules entails. As mentioned above, the second phase aimed at the assembly and integration of the MinDE system (prokaryotic) with actomyosin contractile rings (eukaryotic) to enable controlled localization of forces at the equator for synthetic cell division. While these two synthetic modules independently showed their efficient functioning inside GUVs, their combined reconstitution required fine-tuning and optimization of encapsulating conditions. To tackle this challenge, the following objectives were set:

- Consider the design variables for both the positioning and contractile module and find the experimental conditions allowing the correct functioning of both modules and the showcase of their characteristic behaviour inside vesicles (i.e., generation of MinDE pole to pole oscillations, actin-bundling, bundle-membrane attachment, actomyosin ring contraction, etc.).

- Achieve the diffusiophoresis-mediated positioning of actomyosin rings at mid-cell by the MinDE system.

- Demonstrate equatorial furrowing arising from myosin-driven contractile forces within the recapitulated division ring.

- Investigate the emergence of unexpected effects and behaviours resulting from the integration of these two modules inside minimal cell models.

Taken together, my ultimate goal was to implement a modular engineering approach and show the efficient positioning of actomyosin rings at the equator of GUVs by employing the MinDE system. To attain this goal, this thesis thus pursued two specific aims: (1) to consolidate the MinDE system as a synthetic module for the positioning of any membrane-bound molecule or high-order structure, and (2) to harness its capabilities to overcome current challenges hindering progress in synthetic biology and other fields.

3 Publications

3.1 Publication P1

Protein-Based Patterning to Spatially Functionalize Biomimetic Membranes

María Reverte-López, Svetozar Gavrilovic, Adrián Merino-Salomón, Hiromune Eto, Ana Yagüe Relimpio, Germán Rivas, and Petra Schwille

Summary:

In this publication, we demonstrate the versatility of the MinDE protein system as a synthetic positioning module. To show that Min proteins can be employed as a benign patterning tool to functionalize 3D synthetic systems, we set out to investigate their capabilities on microcarriers and vesicular cell mimics. Due to their use in targeted drug delivery, we 3D-printed microswimmer-like robotic structures as solid microcarrier platforms and selected a wide variety of biomolecules with contrasting properties to test their MinDE-driven patterning. We coated the surface of microrobot-like architectures with lipid bilayers and effectively functionalized their surface with biomedically-relevant proteins and polymers (streptavidin, PEG), as well as higher-order DNA and protein structures (DNA origami, FtsZ filaments). We reveal that both MinDE dynamic and Turing-like patterns can spatiotemporally control any diffusible cargo on 3D-supported lipid bilayers and the inner leaflet of GUVs. These findings consolidate the MinDE system as a robust synthetic positioning module for diverse applications in fields such as synthetic biology and biotechnology.

To cite this article:

Reverte-López, M., Gavrilovic, S., Merino-Salomón, A., Eto, H., Yagüe Relimpio, A., Rivas, G., Schwille, P., Protein-Based Patterning to Spatially Functionalize Biomimetic Membranes. *Small Methods* 7, 2300173 (2023). https://doi.org/10.1002/smtd.202300173.

RESEARCH ARTICLE

small methods
www.small-methods.com

Protein-Based Patterning to Spatially Functionalize Biomimetic Membranes

*María Reverte-López, Svetozar Gavrilovic, Adrián Merino-Salomón, Hiromune Eto, Ana Yagüe Relimpio, Germán Rivas, and Petra Schwille**

The bottom-up reconstitution of proteins for their modular engineering into synthetic cellular systems can reveal hidden protein functions in vitro. This is particularly evident for the bacterial Min proteins, a paradigm for self-organizing reaction-diffusion systems that displays an unexpected functionality of potential interest for bioengineering: the directional active transport of any diffusible cargo molecule on membranes. Here, the MinDE protein system is reported as a versatile surface patterning tool for the rational design of synthetically assembled 3D systems. Employing two-photon lithography, microswimmer-like structures coated with tailored lipid bilayers are fabricated and demonstrate that Min proteins can uniformly pattern bioactive molecules on their surface. Moreover, it is shown that the MinDE system can form stationary patterns inside lipid vesicles, which allow the targeting and distinctive clustering of higher-order protein structures on their inner leaflet. Given their facile use and robust function, Min proteins thus constitute a valuable molecular toolkit for spatially patterned functionalization of artificial biosystems like cell mimics and microcarriers.

1. Introduction

Bottom-up synthetic biology is an interdisciplinary field where engineering principles are applied to biochemical processes with the goal of building cell-like systems from a set of minimal functional modules.[1] In the search for these modules, for the past 20 years the scientific community has applied a "building to understand" strategy.[2] Gene networks, protein systems, synthetic molecules, and biomaterials have been rationally designed and reconstituted in vitro, and extensive knowledge of their discrete properties and working principles has been harnessed.[3–5] Similarly to a tinkerer with a versatile toolbox, researchers are now working on integrating these well-defined modules in synthetically-assembled systems for their use in a wide range of applications like theragnostics, targeted drug delivery, bioremediation, and biocatalysis.

Intriguingly, the reconstitution of biological systems for their engineering into functional modules has revealed new sets of functions far-off the ones observed in vivo.[6] A very recent example involves the *Escherichia coli* (*E. coli*) Min system,[7] a reaction-diffusion system that regulates the positioning of the division FtsZ-ring at mid-cell in *E. coli*.[8,9] Considered a paradigm of molecular self-organization, Min proteins are a well-established model for the study of biological pattern formation.[10] Using ATP as fuel and the plasma membrane as catalytic matrix, the reversible switching of proteins MinD and MinE from membrane-bound to cytosolic state generates a plethora of patterns determined by controllable parameters in the system (**Figure 1**a).

In rod-shaped *E. coli*, MinDE dynamics result in pole-to-pole oscillations driven by ATP hydrolyzation. Inside lipid vesicles, however, a broader range of dynamic oscillation modes beside pole-to-pole has been shown.[11] Moreover, in 2D-reconstituted supported lipid bilayers (SLBs) both traveling and standing waves have been generated,[12–14] as well as quasi-stationary "Turing" patterns.[15] In particular, these stationary patterns are of great interest due to their variability and controllability of shapes. Meshes, spots, inverse spots, and labyrinth-type patterns remain quasi-stationary over time upon ATP consumption and can span hundreds of microns on SLB-coated glass surfaces.

M. Reverte-López, S. Gavrilovic, A. Merino-Salomón, P. Schwille
Department of Cellular and Molecular Biophysics
Max Planck Institute of Biochemistry
82152 Martinsried, Germany
E-mail: schwille@biochem.mpg.de

H. Eto
Hubrecht Institute-KNAW (Royal Netherlands Academy of Arts and Sciences)
Utrecht 3584 CT, The Netherlands

A. Yagüe Relimpio
Department of Cellular Biophysics
Max Planck for Medical Research
69120 Heidelberg, Germany

G. Rivas
Centro de Investigaciones Biológicas Margarita Salas
Consejo Superior de Investigaciones Científicas (CSIC)
Madrid 28040, Spain

The ORCID identification number(s) for the author(s) of this article can be found under https://doi.org/10.1002/smtd.202300173

DOI: 10.1002/smtd.202300173

ADVANCED SCIENCE NEWS
www.advancedsciencenews.com

small methods
www.small-methods.com

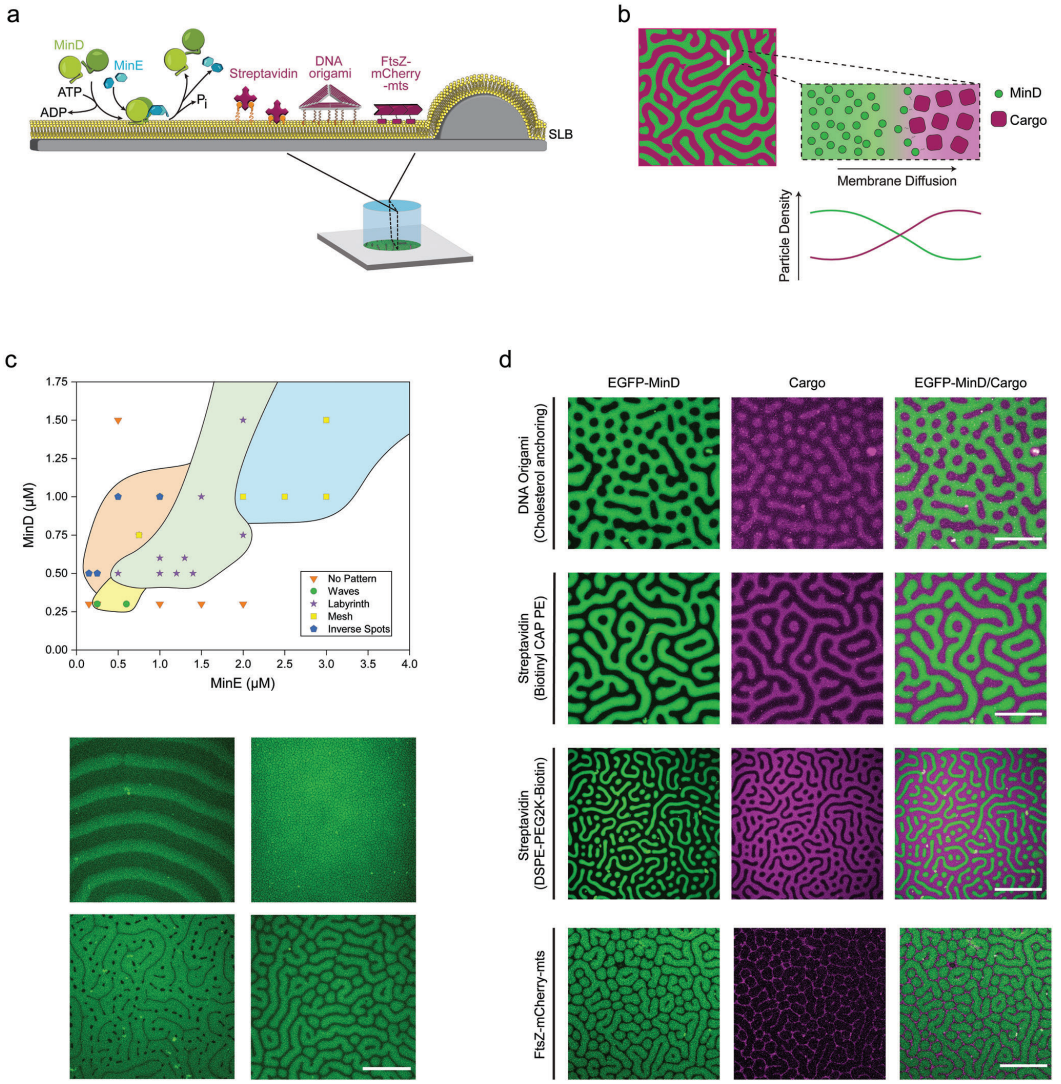

Figure 1. Diffusiophoresis-mediated patterning of membrane-bound molecules by the MinDE system. a) Schematic illustration of the molecular mechanism behind MinDE reaction-diffusion on membranes and the cargo molecules used in this study: DNA origami, streptavidin, and FtsZ filaments. b) The MinDE system can transport membrane-bound molecules. The active flux of MinDE proteins on the membrane establishes a frictional force when non-specifically interacting with cargo, inducing cargo transport toward areas of low MinD density. c) Phase diagram of the MinDE patterns generated when concentrations of MinD and MinE are varied on planar OrmoComp-supported lipid bilayers. Single data points represent patterns obtained on separate OrmoComp-coated surfaces. Colored areas aim to facilitate the interpretation of the patterns expected for further protein ratios. Confocal images illustrating pattern diversity: traveling waves (top left), mesh (top right), inverse spots at a phase boundary (bottom left), and labyrinth (bottom right). Scale bar, 100 μm. d) Confocal images demonstrating the 2D patterning of 4 types of cargo constructs: DNA origami-Cy3, Atto655-streptavidin bound to biotin, Atto655-streptavidin bound to biotin functionalized with a 2000 Da PEG spacer, and FtsZ-mCherry-mts, on SLBs generated over planar OrmoComp surfaces. SLBs contain 1% of Biotinyl-CAP-PE in experiments performed with streptavidin. DNA origami structures were attached to the membrane via TEG-cholesteryl oligonucleotides. Scale bars are 50 μm for origami, streptavidin bound to Biotinyl-Cap-PE and FtsZ-mCherry-mts. For streptavidin bound to PEG2K-Biotin scale bar is 100 μm.

ADVANCED SCIENCE NEWS
www.advancedsciencenews.com

small methods
www.small-methods.com

In addition to deciphering the role of MinDE oscillations in bacteria, and extensively characterizing their patterns in vitro, recent studies revealed a hidden function of these proteins in reconstituted systems: the directional transport and patterning of unrelated molecules on lipid membranes. Through a diffusiophoretic transport mechanism, Min proteins can non-specifically sort and spatiotemporally control membrane-bound diffusible molecules, which results in their distinct patterning on lipid surfaces (Figure 1b).[16,17] However, despite the striking visual effect of this new functionality, MinDE-induced patterning has not been exploited in artificially developed systems yet.

To date, molecular tools that spatiotemporally arrange scaffold components are indeed scarce. Despite the importance and efforts to endow systems like micromotors and microcarriers with sophisticated functionalities, engineering local modifications to confer chemical versatility and novel properties remains a difficult task. To circumvent the difficulties that this site-specific arrangement of molecules entails, recent alternatives have been developed in fields like soft robotics where systems are being engineered to execute complex mechanical operations.[18] For example, the arrangement of active motor proteins with nanoscopic precision is still a challenge to overcome in these systems. Jia et al. recently achieved local actuation of motor-decorated biorobot modules using soluble caged ATP as a spatially addressable light sensor.[18] Although this approach indeed showed the differential deformation of soft biorobots, an exciting avenue to further extend their functional complexity is the controlled spatial targeting of functional biomolecules themselves. In this regard, chemical patterning approaches and lipid-based strategies to spatially reorganize and cluster molecules on microdevices and synthetic vesicles have shown promising results.[19–21] Particularly, the use of phospholipids to create patterned membranes through the formation of spotted domains, Janus assemblies, or the demixing of lipid/polymer hybrid vesicles, has become a strategy whereby challenges like biofouling, efficient antigen presentation, enhanced T-Cell signaling, and adaptability to complex environments could be tackled.[22–25] However, further development of this domain-based surface patterning is still required; instabilities caused by the disjunctive properties of these membrane domains induce their budding or fission into homogeneous morphologies, which ultimately hampers their use for translational applications. Hence, to build synthetic systems with advanced properties and cutting-edge functionalities, new strategies to control the spatial distribution of their elements on surfaces are still required.

In this study, we demonstrate the capability of the MinDE system to spatiotemporally control and distinctively target unrelated cargo molecules on the surface of synthetic 3D systems. For this purpose, we assess the MinDE-driven patterning of biomedically-relevant molecules and high-order protein structures on two model microcarrier systems: membrane-coated 3D-printed microswimmer-like structures and giant unilamellar vesicles (GUVs). Based on the experimental insights here reported, we propose the use of Min proteins as a physiologically benign biochemical patterning tool for the integration of synergistic functionalities in lipid-based systems, including areas of translational research where complex rational design is required.

2. Results

2.1. Quasi-Stationary MinDE Patterns on a UV-Curable Hybrid Polymer

To examine the conditions needed to reconstitute quasi-stationary MinDE patterns on 3D printed microstructures, we carried out MinD-MinE titrations on planar OrmoComp surfaces. First, we set out to choose the photoresist that, as a representative model, demonstrates the versatility of our system. OrmoComp, with an organic-inorganic hybrid composition, was chosen for this purpose due to its facile and ample surface modifications, and its crucial features for biomedical applications like biocompatibility and non-cytotoxicity.[26] As the MinDE reaction-diffusion system relies on a lipid membrane as the catalytic matrix for the spatiotemporal localization of its proteins, following an already reported pipeline,[27] we silanized cured OrmoComp surfaces to enable SLB formation through a vesicle bursting strategy. By (3-aminopropyl)triethoxysilane (APTES) treatment, the terminal positively-charged amine groups of this organosilane coated the surface of the photoresist and through electrostatic interactions facilitated the rupture and fusion of negatively-charged small unilamellar vesicles (SUVs), which ultimately formed SLBs on the OrmoComp surfaces. Subsequently, to quantitatively assess the MinD/MinE ratios needed to generate quasi-stationary patterns on OrmoComp surfaces, we used our well-established in vitro reconstitution assay.[28] We systematically varied protein concentration and confirmed by confocal microscopy the formation of different types of stationary MinDE patterns. Mapping out these patterns thereby gives rise to a phase diagram where, according to protein concentration, areas of dynamic, stationary, and mixed patterns at phase boundaries can be inferred (Figure 1c). In agreement with previous reports, the stationary patterns obtained include labyrinths, meshes, and inverse spots; shapes that emerge when MinE occupies the outer rim of areas with high MinD density.[12]

2.2. Spatiotemporal Positioning of Membrane-Bound Molecules on OrmoComp Surfaces by the MinDE System

Having established the conditions to controllably create stationary MinDE patterns on OrmoComp surfaces, we investigated the MinDE-driven transport of unrelated membrane-bound molecules on these surfaces. To this end, we incubated SLB-coated OrmoComp surfaces with our target cargo molecules, and then incorporated MinDE in our assay chambers to reconstitute labyrinth-type stationary patterns. The robustness of the MinDE ATP-driven transport mechanism was assessed by testing molecules with contrasting size, nature, complexity, and membrane-anchoring type.

Due to its programmability and wide range of applications,[29] DNA origami was first employed to perform this evaluation. With prior incubation of SLBs with triethylene glycol (TEG)-cholesteryl functionalized oligonucleotides, the DNA origami structure incorporated into the chambers was the Rothemund triangle,[30] which was modified with 12 oligonucleotide handles for cholesterol-mediated membrane attachment and 9 oligonucleotide handles for fluorophore attachment. Similarly shown in extensive studies,[17] once stationary MinDE patterns were

ADVANCED SCIENCE NEWS
www.advancedsciencenews.com

small methods
www.small-methods.com

obtained on the membrane, the origami structures were effectively transported toward areas of low MinD density (Figure 1d, top panel). As a result, an anticorrelated pattern of origami structures was formed.

To further verify the MinDE-induced spatiotemporal targeting of biomedically utilized molecules on OrmoComp-supported membranes, we then turned to streptavidin. Given its use as an affinity nano-tag for drug delivery and diagnosis,[31] we tested whether both simple biotinylated lipids and polyethylene glycol (PEG)-lipid conjugates linked to streptavidin could be transported by the diffusive fluxes of MinDE proteins. Notably, when in vitro reconstitutions were carried out with lipids containing a 2000 Da PEG chain, streptavidin was spatiotemporally regulated and rearranged on the membrane to occupy MinD-depleted areas similarly to assays conducted on SLBs containing simple biotin-lipid constructs (Figure 1d, middle panels). Despite the presence of the mushroom-like PEG spacer, which extends the biotin-streptavidin bond up to 3.5 nm above the membrane,[32] the frictional force exerted by the MinD flux on the membrane successfully transported streptavidin, patterning this cargo molecule on OrmoComp surfaces.

To follow up on this observation, we then examined if proteins organized in high-order structures like filaments were also susceptible to rearrangement on the membrane by the MinDE system. To this end, we used FtsZ-mCherry-mts. This protein construct, responsible for the formation of the bacterial division ring, binds directly to reconstituted lipid membranes via an amphipathic helix termed membrane-targeting sequence (MTS).[33] To circumvent any specific interaction between FtsZ and MinD, the effector protein MinC responsible for depolymerizing FtsZ was not included in the assays. In this way, as previous studies performed with FtsZ,[16] we ensured that nonspecific frictional coupling between FtsZ and Min proteins was the only interaction taking effect in the system. Interestingly, after FtsZ-mCherry-mts filaments were incorporated to OrmoComp-supported lipid membranes, a labyrinth-like MinDE pattern was generated on the surface, and this complex cargo structure was reorganized via diffusiophoresis creating anticorrelated patterns similar to the ones described with origami and streptavidin (Figure 1d, fourth panel).

Taken together, our experiments show that MinDE diffusive fluxes enable the active transport of biomedically relevant cargo molecules and high-order protein structures on membrane-coated OrmoComp surfaces.

2.3. Fabrication and Functionalization of Microstructures with Supported Lipid Bilayers

We further explored whether we can obtain MinDE-induced cargo patterning in 3D, and most importantly, on microstructures that could exploit this multidimensional sorting of molecules. Inspired by the engineering of microrobots for translational applications, we 3D-printed microstructures analogous to microswimmers utilized for cargo transport and targeted drug delivery. The designs explored were: 1) a cut sphere connected to a helical tail; 2) a rod-like bacterium mimic with a half-capsule body linked to a thin helical tail. To reach the highest resolution possible at the micron scale, we crosslinked our photoresist (OrmoComp) by two-photon direct laser writing. Due to the shape of the laser focal spot – a spheroid termed voxel – a thorough evaluation of the printing parameters was conducted to circumvent spherical aberrations in the main body of the microswimmer-like structures, especially in design 1. Using scanning electron microscopy (SEM) (**Figure 2**a) we assessed the quality of the structures and found that increasing voxel overlap, while maintaining high scan speeds and low laser doses to avoid micro-explosions, generated optimum features with smooth surfaces.

To further enhance the surface functionalities of the 3D-printed structures, we next coated them with lipid bilayers. We carried out the functionalization strategy employed in 2.1 and obtained fluid lipid membranes on the surface of our OrmoComp microstructures. To exemplify properties that microstructures can acquire by incorporating membranes on their surfaces, we added PEG-lipid conjugates and TEG-cholesteryl functionalized oligonucleotides to our lipid formulations.

Thus, we show that microswimmer-like structures printed with OrmoComp can be functionalized with lipid bilayers, thereby enabling surface coating of these microstructures with stealth molecules for augmented biocompatibility and stability in diverse environments.

2.4. 3D Patterning of Functional Molecules on Lipid-Coated Microstructures

Since the coating of microstructures with tailored lipid membranes provided a versatile matrix from which we could build upon, we next explored the idea of using the MinDE system to spatially functionalize this surface with patterned molecules. To comparably test MinDE-driven cargo transport in 3D, we followed the same experimental strategy employed in 2D and incubated the SLB-coated microstructures with our cargo molecules of interest: DNA origami, streptavidin, and FtsZ-mCherry-mts.

Strikingly, MinDE stationary patterns like spots, inverse spots, and labyrinths also formed on the surface of both microswimmer-like structures and, in accordance with our initial hypothesis, all three cargo molecules were spatiotemporally reorganized, irrespective of microswimmer shape, into anticorrelated stationary patterns – spots, mesh, and labyrinth – (Figure 2b; Figure S1, Supporting Information). MinDE-driven patterning, dependent on cargo intrinsic characteristics (e.g., membrane diffusion and membrane footprint),[17] allowed the positioning of molecules over the entire body of the microswimmer-like structures and remained uniform for hours before ATP depletion (Figure S2, Supporting Information). In addition, anticorrelated positioning of cargo on 3D-printed structures was also obtained with dynamic MinDE traveling waves (Video S1, Supporting Information).

To quantitatively scrutinize the spatiotemporal reorganization of molecules on the surface of 3D-printed structures, we reconstructed the confocal images acquired into 3D projections and quantified the Michelson contrast, $(I_{max} - I_{min}) / (I_{max} + I_{min})$, along lines drawn over the body of the microswimmer-like structures. The normalized fluorescence intensity line plots obtained illustrate how all three cargo molecules converged to MinD-depleted areas on the surface. Moreover, the sharp contrast

ADVANCED SCIENCE NEWS
www.advancedsciencenews.com

small methods
www.small-methods.com

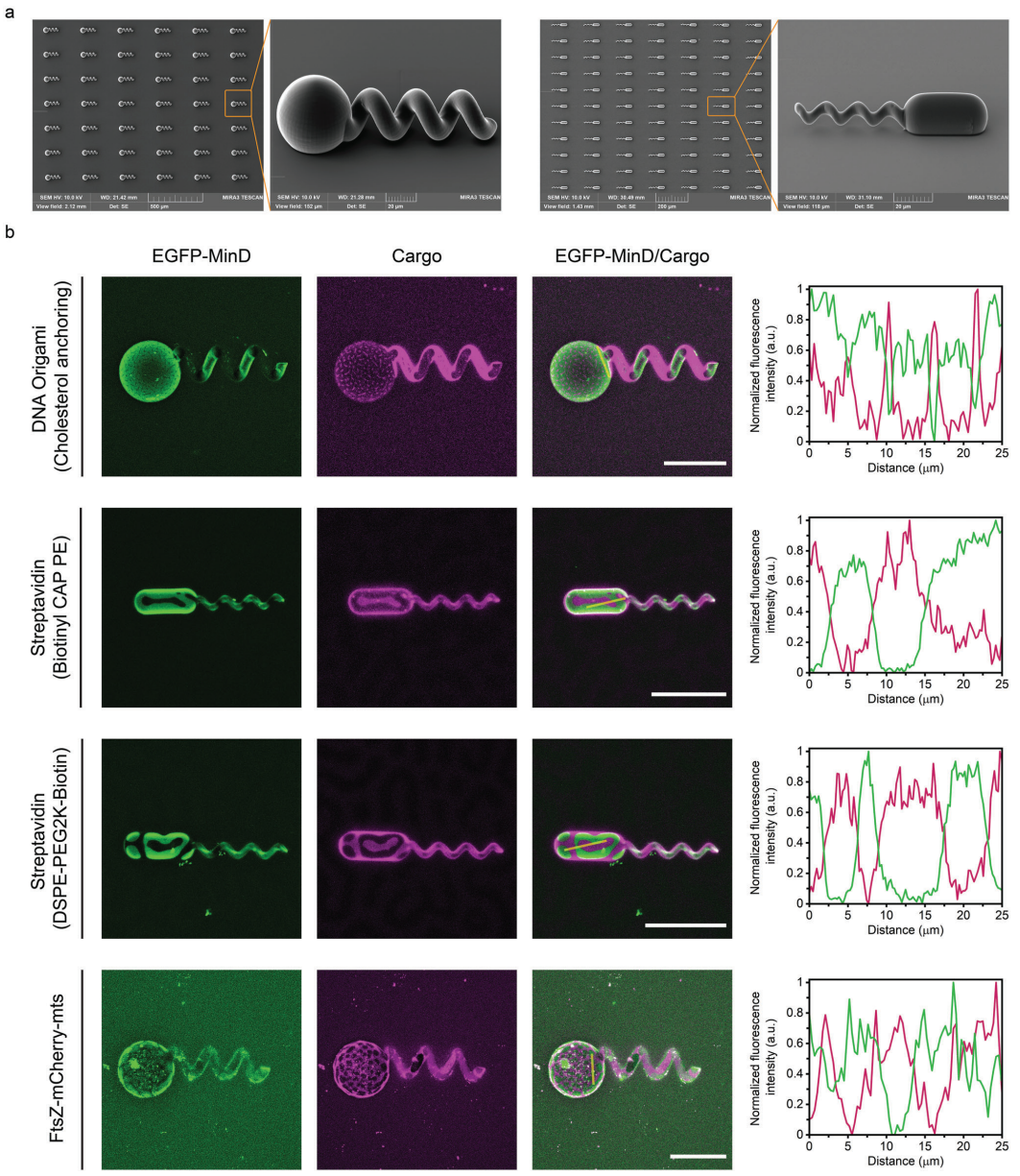

Figure 2. Patterning of membrane-bound molecules on 3D printed microswimmer-like structures. a) Scanning electron microscope (SEM) images of two types of 3D-printed OrmoComp microstructures. b) Z-Projections of confocal images showing the patterning of the 4 types of cargo on 3D-printed structures. SLBs were formed by functionalizing the surface with amine groups and bursting negatively-charged SUVs on their surface. After incubating the printed structures with our cargo molecules (DNA origami, streptavidin, and FtsZ-mCherry-mts), MinDE proteins spatiotemporally rearrange the aforementioned molecules into 3D patterns over their surfaces. Fluorescence intensity line plots of EGFP-MinD (green) and cargo molecules (magenta) demonstrate the demixing with varied contrast of MinD and cargo on both the top and lateral sides of the microswimmer-like structures. Line selections are depicted in yellow in EGFP-MinD/Cargo merged images. Scale bars in white are 50 μm.

ADVANCED SCIENCE NEWS
www.advancedsciencenews.com

small methods
www.small-methods.com

observed at boundary regions further validated the demixing of both MinDE and unrelated membrane-bound cargo.

Hence, our experiments demonstrate that MinDE proteins can be used for the molecular patterning of cargo on membrane-coated microswimmer-like structures, and thus for the advanced functionalization of these microcarriers with spatially-organized molecules of interest.

2.5. Quasi-Stationary MinDE Patterns Spatially Distribute FtsZ-mCherry-mts Bundles Inside GUVs

Having established MinDE patterning on complex 3D structures, we then wondered whether we could incorporate this spatial functionalization tool into fully lipid-based systems. Inspired by studies in the field of synthetic biology and drug delivery,[25,34] where GUVs have become well-established models of artificial cells and biomimetic carriers, we decided to investigate the conditions required to pattern molecules inside these vesicles using MinDE proteins.

Following a bottom-up approach, we encapsulated our reaction mix – MinDE, cargo, and ATP – inside GUVs using a standardized double-emulsion transfer method for purified proteins.[35] As a cargo model, we chose again FtsZ-mCherry-mts to evaluate the transport of complex protein-based structures, this time on the inner leaflet of vesicles (**Figure 3**a). Strikingly, when a high concentration of a macromolecular crowding agent Dextran70 was added to our inner reaction mix, we observed a distinct organization of MinDE and FtsZ-mCherry-mts on the GUV membrane due to crowding-driven membrane exclusion effects (Figure 3b).[35] In stark contrast to earlier experiments on Min proteins reconstituted inside vesicles and droplets,[11,36] MinDE here not only displayed spatial oscillations but also exhibited MinDE quasi-stationary patterns as a key prerequisite for the robust spatial targeting of cargo (Figure 3d,e). These patterns, which resembled the mesh and spot-type Turing-like patterns reconstituted on SLBs, remained uniform over long periods of time and were indeed able to position FtsZ-mCherry-mts into steady large-scale assemblies (Figure 3c). As a consequence, the MinDE diffusive fluxes on the membrane drove the transport of FtsZ-mCherry-mts bundles to the periphery of the MinDE patterns. The cargo thus assembled into characteristic configurations occupying the areas available on the membrane (Videos S2, S3, Supporting Information).

In summary, we show that, in the presence of crowding agents, quasi-stationary Turing patterns can be successfully generated inside GUVs, and MinDE-driven patterning of complex structural cargo is possible on the inner lipid leaflet of these vesicles.

3. Discussion

In this study, we have demonstrated that Min proteins can be employed to induce robust surface patterning of diffusible molecules and molecular assemblies on complex 3D lipid-based systems. Remarkably, we provide direct evidence that MinDE Turing patterns can be generated on both SLB-coated printed microstructures and on the inner lipid leaflet of GUVs. Thus, the here shown variety of membrane-based systems where stationary patterning is possible demonstrates the universality of this recently discovered MinDE function. Specifically, we have conclusively shown that this universality not only applies to the properties of the synthetic membrane environment – a free-standing membrane in the case of synthetic cell mimics and a supported one for microswimmer-like structures -, but also to the nature of the cargo molecules. Besides biomedically relevant molecules for ligand binding and anti-biofouling, like streptavidin and PEG chains, the frictional force induced by Min protein fluxes is able to stationary redistribute DNA assemblies and protein filaments, two types of slow-diffusive cargo molecules which were considered complex to differentially pattern by the MinDE system.[17] Therefore, our findings lend further credence that, under the right concentration and crowding conditions, complex high-order assemblies can also be spatiotemporally regulated by Min proteins.

Contrary to chemical/optical patterning approaches of 3D-printed structures, where molecules are mixed in bulk with a photoresist before polymerization or infiltrated for later crosslinking,[37,38] in this study the MinDE-induced patterning of microstructures is performed after photoresist development through surface chemistry modifications. For fabrication purposes, this strategy presents several advantages. First, the printing and patterning steps are independent. The fabrication process does not involve intricate steps with photoactive reagent mixes which may limit the selection of photoresist. As a result, MinDE-driven patterning of microstructures neither requires arduous optimization of printing parameters to obtain stable structures nor induces potential photodamage to the patterned biomolecules. Moreover, because swelling and shrinking of materials are not required, microstructures retain their physical properties.[18,19] Secondary, the patterning of molecules here shown occurs in minutes and is reversible. After several hours of robust and uniform patterning without buffer exchanges,[12] since the reaction-diffusion mechanism of MinDE proteins is ATP-fueled, it is possible to disperse the established cargo arrangement as well as reorganize molecules into a completely different pattern by modulating ATP concentration. Control over ATP levels thus grants the possibility to, for example, reuse the printed structures for further patterning with new biomolecules. Finally, in the process of constructing compatible surface chemistry for Min proteins, we indirectly incorporate additional functionalities to printed structures beyond those conferred by MinDE-driven patterning.

It should be noted that we fabricated our two model carrier systems coated with lipid bilayers. Indeed, negatively charged membranes, lipid or polymer-based,[39] act as enabling platforms for our protein-based patterning tool. Therefore, by generating lipid vesicles and coating 3D-printed microstructures with SLBs, we incorporate a multi-purpose layer to which diverse functional ligands can be anchored, resulting in the endowment of the coated structures with well-defined properties for interacting or sensing the environment around them.

Furthermore, due to the design of our microstructures and the photoresist chosen, it is possible to functionalize their surface to achieve propulsion in fluid environments. For instance, if magnetic actuation is required, the 3D-printed microstructures can be coated with nickel and gold to allow movement and protect them from oxidation.[40,41] Importantly, this intermediate metallization step is compatible with subsequent SLB coating. By thiol chem-

ADVANCED SCIENCE NEWS
www.advancedsciencenews.com

small methods
www.small-methods.com

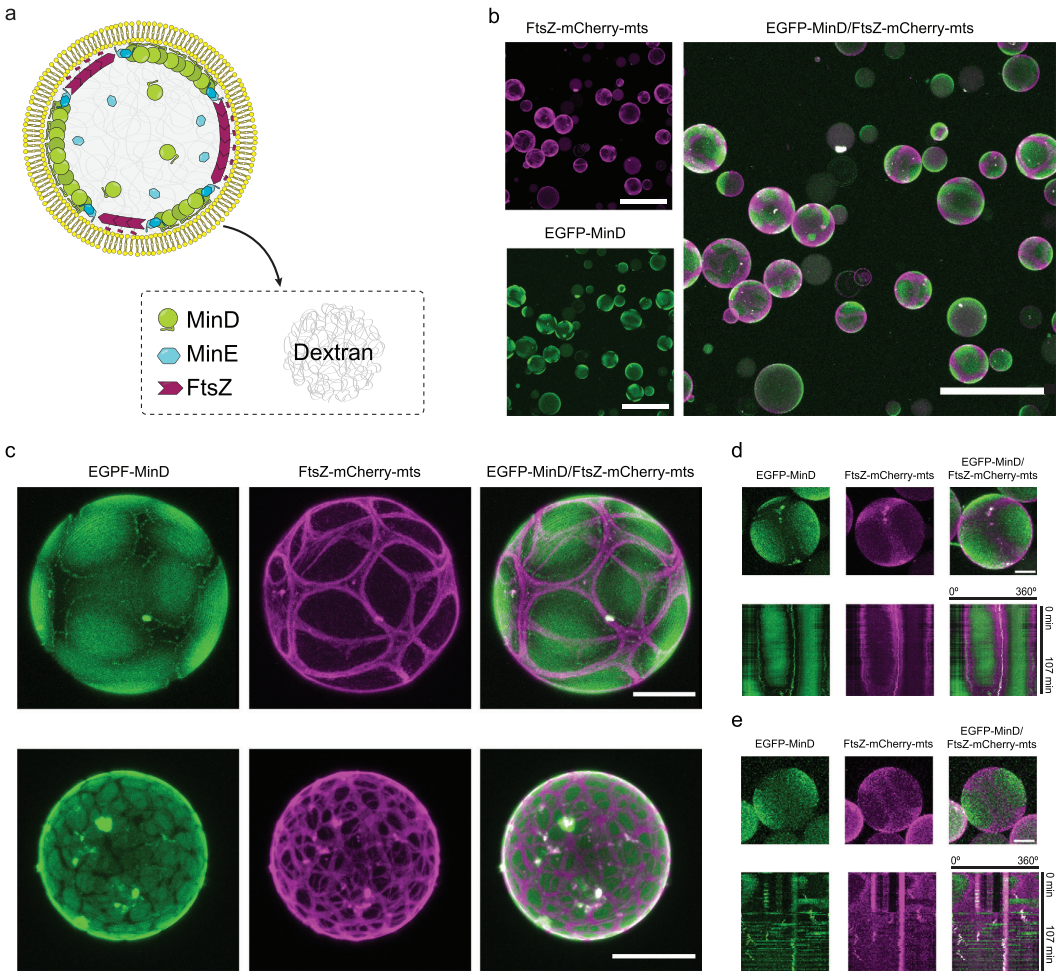

Figure 3. Spatiotemporal positioning of FtsZ-mCherry-mts inside lipid vesicles by MinDE patterns. a) Schematic illustration of the content inside giant unilamellar vesicles after encapsulation. MinDE and FtsZ-mCherry-mts bind to the membrane via MTS domains while Dextran70 generates a volume exclusion effect at the vesicle lumen. b) The addition of Dextran70 as a crowding element promotes the formation of both FtsZ-mCherry-mts bundles and robust MinDE Turing patterns on the inner lipid leaflet of vesicles. FtsZ-mCherry-mts bundles (magenta) are therefore redistributed according to these patterns. Scale bars are 100 µm. c) Z-projections of confocal stacks depicting two examples of FtsZ-mCherry-mts patterning induced by the MinDE system. FtsZ-mCherry-mts bundles assemble into a membrane-bound framework inside the vesicles. Scale bars are 20 µm. d) Belt-type patterning of FtsZ-mCherry-mts inside a GUV observed after performing Z-projections over confocal stacks. The kymographs below the individual and overlaid channels were generated from a spline along the equator of the GUV and are meant to visually define the position of a fluorescent feature inside the spline over time. Here, the FtsZ-mCherry-mts and overlaid kymographs demonstrate that FtsZ-mCherry-mts bundles are effectively patterned into a static belt-type configuration for almost two hours. The scale bar is 10 µm. e) The heterogeneous distribution of protein and crowder concentration after encapsulation generates dynamic MinDE patterns inside some GUVs. Kymographs generated at the GUV equator show how FtsZ-mCherry-mts bundles are localized to areas of low MinD density and create dynamic anti-correlated patterns inside the GUV. The scale bar is 10 µm.

istry, a monolayer of hydrophilic functional groups can be added to the metal-coated surface to induce SUV bursting and SLB formation, thereby allowing particle patterning by MinDE.[42]

In addition, the demonstrated universality of the MinDE-induced surface patterning opens an intriguing avenue of research for future studies: the simultaneous patterned deposition of several unrelated molecules on the same surface. In *E.coli*, MinD acts as a carrier protein responsible for the directional transport of MinC, which competes with MinE for MinD binding. Using the MinC binding interface, we could use protein en-

ADVANCED SCIENCE NEWS
www.advancedsciencenews.com

small methods
www.small-methods.com

gineering to attach other molecules of interest to MinD. As a result, two different molecules could be separated and patterned in an anticorrelated fashion. While one cargo molecule would be positioned at MinDE-depleted areas via diffusiophoresis, another molecule of different nature could bind MinD and overlay the MinDE pattern already formed, causing the disjunctive distribution of the two molecules into two distinct patterns.

Moreover, if the control over pattern formation given by ATP is exploited while simultaneously positioning two biomolecules, this might allow the design of active systems in which reactions could be triggered by the mixing or demixing of cargo molecules. Conversely, to achieve immobile and ATP-independent patterning of biomolecules after their diffusiophoretic positioning, crosslinking strategies can be applied. In this regard, physical and chemical crosslinking of proteins,[43] cation-mediated fixing of DNA origami on membranes,[44] or the UV crosslinking of Min patterns would allow to utilize systems patterned by Min proteins on diverse buffer conditions and experimental set-ups.

Finally, although the microstructures here presented do not induce a change in Min protein dynamics, further use of the 3D-printing and surface functionalization techniques here described could help describe how curvature and 3D geometrical cues affect Min patterns.[45–47] Besides obtaining more experimental data, and thus revealing quantitative parameters behind the observed behavior, an insightful future approach would involve the integration of these input parameters in new computational tools.[48] In particular, the combination of physics-informed neural networks with numerical methods presents a promising future where machine learning could aid in accelerating the computationally costly steps in computer simulations,[49,50] thereby advancing the understanding of the fundamental principles behind reaction-diffusion systems and the prediction of patterns from given input parameters.[51,52]

4. Conclusion

In summary, we demonstrate that the MinDE system is a versatile and robust synthetic tool for the 3D surface patterning of molecules. From small ligands like streptavidin to high-order assemblies like protein bundles and DNA origami, Min proteins can be tuned to asymmetrically arrange molecules into macrodomains on membrane-functionalized surfaces. Given the demand for novel strategies to create heterogeneous surface functionalities, harnessing MinDE capabilities could be an attractive alternative in fields of research working on developing soft biorobots or active microcarriers for theragnostics and drug delivery. For example, cluster-based distribution of antibodies for enhanced T-Cell activation, or asymmetric coverage of proteins and enzymes to facilitate microcarrier movement, are some of the challenges that fixed patterns obtained by MinDE-driven positioning could help tackling.[20,53] Consequently, beyond the great value of the Min proteins as a quantitative general model for reaction-diffusion systems and in harnessing its physiological function in minimal cell division,[35,54] we could also expand the potential applications of this protein-based patterning tool and the systems that can be functionalized by it.

Collectively, the findings presented here lend further evidence to the versatility of this protein system as a functional toolbox.[16] As part of the synthetic division machinery and a spatiotemporal patterning agent, the Min system presents itself as a non-disruptive module compatible with the chassis and energy-storing molecules predicted to take part in the construction of a synthetic cell.[55] Thus, we consider this protein system a powerful spatial regulator for its use in synthetically designed systems.

Lastly, this paper sets an example of the importance of studying protein functions in vitro that, at first glance, are not physiologically relevant or have no direct involvement in in vivo processes. Only by characterizing and scrutinizing such hidden protein functions the scientific community can utilize these across disciplines and devise novel valuable applications.[6]

5. Experimental Section

Fabrication of 3D-Printed Swimmer-Like Structures: Glass coverslips (22 mm × 22 mm Menzel, Germany) were first pre-treated to facilitate the adhesion of the microstructures to the surface. First, coverslips were exposed to O_2 plasma (Zepto, Diener Electronic, Germany) (30% power, 0.3 mbar pressure) for 60 s. Coverslips were then spin-coated with OrmoPrime (Microresist Technology, Germany) at 6000 rpm for 40 s and then baked at 150 °C for 5 min on a hotplate. Once primed, to generate planar surfaces available for patterning, coverslips were spin-coated with OrmoComp (Microresist Technology, Germany) at 6000 rpms for 60 s and UV exposed (Form Cure Formlabs, USA) for 15 min at 60 °C. 3D printing of swimmer-like microstructures was performed with a commercially available two-photon polymerization system (Photonic Professional Nanoscribe GmbH, Germany) equipped with a Zeiss LCI Plan-Neofluar 25×/0.8 objective set for oil immersion. OrmoComp was drop-cast on the primed slides and exposed in dip-in laser lithography mode. Microswimmer-like structures were designed in SOLIDWORKS and their slicing and hatching parameters were set with the Describe software (Nanoscribe GmbH, Germany) to obtain continuous structures and fine details with a surface roughness which had no effect on Min protein dynamics. Rod-like microswimmers: slicing 0.1 µm, hatching 0.2, laser power 50%, scanning speed 15 000 µm s^{-1}. Spherical-shaped microswimmers: slicing 0.1 µm, hatching 0.4, contour count 2, contour distance 0.4, laser power 50%, scanning speed 15 000 µm s^{-1}. Printed structures were developed in acetone and dried using a critical point drier (Leica EM CPD300, Leica Microsystems, Germany). For patterning experiments, to avoid confocal imaging artifacts which appeared at the lateral areas of tall microstructures (the refractive index mix-match caused laser scattering and a lower fluorescence intensity signal on the sides) the spherical and capsule bodies of the microswimmer-like structures used were reduced in height maintaining their scale. Nevertheless, Min proteins could form patterns on all variants of these printed 3D microstructures.

Scanning Electron Microscopy: Samples were first sputter-coated with platinum on a high-resolution automatic sputter coater (Cressington 208HR, Leica Microsystems, Germany) at 20 mA and 0.1 mbar Argon 3 times for 20 s. The thickness of the applied coatings was measured with a built-in thickness controller to be 2.0 nm. Microstructures were then imaged using TESCAN MIRA3 FESEM (TESCAN, Czech Republic) operating at an accelerating voltage of 10 kV in SE mode.

Protein Purification: MinE-His and His-MinD were purified as previously reported.[13] The FtsZ-mCherry-mts was constructed by substituting the *YFP* with a *mCherry* gene using the pET11b-FtsZ-YFP-mts vector published by Osawa et al. and named as pET-FtsZ-mCherry-mts.[56] The protein was purified as previously described.[56] Briefly, E. coli strain BL21 was transformed with pET11b-FtsZ-mCherry-mts and O/N overexpression was performed at 20 °C. Cells were lysed by sonication and separated by centrifugation. The protein was precipitated by adding 30% ammonium sulfate and the mixture was incubated for 20 min on ice with slow shaking. After subsequent centrifugation and resuspension of the pellet, the protein was purified by anion exchange chromatography using a 5 × 5 ml Hi-Trap Q-Sepharose column (GE Healthcare). The purity of the protein

was confirmed by SDS-PAGE and mass spectrometry. The activity of the protein was measured by a colorimetric GTPase activity assay.

DNA Origami Structure Folding and Purification: The used DNA origami structures were based on a well-known design and modified using caDNAno (v.2.1).[30,57] Scaffold DNA (p7249, tilibit nanosystems, 10 nM in folding buffer) was mixed with a 10-fold molar excess of unmodified staple strands or staple strands with TEG-cholesteryl extensions for anchoring to membranes. Staple strands with the adapter sequence for "imager strands" were added in a 100-fold molar excess. The folding reaction was performed via melting for 15 min at 60 °C and temperature ramping from 60 to 4 °C over 15 h. The folded origami structures were purified using Amicon Ultra 0.5 mL Ultracel filters, 100K (Merck, Darmstadt, Germany) in purification buffer (500 mM NaCl, 10 mM Tris–HCl and 1 mM EDTA, pH 7.5) with two rounds of centrifugation (15 min, 3000 rcf), and resuspension in folding buffer (12.5 mM $MgCl_2$, 10 mM Tris–base, 1 mM EDTA, pH 8.0) for 5 min at 3000 rcf. Proper folding of the DNA origami structures was confirmed using atomic force microscopy (AFM) (Figure S3, Supporting Information).

Atomic Force Microscopy: Measurements were performed on a JPK Nanowizard 3. AFM images were taken in QI (quantitative imaging) mode using PEAKFORCE-HIRS-F-B (Bruker). The set point force was 0.15–0.25 nN, acquisition speed 66.2 µm s−1, Z-range 106 nm; 1 × 1 μm^2 fields of view were acquired with a 512 × 512 resolution. Images were first processed in JPKSPM Data Processing (JPK, v6.1.142) performing a line-wise second-degree polynomial leveling followed by another second-degree polynomial leveling with limited data range (0% lower limit, 70% upper limit). Subsequent plane leveling, third-degree polynomial row alignment, and scar correction were performed in Gwyddion (v2.58).[58]

Lipid Bilayer Coating of 3D-Printed Microstructures: All lipids were purchased from Avanti Polar Lipids (USA). To generate SLBs on planar OrmoComp-coated and 3D-printed surfaces, silanization of the surface was performed. Samples were plasma treated with Argon plasma for 60 s with a Model 950 Advanced Plasma System (Gatan, USA) and submerged for 5 min in a solution of 0.5% (v/v) APTES (Sigma–Aldrich, St. Louis, USA) in ethanol. After rinsing with ethanol and water, samples were kept in water as a silicone isolator chamber (Grace Bio-Labs, 665 301, USA) were pressed on the coverslips, enclosing the area where the resist was exposed. SLB formation was obtained by SUV fusion in Min Buffer (150 mM KCl, 25 mM Tris–HCl, and 5 mM $MgCl_2$, pH 7.5) as previously described.[27] SLBs for FtsZ and origami patterning were composed of 1,2-dioleoyl-sn-glycero-3-phosphocholine (DOPC) and 1,2-dioleoyl-sn-glycero-3-phospho-(1'-rac-glycerol) (DOPG) at a 7 : 3 molar ratio. DOPC/DOPG/DSPE-PEG(2000) biotin (1,2-distearoyl-sn-glycero-3-phosphoethanolamine-*N*-[biotinyl(polyethylene glycol)−2000]) and DOPC/DOPG/Biotinyl Cap PE (1,2-dioleoyl-sn-glycero-3-phosphoethanolamine-*N*-(cap biotinyl)) were both mixed at a 6.9 : 3 : 0.1 molar ratio for streptavidin patterning.

Cargo Patterning Assays on 3D Printed Structures: For DNA origami assays, TEG-cholesteryl functionalized anchoring oligonucleotides were incubated for 10 min at a final concentration of 10 nM, during this time cholesterol molecules were incorporated into the lipid bilayer. Afterward, DNA origami structures were added at a final concentration of 0.5 nM and incubated for 15 min. Finally, Cy3-functionalized oligonucleotides were added at a concentration of 10 nM and incubated for 5 min, after which the samples were washed with 0.5 mL of Min Buffer. For streptavidin assays, Atto655-streptavidin was added to chambers at a final concentration of 1 µg mL^{-1} and incubated for 30 min. Excess of Atto655-streptavidin was removed by washing with a total 1 mL Min Buffer. Once these two cargo molecules were bound to SLBs, a mixture of 2.1 µM MinD, 0.9 µM EGFP-MinD, and 4 MinE was prepared and added to the chamber for a final concentration of 1.05 µM MinD, 0.45 µM EGFP-MinD, 2 µM MinE. To trigger Min pattern formation, 2.5 mM ATP was incorporated into the chamber and gently mixed. Chambers were incubated for 30 min before imaging. For FtsZ-mCherry-mts experiments, Min proteins and ATP were first added to the chamber at a final concentration of 1.75 µM MinD, 0.75 µM EGFP-MinD, 2 µM MinE, and 2.5 mM ATP. Afterward, 1 µM of FtsZ-mCherry-mts was incubated with the 3D-printed microstructures, and polymerization was triggered by adding 0.04 µM GTP.

Vesicle Formation: The double emulsion transfer method was employed for the production of giant unilamellar vesicles.[59] For the lipid-oil suspension, a mixture of 1-palmitoyl-2-oleoyl-sn-glycero-3-phosphocholine (POPC) and 1-palmitoyl-2-oleoyl-sn-glycero-3-phospho-(1'-rac-glycerol) (POPG) at 7 : 3 molar ratio was dissolved in chloroform at 1.5 mg mL^{-1} and dried under a nitrogen stream. Lipids were then placed in a vacuum-sealed desiccator for 1 h for complete chloroform evaporation. Inside a glove box, 37 µL decane (TCI Deutschland GmbH, Germany) was added to the lipid film and, once dissolved, 1 mL mineral oil (Carl Roth GmbH, Germany) was incorporated and the lipid-oil suspension vigorously vortexed until a clear solution was obtained. To form the GUVs, a previously reported protocol for the encapsulation of purified proteins was followed.[35] In this case, the inner solution contained 1.5 µM MinD, 1.5 µM EGFP-MinD, 3 µM MinE, 2 µM FtsZ-mCherry-mts, 100 mg mL^{-1} Dextran70 (Sigma–Aldrich, USA), 2.5 mM ATP and 2 mM GTP in Min Buffer. To prepare the crowder solution, Dextran70 was dissolved in Millipore water, and concentration was calculated from its weight and the total volume of the solution. Crowding solutions were stored at −20 °C until further use.

Fluorescence Microscopy: Imaging of Min patterns on OrmoComp-supported bilayers (Figure 1c) was conducted with a Nikon Eclipse Ti in a spinning disk confocal set-up using a Nikon Plan Fluor 20×/0.75 water immersion objective (both Nikon GmbH, Germany) and exciting EGFP with a 490 nm diode laser. Imaging of vesicles and 3D printed structures was performed on Zeiss LSM780 and LSM800 confocal laser scanning microscopes using a C-Apochromat 40×/1.2 water-immersion objective (Carl Zeiss, Germany). Fluorophores were excited using diode-pumped solid-state lasers: 488 nm (EGFP-MinD), 561 nm (Cy3-labelled DNA origami, FtsZ-mCherry-mts), and 640 nm (Atto655-streptavidin). Processing and analysis of all acquired images were conducted using Fiji (v1.53f51).[60] Z-Stacks were reconstructed using the Standard Deviation Z Project function and in the case of microstructures, the first 5–6 bottom slices were discarded to remove surface signal. Kymographs were generated with the Multi Kymograph function. ROIs were drawn manually following the GUVs' fluorescence intensity at their equatorial cross section.

Supporting Information

Supporting Information is available from the Wiley Online Library or from the author.

Acknowledgements

The authors would like to thank the MPIB Core Facility for assistance in protein purification, Michaela Schaper for plasmid cloning, Sigrid Bauer for lipid preparation and Kerstin Röhrl for protein purification. The authors would also like to thank Gereon Brüggenthies for providing the DNA origami design, Jan-Hagen Krohn and Yusuf Qutbuddin for assistance in confocal microscopy and helpful discussions, as well as Frank Siedler for his help with SEM imaging. This work was supported by the Max Planck-Bristol Centre for Minimal Biology (A.M.-S., H.E.) and the Deutsche Forschungsgemeinschaft (P.S.). M.R.-L., S.G. and A.M.-S. are part of IMPRS-LS, and M.R.-L. and S.G. are part of the ONE MUNICH Project supported by the Federal Ministry of Education and Research (BMBF) as well as the Free State of Bavaria under the Excellence Strategy of the Federal Government and the Länder.

Open access funding enabled and organized by Projekt DEAL.

Conflict of Interest

The authors declare no conflict of interest.

Author Contributions

M.R.-L., S.G., and A.M.-S. contributed equally to this work. M.R.-L., S.G., A.M.-S., and P.S. conceived the study. M.R.-L., S.G., A.M.-S., and H.E. performed the patterning experiments. M.R.-L. and H.E. designed geometries

ADVANCED SCIENCE NEWS
www.advancedsciencenews.com

small methods
www.small-methods.com

and M.R.-L. printed the 3D microstructures. S.G. performed SEM imaging and DNA origami validation. A.M.-S. and A.Y-R. performed encapsulation in lipid vesicles. G.R. provided technical advice on crowding conditions. M.R.-L. wrote the original draft. M.R.-L., S.G., A.M.-S., and P.S. revised the manuscript and figures. All authors discussed the results and revised the manuscript.

Data Availability Statement

The data that support the findings of this study are available from the corresponding author upon reasonable request.

Keywords

3D-printing, lipid vesicles, microswimmers, patterning, reaction-diffusion systems, surface functionalization, synthetic biology

Received: February 10, 2023
Revised: May 8, 2023
Published online: June 23, 2023

[1] S. Hirschi, T. R. Ward, W. P. Meier, D. J. Müller, D. Fotiadis, *Chem. Rev.* **2022**, *122*, 16294.
[2] G. M. Church, M. B. Elowitz, C. D. Smolke, C. A. Voigt, R. Weiss, *Nat. Rev. Mol. Cell Biol.* **2014**, *15*, 289.
[3] T. Ellis, X. Wang, J. J. Collins, *Nat. Biotechnol.* **2009**, *27*, 465.
[4] D. Wu, N. Sinha, J. Lee, B. P. Sutherland, N. I. Halaszynski, Y. Tian, J. Caplan, H. V. Zhang, J. G. Saven, C. J. Kloxin, D. J. Pochan, *Nature* **2019**, *574*, 658.
[5] S. Deshpande, T. Pfohl, *PLoS One* **2015**, *10*, e0116521.
[6] P. Schwille, B. P. Frohn, *Trends Cell Biol.* **2022**, *32*, 102.
[7] B. Ramm, T. Heermann, P. Schwille, *Cell. Mol. Life Sci.* **2019**, *76*, 4245.
[8] P. A. J. de Boer, R. E. Crossley, L. I. Rothfield, *Cell* **1989**, *56*, 641.
[9] D. M. Raskin, P. A. J. de Boer, *Proc. Natl. Acad. Sci. U. S. A.* **1999**, *96*, 4971.
[10] J. Halatek, E. Frey, *Nat. Phys.* **2018**, *14*, 507.
[11] T. Litschel, B. Ramm, R. Maas, M. Heymann, P. Schwille, *Angew. Chem., Int. Ed.* **2018**, *57*, 16286.
[12] P. Glock, B. Ramm, T. Heermann, S. Kretschmer, J. Schweizer, J. Mücksch, G. Alagöz, P. Schwille, *ACS Synth. Biol.* **2019**, *8*, 148.
[13] M. Loose, E. Fischer-Friedrich, J. Ries, K. Kruse, P. Schwille, *Science* **2008**, *320*, 789.
[14] S. Kretschmer, T. Heermann, A. Tassinari, P. Glock, P. Schwille, *ACS Synth. Biol.* **2021**, *10*, 939.
[15] A. M. Turing, *Philos. Trans. R. Soc., B* **1952**, *237*, 37.
[16] B. Ramm, P. Glock, J. Mücksch, P. Blumhardt, D. A. García-Soriano, M. Heymann, P. Schwille, *Nat. Commun.* **2018**, *9*, 3942.
[17] B. Ramm, A. Goychuk, A. Khmelinskaia, P. Blumhardt, H. Eto, K. A. Ganzinger, E. Frey, P. Schwille, *Nat. Phys.* **2021**, *17*, 850.
[18] H. Jia, J. Flommersfeld, M. Heymann, S. K. Vogel, H. G. Franquelim, D. B. Brückner, H. Eto, C. P. Broedersz, P. Schwille, *Nat. Mater.* **2022**, *21*, 703.
[19] H. Ceylan, I. C. Yasa, M. Sitti, *Adv. Mater.* **2017**, *29*, 1605072.
[20] B. R. Olden, C. R. Perez, A. L. Wilson, I. I. Cardle, Y.-S. Lin, B. Kaehr, J. A. Gustafson, M. C. Jensen, S. H. Pun, *Adv. Healthcare Mater.* **2019**, *8*, 1801188.
[21] P. A. Beales, J. Nam, T. K. Vanderlick, *Soft Matter* **2011**, *7*, 1747.
[22] D. A. Christian, A. Tian, W. G. Ellenbroek, I. Levental, K. Rajagopal, P. A. Janmey, A. J. Liu, T. Baumgart, D. E. Discher, *Nat. Mater.* **2009**, *8*, 843.
[23] M. Schulz, W. H. Binder, *Macromol. Rapid Commun.* **2015**, *36*, 2031.
[24] J. A. Nye, J. T. Groves, *Langmuir* **2008**, *24*, 4145.
[25] J. Shin, B. D. Cole, T. Shan, Y. Jang, *Biomacromolecules* **2022**, *23*, 1505.
[26] F. Qiu, L. Zhang, K. E. Peyer, M. Casarosa, A. Franco-Obregón, H. Choi, B. J. Nelson, *J. Mater. Chem. B* **2014**, *2*, 357.
[27] H. Eto, H. G. Franquelim, M. Heymann, P. Schwille, *Soft Matter* **2021**, *17*, 5456.
[28] B. Ramm, P. Glock, P. Schwille, *J. Vis. Exp.* **2018**, *137*, 58139.
[29] F. Hong, F. Zhang, Y. Liu, H. Yan, *Chem. Rev.* **2017**, *117*, 12584.
[30] P. W. K. Rothemund, *Nature* **2006**, *440*, 297.
[31] C. M. Dundas, D. Demonte, S. Park, *Appl. Microbiol. Biotechnol.* **2013**, *97*, 9343.
[32] O. Tirosh, Y. Barenholz, J. Katzhendler, A. Priev, *Biophys. J.* **1998**, *74*, 1371.
[33] M. Osawa, D. E. Anderson, H. P. Erickson, *Science* **2008**, *320*, 792.
[34] O. Staufer, S. Antona, D. Zhang, J. Csatári, M. Schröter, J.-W. Janiesch, S. Fabritz, I. Berger, I. Platzman, J. P. Spatz, *Biomaterials* **2021**, *264*, 120203.
[35] S. Kohyama, A. Merino-Salomón, P. Schwille, *Nat. Commun.* **2022**, *13*, 6098.
[36] S. Kohyama, N. Yoshinaga, M. Yanagisawa, K. Fujiwara, N. Doi, *Elife* **2019**, *8*, e44591.
[37] T. K. Claus, B. Richter, V. Hahn, A. Welle, S. Kayser, M. Wegener, M. Bastmeyer, G. Delaittre, C. Barner-Kowollik, *Angew. Chem., Int. Ed.* **2016**, *55*, 3817.
[38] C. A. Koepele, M. Guix, C. Bi, G. Adam, D. J. Cappelleri, *Adv. Intell. Syst.* **2020**, *2*, 1900147.
[39] A. M. Wagner, H. Eto, A. Joseph, S. Kohyama, T. Haraszti, R. A. Zamora, M. Vorobii, M. I. Giannotti, P. Schwille, C. Rodriguez-Emmenegger, *Adv. Mater.* **2022**, *34*, 2202364.
[40] X. Wang, C. Hu, L. Schurz, C. De Marco, X. Chen, S. Pané, B. J. Nelson, *ACS Nano* **2018**, *12*, 6210.
[41] A. Bonabi, S. Tähkä, E. Ollikainen, V. Jokinen, T. Sikanen, *Micromachines* **2019**, *10*, 605.
[42] J. T. Marquês, R. F. M. de Almeida, A. S. Viana, *Electrochim. Acta* **2014**, *126*, 139.
[43] B. Jayachandran, T. N. Parvin, M. M. Alam, K. Chanda, B. Mm, *Molecules* **2022**, *27*, 8124.
[44] S. Kempter, A. Khmelinskaia, M. T. Strauss, P. Schwille, R. Jungmann, T. Liedl, W. Bae, *ACS Nano* **2019**, *13*, 996.
[45] L. Wettmann, M. Bonny, K. Kruse, *PLoS One* **2018**, *13*, e0203050.
[46] K. Zieske, J. Schweizer, P. Schwille, *FEBS Lett.* **2014**, *588*, 2545.
[47] J. Schweizer, M. Loose, M. Bonny, K. Kruse, I. Mönch, P. Schwille, *Proc. Natl. Acad. Sci. U. S. A.* **2012**, *109*, 15283.
[48] I. Ali, M. T. Saleem, *Mathematics* **2023**, *11*, 1459.
[49] F. Giampaolo, M. De Rosa, P. Qi, S. Izzo, S. Cuomo, *Adv. Model. Simul. Eng. Sci.* **2022**, *9*, 5.
[50] J. Q. Toledo-Marín, G. Fox, J. P. Sluka, J. A. Glazier, *Front. Physiol.* **2021**, 12.
[51] A. Li, R. Chen, A. B. Farimani, Y. J. Zhang, *Sci. Rep.* **2020**, *10*, 3894.
[52] J. Kho, W. Koh, J. C. Wong, P.-H. Chiu, C. C. Ooi, arXiv Preprint, arXiv:2211.13464v1, submitted: November, **2022**.
[53] K. Zhang, Y. Ma, D. Wang, J. Liu, J. An, Y. Li, C. Ma, Y. Pei, Z. Zhang, J. Liu, J. Shi, *Nano Lett.* **2022**, *22*, 1937.
[54] L. Würthner, F. Brauns, G. Pawlik, J. Halatek, J. Kerssemakers, C. Dekker, E. Frey, *Proc. Natl. Acad. Sci. U. S. A.* **2022**, *119*, e2206888119.
[55] K. Powell, *Nature* **2018**, *563*, 172.
[56] M. Osawa, D. E. Anderson, H. P. Erickson, *EMBO J.* **2009**, *28*, 3476.
[57] S. M. Douglas, A. H. Marblestone, S. Teerapittayanon, A. Vazquez, G. M. Church, W. M. Shih, *Nucleic Acids Res.* **2009**, *37*, 5001.
[58] D. Nečas, P. Klapetek, *Open Phys.* **2012**, *10*, 181.
[59] S. Pautot, B. J. Frisken, D. A. Weitz, *Proc. Natl. Acad. Sci. U. S. A.* **2003**, *100*, 10718.
[60] J. Schindelin, I. Arganda-Carreras, E. Frise, V. Kaynig, M. Longair, T. Pietzsch, S. Preibisch, C. Rueden, S. Saalfeld, B. Schmid, J.-Y. Tinevez, D. J. White, V. Hartenstein, K. Eliceiri, P. Tomancak, A. Cardona, *Nat. Methods* **2012**, *9*, 676.

3.2 Publication P2

Self-Organized Spatial Targeting of Contractile Actomyosin Rings for Synthetic Cell Division

María Reverte-López, Nishu Kanwa, Yusuf Qutbuddin, Viktoriia Belousova, Marion Jasnin, Petra Schwille

Summary:

In this publication, we achieve the positioning of contractile actomyosin rings inside vesicles for the synthetic division of minimal cells. To reach this important milestone for the eukaryotic-based synthetic division approach, we exploited the MinDE system as a positioning module. Co-reconstitution of both the MinDE system and actomyosin rings under suitable conditions resulted in the spatial localization of contractile rings at the equator of vesicles, where myosin-driven forces yielded mid-cell furrowing. We also report the emergence of MinDE-induced membrane transformations, such as blebbing, and study this membrane-remodelling phenomenon in closer detail with phase-separated vesicles. This study demonstrates that combining synthetic modules of contrasting origin (eukaryotic for the contractile module and bacterial for the positioning module) is a feasible strategy to build artificial cells with pre-designed features and emergent functions.

To cite this article:

Reverte-López, M., Kanwa, N., Qutbuddin, Y., Belousova, V., Jasnin, M., Schwille, P., Self-organized spatial targeting of contractile actomyosin rings for synthetic cell division. *Nat Commun* 15, 10415 (2024). https://doi.org/10.1038/s41467-024-54807-9.

nature communications

Article

https://doi.org/10.1038/s41467-024-54807-9

Self-organized spatial targeting of contractile actomyosin rings for synthetic cell division

Received: 13 May 2024

Accepted: 18 November 2024

Published online: 29 November 2024

Check for updates

María Reverte-López[1], Nishu Kanwa[1], Yusuf Qutbuddin[1], Viktoriia Belousova[1], Marion Jasnin[2] & Petra Schwille[1]

A key challenge for bottom-up synthetic biology is engineering a minimal module for self-division of synthetic cells. Actin-based cytokinetic rings are considered a promising structure to produce the forces required for the controlled excision of cell-like compartments such as giant unilamellar vesicles (GUVs). Despite prior demonstrations of actin ring targeting to GUV membranes and myosin-induced constriction, large-scale vesicle deformation has been precluded due to the lacking spatial control of these contractile structures. Here we show the combined reconstitution of actomyosin rings and the bacterial MinDE protein system within GUVs. Incorporating this spatial positioning tool, able to induce active transport of membrane-attached diffusible molecules, yields self-organized equatorial assembly of actomyosin rings in vesicles. Remarkably, the synergistic effect of Min oscillations and the contractility of actomyosin bundles induces mid-vesicle deformations and vesicle blebbing. Our system showcases how functional machineries from various organisms may be combined in vitro, leading to the emergence of functionalities towards a synthetic division system.

Bottom-up synthetic biology is an interdisciplinary field currently fostering promising technological advancements to tackle the environmental and biomedical challenges of the future while it strives towards a fundamental goal: the construction of an artificial cell from a set of minimal functional modules[1–4]. As protocell models, the biomimetic chassis commonly used in the field are giant unilamellar vesicles (GUVs), membrane-enclosed containers capable of hosting biochemical reactions[5]. To ensure the autonomy and continuity of our artificial vesicular systems, key cellular features and processes must be recapitulated within protocells; particularly, their ability to divide and self-replicate, a critical step in a cell's life cycle[1,6].

In this regard, several strategies have been conceived to engineer a synthetic division module capable of mechanical membrane abscission[7]. While the reconstitution of well-characterized bacterial divisome machinery is a very promising approach[8,9], recapitulating division with a eukaryotic cytoskeleton-based toolbox is another intriguing strategy, due to the versatility and modularity of eukaryotic division proteins. Inspired by eukaryotic cytokinesis, the so-called engineering route works on assembling an actomyosin contractile ring at the GUV equator which, upon its controlled diameter reduction, is supposed to constrict the vesicle membrane until scission[10]. Two main cytoskeletal components are required for this in vitro ring assembly route: actin and myosin. Actin, in its filamentous form and together with its many regulatory binding proteins, assembles into bundles which positioned at mid-cell constitute the ring scaffold. To generate the tension required for ring constriction, actin must interact with many membrane-associated and scaffolding proteins like anillin, septins and the motor protein myosin. The interplay of these cytokinetic constituents and the contraction generated by myosin and other passive crosslinkers are presumably behind the contractility of the actin assembly and furrow ingression[11–13].

[1]Department of Cellular and Molecular Biophysics, Max Planck Institute of Biochemistry, Martinsried, Germany. [2]Helmholtz Pioneer Campus, Helmholtz Munich, Neuherberg, Germany; Department of Chemistry, Technical University of Munich, Garching, Germany. e-mail: schwille@biochem.mpg.de

Article https://doi.org/10.1038/s41467-024-54807-9

Several studies have shown the successful reconstitution of contractile actomyosin rings in vitro[14–16]. Of particular interest is the reconstitution inside GUVs by Litschel et al.[15]. Using talin-vinculin as bundlers, membrane-bound actomyosin rings induced transient deformation in vesicles. However, bundles slipped on the membrane and formed condensate clusters, impeding the radial targeting of contractile forces on the vesicle membrane. Indeed, a key requirement for the cytokinetic engineering route to succeed is the stable circumferential positioning of the contractile ring during constriction of the vesicle, ideally at mid-cell. To date, however, spatiotemporal control of actomyosin rings in GUVs has not been achieved. For the eukaryotic reconstitution approach this challenge is of particular complexity, since reconstitution of in vivo mechanisms to maintain mid-cell ring placement would require the synergistic integration of many proteins systems and signalling molecules, a currently unattainable feat[10].

Interestingly, recent studies have shown the robustness and versatility of a protein-based spatial positioning toolset: the MinDE system[17–19]. The *Escherichia coli* (*E. coli*) Min proteins are a reaction-diffusion system able to self-organize on membranes through ATP hydrolysis. Composed of three proteins—MinD, MinE and MinC—the Min complex has a particular function in vivo: the localization of the FtsZ division ring (Z-ring) in the middle of rod-shape bacteria. Their self-organization mechanism consists of three steps: (1) ATP-dependent dimerization of MinD promoting membrane attachment, (2) MinE recruitment to membrane-bound MinD stimulating MinD's ATP-ase activity, (3) ATP hydrolysis and detachment of the MinDE complex from the membrane. Following this mechanism of pattern formation, MinD and MinE oscillate from one pole of the cell to the other and inhibit the assembly of the Z-ring near the poles via depolymerization of FtsZ through MinC, the functional cargo protein that is not involved in MinDE self-assembly[20]. In vitro, however, a surprising functionality of the MinDE system was discovered[21]. When reconstituted on planar supported lipid bilayers and inside GUVs, the proteins MinD and MinE can non-specifically sort and position any membrane-bound cargo. More precisely, through a diffusiophoretic transport mechanism, MinD fluxes can spatiotemporally control molecules on the membrane by frictional forces and generate anti-correlated molecular patterns[17]. This biochemical function, although possibly irrelevant in vivo, could thus be exploited for the positioning of membrane-attached molecules and other biomimetic features in artificial systems[18,19].

In this study, we demonstrate the successful co-reconstitution of actomyosin architectures and the MinDE system inside GUVs. Upon optimization of encapsulation conditions, time-lapse imaging revealed the MinDE-driven diffusiophoretic positioning of actomyosin rings and bundle networks at mid-cell, where we observed equatorial furrow-like invaginations breaking spherical symmetry. Moreover, we show that, besides the spatiotemporal control of actomyosin bundles at the membrane, MinDE binding can induce bleb-like outward protrusions in single-phase vesicles and domain-specific deformations in phase-separated GUVs. Thus, the experimental insights here reported demonstrate that upon ATP hydrolysis, MinDE proteins not only aid in active contractile ring localization, but also generate mechanical work to remodel vesicle membranes during synthetic division. Overall, these results showcase the advantages of integrating synthetic toolsets of different origin to engineer artificial cells with advanced functionalities.

Results

Co-reconstitution of actomyosin networks and the MinDE system inside GUVs

To achieve the co-reconstitution of actomyosin networks and Min oscillations inside vesicles, we carried out encapsulation experiments via double emulsion transfer to identify optimal experimental conditions for the dynamic and functional interplay of both systems' components.

First, since G-actin and Min protein self-organization depend on factors like salt concentration, supply of ATP and the presence of divalent cations in solution, we tuned the inner environment of the vesicles to simultaneously facilitate actin filament polymerization and MinD dimerization, critical for MinD interaction with negatively charged amphiphiles and its cooperative binding to membranes. Given the importance of the membrane as catalytic matrix for the spatiotemporal organization of MinDE proteins, we generated vesicles containing negative charge in the bilayer to enable the self-organization of Min proteins into different oscillation modes[22,23]. In addition, we incorporated biotinylated lipids to link biotinylated actin filaments to the inner leaflet of the GUVs. Anchoring actin assemblies to the membrane through neutravidin-biotin bonds allowed us to exploit the diffusiophoretic capabilities of Min proteins, which require membrane-bound cargo to induce the ATP-driven transport of molecules on membranes[17].

Once optimal buffer conditions and membrane composition were identified, we chose fascin as the crosslinking protein to generate high-order actin bundle structures. As previously reported[15], by binding fascin-assembled bundles to the membrane via neutravidin-biotin bonds we obtained long and curved bundles that robustly bound to the membrane adapting to the vesicle curvature. Additionally, to accelerate actin polymerization kinetics and decrease MinDE wavelength and oscillation velocity, we employed Ficoll70 as macromolecular crowder[9,24,25], which also facilitated vesicle production. Finally, to make our actin assemblies contractile and render membrane deformations[14,15], the motor protein myosin II was added to the inner solution mix (Fig. 1a).

To investigate the effects of MinDE oscillations on the formation of actin-bundle architectures under crowding conditions, we encapsulated actin and fascin at different molar ratios together with myosin II in the presence and absence of Min proteins. To this end, we analyzed actin architecture types and quantified their frequency of appearance in terms of GUV sizes. Similar to recent cytoskeletal reconstitutions in GUVs[16,26], we observed four main actin phenotypes in both the presence and absence of Min proteins: soft bundle webs, actomyosin asters, flexible rings and stiff-straight bundles (Fig. 1b).

Although phenotype yields differed, Min oscillations supported the bundling and assembly of actomyosin architectures on GUV membranes. In particular, at a 0.25 fascin/actin molar ratio (Fig. 1c), when Min proteins were part of the reaction mix, we detected an increase in flexible ring yields, as well as a lower probability of stiff bundle formation, irrespective of vesicle size. As previously reported, the size of a spherically confining environment impacts actin-bundle architecture due to the persistence length of actin filaments and the spontaneous equatorial assembly of bundles to minimize their bending energy[14,26]. In both samples containing or in absence of Min proteins, the probability of flexible ring formation was significantly higher in small diameter vesicles (diameter $< 15\,\mu m$), whereas for medium and big vesicles the predominant phenotype was aster, reaching almost 50% formation probability in vesicles between 20–25 μm in diameter and 80% for vesicles bigger than 25 μm. Similarly, when a 0.5 fascin/actin molar ratio was employed and a higher fascin/actin concentration was encapsulated, we observed the four aforementioned phenotypes in the presence and absence of Min proteins (Fig. 1c). Under these conditions, however, only the frequency of stiff bundle formation decreased upon addition of Min proteins and the probability of flexible ring formation drastically decreased for GUVs bigger than 15 μm diameter in samples containing Min proteins or in their absence.

Furthermore, to study the evolution of this co-reconstituted system over time, we performed experiments in the presence of MinDE at 0.25 fascin/actin ratio and quantified the frequency of actin phenotypes observed on the sample at three timepoints: right after encapsulation, 7 h and 24 h after vesicle production (Supplementary Fig. 1a).

Article https://doi.org/10.1038/s41467-024-54807-9

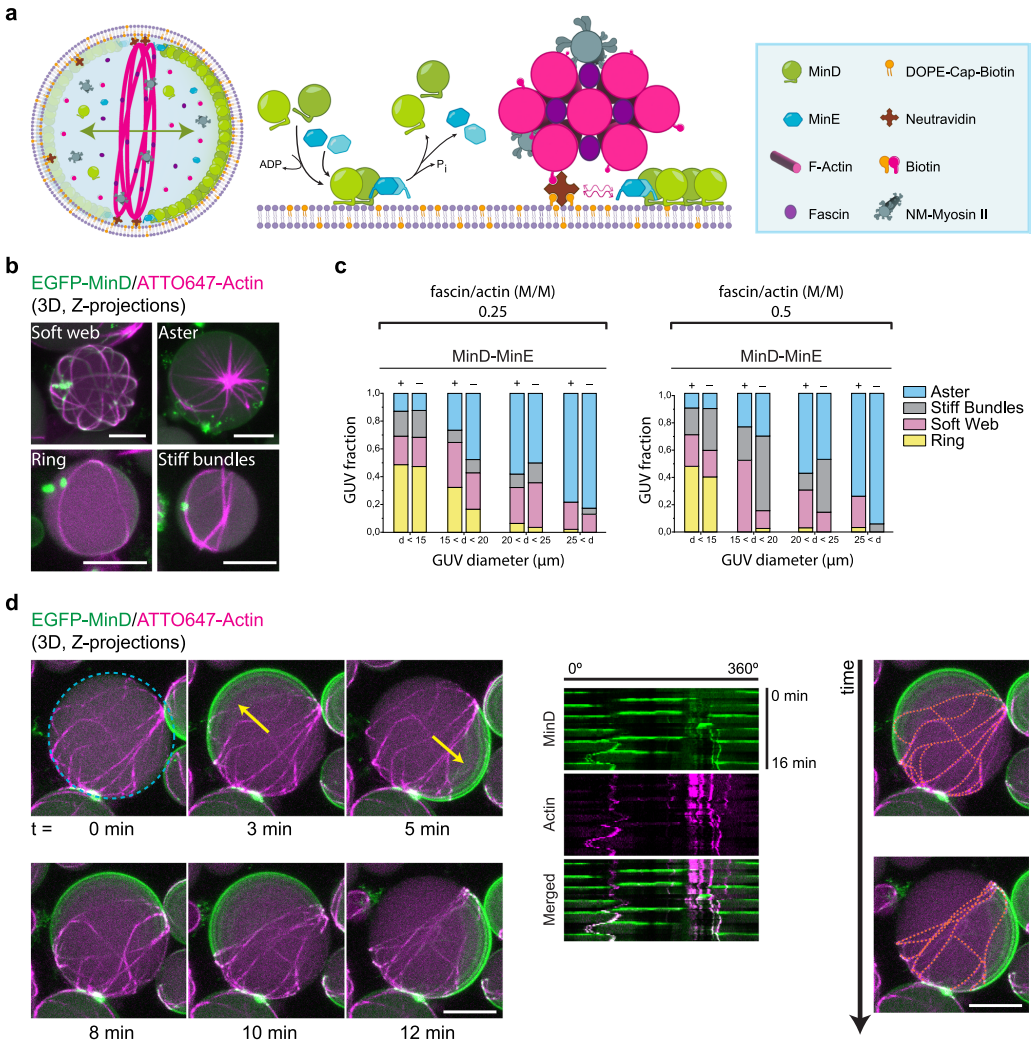

Fig. 1 | Co-reconstitution of actomyosin networks and the MinDE system enables the reorganization and positioning of actomyosin bundles at mid-cell. **a** Schematic illustration of the GUV content and the two macromolecular reactions at membrane level: the MinDE self-assembly mechanism behind pattern formation and the diffusiophoresis-mediated transport of neutravidin-bound actomyosin bundles by Min proteins. The active flux of MinDE proteins on the vesicle membrane interacts non-specifically via frictional forces with membrane-bound neutravidin inducing the transport and positioning of these molecules, and consequently the actomyosin bundles linked to them, towards areas of low MinD density. **b** 3D projections of confocal images showing the 4 phenotypes of actin architectures obtained after encapsulating 2.4 μM actin, 0.6 μM fascin (fascin/actin molar ratio = 0.25), 0.05 μM myosin II, 50 g/L Ficoll70, 3 μM MinD, 3 μM MinE and 5 mM ATP. Scale bars: 10 μm. **c** Bar graphs with the frequencies of the four actomyosin phenotypes observed at different vesicle diameters when encapsulation experiments were performed at 0.25 and 0.5 fascin/actin molar (M/M) ratio in the presence and absence of Min proteins and protein/crowding conditions specified in (**b**). Total number of GUVs analyzed per condition = 150. **d** 3D projections of time-lapse confocal images depicting the reorganization and stacking of actomyosin bundles towards the vesicle equator driven by the diffusiophoretic transport of Min pole-to-pole oscillations. Yellow arrows indicate the perpendicular orientation of MinDE oscillations with respect to actomyosin bundles, which get antagonistically positioned at mid-cell. Kymographs generated at the vesicle equator (blue dashed circle) are meant to visually define the position of fluorescent features at this region over time. Orange dotted lines depict the approximate distribution of actin bundles on the membrane at two time points. Vesicle content as specified in (**b**). Scale bars: 10 μm. Source data are provided as a Source Data file.

Interestingly, we found that aster formation was immediate after vesicle generation, as the frequency of these star-like condensates remained markedly similar at 7 and 24 h: 34% and 38%, respectively. Conversely, vesicles initially presenting no distinguishable phenotype (but filled with G-actin on their lumen) showed a frequency as high as asters right after encapsulation (40%), which progressively decreased over time reaching 6% at 24 h. Concomitantly, we observed that the number of vesicles containing rings and soft webs increased after 7 h, the latter phenotype showing progressive increment in number as we prolonged sample incubation time to 24 h.

Article https://doi.org/10.1038/s41467-024-54807-9

Taken together, we show the successful co-reconstitution of the actomyosin system together with Min proteins and demonstrate that MinDE oscillations are compatible with the assembly of membrane-bound actomyosin architectures inside GUVs, and vice versa. Notably, addition of Min proteins promotes the formation of flexible actomyosin rings in all vesicle sizes encapsulated with a 0.25 fascin/actin ratio.

Diffusiophoresis-mediated positioning of actomyosin bundles at mid-cell by the MinDE system

Having established the conditions to reconstitute dynamic Min oscillations together with actomyosin-bundle assemblies inside GUVs, we then investigated whether Min proteins could effectively reorganize these assemblies and position them at mid-cell via their diffusiophoretic mechanism of molecular transport. Since flexible rings and soft bundle webs are the two types of actin architectures that could efficiently transmit contractile forces to the membrane, we studied the spatiotemporal organization of these two phenotypes by Min oscillations with time-lapse microscopy.

In agreement with past studies[27], we observed three main Min oscillation modes resultant from the reaction-diffusion fluxes of Min proteins on the inner leaflet of vesicles (Supplementary Fig. 1b): pulsing (oscillation characterized by the consecutive binding and unbinding of MinD to the entire vesicle membrane), pole-to-pole (sequential binding of MinD to the hemispheres of the vesicle), and circling waves (MinDE waves revolving around the inner leaflet of the membrane).

As MinDE pole-to-pole oscillations are the desired phenotype to actively transport molecules to the mid-cell region via diffusiophoresis[9,21], we first scrutinized actomyosin-containing vesicles exhibiting this dynamic pattern. Strikingly, in vesicles containing actomyosin bundles isotropically distributed all over the membrane, MinDE pole-to-pole oscillations yielded an anticorrelated and directional movement of the bundles perpendicular to the oscillation axis, reducing bundle interdistance and accumulating them at mid-cell (Fig. 1d, Supplementary Movie 1). Subjected to the highly dynamic MinDE pattern, the actomyosin bundles still showed positional fluctuations at the GUV equator over time, but maintained a perpendicular orientation to the oscillation axis.

Subsequently, to test the robustness of the MinDE diffusiophoretic transport in our actin-based encapsulation system, we varied the experimental conditions from our standard inner solution mix. We found that, in the absence of myosin II, under varying Ficoll70 concentrations (10-50 g/L), and employing different molar ratios for fascin/actin (0.25 or 0.5) as well as MinD/MinE ratios (1 or 2), Min proteins were capable of actively arranging membrane-bound actin bundles via diffusiophoresis when patterns different from pulsing developed on the vesicle membrane. Importantly, and as expected from our previous experiments, MinDE pole-to-pole patterns rotated and positioned fascin-assembled actin rings in the absence of myosin II, maintaining ring orientation perpendicular to MinDE oscillations (Supplementary Fig. 2b). In addition, when MinDE circling patterns emerged on vesicles containing fascin-bundled actin rings, we observed that the frictional forces induced by the directional MinD protein flux promoted the circular displacement of one end of the ring towards the opposite end (Supplementary Fig. 2c), resulting in the complete folding of the ring in less than 15 minutes (Supplementary Fig. 2d). Moreover, we detected that chaotic MinDE patterns—a dynamic mode in which Min proteins bind and unbind membrane areas in stochastic direction—could also alter the distribution of actomyosin bundles and, in some instances, buckle and collapse the network (Supplementary Figs. 1c, d).

Thus, our data demonstrate that the MinDE system can be used to regulate the spatiotemporal localization of membrane-bound actomyosin bundles and most importantly, position contractile actomyosin architectures at mid-cell via its characteristic pole-to-pole oscillation mode.

Equatorial constriction of vesicles induced by positioned actomyosin architectures

In our system, myosin II not only acts as a crosslinking agent but also provides the contractile force required to induce membrane deformations. Having shown that the MinDE system localized actomyosin assemblies at the vesicle equator, we next investigated whether the positioned contractile assemblies could generate furrow-like membrane deformations.

First, to explore the contractile effect of myosin II on positioned actin structures, we carried out encapsulation experiments at 0.25 and 0.5 fascin/actin molar ratio with 50 g/L Ficoll70 and examined the vesicles presenting pole-to-pole oscillations with time-lapse confocal microscopy. Interestingly, when we employed a 0.5 fascin/actin molar ratio, mid-cell deformation induced by actomyosin ring constriction could be observed (Fig. 2a). This furrow-like invagination of the membrane, sustained over time (Supplementary Movie 2), generated two lobes where MinD proteins continued oscillating in a pole-to-pole pattern maintaining the localization of the ring at mid-cell.

In line with these observations, we also detected vesicle deformation at 0.25 fascin/actin molar ratio. Contrary to single rings, soft actomyosin bundle networks positioned at the vesicle equator formed a constriction band resulting in the loss of spherical vesicle shape (Fig. 2b). In addition to this large-scale membrane deformation, the vesicle presented an actin-filled membrane out-bud at the constriction site (Supplementary Fig. 3, Supplementary Movie 3). Although we could not acquire the formation process of this bud, Litschel et al. already reported on this type of membrane deformation, which results from the sliding of actomyosin bundles along the membrane to one side of the vesicle and their collapse into a condensate[15]. Notably, the membrane bud we observed was localized closely to the actomyosin band constricting the vesicle at the equator, while MinDE pole-to-pole oscillations continued at the two hemispheres generated at each side of the actomyosin band. To quantitatively assess vesicle deformation, we calculated the vesicle aspect ratio (AR) as the ratio between their major (a) and minor (b) axes. In both examples presented, aspect ratios indicated a vesicle deformation towards a rod-like shape ($AR < 0.9$), with the lowest AR obtained (0.75) 24 h after encapsulation, where a vesicle with a centered actomyosin network exhibited a distinct elongated shape (Supplementary Fig. 4a).

Furthermore, given that macromolecular crowders can impact both actin bundle architecture and the mechanical properties of the vesicle membrane[28,29], we subsequently performed encapsulation experiments at lower crowding concentration (20 g/l Ficoll70) and found membrane deformations in line with those already showed. Furthermore, under these experimental conditions, we detected an example of eccentric membrane deformation caused by an actomyosin ring when the established MinDE oscillation pattern inside the vesicle was different from the pole-to-pole mode (Fig. 2c). More specifically, the MinDE pattern at the vesicle membrane transitioned into a circling and less dynamic MinDE oscillation (possibly due to ATP depletion). Contrary to vesicles presenting mid-cell constriction, the membrane deformation observed induced a characteristic asymmetric dumbbell shape with two differently sized sub-compartments. Nevertheless, this asymmetric deformation, sustained over time (average AR over 20 minutes = 0.79), did not collapse after more than an hour of imaging (Supplementary Movie 4). Myosin II and ATP concentration added were 0.05 μM and 5 mM, respectively. Further experiments are therefore required to find the optimal encapsulating conditions enabling MinDE-stabilized rings positioned at mid-cell to undergo progressive contraction and controllably reduce their diameter by the action of myosin II motors.

Article https://doi.org/10.1038/s41467-024-54807-9

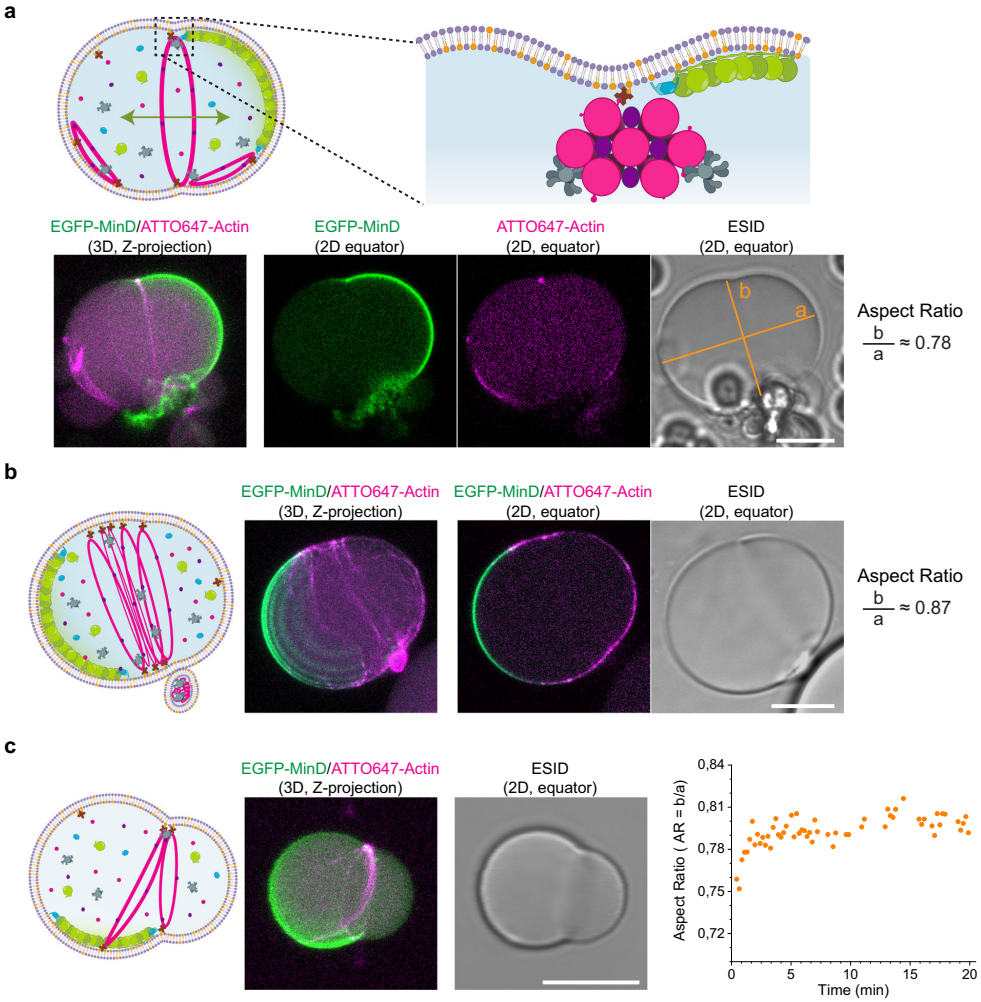

Fig. 2 | Positioned actomyosin rings and soft webs constrict vesicles at mid-cell. **a** Schematic illustration behind the mechanism of membrane deformation. Contractile actomyosin bundles positioned by MinDE proteins at mid-cell induce furrow-like membrane invaginations. 3D projections and 2D confocal images show an actomyosin ring constricting the vesicle at its equator. Orange lines indicate the major (a) and minor (b) axes measured to calculate the aspect ratio of the deformed vesicle (for spherical vesicles: aspect ratio = 1). Inner solution mix: 4 μM actin, 2 μM fascin (fascin/actin molar ratio = 0.5), 0.05 μM myosin II, 50 g/L Ficoll70, 3 μM MinD, 3 μM MinE and 5 mM ATP. Scale bar: 10 μm. **b** Schematic illustration, 3D projections and 2D confocal images of a vesicle containing a soft web of actomyosin bundles at the vesicle center being positioned by pole-to-pole Min oscillations. The contractile actomyosin band formed causes the deformation of the vesicle (aspect ratio < 1). Inner solution mix: 2.4 μM actin, 0.6 μM fascin (fascin/actin molar ratio = 0.25), 0.05 μM myosin II, 50 g/L Ficoll70, 3 μM MinD, 3 μM MinE and 5 mM ATP. Scale bar: 10 μm. **c** Schematic illustration, 3D projection and 2D confocal image of a vesicle with a non-positioned contractile actomyosin assembly due to the loss in pole-to-pole MinDE oscillations. Constriction of the actomyosin bundles results in the deformation of the vesicle membrane into an asymmetric dumbbell shape. Scatter plot depicts the aspect ratio of the vesicle at different time points. Inner reaction mix: 4 μM actin, 2 μM fascin (fascin/actin molar ratio = 0.5), 0.05 μM myosin II, 20 g/L Ficoll70, 3 μM MinD, 3 μM MinE and 5 mM ATP. Scale bar: 10 μm. Source data are provided as a Source Data file.

In summary, we show that MinDE pole-to-pole oscillations can target the constriction of actomyosin architectures at the vesicle equator, resulting in the generation of sustained furrow-like membrane deformations.

MinDE-induced blebbing in reconstituted actomyosin vesicles

When thicker and more abundant actomyosin bundles developed at the membrane in the form of soft webs, we detected the establishment of more chaotic and static MinDE patterns. Thus, to further characterize the system, we performed time-lapse imaging on vesicles presenting chaotic or static-like MinDE patterns.

Interestingly, a large number of vesicles exhibiting these patterns developed membrane deformations similar to bleb-like morphologies (Fig. 3a, Supplementary Movie 5). To get further insights into the underlying mechanism behind bleb formation, we analyzed the interaction between our co-reconstituted protein systems and the vesicle

Article https://doi.org/10.1038/s41467-024-54807-9

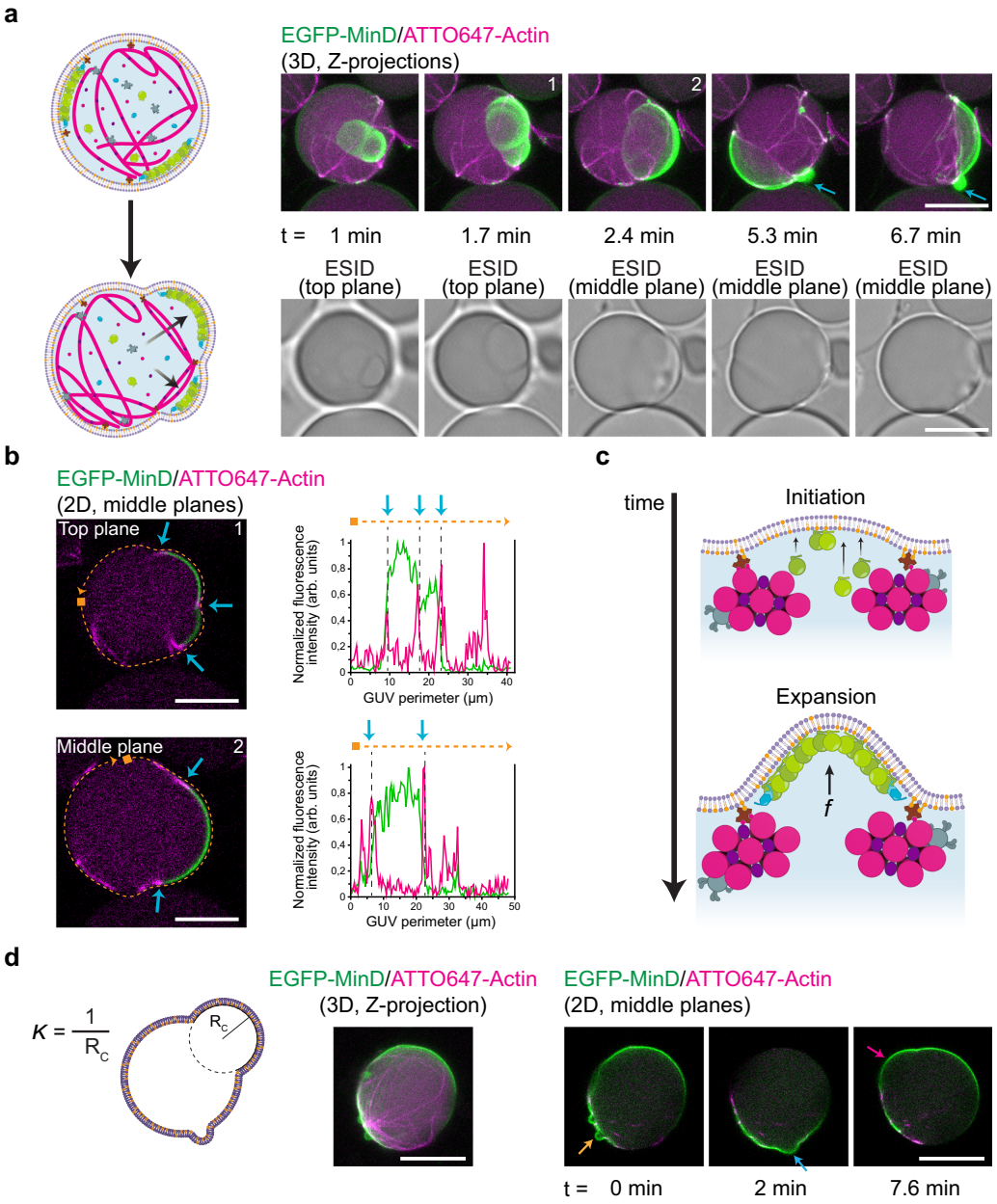

membrane. Closer inspection of the blebs' cross-sections revealed that the actomyosin soft web inside the vesicle compartmentalized the membrane into areas delimited by the peripheral attachment of bundles (Figs. 3b, Supplementary Fig. 5a). Due to this compartmentalization, container symmetry was lost and MinDE proteins generated a chaotic oscillation capable of deforming the membrane. More specifically, we found that the initial spontaneous curvature induced on these compartments by MinDE binding increased as more MinD molecules were recruited to the membrane, resulting in the outward growth of the dynamic bleb-like protrusions (Fig. 3c, Supplementary Fig. 5b). Subsequently, after MinDE-driven membrane deformations, we observed that the reduction in bilayer tension and the recovery of the initial vesicle shape was accompanied by the generation of a membrane out-bud (Fig. 3a, blue arrows), which was not reabsorbed into the mother vesicle (Supplementary Fig. 5c)[30].

Furthermore, consistent with our previous observations and simultaneous to this membrane remodelling effect, the diffusiophoretic transport of actomyosin bundles reorganized the network at

Article https://doi.org/10.1038/s41467-024-54807-9

Fig. 3 | MinDE-induced blebbing in vesicles containing reconstituted actomyosin architectures. a Schematic illustration depicting the change in vesicle shape due to MinDE chaotic oscillations. Min proteins attach to areas delimited by soft actomyosin bundles and deform the membrane generating dynamic bleb-like protrusions. Fluorescence and brightfield confocal time-series show a blebbing vesicle. After bleb retraction, the reduction in bilayer tension generates an outward lipid bud (blue arrows). Encapsulation conditions: 2.4 μM actin, 0.6 μM fascin, 0.05 μM myosin II, 50 g/L Ficoll70, 3 μM MinD, 3 μM MinE and 5 mM ATP. Scale bars: 10 μm. **b** Confocal cross-section images at two time points of the vesicle in section a. Peripheral actomyosin anchoring creates a delimiting area which deforms upon MinDE binding. Additionally, MinDE diffusiophoretic transport changes the position of actomyosin bundles and the shape of the membrane area available for Min protein recruitment (blue arrows). Fluorescence intensity line plots of EGFP-MinD (green) and ATTO647-actin (magenta) demonstrate the demixing of both protein systems at the membrane perimeter (orange dotted line). Scale bars: 10 μm. **c** Schematic illustration of the proposed mechanism behind MinDE-induced blebbing. The recruitment of MinDE proteins to the compartmentalized inner leaflet of the bilayer generates the effect of a membrane outward protrusion in bleb form. **d** Schematic illustration depicting the radius of curvature R_C used to calculate the curvature ($K = 1/R_C$) of the blebs. 3D projection and 2D time-lapse confocal images show a vesicle with diverse bleb-like deformations emerging over time. Orange arrow points at a bleb with $K = 0.73\ \mu m^{-1}$. Blue arrow, $K = 0.27\ \mu m^{-1}$. Magenta arrow, $K = 0.10\ \mu m^{-1}$. Encapsulation mix: 4 μM actin, 2 μM fascin, 0.05 μM myosin II, 50 g/L Ficoll70, 3 μM MinD, 3 μM MinE and 5 mM ATP. Scale bars: 20 μm. Source data are provided as a Source Data file.

the membrane. As a result, membrane compartments changed in size and the oscillations maintained a chaotic mode inducing dynamic blebs in other areas of the vesicle (Fig. 3b).

To further scrutinize the membrane-remodelling capabilities of Min proteins along with our actomyosin architectures, we performed encapsulation experiments at 0.5 fascin/actin molar ratio and calculated the curvature of the blebs observed. Similar to our non-deflated vesicles encapsulated with 0.25 fascin/actin ratio, MinDE binding induced blebbing in a subset of vesicles (Supplementary Movie 6). Time-lapse imaging revealed that Min proteins can induce blebs with a wide range of curvatures (K, calculated as the inverse of the radius of a circle that fits the bleb). As MinDE established a chaotic oscillation inside the vesicle, small blebs ($K = 0.73\ \mu m^{-1}$), medium size ($K = 0.27\ \mu m^{-1}$) and big ($K = 0.10\ \mu m^{-1}$) deformations emerged (Fig. 3d, orange, blue, and magenta arrows, respectively).

Hence, our results show that, when co-reconstituted with actomyosin bundle networks, the MinDE system can generate dynamic bleb-like outward protrusions in vesicles encapsulated at iso-osmolar conditions, confirming its capabilities as a membrane remodelling protein system as previously observed[27,31].

Co-reconstitution of actomyosin bundle networks and the MinDE system in phase-separated vesicles show remodelling of membrane domains

Lastly, to increase the complexity of the system and test its compatibility with other shape-remodelling strategies, we first tested its reconstitution in vesicles of ternary lipid mixtures. Due to their tuneable mechanical and biochemical properties, phase-separated lipid membranes constitute another approach to aid in the remodelling of biomimetic systems by altering membrane curvature, fluidity, etc[32–34]. Furthermore, two-phase vesicles constitute an additional strategy to study the reorganization and deformation of free-standing lipid domains by actomyosin networks[35–37].

To achieve the co-reconstitution of the two protein systems in GUVs with phase-separated lipid domains we again employed the double emulsion transfer method. At room temperature (25 °C), GUVs demixed into coexisting Liquid-ordered (Lo) and Liquid-disordered (Ld) domains, where Ld domains consisted of DOPE-Biotin to facilitate actin binding (Fig. 4a). To study the successful reconstitution of the system inside phase-separated vesicles, we again performed time-lapse confocal imaging and observed that Min proteins could oscillate by binding to Ld domains on the vesicle membrane. Notably, due to the high frequency of soft actomyosin bundle webs formed, MinDE proteins also established chaotic oscillations on the Ld domains of the vesicle. The flexible bundles, however, spanned and crossed both lipid domains.

Interestingly, MinDE-driven diffusiophoretic transport displaced the actomyosin bundles bound at Ld/Lo boundaries, reorganizing the actomyosin network inside the vesicle. Moreover, consistent with our previous experiments performed on single-phase GUVs, MinDE binding to areas delimited by actomyosin bundles at domain boundaries deformed Ld domains into dynamic bleb-like protrusions (Figs. 4b, Supplementary Movie 7). In contrast to studies in which bulging or budding of phase-separated GUVs is externally induced by tuning membrane composition or changing osmotic conditions, and where deformations arise by an imbalance between surface tension and interfacial line tension[34,38], our phase-separated GUVs remained spherical over time in the absence of Min proteins, and no deformations in the form of blebbing or budding were observed (Supplementary Figs. 6, Supplementary Movie 8). Only in the presence of MinDE oscillations in GUVs containing actomyosin networks, timelapses showed the active—i.e., energy-consuming—deformation of Ld domains into outward blebs (Fig. 4c). During the course of these transient outward deformations, we also observed the remodelling of domains at the membrane such as their maneuvering followed by splitting (Supplementary Movie 7). As a result of MinD binding to Ld domains, the initial demixing of lipid phases on the vesicle thus changed, and domain reorganization occurred on the entire vesicle. Interestingly, while the resultant dynamic protrusions in the membrane comprised of Ld domains, Lo domains stayed intact.

In addition, to test the compatibility of our system with other membrane-based strategies for the enhancement of GUV deformation, we generated vesicles containing DOPE, a lipid with intrinsic negative curvature due to its inverse-cone shape[39]. Although the yield of vesicle production dramatically decreases at 15% DOPE molar ratio, successful encapsulation of our co-reconstituted system is possible when 10% DOPE is added to the lipid mix together with 60% POPC and 30% POPG. Importantly, in vesicles generated under these conditions, we observed generation of the three standard Min oscillations, actomyosin-driven equatorial deformation of vesicles and the formation of highly protruding blebs due to MinDE chaotic oscillations (Supplementary Fig. 4b).

In conclusion, we demonstrate that the co-reconstitution of Min proteins and actomyosin can deform DOPE-containing and complex ternary vesicle membranes, and dynamically remodel phase-separated lipid domains by rearranging and reshaping them on the membrane.

Discussion

In this study, we have successfully co-reconstituted contractile actomyosin rings and other assemblies with a protein-based spatial positioning toolset, the MinDE system. Our results demonstrate that, under optimal encapsulating conditions, actomyosin bundles can be spatiotemporally controlled at the membrane and positioned at mid-cell via pole-to-pole MinDE oscillations. Notably, the positioned bundles, due to their contractile nature, induced membrane deformations, breaking GUV spherical symmetry and generating furrow-like invaginations. In addition to the observed actomyosin-driven membrane remodelling, we provide direct evidence that MinDE proteins generate dramatic bleb-like deformations upon dynamic binding to the membrane, another source of symmetry breaking for the GUVs. Thus, our findings lend further credence to the hypothesis that the diffusiophoretic function of the MinDE system can be exploited to maintain actomyosin

Article https://doi.org/10.1038/s41467-024-54807-9

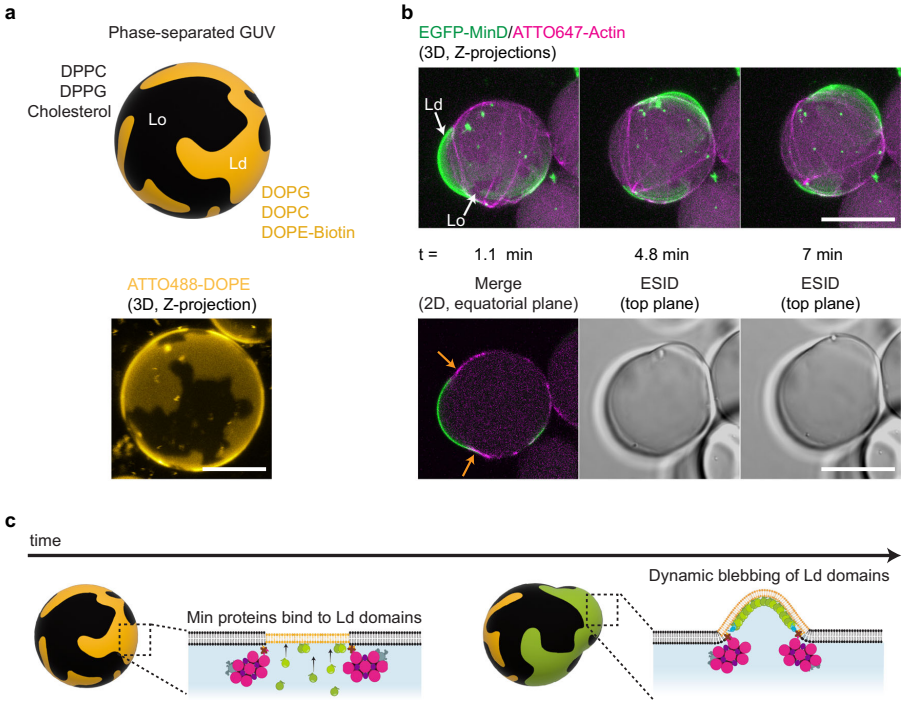

Fig. 4 | MinDE-induced bleb morphologies on phase-separated GUVs with encapsulated actomyosin architectures. a Schematic illustration (top) and 3D confocal image (bottom) show the membrane composition employed to generate phase-separated vesicles and the domains obtained. Scale bar: 10 μm. **b** 3D projections and 2D confocal images depict a blebbing phase-separated vesicle. MinDE proteins bind and oscillate on Ld domains. Actomyosin bundles remain at lipid-phase boundaries as Min proteins transiently deform Ld domains (orange arrows). Inner encapsulation mix: 2.4 μM actin, 0.6 μM fascin (fascin/actin molar ratio = 0.25), 0.05 μM myosin II, 20 g/L Ficoll70, 3 μM MinD, 3 μM MinE and 5 mM ATP. Scale bars: 20 μm. **c** Schematic illustration of the proposed mechanism behind the dynamic deformation of Ld domains by MinDE protein oscillations.

ring localization at mid-cell, one of the key milestones so far not successfully reported in the eukaryotic-based approach to synthetic cell division.

It should be noted that, after the adjustment in encapsulating conditions, our reconstitution conclusively showed the robustness of the MinDE system when integrated with the contractile actomyosin toolset. Not only did we observe the main MinDE-oscillation phenotypes extensively reported in past studies[9,27], our results also indicate that the establishment of Min patterns on the membrane had no detrimental effect of the formation of lipid-linked actomyosin structures. Indeed, we observed an increase in the frequency of GUVs containing membrane-bound rings when Mins were part of the inner encapsulation mix. Moreover, in agreement with previous MinDE geometry-sensing studies and the spatiotemporal feedback observed with FtsZ[40,41], our results demonstrate that Min oscillations orient themselves in a pole-to-pole fashion perpendicular to the spatially positioned ring structures while vesicles acquired ellipsoidal shape due to actomyosin contraction, an important aspect to consider as constriction progresses.

Alternative strategies for ring localization, like the use of microfluidic traps and curvature inducing/sensing biomolecules (e.g., septins, BAR domains, DNA origami), propose the use of external mechanical forces or biomolecules to generate a furrow-like negative curvature that could favor ring assembly[42–46]. However, due to progressive membrane deformation, ring alignment could be lost[42]. The MinDE system, by contrast, dynamically responds to vesicle shape changes, as MinDE pole-to-pole oscillations block any membrane binding on the poles, thereby enabling the targeting of mechanical forces at the center[9]. Nonetheless, to keep the actomyosin ring in place and prevent slippage of the bundles on the membrane, future research should investigate the co-reconstitution of scaffold (e.g., anillin, septins) and severing/de-polymerizing proteins to increase turnover dynamics within actin bundles at the membrane as myosin contraction remodels the ring[47,48].

Besides accomplishing the active positioning of actomyosin architectures, time-lapse imaging revealed a surprising finding, the MinDE-driven blebbing of vesicles. In vivo, blebbing occurs at the cell poles as a mechanism to reduce cortical tension and ensure the stability of cellular shape during eukaryotic cytokinesis[49]. In our in vitro reconstitution, however, blebs originate because of a chemo-mechanical force induced by MinDE on free-standing membranes and constitute a source of asymmetric remodelling of the membrane[50,51].

Interestingly, whereas previous studies on Min proteins enclosed in GUVs have shown shape fluctuations in vesicles due to dynamic MinDE pulsing patterns under hypertonic and (near)-isotonic conditions[27,31,52], our results reveal MinDE-driven deformations of localized membrane regions which bend away from the inner leaflet where Min proteins attach. This observation leads us to speculate that the dramatic bleb-like protrusions shown here are due to confinement

effects induced by actomyosin bundles acting as lateral diffusion barriers for Min protein fluxes[53]. Consequently, and in accordance with previous studies, this partitioning of the vesicle membrane would in turn alter the membrane-to-bulk ratio and thus MinDE membrane kinetics[9,40]. The exact structural mechanism by which Min protein dynamics may induce local membrane deformations still remains opaque. Although previous reports have indicated the ability of Min proteins to increase membrane viscosity and change membrane topology by inserting their alpha helix[54,55], these two effects would not explain the outward budding force observed here[30,56]. Furthermore, while MinD-ATP forms flexible 2D oligomers on membranes, possible scaffolding effects due to their clustering at the inner leaflet remain unknown, and a potential intrinsic curvature of these oligomers is yet to be elucidated[57–59].

However, numerous theoretical and in vitro studies have already reported on the forces induced by reaction-diffusion systems such as Min proteins to deform open or confined dynamic surfaces[31,51,60,61]. More specifically, Fu et al. showed that only in the presence of MinE and ATP, MinDE oscillations could generate up to ~0.84 pN forces resulting in membrane extension and spreading of flat vesicles[31]. In contrast to other non-oscillatory protein-binding systems, which were shown to induce an opposite bending curvature due to protein-crowding effects[56,62], our MinDE protein system presents non-equilibrium dynamics at the inner leaflet and oscillatory membrane-bulk exchange due to ATP consumption. Therefore, to explain the outward membrane bending in our blebbing vesicles, we hypothesize that reactive MinDE fluxes localized to bundle-delimited regions exert an osmotic pressure arising from ATP-driven forces with normal components (Fig. 3c)[53,63]. In particular, the collisions resulting from the dynamic and highly cooperative binding and disassociation of MinD and MinE on the membrane patches, and the protein gradients generated on the proximal bulk, could first drive the straightening of nanoscale membrane undulations to release new membrane area, and ultimately, lead to outward blebbing[54,64].

Nevertheless, as some phenomenological aspects of the MinDE-membrane dynamics are still under investigation[58,65], future theoretical studies using modelling approaches combining reaction-diffusion dynamics and deformable surfaces should provide further insights to analyze this non-equilibrium process and underpin the precise molecular mechanism by which MinDE reactive fluxes are translated into shape-remodelling forces.

In addition, we observed an interesting mechanical effect on actin bundles themselves, arising via diffusiophoresis from MinDE dynamic patterns like chaotic or circling oscillations. Interestingly, time-lapse imaging showed bundles bending, collapsing, and stretching due to the diffusiophoretic frictional force of MinD fluxes. Thus, the system here reconstituted presents itself as another approach to study the crosslinker-dependent mechanical properties of actomyosin bundles and investigate the extent of diffusiophoresis when stiff supramolecular structures are bound to the membrane.

Importantly, and in accordance with previous studies, we observed actomyosin-driven deformation of GUVs under (near)-isosmotic conditions towards both ellipsoidal and asymmetric lobe shapes[15,16]. In this context, Bashirzadeh et al. calculated the force (~176 pN) generated by actomyosin rings on GUVs to induce asymmetric dumbbell deformations similar to those we observed (Fig. 2c)[16]. In contrast to bleb-like morphologies (Figs. 3 and 4), where forces arising from Min oscillations were essential to generate these deformations (Supplementary Fig. 6), in this study we also showed vesicles that exhibited sustained equatorial constriction and asymmetric dumbbell shape after Min oscillation decay on the membrane (Fig. 2, Supplementary Movie 4). This observation therefore suggests that, in these vesicles, the actomyosin bundles pinching the membrane are solely responsible for the sustained deformation obtained, and the observed constriction force (three orders of magnitude higher than the one Min proteins could generate) is similar in nature to that characterized by Bashirzadeh et al.

However, after the stalling of myosin II on bundles occurred, contraction was arrested and deformation did not progress. It should be borne in mind that, in our system, myosin II also crosslinks actin and consumes ATP, an energy source employed by actin as well as MinD. Thus, we consider reasonable to suggest that under our encapsulating conditions with fascin as bundling agent, myosin II contracts the actin assembly until it reaches full condensate formation or stalls due to a compacted actin architecture or ATP shortage[28,66].

Enhancement of actin contraction is an important aspect that requires improvement, as our actomyosin architectures become stagnant over time and progression of the cytokinetic contraction is hampered. To effectively achieve a controlled contraction of the ring and its decrease in diameter on the membrane, there are a few approaches that could be implemented in our system. From the activation of latent myosin II with blebbistatin to trigger contraction late after encapsulation[67,68], to the assembly of a mix-polarity cortex remodelled by actin turnover (naturalistic route for synthetic division)[10,47,66], the use of this motor protein could render promising results. Alternatively, as Kučera et al. showed[13], an interesting element that could substitute or supplement myosin activity is anillin, a passive actin crosslinker capable of generating contractile forces. Regardless of the approach, future studies with optimized contractile toolsets could include the MinDE system to efficiently position these actin-based assemblies at mid-cell and deform lipid vesicles.

Collectively, the findings here provide a potential avenue for the equatorial localization of contractile actomyosin rings and the spatial targeting of mechanical forces at the vesicle membrane. Hence, being one step closer to a well-defined self-division of artificial minimal cells, future investigations should consider expanding the system reconstituted here with other division toolsets like a membrane expansion system to engineer membrane growth, an imperative to achieve sustained synthetic division.

Towards the integration of different functional modules to build a synthetic cell

In conclusion, we show that positioning and confinement of contractile actomyosin rings in vesicles to a defined zone of future constriction, ideally in the equatorial region, is possible by employing the versatile MinDE protein system. We thus provide an example of a successful synthetic integration of functional toolkits from different organisms for the division of minimal vesicular systems. As synthetic biology strives to achieve the construction of an artificial cell, minimal modules reconstituted separately must be combined. Working towards the optimization of experimental conditions to meet the needs of all components may be the next challenge of the field. However, the efforts to interlace diverse functional modules might provide the field with interesting outcomes, like emergent protein functions or unexpected advantageous effects arising from the interplay of completely unrelated families of biomolecules.

Methods

Proteins

Actin (alpha-actin skeletal muscle, rabbit), ATTO647-Actin (alpha-actin skeletal muscle, rabbit) and Biotin-Actin (alpha-actin skeletal muscle, rabbit) were purchased from HYPERMOL (Germany). Myosin (rabbit muscle) was purchased from Cytoskeleton Inc (Tebubio GmbH, Offenbach, Germany). Fascin (human, recombinant) was purchased from Cytoskeleton Inc (Tebubio GmbH, Offenbach, Germany) and HYPERMOL (Germany). Stock solutions for all purchased cytoskeletal proteins were obtained by following the handling instructions of the manufacturer. Stock solutions of neutravidin (Thermo Fisher Scientific Inc., Massachusetts, USA, Cat# 31000) were prepared by dissolving the protein in water according to reconstitution instructions.

Article https://doi.org/10.1038/s41467-024-54807-9

MinE-His, His-MinD and His-EGFP-MinD were purified as described in previous reports[69,70]. Briefly, His-tag carrying proteins were purified via affinity chromatography using Ni-NTA columns. Transformed *E.coli* BL21 cells were lysed by sonication and cell lysates were centrifuged to discard debris. Supernatants were loaded into Ni-NTA columns and proteins were eluted in storage buffer (50 mM HEPES, pH 7.25, 150 mM KCl, 0.1 mM EDTA, 1 mM TCEP, 10% Glycerin). Protein purity was confirmed via SDS-PAGE. Protein concentration and protein activity were determined via Bradford assay and ATPase assay, respectively.

Crowder and density gradient solutions

BSA (Sigma-Aldrich, St. Louis, USA, Cat# A6003) stock solutions were prepared by dissolving the lyophilized powder in Millipore water at ~100 g/L as previously described[9]. To remove undesired debris from BSA solutions, three washing steps were performed with Millipore water using Amicon Ultra-0.5 centrifugal filters 50 kDa MWCO (Merck KGaA, Darmstadt, Germany). Concentration of final stock solutions (ranging from 170 to 300 g/l) were determined via Bradford Assays and stored at -20 °C. Ficoll70 (Sigma-Aldrich, St. Louis, USA, Cat# F2878) was dissolved in Millipore water and left at 4 °C in a rotary shaker for 24 h. Stock concentrations were calculated from the weight of Ficoll70 added and the final volume of solution obtained (625 g/L). Ficoll70 stocks were subsequently stored at -20 °C. 60% Iodixanol (OptiPrep™, Cat# D1556) was purchased from Sigma-Aldrich (St. Louis, USA).

Vesicle production

All lipids were purchased from Avanti Polar Lipids (USA). For single-phase vesicles, a lipid-oil emulsion was prepared by dissolving 1-palmitoyl-2-oleoyl-sn-glycero-3phosphocholine (POPC), 1-palmitoyl-2-oleoyl-sn-glycero-3-phospho(1'-rac-glycerol) (POPG) and 1,2-dioleoyl-sn-glycero-3-phosphoethanolamine-N-(cap biotinyl) (sodium salt) (18:1 Biotinyl CAP PE) at a 6.9: 3: 0.1 molar ratio in 2.5 g/L final concentration and drying the mixture for 15 min under a nitrogen stream. In the case of experiments employing 1,2-dioleoyl-sn-glycero-3-phosphoethanolamine (DOPE), a mixture of POPC, POPG, Biotinyl CAP PE and DOPE were prepared in a 6: 3: 0.9: 0.1 molar ratio. For all lipid mixes, to ensure full evaporation of chloroform, mixtures were placed in a vacuum-sealed desiccator for at least 2 h. Inside a glove box (right before encapsulation experiments) 37.5 μL of decane (TCI Deutschland GmbH, Germany) was added to the dried lipid film and, once dissolved, 1 mL mineral oil (Carl Roth GmbH, Germany) was added and the lipid-oil suspension vigorously vortexed until a clear solution was obtained. For phase-separated vesicles, the lipid mix used was DOPC: DOPG: DPPC: DPPG: Chol (17.5: 7.5: 31.5: 13.5: 30) labeled with 0.001 mol% ATTO-655 DOPE binding to the Ld phase. The lipid mix (3.2 mM) was dissolved in chloroform and dried in a glass vial under N_2 flow for ~15 minutes. The dried film was then suspended in a mixture of decane (20 μL) and mineral oil (480 μL) and sonicated at elevated temperatures for ~30 minutes. Both single single-phase and phase-separated GUVs were produced with the double emulsion transfer method following a recently reported protocol for vesicle generation with purified proteins in 96 well-plates[9,71]. To ensure iso-osmolar conditions between the inside and outside of GUVs, the osmolarity of inner encapsulating solutions was measured with a osmometer (Fiske Micro-Osmometer model 120, Fiske Associates, Norwood, MA, USA) and outer glucose solutions with matching osmolarities were used as outer aqueous environment where GUVs are collected after production for subsequent imaging. The density of the inner mixture depends on the experimental conditions tested but to generate all the vesicles here reported we centrifuged well-plates at 600 × *g* for 10 min. In the case of single-phase vesicles centrifugation was performed at RT. For phase-separated GUVs, well-plates were centrifuged at 37 °C and the sample was allowed to cool to RT for ~30 min before imaging.

Encapsulation of the system in single and double-phase GUVs

Depending on the experimental conditions tested, the final concentrations of the proteins varied but the procedure remained the same. All the steps were performed on ice except for the final encapsulation on 96 well-plates. First, we prepared a 35 μM actin mix (A-Mix) comprised of 86% G-actin, 10% ATTO647-actin and 4% biotinylated actin in water. Once we were ready to encapsulate, we prepared the following inner reaction mix: 4% OptiPrep™, 0.01 g/L Neutravidin, 10 g/L BSA, 10-50 g/L Ficoll70, 3-3.2 MinD (70% His-MinD, 30% EGDP-MinD), 1.6-3 MinE, 1.5-4 μM Actin (from the A-Mix), 0.3-2 μM fascin, 0-0.05 μM Myosin and 5 mM ATP (frozen stocks supplemented with 5 mM $MgCl_2$) in a final buffer concentration of 50 mM KCl, 10 mM Tris-HCl and 5 mM $MgCl_2$. To ensure no pre-polymerization, bundling or contraction of actin occurs prior encapsulation, actin, fascin, myosin and ATP were added in that order seconds before generating the vesicles via centrifugation.

Fluorescence microscopy

Imaging of vesicles was performed on a LSM800 confocal laser scanning microscope using a C-Apochromat 40 × /1.2 water-immersion objective (Carl Zeiss, Germany). Fluorophores were excited using diode-pumped solid-state lasers: 488 nm (EGFP-MinD) and 640 nm (ATTO647-Actin).

Image analysis

Processing and analysis of all acquired images were conducted using Fiji (v1.53f51)[72], a custom-written script in MATLAB (R2022a) and OriginPro (2021b), the latter also being used for plotting datasets. Z-Stacks were reconstructed in Fiji using the Standard Deviation Z-Projection. For kymographs, the Multi Kymograph function was used and ROIs were drawn manually following the GUVs' fluorescence intensity at their equatorial cross section with the free-hand selection, fitting them to splines before kymograph retrieval. For aspect ratio calculations, Fig. 2a, b and Supplementary Fig. 4a GUVs were traced by hand using the free-hand selection and major and minor axes were retrieved from Fiji measurements. For Fig. 2c, all time frames from the EGFP channel were processed first with a Gaussian filter of radius 1 and then Otsu-thresholded (frames where GUV contours where incorrectly thresholded were discarded). After filling holes, ROIs retrieved from the particle analyzer were fitted to an ellipse to measure the major and minor axes. Intensity profiles in Fig. 3b were obtained applying the Plot Profile Fiji function to segmented lines after being fitted to splines. For the waterfall 3D plot in Supplementary Fig. 5b, a 5 μm intensity line-plot at the bleb was drawn in Fiji to obtain fluorescence intensity values at six different time points. The data were plotted in Origin using the 3D waterfall plot. In Fig. 3d, curvatures were calculated by drawing ROI circles fitting the blebs and retrieving radii measurements from Fiji.

Analysis and quantification of actomyosin phenotypes inside GUVs

For Fig. 1c, data for both fascin/actin molar ratios studied were obtained by acquiring Z-stacks of 3 separate experiments (triplicates for presence and absence of Min proteins) after Min oscillation decay for those where Min proteins were added. 150 GUVs of different sizes taken from these 3 experimental runs were pooled and analyzed together. Those presenting encapsulated actin bundles were classified into four categories (rings, asters, stiff-straight bundles and soft webs) by analyzing the acquired Z-stacks and their Standard Deviation Z-Projection. GUV diameters were obtained by manually drawing circle ROIs at the vesicle equator and vesicles were grouped into 4 categories according to their size. GUVs with no actin assemblies inside were not considered for the analysis. Frequencies were calculated from the number of vesicles belonging to each actin-assembly category and the total number of pooled GUVs analyzed per condition (150 vesicles). Datasets were normalized using the total number of vesicles analyzed

in each size group. For Supplementary Fig. 1a, three independent experiments were perfomed with a total of 336 GUVs analyzed per experimental run (GUVs analyzed per timepoint = 112). GUVs with a diameter above 25 μm were not considered for the analysis. To be rigorous on the time, 1 hour was considered as the first timepoint as it takes ~20 min for vesicle production and ~30 min to complete the acquisition of a high-resolution Tilescan in 3D. Samples were kept at 20 °C and later imaged at 7 and 24 h.

Analysis of MinDE-induced folding of actin bundles

To quantify the angle between the two bundle ends attached to the vesicle membrane, the equator of the ATTO647-Actin channel was taken, and this time-series segmented using the "Moments" threshold method. To automatically detect both bundle ends as features and track their position over time, the Fiji plugin 'TrackMate' was employed[73]. The LoG detector was configured with threshold 7, radius 6 px, median filtering, and subpixel localization. Coordinates of the spots detected (two per time frame corresponding to the bundle ends) were obtained with TrackMate's Simple LAP tracker using the following settings: linking max distance 1 px, gap-closing max distance 15 px, gap-closing max frame gap 1. The angles between the two bundle ends over time were obtained with a MATLAB custom script taking spot coordinates as vector with the vesicle's center point as origin.

Statistics & reproducibility

Sample sizes for vesicle classification were not predetermined prior to experiments. The sample size was chosen from a standard number relevant for the field and taken from at least three independent replicates (total number of GUVs analyzed per experimental run between 150 and 336, number specified in each figure caption). Employing this sample size for vesicle classification allowed actin morphologies to be clearly distinguished and classified with sufficient representation. Exclusion criteria was pre-established before data analysis. Vesicles containing two different actin phenotypes in their lumen and vesicles with encapsulated lipid or protein aggregates were excluded to ensure that only high quality GUV data was employed in this study. Empty vesicles were not taken into consideration for Fig. 1c but we analyzed their frequency in Supplementary Fig. 1b.

For actin phenotype classification in Fig. 1c, three independent experimental replicates were performed for each condition and GUVs from these replicates were pooled together for their analysis. For Supplementary Fig. 1b, three independent experimental runs were performed, with a total of 336 GUVs analyzed per experimental run (GUVs analyzed per timepoint = 112). All qualitative data in the form of microscopy images were replicated with at least ten independent experiments for each protein molar ratio specified. From these experiments ($n = 25$) diffusiophoresis, blebbing and membrane deformations were observed on many different vesicles from different experimental runs confirming their reproducibility. The vesicles with the most notable effects were then chosen for the analysis. For phase separation experiments, three independent control experiments were performed. For the encapsulation of actomyosin with Min proteins inside phase-separated vesicles, five independent encapsulation experiments were performed and similar results observed. Finally, the experiments were not randomized and the investigators were not blinded to allocation during experients and outcome assessment.

Reporting summary

Further information on research design is available in the Nature Portfolio Reporting Summary linked to this article.

Data availability

All data sets supporting the findings of this study are provided in the Source Data file. The Source Data have been deposited in the Figshare database under accession code: https://doi.org/10.6084/m9.figshare.26893822[74]. Due to large file size, the original acquired images and timelapse videos are freely available upon access request. This access can be obtained by contacting the corresponding author, who will aim to process requests within a week. Source data are provided with this paper.

Code availability

The custom MATLAB script employed to calculate the folding angle of actin rings over time is available with full access in the GitHub repository: https://github.com/MariaReverteLopez/Ring-Folding-Analysis-inside-GUVs.

References

1. Hirschi, S., Ward, T. R., Meier, W. P., Müller, D. J. & Fotiadis, D. Synthetic biology: bottom-up assembly of molecular systems. *Chem. Rev.* **122**, 16294–16328 (2022).
2. Lee, K. Y. et al. Photosynthetic artificial organelles sustain and control ATP-dependent reactions in a protocellular system. *Nat. Biotechnol.* **36**, 530–535 (2018).
3. Miller, T. E. et al. Light-powered CO2 fixation in a chloroplast mimic with natural and synthetic parts. *Science* **368**, 649–654 (2020).
4. Gadok, A. K. et al. Connectosomes for direct molecular delivery to the cellular cytoplasm. *J. Am. Chem. Soc.* **138**, 12833–12840 (2016).
5. Litschel, T. & Schwille, P. Protein reconstitution inside giant unilamellar vesicles. *Annu. Rev. Biophys.* **50**, 525–548 (2021).
6. Schwille, P. et al. MaxSynBio: avenues towards creating cells from the bottom up. *Angew. Chem. Int. Ed.* **57**, 13382–13392 (2018).
7. Kretschmer, S., Ganzinger, K. A., Franquelim, H. G. & Schwille, P. Synthetic cell division via membrane-transforming molecular assemblies. *BMC Biol.* **17**, 43 (2019).
8. Rivas, G., Vogel, S. K. & Schwille, P. Reconstitution of cytoskeletal protein assemblies for large-scale membrane transformation. *Curr. Opin. Chem. Biol.* **22**, 18–26 (2014).
9. Kohyama, S., Merino-Salomón, A. & Schwille, P. In vitro assembly, positioning and contraction of a division ring in minimal cells. *Nat. Commun.* **13**, 6098 (2022).
10. Baldauf, L., van Buren, L., Fanalista, F. & Koenderink, G. H. Actomyosin-driven division of a synthetic cell. *ACS Synth. Biol.* **11**, 3120–3133 (2022).
11. Green, R. A., Paluch, E. & Oegema, K. Cytokinesis in animal cells. *Annu. Rev. Cell Dev. Biol.* **28**, 29–58 (2012).
12. O'Shaughnessy, B. & Thiyagarajan, S. Mechanisms of contractile ring tension production and constriction. *Biophys. Rev.* **10**, 1667–1681 (2018).
13. Kučera, O. et al. Anillin propels myosin-independent constriction of actin rings. *Nat. Commun.* **12**, 4595 (2021).
14. Miyazaki, M., Chiba, M., Eguchi, H., Ohki, T. & Ishiwata, S. Cell-sized spherical confinement induces the spontaneous formation of contractile actomyosin rings in vitro. *Nat. Cell Biol.* **17**, 480–489 (2015).
15. Litschel, T. et al. Reconstitution of contractile actomyosin rings in vesicles. *Nat. Commun.* **12**, 2254 (2021).
16. Bashirzadeh, Y., Moghimianavval, H. & Liu, A. P. Encapsulated actomyosin patterns drive cell-like membrane shape changes. *iScience* **25**, 104236 (2022).
17. Ramm, B. et al. A diffusiophoretic mechanism for ATP-driven transport without motor proteins. *Nat. Phys.* **17**, 850–858 (2021).
18. Reverte-López, M. et al. Protein-based patterning to spatially functionalize biomimetic membranes. *Small Methods* **7**, 2300173 (2023).
19. Gavrilović, S., Brüggenthies, G. A., Weck, J. M., Heuer-Jungemann, A. & Schwille, P. Protein-assisted large-scale assembly and differential patterning of DNA origami lattices. *Small* **20**, 2309680 (2024).

20. Ramm, B., Heermann, T. & Schwille, P. TheE. coli MinCDE system in the regulation of protein patterns and gradients. *Cell Mol. Life Sci.* **76**, 4245–4273 (2019).
21. Ramm, B. et al. The MinDE system is a generic spatial cue for membrane protein distribution in vitro. *Nat. Commun.* **9**, 3942 (2018).
22. Renner, L. D. & Weibel, D. B. MinD and MinE interact with anionic phospholipids and regulate division plane formation in Escherichia coli*. *J. Biol. Chem.* **287**, 38835–38844 (2012).
23. Vecchiarelli, A. G., Li, M., Mizuuchi, M. & Mizuuchi, K. Differential affinities of MinD and MinE to anionic phospholipid influence Min patterning dynamics in vitro. *Mol. Microbiol.* **93**, 453–463 (2014).
24. Rashid, R., Chee, S. M. L., Raghunath, M. & Wohland, T. Macromolecular crowding gives rise to microviscosity, anomalous diffusion and accelerated actin polymerization. *Phys. Biol.* **12**, 034001 (2015).
25. Gao, M. & Winter, R. Kinetic insights into the elongation reaction of actin filaments as a function of temperature, pressure, and macromolecular crowding. *ChemPhysChem.* **16**, 3681–3686 (2015).
26. Bashirzadeh, Y. et al. Actin crosslinker competition and sorting drive emergent GUV size-dependent actin network architecture. *Commun. Biol.* **4**, 1–11 (2021).
27. Litschel, T., Ramm, B., Maas, R., Heymann, M. & Schwille, P. Beating vesicles: encapsulated protein oscillations cause dynamic membrane deformations. *Angew. Chem. Int Ed. Engl.* **57**, 16286–16290 (2018).
28. Park, J. et al. Crowding tunes the organization and mechanics of actin bundles formed by crosslinking proteins. *FEBS Lett.* **595**, 26–40 (2021).
29. Quinn, S. D. et al. Crowding-induced morphological changes in synthetic lipid vesicles determined using smFRET. *Front Bioeng. Biotechnol.* **10**, 958026 (2022).
30. Lipowsky, R. Remodeling of membrane shape and topology by curvature elasticity and membrane tension. *Adv. Biol.* **6**, 2101020 (2022).
31. Fu, M., Franquelim, H. G., Kretschmer, S. & Schwille, P. Non-equilibrium large-scale membrane transformations driven by MinDE biochemical reaction cycles. *Angew. Chem. Int. Ed.* **60**, 6496–6502 (2021).
32. Baumgart, T., Hess, S. T. & Webb, W. W. Imaging coexisting fluid domains in biomembrane models coupling curvature and line tension. *Nature* **425**, 821–824 (2003).
33. Baumgart, T., Das, S., Webb, W. W. & Jenkins, J. T. Membrane elasticity in giant vesicles with fluid phase coexistence. *Biophys. J.* **89**, 1067–1080 (2005).
34. Dreher, Y., Jahnke, K., Bobkova, E., Spatz, J. P. & Göpfrich, K. Division and regrowth of phase-separated giant unilamellar vesicles. *Angew. Chem. Int. Ed.* **60**, 10661–10669 (2021).
35. Liu, A. P. & Fletcher, D. A. Actin polymerization serves as a membrane domain switch in model lipid bilayers. *Biophysical J.* **91**, 4064–4070 (2006).
36. Honigmann, A. et al. A lipid bound actin meshwork organizes liquid phase separation in model membranes. *eLife* **3**, e01671 (2014).
37. Vogel, S. K., Greiss, F., Khmelinskaia, A. & Schwille, P. Control of lipid domain organization by a biomimetic contractile actomyosin cortex. *eLife* **6**, e24350 (2017).
38. Bacia, K., Schwille, P. & Kurzchalia, T. Sterol structure determines the separation of phases and the curvature of the liquid-ordered phase in model membranes. *Proc. Natl Acad. Sci. Usa.* **102**, 3272–3277 (2005).
39. Cullis, P. R., Hope, M. J. & Tilcock, C. P. S. Lipid polymorphism and the roles of lipids in membranes. *Chem. Phys. Lipids* **40**, 127–144 (1986).
40. Schweizer, J. et al. Geometry sensing by self-organized protein patterns. *Proc. Natl Acad. Sci. USA* **109**, 15283–15288 (2012).
41. Wu, F., van Schie, B. G. C., Keymer, J. E. & Dekker, C. Symmetry and scale orient Min protein patterns in shaped bacterial sculptures. *Nat. Nanotechnol.* **10**, 719–726 (2015).
42. Ganzinger, K. A. et al. FtsZ reorganization facilitates deformation of giant vesicles in microfluidic traps. *Angew. Chem. Int Ed. Engl.* **59**, 21372–21376 (2020).
43. Bridges, A. A., Jentzsch, M. S., Oakes, P. W., Occhipinti, P. & Gladfelter, A. S. Micron-scale plasma membrane curvature is recognized by the septin cytoskeleton. *J. Cell Biol.* **213**, 23–32 (2016).
44. Czogalla, A. et al. Amphipathic DNA origami nanoparticles to scaffold and deform lipid membrane vesicles. *Angew. Chem. Int. Ed.* **54**, 6501–6505 (2015).
45. Franquelim, H. G., Khmelinskaia, A., Sobczak, J.-P., Dietz, H. & Schwille, P. Membrane sculpting by curved DNA origami scaffolds. *Nat. Commun.* **9**, 811 (2018).
46. Le Roux, A.-L. et al. Dynamic mechanochemical feedback between curved membranes and BAR protein self-organization. *Nat. Commun.* **12**, 6550 (2021).
47. Pontani, L.-L. et al. Reconstitution of an actin cortex inside a liposome. *Biophys. J.* **96**, 192–198 (2009).
48. Simon, C. et al. Actin dynamics drive cell-like membrane deformation. *Nat. Phys.* **15**, 602–609 (2019).
49. Sedzinski, J. et al. Polar actomyosin contractility destabilizes the position of the cytokinetic furrow. *Nature* **476**, 462–466 (2011).
50. Schwille, P. & Frohn, B. P. Hidden protein functions and what they may teach us. *Trends Cell Biol.* **32**, 102–109 (2022).
51. Fu, M. et al. Mechanochemical feedback loop drives persistent motion of liposomes. *Nat. Phys.* **19**, 1211–1218 (2023).
52. Godino, E. et al. De novo synthesized Min proteins drive oscillatory liposome deformation and regulate FtsA-FtsZ cytoskeletal patterns. *Nat. Commun.* **10**, 4969 (2019).
53. Derganc, J. & Čopič, A. Membrane bending by protein crowding is affected by protein lateral confinement. *Biochimica et. Biophysica Acta (BBA) - Biomembranes* **1858**, 1152–1159 (2016).
54. Mazor, S. et al. Mutual effects of MinD–membrane interaction: I. changes in the membrane properties induced by MinD binding. *Biochimica et. Biophysica Acta (BBA) - Biomembranes* **1778**, 2496–2504 (2008).
55. Zhou, H. & Lutkenhaus, J. Membrane binding by MinD involves insertion of hydrophobic residues within the C-terminal amphipathic helix into the bilayer. *J. Bacteriol.* **185**, 4326–4335 (2003).
56. Stachowiak, J. C. et al. Membrane bending by protein–protein crowding. *Nat. Cell Biol.* **14**, 944–949 (2012).
57. Hu, Z., Gogol, E. P. & Lutkenhaus, J. Dynamic assembly of MinD on phospholipid vesicles regulated by ATP and MinE. *Proc. Natl Acad. Sci.* **99**, 6761–6766 (2002).
58. Miyagi, A., Ramm, B., Schwille, P. & Scheuring, S. High-speed atomic force microscopy reveals the inner workings of the MinDE protein oscillator. *Nano Lett.* **18**, 288–296 (2018).
59. Jarsch, I. K., Daste, F. & Gallop, J. L. Membrane curvature in cell biology: an integration of molecular mechanisms. *J. Cell Biol.* **214**, 375–387 (2016).
60. Christ, S., Litschel, T., Schwille, P. & Lipowsky, R. Active shape oscillations of giant vesicles with cyclic closure and opening of membrane necks. *Soft Matter* **17**, 319–330 (2021).
61. Tamemoto, N. & Noguchi, H. Pattern formation in reaction–diffusion system on membrane with mechanochemical feedback. *Sci. Rep.* **10**, 19582 (2020).
62. Busch, D. J. et al. Intrinsically disordered proteins drive membrane curvature. *Nat. Commun.* **6**, 7875 (2015).
63. Derganc, J. & Antonny, B. & Čopič, A. Membrane bending: the power of protein imbalance. *Trends Biochemical Sci.* **38**, 576–584 (2013).
64. Shi, Z. & Baumgart, T. Dynamics and instabilities of lipid bilayer membrane shapes. *Adv. Colloid Interface Sci.* **208**, 76–88 (2014).

65. Ye, W. et al. Plasmonic nanosensors reveal a height dependence of MinDE protein oscillations on membrane features. *J. Am. Chem. Soc.* **140**, 17901–17906 (2018).
66. Weirich, K. L., Stam, S., Munro, E. & Gardel, M. L. Actin bundle architecture and mechanics regulate myosin II force generation. *Biophysical J.* **120**, 1957–1970 (2021).
67. Sakamoto, T., Limouze, J., Combs, C. A., Straight, A. F. & Sellers, J. R. Blebbistatin, a Myosin II Inhibitor, Is Photoinactivated by Blue Light. *Biochemistry* **44**, 584–588 (2005).
68. Schuppler, M., Keber, F. C., Kröger, M. & Bausch, A. R. Boundaries steer the contraction of active gels. *Nat. Commun.* **7**, 13120 (2016).
69. Loose, M., Fischer-Friedrich, E., Ries, J., Kruse, K. & Schwille, P. Spatial regulators for bacterial cell division self-organize into surface waves in vitro. *Science* **320**, 789–792 (2008).
70. Ramm, B., Glock, P. & Schwille, P. In vitro reconstitution of self-organizing protein patterns on supported lipid bilayers. *J. Vis. Exp.* https://doi.org/10.3791/58139 (2018).
71. Pautot, S., Frisken, B. J. & Weitz, D. A. Engineering asymmetric vesicles. *Proc. Natl Acad. Sci.* **100**, 10718–10721 (2003).
72. Schindelin, J. et al. Fiji: an open-source platform for biological-image analysis. *Nat. Methods* **9**, 676–682 (2012).
73. Ershov, D. et al. TrackMate 7: integrating state-of-the-art segmentation algorithms into tracking pipelines. *Nat. Methods* **19**, 829–832 (2022).
74. Reverte-López, M. et al. Self-organized spatial targeting of contractile actomyosin rings for synthetic cell division Dataset. figshare https://doi.org/10.6084/m9.figshare.26893822 (2024).

Acknowledgements

The authors would like to thank the MPIB Core Facility for assistance in protein purification, Michaela Schaper for plasmid cloning, Kerstin Röhrl for protein purification, Sandra Ortmeier for lipid preparations and Sigrid Bauer for her advice on vesicle formation and unconditional scientific support. The authors would also like to thank Jan-Hagen Krohn for assistance in confocal microscopy, as well as Adrián Merino-Salomón and Shunshi Kohyama for helpful discussions on crowder conditions and protein encapsulation. For insightful discussions on the mechanism behind vesicle blebbing, the authors would like to thank Prof. Erwin Frey, Dr. Henri Franquelim, Dr. Ivan Maryshev and Henrik Weyer. This work was supported by the Deutsche Forschungsgemeinschaft (P.S. and M.J.). Y.Q. received funding from the European Union's Horizon 2020 research and innovation programme under the Marie Skłodowska-Curie grant agreement no. 859416. M.R.-L., Y.Q. and V.B are part of IMPRS-ML, and M.R.-L. is part of the ONE MUNICH Project supported by the Federal Ministry of Education and Research (BMBF) as well as the Free State of Bavaria under the Excellence Strategy of the Federal Government and the Länder. The authors would also like to acknowledge the support of the Center for Nanoscience (CeNS), Munich.

Author contributions

M.R.-L. and P.S. conceived the study. M.R.-L. designed and performed encapsulation experiments, analyzed data and interpreted results. N.K and M.R.-L. designed and carried out phase-separation experiments. M.R.-L and Y.Q analyzed blebbing vesicles. V.B. assisted with the supplementary experiments. M.J. provided technical advice on protein conditions for encapsulation. M.R.-L. and P.S. wrote the manuscript and all authors revised and approved the final version of the manuscript.

Funding

Open Access funding enabled and organized by Projekt DEAL.

Competing interests

The authors declare no competing interests.

Additional information

Supplementary information The online version contains supplementary material available at https://doi.org/10.1038/s41467-024-54807-9.

Correspondence and requests for materials should be addressed to Petra Schwille.

Peer review information *Nature Communications* thanks the anonymous reviewers for their contribution to the peer review of this work. A peer review file is available.

4 Discussion

In this thesis, I describe my contributions to the field of synthetic biology, more specifically to the efforts towards the reconstitution of an artificial cell capable of division. By adhering to a multidisciplinary approach, I employed a diverse assortment of technologies and methods that allowed me to show the applicability of biochemical findings across disciplines. From 3D-printing of microstructures employing 2PP lithography to the production of vesicular systems via encapsulation methods, the research presented here showcases a wide variety of *in vitro* reconstituted models and the technologies involved in their study and integration.

While collaborating with Dr. Adrián Merino Salomón and Svetozar Gavrilovic (publication P1), the fabrication of microswimmer-like robotic structures allowed us to explore the use of the MinDE system as a micropatterning tool for biomedically-relevant microcarrier technologies. Through surface chemistry modifications and the alteration of MinDE dynamics with crowding agents, we demonstrated that this bacterial protein system can be employed as a benign positioning module for the functionalization of microswimmer surfaces and cargo-delivery systems like giant vesicles with bioactive molecules.

Confirming the robustness of this MinDE positioning module, I then set out to harness its capabilities to provide an alternative solution for the control of actomyosin-based division rings inside vesicles. The positioning of eukaryotic-based synthetic rings via MinDE oscillations demonstrated in publication P2 marks an important milestone for this synthetic division approach. The spatiotemporal control of myosin-driven forces at the equator yielded vesicles with mid-cell deformations, providing an example of a self-assembled and self-organized system with no external aid for contractile ring localization. Furthermore, by doing so, I have addressed one of the current challenges in the synthetic biology field: the design of a system from the modular assembly of independent components which exhibit singular functions both separately and co-reconstituted inside cellular mimics. In agreement with the field's predictions regarding the combination and integration of synthetic modules, closer inspection of the reconstituted system uncovered emergent behaviours arising from MinDE oscillations, such as the outward deformation of vesicles and the remodelling of phase-separated lipid domains.

In the following sections, I will discuss the two studies included in this thesis in detail, with particular emphasis on the new questions this research has unveiled and the potential future avenues to overcome some of the new challenges posed.

4.1 Beyond *in vivo* functions: applications of the MinDE system as a micropatterning tool

Studying the mechanistic intricacies of the MinDE system has enabled the in-depth characterization of its properties and features. The more we uncover, the greater our inventiveness is incited. One clear example is the study by Heeermann *et al.* [345]. Utilizing MinDE protein pattern formation as a visual readout for biomolecular interaction screening, this study evidences how exploiting an apparently trivial protein system can yield applications beyond its *in vivo* context.

Besides its use as a generic sensor, in publication P1, we show another potential application of the MinDE system: its use as a micropatterning and positioning tool. In the fabrication of microactuators and microcarriers for biomedical purposes such as diagnostics and active drug delivery, researchers currently struggle to develop strategies to increase their chemical versatility and expand their functions. To enrich printed structures and liposomes with new capabilities that could translate into novel applications, some of the developed methods for surface functionalization rely on complex and limiting approaches. On the one hand, although current optical and chemical patterning techniques for 3D-printed microswimmers offer simultaneous and post-fabrication surface modifications, the margin for improvement and refinement is still ample. Some of these approaches involve light-addressed spatial activation of a photoresist mixed with the reaction moieties to be patterned, which limits the selection of functional biomolecules to those resistant to photodamage and also requires custom laser setups and specific polymer base precursors [346, 347]. On the other hand, conjugation methods to decorate microcarriers like liposomes still require further development. Although their cell-membrane coating can engage in biomimicry and biofouling functions via affinity-ligand anchoring, the controlled topological distribution and asymmetric density arrangement of molecules for applications like T-cell activation remains a challenging feat [348, 349].

In this regard, identifying this gap in patterning technology led us to investigate whether Min proteins could spatiotemporally control molecules on the surface of these microcarrier systems. To this end, employing the surface functionalization approach developed by Eto *et al.* [135], we 3D-printed microswimmer-like robots, coated their surface with lipid bilayers, and demonstrated that quasi-stationary MinDE patterns can position bioactive molecules and tethered PEG chains via diffusiophoresis. Given that this is a post-printing type of functionalization, we showed that Min proteins offer a versatile way to design and

use microrobot surfaces. For instance, due to their ability to non-specifically sort cargo molecules, simultaneous multi-patterning with several biomolecules can be achieved [350]. Conversely, if sequential patterning in controlled steps is required, or MinDE removal is needed, experiments performed with Svetozar Gavrilovic demonstrated that crosslinking of reactive biomolecules (e.g., DNA origami) before MinDE washing provides stable and long-lasting biomolecule patterns, which remain unaltered for at least 24 hours (see Appendix III, Figure III.1). Moreover, if anti-correlated patterns of two distinct molecules are desired, conjugation of one of the molecules to the MinD-binding sequence of MinC (residues RSGQ in *E.coli*) could allow its transport to areas of high MinD density.

Similarly to other studies performed on SLBs, we observed that some of the molecules employed as cargo had a distinct "narrowing" effect on the MinDE patterns formed on our microswimmer structures. In particular, the crowding agent PEG had the most significant impact on the distribution and distance between MinD maxima (also termed as pattern sharpening). Although this is expected from membrane-bound molecules with high effective size (high membrane footprint) [334], recent studies have now started to investigate the underlying mechanism by which diffusiophoretic transport affects reaction-diffusion systems. More specifically, the model parameters and conditions behind the diffusiophoretic sharpening of Turing patterns [351]. Thus, our 3D-printed membrane models could provide an additional platform to carefully study this phenomenon *in vitro* and complement simulation and numerical models.

Furthermore, high-resolution printing of microstructures through 2PP and their surface chemistry functionalization with lipids are two emerging technologies suitable for the in-depth study of protein systems and their geometry-sensing properties. Interestingly, this is the case of Min proteins. As shown by past studies employing confined 3D systems and reconstituted 2D membranes, Min proteins have cell geometry detection mechanisms, and not only do they sense 3D shape, buy they also adapt to it [121, 314]. Therefore, studying the effect of varying 3D geometries on quasi-stationary Turing patterns and their diffusiophoretic transport of molecules might provide further insights into their self-organization principles. Indeed, when I performed patterning experiments on complex microstructures of varying curvatures and topologies, MinE minima aligned at concave (negatively curved) groove regions (see Appendix III, Figure III.2b). More precisely, MinE densities appeared to follow the circumferential shape of the 3D structure, creating concentric circles in deep and wide concave regions. Although a thorough analysis of these phenomena will require the use of computational models to describe MinDE self-organization dynamics, these preliminary experiments confirm cargo patterning on other complex 3D structures and showcase their potential application for future geometry-sensing studies.

Finally, together with microswimmers, we also achieved the formation of quasi-stationary Turing patterns inside GUVs, which enabled the patterning of MTS-bound FtsZ-mCherry bundles into spot or mesh distributions. The key to the formation of such patterns was the encapsulation of the crowding agent Dextran70 at high concentration (100 g/L). Studies

on the effect of BSA and other crowding molecules have previously revealed that their addition to *in vitro* reconstituted assays has a direct effect on MinDE dynamics [352, 305]. Indeed, the wavelength and wave velocity of MinDE dynamic patterns decrease, and the transmission of lateral spatiotemporal information appears to be impaired [335, 122]. As suggested by these findings, depletion forces and the increase in solution viscosity induced by crowding agents might change the reaction rate and diffusion constants of Min proteins at the membrane and alter the protein gradients formed in the bulk [122]. Therefore, the quasi-stationary patterns observed in P1 may arise from crowding-mediated effects on MinDE diffusivity and reaction kinetics, which facilitated the stable positioning of FtsZ-mCherry-mts filaments (a cargo with high diffusivity and low membrane footprint) on the inner leaflet of vesicles.

4.2 The MinDE positioning module as a stepping stone for actomyosin-based synthetic division

In the development of a contractile module for synthetic division, the reconstitution of actomyosin architectures promptly revealed a missing piece. If contractile rings or actin cortices were not correctly localized at the vesicle equator, myosin-driven forces did not yield membrane furrowing. For instance, light-mediated pole relaxation of cortices was required to stably deform liposomes at their centre, and external addition of vesicle-shaping components was needed to localize membrane-remodelling proteins like dynamin A [271, 342, 353]. Accordingly, if contractile forces are globally initiated, a tug-of war effect unfolds and a cleavage furrow forms slowly and asymmetrically [271]. Thus, in this thesis, I set out to reconcile this predicament and provide an alternative solution that does not rely on external devices and effectors.

By exploiting the MinDE system as an already consolidated patterning tool, in publication P2 I showed that actomyosin rings can be spatiotemporally controlled and positioned at mid-cell. The MinDE diffusiophoresis-driven transport of biotin molecules at the inner leaflet of vesicles reorganized actomyosin bundles and yielded centred rings. Indeed, the combination of a self-organized system (MinDE) with a contractile structure (actomyosin rings) rendered the dynamic spatial control of forces within minimal cells. These results therefore demonstrate a successful co-reconstitution of two modules working as an ensemble towards a set purpose: synthetic division.

Since MinDE oscillations sense the 3D geometry of the compartment and align to its longest axis, MinDE pole-to-pole patterns constitute an ideal tool to maintain ring localization while vesicle deformation takes place [314]. Moreover, given the importance of tension redistribution inside dividing cells, this work demonstrates that the MinDE system can become a generic positioning module for synthetic cells containing contractile systems

of different nature. As I will discuss in section 4.4, the reconstitution of a eukaryotic-based division machinery presents many challenges due to its complexity. Owing to these setbacks, many research groups have turned to the development of other synthetic cytoskeletal-mimic systems based on peptide filaments, DNA origami, or polydiacetylenes fibrils [354, 355, 356, 357]. MinDE diffusiophoretic transport could therefore be co-reconstituted with these systems to achieve the spatiotemporal control of cytoskeletal architectures at the membrane and aid in their application as potential contractile modules. Concurrently, the bacterial approach to synthetic division has shown promising results. Aiming at the reconstitution of a minimal set of bacterial components for the formation of a contractile FtsZ ring, the Min system is being employed both as a ring assembly agent (via MinC depolymerization of FtsZ) and a positioning tool (via diffusiophoresis). However, together with Min proteins, further experiments will be required to demonstrate that FtsZ rings can effectively generate the forces enabling minimal cell division.

Taken together, the results presented in publication P2 demonstrate that the MinDE system can be combined with actomyosin contractile structures to develop a synthetic division machinery. Previous mathematical models already pointed to the feasibility of this modular approach for assembling dividing *in silico* protocells. As described by Schneider and colleagues, synchronization of a contractile module with a positioner building block provides the starting functionalities required for a synthetic cell to divide [358, 58]. Thus, this thesis realizes, through *in vitro* experimental work, the modular assembly projected by these theoretical studies. Nevertheless, as I will discuss in section 4.5, we will need to incorporate many other regulatory and complementary components to mend the current deficiencies accompanying the eukaryotic-based division approach.

4.3 The modular assembly of artificial cells unveils synergistic protein interactions and hidden functions

The first step in the co-reconstitution of MinDE oscillations with actomyosin rings consisted in optimizing the encapsulating conditions. These two protein systems, found in different life domains, require particular salt concentrations, divalent cations, and negatively charged lipids to showcase canonical behaviour. Optimization of such conditions, however, led to surprising behaviours initially not predicted.

Firstly, when I investigated the fraction of GUVs containing single actomyosin rings, vesicles comprising MinDE oscillations showed an increase in ring formation frequency in comparison to their MinDE-deficient counterparts. In short, Min oscillations did not impair fascin-mediated bundling of actin at the membrane and, in contrast, seemed to aid in

the assembly of actin bundles into singular rings. This finding thus suggests a synergistic effect arising from their combinatorial ensemble, which provided a benefit to the overall purpose of the system.

However, I also observed other striking effects. Some membrane-bound actomyosin rings and networks underwent bending and collapsed in the presence of MinDE circling and chaotic patterns. In addition, as MinDE waves travelled on the inner leaflet of the vesicles, these bent or collapsed cytoskeletal structures appeared to be "swept " in various directions ahead of MinDE oscillations. Although fascin bundles are relatively stiff supramolecular structures[1], these results may also point to MinDE-driven diffusiophoresis as the mechanism behind these topological transformations. Specifically, the frictional coupling between biotin-anchored fascin bundles and Min proteins might induce the bending of bundles on the membrane and their transport based on Min pattern direction.

Interestingly, when I analysed vesicles simultaneously containing actomyosin networks and MinDE chaotic oscillations, I observed an intriguing phenomenon: the outward blebbing of GUVs. The actomyosin bundles, demarcating the vesicle membrane into partitioned areas, became lateral diffusion barriers for Min proteins. As a result, MinDE oscillations turned chaotic due to the loss of 3D symmetry, and Min binding to these bundled-delimited areas induced outward membrane protrusions reminiscent of bleb morphologies [360]. A closer analysis of these blebs suggests that MinDE binding is crucial for their emergence, since bleb growth is concomitant with an increase in EGFP-MinD fluorescence intensity. Further quantification of the extent of membrane deformation showed that MinDE binding generated protrusions which either increased or decreased local membrane curvature. Indeed, within the same vesicle MinDE oscillations generated small blebs with highly curved membrane surface, as well as larger deformations extending the vesicle membrane and thus losing sphericity. Moreover, the encapsulation of the system inside phase-separated GUVs revealed similar bleb-like bulging of Ld domains. In collaboration with Dr. Nishu Kanwa, we constrained MinDE oscillation to Ld domains and observed that Min proteins can also transiently deform them, triggering the global remodelling of domains on the bilayer.

MinDE-driven deformations of lipid membranes have already been described in the literature. In osmotically deflated vesicles, Litschel *et al.* reported that MinDE pulsing patterns induced extensive deformations, decreasing the intrinsic spontaneous curvature of the vesicle membrane upon protein attachment [338]. Moreover, Fu *et al.* showed periodic membrane spreading/pulling by MinDE membrane attachment cycles and provided further evidence that MinE is required for such deformations [361]. Although another lab reproduced and confirmed these membrane remodelling events [339], the underlying mechanism behind MinDE-driven membrane deformations remains opaque. Some authors have hypothesized that the observed deformations might arise from an increase in local viscosity

[1] bending stiffness of fascin bundles in the presence of 5–20% w/w Ficoll70: $\kappa_B = 2.3\text{–}3.9 \times 10^{-25}$ N·m^2 [359]

mediated by Min proteins or from the insertion of their amphipathic helix (MTS domain) into the lipid bilayer, which could trigger local variations of membrane curvature ("wedging effect"), as well as an area difference between the two leaflets. In addition, recent studies demonstrating the oligomerization of MinD on 2D membranes might suggest a possible scaffolding effect induced by these higher-order protein structures [309, 311]. Nevertheless, I speculate that many of these hypotheses cannot not fully explain the extent of the deformations observed in blebbing vesicles. For instance, as reported by Stachowiak *et al.*, the size and coverage of the protein containing the amphipathic helix limit the membrane occupancy of the inserted domains, thereby reducing their impact on surface area increase [362]. Consequently, it seems likely that MinDE helix insertion cannot account for the membrane deformations and high curvatures I observed in publication P2.

However, it seems evident that energy dissipation through ATP hydrolysis by MinD is behind this non-equilibrium deformation process. Given that confinement is a major feature of this co-reconstituted system, I hypothesize that the deformations I observed result from an osmotic pressure arising from MinDE protein fluxes. As Min proteins bind to the membrane, cooperative recruitment decreases their lateral diffusion at the membrane and enhances protein collisions. The corresponding protein gradients generated at the bulk and membrane could therefore result in the build-up of forces perpendicular to the bundle-delimited regions. These forces might then straighten nanoscale membrane undulations, releasing new membrane area and ultimately yielding the outward bleb morphologies bounded by actin bundles. Importantly, this phenomenon is triggered by energy consumption. In contrast to other studies, where protein crowding at the membrane caused a steric pressure that led to membrane tubulation [362, 363], MinDE-driven deformations do not occur when MinD-ATP binds alone to the membrane. MinE is required to trigger the self-organization of this protein system on the membrane via a reaction-diffusion mechanism [361]. Thus, I find it reasonable to suggest that this deformation mechanism is a non-equilibrium process which requires the consumption of energy to perform mechanical work on lipid bilayers.

To unravel the phenomenological aspects behind vesicle blebbing, we could address the observed deformations with *in silico* frameworks utilizing numerical simulations. Although this approach will face many challenges (it would involve simulating deformable volumes and surfaces in 3D with a reaction-diffusion Min skeleton model), it should provide additional insights to explain the experimental observations presented here [364, 365].

In conclusion, this thesis work demonstrates that in the engineering of synthetic cells, the integration of functional modules can reveal unexpected synergistic effects and protein behaviours. While Min proteins continue to surprise with "hidden" functions emerging from their *in vitro* reconstitution, further use of mathematical models and computer simulations will be needed to underpin the precise mechanistic processes behind the experimental phenomena observed.

4.4 Mechanistic challenges for the eukaryotic-based division approach

Despite the success in the MinDE-driven positioning of actomyosin rings, these eukaryotic protein structures reconstituted in publication P2 showed eventual stagnation. Ring contraction stopped after some time, and the vesicles did not continue symmetrically deforming to yield the characteristic aspect ratio of a two-lobed cell with a high-curvature furrow. In contrast, a high fraction of GUVs presented fully constricted bundled networks into aster-like structures, which remained either attached at the membrane or free-floating in the vesicle lumen. Both phenotypes represent the two contrasting outcomes in the contractility range of the system: little or no constriction and full, rapid contraction. Several possible reasons attributable to the design variables of the system might explain these two undesired phenotypes.

Firstly, the use of skeletal myosin II as molecular motor encompasses several limitations. Taking the form of large bipolar ensembles, skeletal muscle thick filaments comprise hundreds of motor heads which present a low duty ratio, enabling fast and large force generation [366, 367]. Although its features provide many advantageous properties for the construction of synthetic rings, the rapid build-up of contraction forces by skeletal myosin II might be detrimental in relation to the type of division rings reconstituted *in vitro*: ordered fascin bundles. Indeed, as I will discuss in detail below, the spatial organization of f-actin and its degree of connectivity have a direct influence over how forces are transmitted through the actomyosin architecture. Consequently, future reconstitutions might need to explore the use of other myosin isoforms to achieve slower and sustained contraction of actin bundle rings. A potential alternative candidate is non-muscle myosin II (NM II). As an essential component for the *in vivo* construction of cytokinetic rings, NM II assembles into short filaments, maintaining tension and contributing to network connectivity by acting as a stable crosslinker [368, 369]. More precisely, the responsive NM II-A isoform, which presents different behavioural regimes, might provide strong force generation and tension maintenance, at the same time its motor properties are modulated depending on the stiffness and mechanical signals of the contractile network [367, 197].

Secondly, the choice and concentration of ABPs as crosslinker/bundlers of actin markedly affect the structure of the obtained actin bundles. In publication P2, I assembled actin bundles by encapsulating different concentrations of fascin, a small actin crosslinking protein which tightly packs f-actin into hexagonal parallel arrays of the same polarity [370]. As discussed earlier, the architecture of these unipolar bundles, with very small interfilament distance, affects myosin-driven force generation and overall contraction dynamics. Indeed, as both experimental and simulation works confirmed, the flexible but tightly spaced bundles crosslinked with fascin facilitate the unidirectional movement of myosin, resulting in fast contraction and high mechanical work by skeletal myosin II [261, 371]. However, as previous studies have shown, high f-actin network connectivity, arising from an elevated

fascin concentration, increases bundle stiffness [372, 260, 373]. The enhancement in bundle rigidity, together with the high filament packing and persistence length induced by the presence of the crowding agent Ficoll70, could therefore hinder myosin-actin interaction, possibly trapping myosin filaments and inhibiting contraction [359, 374]. Thus, as the rings reconstituted in publication P2 were assembled from ordered fascin bundles, I find it reasonable to suggest that excessive crosslinking might prevent both the sliding and buckling of f-actin within the bundles, ultimately impeding the progression of ring constriction. Conversely, as the inverted emulsion produces a heterogeneous population of vesicles, the aster-like structures observed might arise from variations in the encapsulated [actin]:[myosin]:[biotin]:[fascin] ratio, thereby altering actin bundle architecture and the effective myosin contraction response. Moreover, in contrast to mixed-polarity bundles, unipolar contractile bundles show a high energy conversion efficiency, being the fastest ATP-consuming structures when compared to other crosslinked networks [371]. Considering the amount of ATP-dependent biomolecules in our system (actin, myosin, Min proteins), this is a parameter that might require careful scrutiny.

Finally, I employed biotin-neutravidin bonds as the linker strategy to anchor actomyosin architectures to the inner leaflet of GUVs. Although this allowed the generation of curved fascin bundles over the inner leaflet of vesicles and their positioning by MinDE-driven diffusiophoretic transport, it is still unclear whether this strong non-covalent bond is the optimal anchoring strategy for the transmission of myosin forces to the membrane [183, 375]. The high affinity of this bond might disrupt the dynamic remodelling of both actomyosin rings and the lipid membrane, preventing adhered rings from increasingly deforming furrowed vesicles. Contrary to ring-slippage events reported in other studies, where the highly fluid nature of the membrane caused bundle sliding and condensation [267], the rings generated in publication P2 remained firmly attached while stalled. While other membrane linkers might show enhanced control of vesicle deformation with rings in advanced constriction stages, biotin-neutravidin bonds appear sufficient to enable ring positioning and sustained membrane deformations.

Overall, fine-tuning of parameters like the type and concentration of molecular motors, actin crosslinkers, crowding agents, and lipid membrane anchors remains a complex and poorly explored endeavour. Nevertheless, since controlled contraction of synthetic division rings is the central objective the field strives for, future experiments will need to characterize this parameter space to identify the optimal encapsulating conditions.

4.5 Future perspectives

4.5.1 Overcoming contraction stalling with *in vitro* reconstituted anillo-actin rings

For those working on the division of giant vesicles with eukaryotic proteins, the use of myosin as the main molecular motor constitutes the most fitting choice upon first inspection; innumerable studies report its role in the division of a wide range of organisms, such as mammalian cells, budding and fission yeast, as well as other model organisms like *Dictyostelium* and *C.elegans*. Since synthetic biology relies on biomimicry, it is thus reasonable to consider myosin as the molecular motor with the potential to bring full contraction of division rings inside GUVs.

Nevertheless, including the study presented here (P2), neither the engineering ring route nor the naturalistic cortex assembly strategy for eukaryotic-based synthetic division has achieved a controlled decrease in actomyosin ring diameter or the effective abscission of the membrane via cortex contractility, respectively. On the one hand, actin rings assembled from crosslinkers and bundlers like fascin or α-actinin [263, 344], or focal adhesion/bundling proteins like talin and vinculin [267], progress into unfavourable phenotypes (aster-like structures and stagnant actomyosin rings) when myosin is added to the encapsulation mix. On the other hand, a membrane-bound cortical f-actin network recently assembled by Sakamoto and Murrell also yielded liposome deformations but did not progress to full cortex constriction or attained membrane abscission [271].

However, pioneering work performed by the Lansky & Braun Lab has paved the way for a potential new alternative: the use of anillin in the form of anillo-actin rings. Anillin is a non-motor actin crosslinking and scaffolding protein that plays a pivotal role in cytokinesis. As one of the master organizers of the division ring, in human cells anillin interacts with many cytoskeletal components such as actin, septins, RhoA, and myosin. As a well-conserved protein, anillin presents two main regions. On one side, its N-terminal contains the actin and myosin binding domains, which mediate the crosslinking and bundling of f-actin [376]. On the other side, at its C-terminus, anillin contains the anillin homology region where it binds septins and RhoA. Notably, this region exhibits a pleckstrin-homology domain (PH), which interacts with phosphatidylinositol phosphate (PIP) lipids and binds the cytokinetic ring to the membrane [377, 378].

Interestingly, as demonstrated by Kučera *et al.*, anillin is a passive crosslinker capable of sliding actin filaments to maximize their overlap, generating tens of pico-Newton forces [269]. This f-actin sliding, resulting from the entropic expansion of anillin, does not consume an external energy source such as ATP, and thus brings the system into a configuration of minimal free energy. Nevertheless, experiments performed in solution showed that, when mixed with actin, anillin formed rings which constricted spontaneously over time. This myosin-independent constriction force, albeit of entropic origin, opens

an exciting new avenue for the synthetic division efforts, as this passive crosslinker might constitute a potential substitute or complementary factor to myosin forces. Motivated by this hypothesis, I performed preliminary experiments employing anillin as a substitute for myosin motors (see Appendix IV for supplementary figures and data). Although an extensive characterization of the parameter space is still required, these experiments provided valuable insights.

Firstly, in agreement with my predictions, *in vitro* encapsulation of anillin and actin at different molar ratios inside GUVs yielded three distinct phenotypes: single rings, soft bundle networks, and asters (Figure 4.1). Similarly to their actomyosin counterparts, anchoring anillo-actin structures to the membrane generated curved and isotropic actin bundle networks. Importantly, these structures showed contractility over time. As expected, the anillin-mediated sliding of f-actin induced the folding and remodelling of the anillo-actin bundles within vesicles.

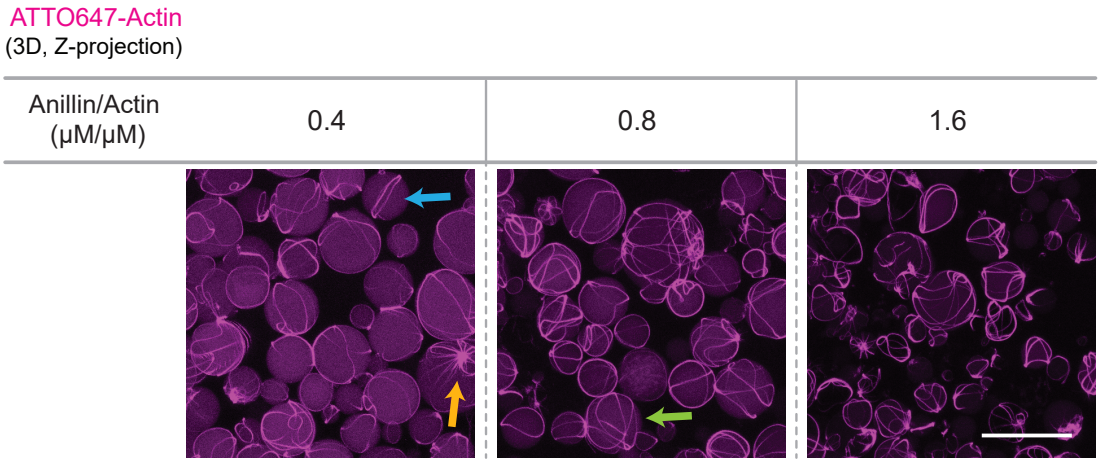

Figure 4.1. Reconstitution of anillo-actin structures inside GUVs. 3D projections of confocal images depicting encapsulation experiments performed at three anillin/actin molar ratios (M/M): 1 μM Anillin/2.4 μM Actin (0.4 M/M), 2 μM Anillin/2.4 μM Actin (0.8 M/M), and 4 μM Anillin/2.4 μM Actin (1.6 M/M). Encapsulation experiments yield three distinct anillo-actin phenotypes inside GUVs: single rings (blue arrow), asters (yellow arrow), and soft bundle networks (green arrow). GUV inner solution mix: 0.01 g/L Neutravidin, 50 g/L Ficoll70, 10 g/L BSA and 5mM ATP. Scale bar is 50 μm.

Secondly, time-lapse confocal imaging of vesicles containing high anillin/actin molar ratios revealed that, upon network collapse, GUVs burst and released their content into the outer solution (see Appendix IV, Figure IV.1). The contraction of densely-packed anillo-actin architectures, which were tightly bound to the lipid membrane via biotin-neutravidin bonds, might be behind these bursting events. As previous studies have reported, membranes can rupture and nanopores emerge when bilayers are subjected to high loads [379]. Although tension-induced nanopores can reseal to restore membrane integrity, I speculate

that forces arising from anillo-actin contractility might induce their growth into micropores, resulting in the bursting of the vesicles [380, 381].

Thirdly, when I co-reconstituted these anillo-actin structures with the MinDE system, very few vesicles showed MinDE-driven transport of these bundle structures. Since the concentrations of biotinylated lipids, biotin-actin, and neutravidin were not fully optimized in these experiments, I hypothesize that the anillo-actin bundles obtained contained a high number of anchoring sites which resulted in bundles with very low diffusivity and large effective size (membrane footprint). Consequently, these anchoring conditions might have hindered the diffusiophoretic transport of anillo-actin bundles by Min proteins [334]. However, some GUVs containing anillo-actin rings did show significant mid-cell furrowing while Min proteins oscillated at the poles of the vesicle (Figure 4.2). These rare observations demonstrate the potential improvements anillin could bring to the system studied here under the right experimental conditions. In addition, these experiments provided further evidence of the importance of including a positioning module inside our GUVs. Indeed, although anillo-actin networks substantially deformed vesicles at mid-cell, the lack of a system enabling the spatiotemporal control of these forces at the membrane resulted in the lateral collapse of the network, as well as the regression to the spherical vesicle shape (Figure 4.3, Figure IV.2 in Appendix IV).

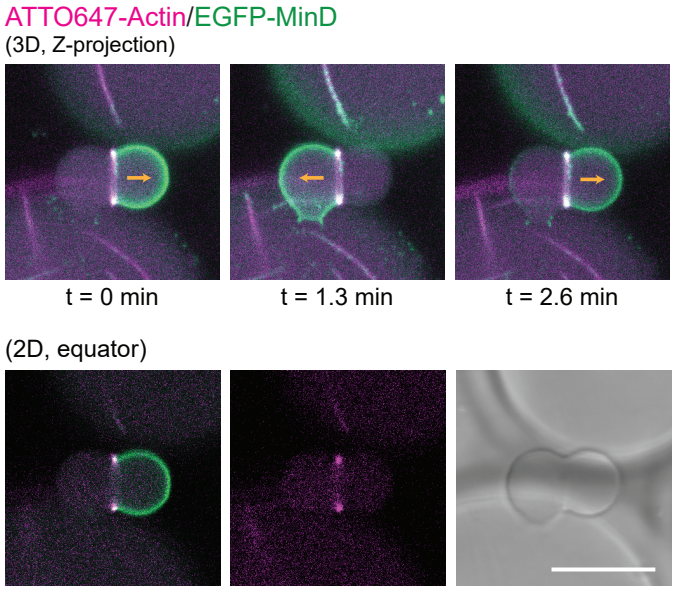

Figure 4.2. Contractile anillo-actin ring co-reconstituted with MinDE induce mid-vesicle furrowing. 3D projections and 2D images from confocal microscopy show a two-lobed shaped vesicle exhibiting mid-cell furrowing due to a contractile anillo-actin ring. Yellow arrows point to the pole-to-pole oscillations of Min proteins at the two vesicle lobes. GUV inner mix: 3 μM Anillin/3 μM Actin (1 M/M), 3 μM MinD, 3 μM MinE, 0.01 g/L Neutravidin, 50 g/L Ficoll70, 10 g/L BSA, and 5mM ATP. Scale bar is 20 μm.

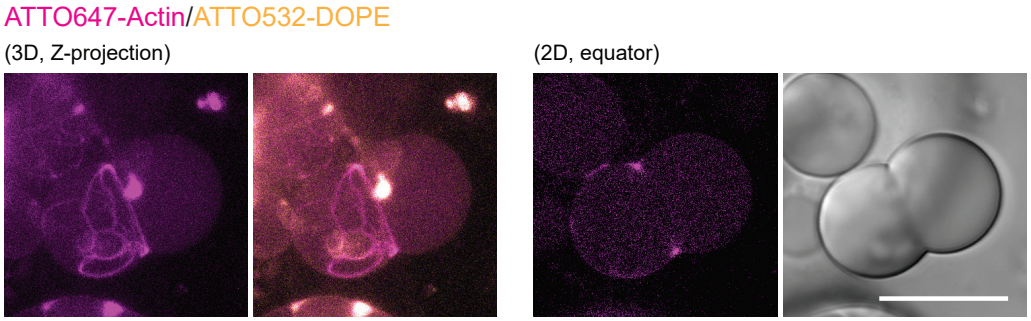

Figure 4.3. Vesicle constriction induced by contraction of anillo-actin networks. 3D projections of a confocal z-stack and 2D images of the equatorial plane of a vesicle exhibiting furrowing. The anillo-actin architecture inside the vesicle deforms the membrane as it contracts. GUV inner solution mix: 2 μM Anillin/2.4 μM Actin (0.8 M/M), 3 μM MinD, 3 μM MinE, 0.01 g/L Neutravidin, 4% OptiPrep, 50 g/L Ficoll70, 10 g/L BSA, and 5mM ATP. Scale bar is 20 μm.

Finally, to minimize vesicle bursting and facilitate MinDE-driven transport, I changed the membrane-anchoring strategy. With the aim of efficiently transmitting localized forces to the membrane, I replaced biotinylated lipids with phosphatidylinositol (3,4,5)-triphosphate (PIP3). Given that the PH domain of anillin has been shown to interact with PIP lipids [382], and following the premise that Min proteins are capable of creating anti-correlated lipid patterns [383, 384], I encapsulated anillo-actin structures in POPC lipid vesicles containing 5% PIP3. Interestingly, not only did the anillo-actin bundles appeared to be bound to the membrane of these vesicles, their contractile force also induced smaller-scale deformations like blebs and membrane tubes (Figure IV.3). In the future, further experiments will be needed to effectively incorporate MinDE oscillations and fine-tune anillin/actin molar ratios to achieve the spatiotemporal control of contractile anillo-actin rings at mid-cell.

To sum up, preliminary experiments shown in this thesis provide new insights into the use of anillin as a potential contractile agent in the division of synthetic cells. To this end, once the optimal stoichiometry of modular parameters is achieved, anillin-driven forces might constitute a promising alternative or complementary component to myosin-based division systems.

4.5.2 Next steps: building up complexity in synthetic division studies

In the roadmap towards the construction of a dividing synthetic cell, the research presented in this thesis highlights the promising outlook of synthetic biology and the many aspects which remain open for development. In this regard, actomyosin-based contractile modules require further improvement. As already explored in previous studies, adding

new layers of complexity might facilitate the dynamic remodelling of contractile rings. For instance, our reconstituted systems could combine myosin-driven contractility with a rapid actin turnover rate. Indeed, incorporating f-actin severing proteins like cofilin and gelsolin might aid in maintaining a dynamic steady state, which would potentially increase the efficiency of actomyosin contractility and thus circumvent irreversible ring contraction stalling [371]. In addition, for the present cases where actin contractility progresses but membrane abscission is not achieved, incorporating the ESCRT and Cdv protein machineries might drive the reconstituted vesicular systems towards attaining full cell division.

In parallel, the development of new functional modules will be crucial to endow artificial cells with additional functions which are essential to accomplish their self-division. In particular, a module to induce membrane growth via *in situ* lipid synthesis or lipid reservoirs will become key to supplying vesicles with the additional membrane area needed for division [385]. Besides aiding in the mechanical remodelling of dividing membranes, a synthetic module for lipid supply will enable the growth and continuity of subsequent daughter cells, ensuring the self-sustainability of our artificial systems.

Overall, although the integration of a high number of complex synthetic modules will be a pressing challenge that we will need to address, many technological advancements will accompany these research studies, bringing further progress to the synthetic biology field.

4.6 Concluding remarks

In conclusion, the research work presented in this thesis shows the successful assembly and integration of two synthetic functional modules for the division of minimal cells. These new insights not only demonstrate that the MinDE protein system can be exploited as a positioning module for actomyosin-based synthetic division, but also show its versatility and robustness for applications that go far beyond the study of self-organized systems.

Although it took life millions of years to exist as we know it, imitating its working principles will be crucial to progressively increase the complexity of our synthetic systems. Thus, the development and improvement of bio-inspired modules, together with a simultaneous characterization of their design variables, will open new exciting questions and ultimately bring us closer to our goal of building a synthetic cell capable of self-division.

Bibliography

[1] Philip Shapira, Seokbeom Kwon, and Jan Youtie. Tracking the emergence of synthetic biology. *Scientometrics*, 112(3):1439–1469, 2017. ISSN 0138-9130. doi: 10.1007/s11192-017-2452-5.

[2] B. Hobom. Gene surgery: on the threshold of synthetic biology. *Medizinische Klinik*, 75(24):834–841, November 1980. ISSN 0025-8458.

[3] Maureen A. O'Malley, Alexander Powell, Jonathan F. Davies, and Jane Calvert. Knowledge-making distinctions in synthetic biology. *BioEssays*, 30(1):57–65, 2008. ISSN 1521-1878. doi: 10.1002/bies.20664.

[4] Drew Endy. Foundations for engineering biology. *Nature*, 438(7067):449–453, November 2005. ISSN 1476-4687. doi: 10.1038/nature04342.

[5] Steven A. Benner and A. Michael Sismour. Synthetic biology. *Nature Reviews. Genetics*, 6(7):533–543, 2005. ISSN 1471-0056. doi: 10.1038/nrg1637.

[6] Mamta Singh and Anuradha Vaidya. Translational synthetic biology. *Systems and Synthetic Biology*, 9(4):191–195, December 2015. ISSN 1872-5325. doi: 10.1007/s11693-015-9181-y.

[7] Pablo Schyfter. How a 'drive to make' shapes synthetic biology. *Studies in History and Philosophy of Science Part C: Studies in History and Philosophy of Biological and Biomedical Sciences*, 44(4, Part B):632–640, December 2013. ISSN 1369-8486. doi: 10.1016/j.shpsc.2013.05.010.

[8] Renan Gonçalves Leonel da Silva, Jakob Schweizer, Kalina Kamenova, Larry Au, Alessandro Blasimme, and Effy Vayena. Organizational change of synthetic biology research: Emerging initiatives advancing a bottom-up approach. *Current Research in Biotechnology*, 7:100188, January 2024. ISSN 2590-2628. doi: 10.1016/j.crbiot.2024.100188.

[9] iGEM. https://igem.org, accessed on 01-02-2025.

[10] SynCellEU. https://syntheticcell.eu/, accessed on 01-02-2025.

[11] EUSynBioS. https://www.eusynbios.org, accessed on 01-02-2025.

[12] Stefano Donati, Içvara Barbier, Daniela A. García-Soriano, Stefano Grasso, Paola Handal-Marquez, Koray Malcı, Louis Marlow, Cauã Westmann, and Adam Amara. Synthetic biology in Europe: Current community landscape and future perspectives. *Biotechnology Notes*, 3:54–61, January 2022. ISSN 2665-9069. doi: 10.1016/j.biotno.2022.07.003.

[13] Roberta Kwok. Five hard truths for synthetic biology. *Nature*, 463(7279):288–290, January 2010. ISSN 1476-4687. doi: 10.1038/463288a.

[14] Christopher A. Voigt. Synthetic biology 2020–2030: Six commercially-available products that are changing our world. *Nature Communications*, 11(1):6379, December 2020. ISSN 2041-1723. doi: 10.1038/s41467-020-20122-2.

[15] Marleen H. M. E. van Stevendaal, Jan C. M. van Hest, and Alexander F. Mason. Functional Interactions Between Bottom-Up Synthetic Cells and Living Matter for Biomedical Applications. *ChemSystemsChem*, 3(5):e2100009, 2021. ISSN 2570-4206. doi: 10.1002/syst.202100009.

[16] Stephan Hirschi, Thomas R. Ward, Wolfgang P. Meier, Daniel J. Müller, and Dimitrios Fotiadis. Synthetic Biology: Bottom-Up Assembly of Molecular Systems. *Chemical Reviews*, 122(21):16294–16328, November 2022. ISSN 0009-2665, 1520-6890. doi: 10.1021/acs.chemrev.2c00339.

[17] Camila Guindani, Lucas Caire da Silva, Shoupeng Cao, Tsvetomir Ivanov, and Katharina Landfester. Synthetic Cells: From Simple Bio-Inspired Modules to Sophisticated Integrated Systems. *Angewandte Chemie International Edition*, 61(16): e202110855, 2022. ISSN 1521-3773. doi: 10.1002/anie.202110855.

[18] Katharina Landfester and Kai Sundmacher. Bottom-Up Synthetic Biology: Towards the Modular Design of Artifical Cells from Functional Modules. *Advanced Biosystems*, 3(6):1900095, 2019. ISSN 2366-7478. doi: 10.1002/adbi.201900095.

[19] Kendall Powell. How biologists are creating life-like cells from scratch. *Nature*, 563 (7730):172–175, November 2018. doi: 10.1038/d41586-018-07289-x.

[20] Rebecca L. Tarnopol, Sierra Bowden, Kevin Hinkle, Krithika Balakrishnan, Akira Nishii, Caleb J. Kaczmarek, Tara Pawloski, and Anthony G. Vecchiarelli. Lessons from a Minimal Genome: What Are the Essential Organizing Principles of a Cell Built from Scratch? *ChemBioChem*, 20(20):2535–2545, 2019. ISSN 1439-7633. doi: 10.1002/cbic.201900249.

[21] Christine M. E. Kriebisch, Olga Bantysh, Lorena Baranda Pellejero, Andrea Belluati, Eva Bertosin, Kun Dai, Maria de Roy, Hailin Fu, Nicola Galvanetto, Julianne M. Gibbs, Samuel Santhosh Gomez, Gaetano Granatelli, Alessandra Griffo, Maria Guix, Cenk Onur Gurdap, Johannes Harth-Kitzerow, Ivar S. Haugerud, Gregor Häfner, Pranay Jaiswal, Sadaf Javed, Ashkan Karimi, Shuzo Kato, Brigitte A. K. Kriebisch,

Sudarshana Laha, Pao-Wan Lee, Wojciech P. Lipinski, Thomas Matreux, Thomas C. T. Michaels, Erik Poppleton, Alexander Ruf, Annemiek D. Slootbeek, Iris B. A. Smokers, Héctor Soria-Carrera, Alessandro Sorrenti, Michele Stasi, Alisdair Stevenson, Advait Thatte, Mai Tran, Merlijn H. I. van Haren, Hidde D. Vuijk, Shelley F. J. Wickham, Pablo Zambrano, Katarzyna P. Adamala, Karen Alim, Ebbe Sloth Andersen, Claudia Bonfio, Dieter Braun, Erwin Frey, Ulrich Gerland, Wilhelm T. S. Huck, Frank Jülicher, Nadanai Laohakunakorn, L. Mahadavan, Sijbren Otto, James Saenz, Petra Schwille, Kerstin Göpfrich, Christoph A. Weber, and Job Boekhoven. A roadmap toward the synthesis of life. *Chem*, page 102399, February 2025. ISSN 2451-9294. doi: 10.1016/j.chempr.2024.102399.

[22] J. Craig Venter, John I. Glass, Clyde A. Hutchison, and Sanjay Vashee. Synthetic chromosomes, genomes, viruses, and cells. *Cell*, 185(15):2708–2724, July 2022. ISSN 00928674. doi: 10.1016/j.cell.2022.06.046.

[23] Daniel G. Gibson, Gwynedd A. Benders, Cynthia Andrews-Pfannkoch, Evgeniya A. Denisova, Holly Baden-Tillson, Jayshree Zaveri, Timothy B. Stockwell, Anushka Brownley, David W. Thomas, Mikkel A. Algire, Chuck Merryman, Lei Young, Vladimir N. Noskov, John I. Glass, J. Craig Venter, Clyde A. Hutchison, and Hamilton O. Smith. Complete Chemical Synthesis, Assembly, and Cloning of a Mycoplasma genitalium Genome. *Science*, 319(5867):1215–1220, February 2008. doi: 10.1126/science.1151721.

[24] Daniel G. Gibson, John I. Glass, Carole Lartigue, Vladimir N. Noskov, Ray-Yuan Chuang, Mikkel A. Algire, Gwynedd A. Benders, Michael G. Montague, Li Ma, Monzia M. Moodie, Chuck Merryman, Sanjay Vashee, Radha Krishnakumar, Nacyra Assad-Garcia, Cynthia Andrews-Pfannkoch, Evgeniya A. Denisova, Lei Young, Zhi-Qing Qi, Thomas H. Segall-Shapiro, Christopher H. Calvey, Prashanth P. Parmar, Clyde A. Hutchison, Hamilton O. Smith, and J. Craig Venter. Creation of a Bacterial Cell Controlled by a Chemically Synthesized Genome. *Science*, 329(5987):52–56, July 2010. doi: 10.1126/science.1190719.

[25] Carole Lartigue, John I. Glass, Nina Alperovich, Rembert Pieper, Prashanth P. Parmar, Clyde A. Hutchison, Hamilton O. Smith, and J. Craig Venter. Genome Transplantation in Bacteria: Changing One Species to Another. *Science*, 317(5838): 632–638, August 2007. doi: 10.1126/science.1144622.

[26] Clyde A. Hutchison, Ray-Yuan Chuang, Vladimir N. Noskov, Nacyra Assad-Garcia, Thomas J. Deerinck, Mark H. Ellisman, John Gill, Krishna Kannan, Bogumil J. Karas, Li Ma, James F. Pelletier, Zhi-Qing Qi, R. Alexander Richter, Elizabeth A. Strychalski, Lijie Sun, Yo Suzuki, Billyana Tsvetanova, Kim S. Wise, Hamilton O. Smith, John I. Glass, Chuck Merryman, Daniel G. Gibson, and J. Craig Venter. Design and synthesis of a minimal bacterial genome. *Science*, 351(6280):aad6253, March 2016. doi: 10.1126/science.aad6253.

[27] Pamela P. Peralta-Yahya, Fuzhong Zhang, Stephen B. del Cardayre, and Jay D. Keasling. Microbial engineering for the production of advanced biofuels. *Nature*, 488 (7411):320–328, August 2012. ISSN 1476-4687. doi: 10.1038/nature11478.

[28] Dae-Kyun Ro, Eric M. Paradise, Mario Ouellet, Karl J. Fisher, Karyn L. Newman, John M. Ndungu, Kimberly A. Ho, Rachel A. Eachus, Timothy S. Ham, James Kirby, Michelle C. Y. Chang, Sydnor T. Withers, Yoichiro Shiba, Richmond Sarpong, and Jay D. Keasling. Production of the antimalarial drug precursor artemisinic acid in engineered yeast. *Nature*, 440(7086):940–943, April 2006. ISSN 1476-4687. doi: 10.1038/nature04640.

[29] John I. Glass, Chuck Merryman, Kim S. Wise, Clyde A. Hutchison, and Hamilton O. Smith. Minimal Cells—Real and Imagined. *Cold Spring Harbor Perspectives in Biology*, 9(12):a023861, December 2017. ISSN 1943-0264. doi: 10.1101/cshperspect.a023861.

[30] Kristina A. Ganzinger and Petra Schwille. More from less – bottom-up reconstitution of cell biology. *Journal of Cell Science*, 132(4):jcs227488, February 2019. ISSN 0021-9533. doi: 10.1242/jcs.227488.

[31] Petra Schwille, Joachim Spatz, Katharina Landfester, Eberhard Bodenschatz, Stephan Herminghaus, Victor Sourjik, Tobias J. Erb, Philippe Bastiaens, Reinhard Lipowsky, Anthony Hyman, Peter Dabrock, Jean-Christophe Baret, Tanja Vidakovic-Koch, Peter Bieling, Rumiana Dimova, Hannes Mutschler, Tom Robinson, T.-Y. Dora Tang, Seraphine Wegner, and Kai Sundmacher. MaxSynBio: Avenues Towards Creating Cells from the Bottom Up. *Angewandte Chemie International Edition*, 57(41):13382–13392, 2018. ISSN 1521-3773. doi: 10.1002/anie.201802288.

[32] Ke Yue, Yingqiu Li, Mengjiao Cao, Lulu Shen, Jingsheng Gu, and Lei Kai. Bottom-Up Synthetic Biology Using Cell-Free Protein Synthesis. In Yuan Lu and Michael C. Jewett, editors, *Cell-Free Macromolecular Synthesis*, pages 1–20. Springer Nature Switzerland, Cham, 2023. ISBN 978-3-031-41287-5. doi: 10.1007/10_2023_232.

[33] Kerstin Göpfrich, Ilia Platzman, and Joachim P. Spatz. Mastering Complexity: Towards Bottom-up Construction of Multifunctional Eukaryotic Synthetic Cells. *Trends in Biotechnology*, 36(9):938–951, September 2018. ISSN 0167-7799. doi: 10.1016/j.tibtech.2018.03.008.

[34] Alexander B. Cook, Sebastian Novosedlik, and Jan C. M. Van Hest. Complex Coacervate Materials as Artificial Cells. *Accounts of Materials Research*, 4(3):287–298, March 2023. ISSN 2643-6728, 2643-6728. doi: 10.1021/accountsmr.2c00239.

[35] Nathaniel J. Gaut and Katarzyna P. Adamala. Reconstituting Natural Cell Elements in Synthetic Cells. *Advanced Biology*, 5(3):2000188, 2021. ISSN 2701-0198. doi: 10.1002/adbi.202000188.

[36] Wentao Jiang, Ziyu Wu, Zheng Gao, Mimi Wan, Min Zhou, Chun Mao, and Jian Shen. Artificial Cells: Past, Present and Future. *ACS Nano*, 16(10):15705–15733, October 2022. ISSN 1936-0851. doi: 10.1021/acsnano.2c06104.

[37] Ivan Ivanov, Sebastián López Castellanos, Severo Balasbas, Lado Otrin, Nika Marušič, Tanja Vidaković-Koch, and Kai Sundmacher. Bottom-Up Synthesis of Artificial Cells: Recent Highlights and Future Challenges. *Annual Review of Chemical and Biomolecular Engineering*, 12:287–308, June 2021. ISSN 1947-5446. doi: 10.1146/annurev-chembioeng-092220-085918.

[38] Songyang Liu, Yanwen Zhang, Mei Li, Li Xiong, Zijian Zhang, Xiaohai Yang, Xiaoxiao He, Kemin Wang, Jianbo Liu, and Stephen Mann. Enzyme-mediated nitric oxide production in vasoactive erythrocyte membrane-enclosed coacervate protocells. *Nature Chemistry*, 12(12):1165–1173, December 2020. ISSN 1755-4349. doi: 10.1038/s41557-020-00585-y.

[39] Sagardip Majumder, Jonathan Garamella, Ying-Lin Wang, Maxwell DeNies, Vincent Noireaux, and Allen P. Liu. Cell-sized mechanosensitive and biosensing compartment programmed with DNA. *Chemical Communications*, 53(53):7349–7352, June 2017. ISSN 1364-548X. doi: 10.1039/C7CC03455E.

[40] Ulrike Kauscher, Margaret N. Holme, Mattias Björnmalm, and Molly M. Stevens. Physical stimuli-responsive vesicles in drug delivery: Beyond liposomes and polymersomes. *Advanced Drug Delivery Reviews*, 138:259–275, January 2019. ISSN 0169-409X. doi: 10.1016/j.addr.2018.10.012.

[41] Felix Lussier, Oskar Staufer, Ilia Platzman, and Joachim P. Spatz. Can Bottom-Up Synthetic Biology Generate Advanced Drug-Delivery Systems? *Trends in Biotechnology*, 39(5):445–459, May 2021. ISSN 0167-7799. doi: 10.1016/j.tibtech.2020.08.002.

[42] Guoshu Wang and Kathrin Castiglione. Light-Driven Biocatalysis in Liposomes and Polymersomes: Where Are We Now? *Catalysts*, 9(1):12, January 2019. ISSN 2073-4344. doi: 10.3390/catal9010012.

[43] Jian Liu, Jueyi Xue, Lu Fu, Jiangtao Xu, Megan S. Lord, and Kang Liang. Genetically Encoded Synthetic Beta Cells for Insulin Biosynthesis and Release under Hyperglycemic Conditions. *Advanced Functional Materials*, 32(18):2111271, 2022. ISSN 1616-3028. doi: 10.1002/adfm.202111271.

[44] M. Dua, A. Singh, N. Sethunathan, and A. Johri. Biotechnology and bioremediation: Successes and limitations. *Applied Microbiology and Biotechnology*, 59(2):143–152, July 2002. ISSN 1432-0614. doi: 10.1007/s00253-002-1024-6.

[45] The intersection of bottom-up synthetic cell engineering and nanobiotechnology. *Nature Nanotechnology*, 19(2):131–131, February 2024. ISSN 1748-3395. doi: 10.1038/s41565-024-01627-z.

[46] Roger Brent. A partnership between biology and engineering. *Nature Biotechnology*, 22(10):1211–1214, October 2004. ISSN 1546-1696. doi: 10.1038/nbt1004-1211.

[47] Bernd Giese, Stefan Koenigstein, Henning Wigger, Jan C. Schmidt, and Arnim von Gleich. Rational Engineering Principles in Synthetic Biology: A Framework for Quantitative Analysis and an Initial Assessment. *Biological Theory*, 8(4):324–333, December 2013. ISSN 1555-5550. doi: 10.1007/s13752-013-0130-2.

[48] Matthias Heinemann and Sven Panke. Synthetic biology—putting engineering into biology. *Bioinformatics*, 22(22):2790–2799, November 2006. ISSN 1367-4803. doi: 10.1093/bioinformatics/btl469.

[49] Barry Canton, Anna Labno, and Drew Endy. Refinement and standardization of synthetic biological parts and devices. *Nature Biotechnology*, 26(7):787–793, July 2008. ISSN 1546-1696. doi: 10.1038/nbt1413.

[50] Kathryn L. Garner. Principles of synthetic biology. *Essays in Biochemistry*, 65(5): 791–811, November 2021. ISSN 0071-1365. doi: 10.1042/EBC20200059.

[51] Sergio Garcia and Cong T. Trinh. Modular design: Implementing proven engineering principles in biotechnology. *Biotechnology Advances*, 37(7):107403, November 2019. ISSN 0734-9750. doi: 10.1016/j.biotechadv.2019.06.002.

[52] Chen Wang, Junzhu Yang, and Yuan Lu. Modularize and Unite: Toward Creating a Functional Artificial Cell. *Frontiers in Molecular Biosciences*, 8:781986, November 2021. ISSN 2296-889X. doi: 10.3389/fmolb.2021.781986.

[53] Leland H. Hartwell, John J. Hopfield, Stanislas Leibler, and Andrew W. Murray. From molecular to modular cell biology. *Nature*, 402(S6761):C47–C52, December 1999. ISSN 0028-0836, 1476-4687. doi: 10.1038/35011540.

[54] Petra Schwille. Bottom-Up Synthetic Biology: Engineering in a Tinkerer's World. *Science*, 333(6047):1252–1254, September 2011. doi: 10.1126/science.1211701.

[55] Günter P. Wagner, Mihaela Pavlicev, and James M. Cheverud. The road to modularity. *Nature Reviews Genetics*, 8(12):921–931, December 2007. ISSN 1471-0064. doi: 10.1038/nrg2267.

[56] Claus Kadelka, Matthew Wheeler, Alan Veliz-Cuba, David Murrugarra, and Reinhard Laubenbacher. Modularity of biological systems: A link between structure and function. *Journal of The Royal Society Interface*, 20(207):20230505, October 2023. doi: 10.1098/rsif.2023.0505.

[57] Registry of Standard Biological Parts. https://parts.igem.org, accessed on 01-02-2025.

[58] Eugenia Schneider and Michael Mangold. Modular assembling process of an in-silico protocell. *Biosystems*, 165:8–21, March 2018. ISSN 0303-2647. doi: 10.1016/j.biosystems.2017.12.004.

[59] Allen P. Liu and Daniel A. Fletcher. Biology under construction: In vitro reconstitution of cellular function. *Nature Reviews Molecular Cell Biology*, 10(9):644–650, September 2009. ISSN 1471-0080. doi: 10.1038/nrm2746.

[60] Maria Manasseina. Julius Wiesner (Hg.): Mikroskopische Untersuchungen . Ausgeführt im Laboratorium für Mikroskopie und technische Waarenkunde am kk polytechischen Institute em Wien . *Julius Wiesner (Hg.): Mikroskopische Untersuchungen. Ausgeführt im Laboratorium für Mikroskopie und technische Waarenkunde am k. k. polytechischen Institute in Wien*, pages 116–128, Stuttgart 1872.

[61] Eduard Buchner. Alkoholische Gährung ohne Hefezellen. *Berichte der deutschen chemischen Gesellschaft*, 30(1):117–124, 1897. ISSN 1099-0682. doi: 10.1002/cber.18970300121.

[62] I. Banga and A. Szent-Györgyi. *Studies from the Institute of Medical Chemistry University Szeged*, volume 1. S. Karger AG, Basel, (ed. szent-györgyi, a.) edition, 1941/1942.

[63] A. Szent-Györgyi. Free-energy relations and contraction of actomyosin. *The Biological Bulletin*, 96(2):140–161, April 1949. ISSN 0006-3185. doi: 10.2307/1538196.

[64] F. B. Straub and G. Feuer. Adenosinetriphosphate the functional group of actin. *Biochimica et Biophysica Acta*, 4:455–470, January 1950. ISSN 0006-3002. doi: 10.1016/0006-3002(50)90052-7.

[65] Ekat Kritikou. To see them contract for the first time. *Nature Reviews Molecular Cell Biology*, 9(1):s5–s5, May 2010. ISSN 1471-0080. doi: 10.1038/nrm2556.

[66] Michael Murrell, Todd Thoresen, and Margaret Gardel. Chapter Fifteen - Reconstitution of Contractile Actomyosin Arrays. In Ronald D. Vale, editor, *Methods in Enzymology*, volume 540 of *Reconstituting the Cytoskeleton*, pages 265–282. Academic Press, January 2014. doi: 10.1016/B978-0-12-397924-7.00015-7.

[67] Michiki Kasai, Eizo Nakano, and Fumio Oosawa. Polymerization of actin free from nucleotide and divalent cations. *Biochimica et Biophysica Acta (BBA) - Biophysics including Photosynthesis*, 94(2):494–503, March 1965. ISSN 0926-6585. doi: 10.1016/0926-6585(65)90058-0.

[68] Thomas P. Loisel, Rajaa Boujemaa, Dominique Pantaloni, and Marie-France Carlier. Reconstitution of actin-based motility of Listeria and Shigella using pure proteins. *Nature*, 401(6753):613–616, October 1999. ISSN 1476-4687. doi: 10.1038/44183.

[69] Lisa A. Cameron, Matthew J. Footer, Alexander van Oudenaarden, and Julie A. Theriot. Motility of ActA protein-coated microspheres driven by actin polymerization. *Proceedings of the National Academy of Sciences*, 96(9):4908–4913, April 1999. doi: 10.1073/pnas.96.9.4908.

[70] Laurent Blanchoin, Kurt J. Amann, Henry N. Higgs, Jean-Baptiste Marchand, Donald A. Kaiser, and Thomas D. Pollard. Direct observation of dendritic actin filament networks nucleated by Arp2/3 complex and WASP/Scar proteins. *Nature*, 404(6781): 1007–1011, April 2000. ISSN 1476-4687. doi: 10.1038/35010008.

[71] Kurt J. Amann and Thomas D. Pollard. Direct real-time observation of actin filament branching mediated by Arp2/3 complex using total internal reflection fluorescence microscopy. *Proceedings of the National Academy of Sciences*, 98(26):15009–15013, December 2001. doi: 10.1073/pnas.211556398.

[72] Laurent Blanchoin, Thomas D. Pollard, and R. Dyche Mullins. Interactions of ADF/cofilin, Arp2/3 complex, capping protein and profilin in remodeling of branched actin filament networks. *Current Biology*, 10(20):1273–1282, October 2000. ISSN 0960-9822. doi: 10.1016/S0960-9822(00)00749-1.

[73] Benjamin A Smith, Shae B Padrick, Lynda K Doolittle, Karen Daugherty-Clarke, Ivan R Corrêa, Jr, Ming-Qun Xu, Bruce L Goode, Michael K Rosen, and Jeff Gelles. Three-color single molecule imaging shows WASP detachment from Arp2/3 complex triggers actin filament branch formation. *eLife*, 2:e01008, September 2013. ISSN 2050-084X. doi: 10.7554/eLife.01008.

[74] Michael D Vahey and Daniel A Fletcher. The biology of boundary conditions: Cellular reconstitution in one, two, and three dimensions. *Current Opinion in Cell Biology*, 26:60–68, February 2014. ISSN 0955-0674. doi: 10.1016/j.ceb.2013.10.001.

[75] Petra Schwille and Béla P. Frohn. Hidden protein functions and what they may teach us. *Trends in Cell Biology*, 32(2):102–109, February 2022. ISSN 09628924. doi: 10.1016/j.tcb.2021.09.006.

[76] Haiyang Jia and Petra Schwille. Bottom-up synthetic biology: Reconstitution in space and time. *Current Opinion in Biotechnology*, 60:179–187, December 2019. ISSN 0958-1669. doi: 10.1016/j.copbio.2019.05.008.

[77] Jonathan Lombard. Once upon a time the cell membranes: 175 years of cell boundary research. *Biology Direct*, 9:32, December 2014. ISSN 1745-6150. doi: 10.1186/s13062-014-0032-7.

[78] Jack W. Szostak, David P. Bartel, and P. Luigi Luisi. Synthesizing life. *Nature*, 409 (6818):387–390, January 2001. ISSN 1476-4687. doi: 10.1038/35053176.

[79] W. Turner. The Cell Theory, Past and Present. *Journal of Anatomy and Physiology*, 24(Pt 2):253–287, January 1890.

[80] Ernst Overton. Ueber die osmotischen Eigenschaften der Zelle in ihrer Bedeutung für die Toxikologie und Pharmakologie: Mit besonderer Berücksichtigung der Ammoniake und Alkaloide. *Zeitschrift für Physikalische Chemie*, 22U(1):189–209, February 1897. ISSN 2196-7156, 0942-9352. doi: 10.1515/zpch-1897-2220.

[81] R. Chambers. A MICRO INJECTION STUDY ON THE PERMEABILITY OF THE STARFISH EGG. *The Journal of General Physiology*, 5(2):189–193, November 1922. ISSN 0022-1295. doi: 10.1085/jgp.5.2.189.

[82] Rudolf Höber. Messungen der inneren Leitfähigkeit von Zellen. *Pflüger's Archiv für die gesamte Physiologie des Menschen und der Tiere*, 150(1):15–45, February 1913. ISSN 1432-2013. doi: 10.1007/BF01681047.

[83] J. Hillier and J. F. Hoffman. On the ultrastructure of the plasma membrane as determined by the electron microscope. *Journal of Cellular and Comparative Physiology*, 42(2):203–247, October 1953. ISSN 0095-9898. doi: 10.1002/jcp.1030420205.

[84] J. D. Robertson. The molecular structure and contact relationships of cell membranes. *Progress in Biophysics and Molecular Biology*, 10:343–418, 1960. ISSN 0079-6107.

[85] D W Deamer. The first living systems: A bioenergetic perspective. *Microbiology and Molecular Biology Reviews*, 61(2):239–261, June 1997. doi: 10.1128/mmbr.61.2.239-261.1997.

[86] Matthew E. Allen, James W. Hindley, Divesh K. Baxani, Oscar Ces, and Yuval Elani. Hydrogels as functional components in artificial cell systems. *Nature Reviews Chemistry*, 6(8):562–578, August 2022. ISSN 2397-3358. doi: 10.1038/s41570-022-00404-7.

[87] Janice L. Robertson. The lipid bilayer membrane and its protein constituents. *Journal of General Physiology*, 150(11):1472–1483, September 2018. ISSN 0022-1295. doi: 10.1085/jgp.201812153.

[88] Takeshi Harayama and Howard Riezman. Understanding the diversity of membrane lipid composition. *Nature Reviews Molecular Cell Biology*, 19(5):281–296, May 2018. ISSN 1471-0080. doi: 10.1038/nrm.2017.138.

[89] Markus Sällman Almén, Karl JV Nordström, Robert Fredriksson, and Helgi B. Schiöth. Mapping the human membrane proteome: A majority of the human membrane proteins can be classified according to function and evolutionary origin. *BMC Biology*, 7(1):50, August 2009. ISSN 1741-7007. doi: 10.1186/1741-7007-7-50.

[90] Jeanne C. Stachowiak and Tomas Kirchhausen. The beauty of simplicity in membrane biology. *Nature Cell Biology*, 24(12):1682–1685, December 2022. ISSN 1476-4679. doi: 10.1038/s41556-022-01015-6.

[91] E. A. Evans and R. M. Hochmuth. Mechanochemical Properties of Membranes. In Felix Bronner and Arnost Kleinzeller, editors, *Current Topics in Membranes and Transport*, volume 10 of *Membrane Properties: Mechanical Aspects, Receptors, Energetics and Calcium-Dependence of Transport*, pages 1–64. Academic Press, January 1978. doi: 10.1016/S0070-2161(08)60833-3.

[92] W. Dowhan. MOLECULAR BASIS FOR MEMBRANE PHOSPHOLIPID DIVERSITY: Why Are There So Many Lipids? *Annual Review of Biochemistry*, 66 (Volume 66, 1997):199–232, July 1997. ISSN 0066-4154, 1545-4509. doi: 10.1146/annurev.biochem.66.1.199.

[93] S. J. Singer and Garth L. Nicolson. The Fluid Mosaic Model of the Structure of Cell Membranes. *Science*, 175(4023):720–731, February 1972. doi: 10.1126/science.175.4023.720.

[94] Garth L. Nicolson. The Fluid—Mosaic Model of Membrane Structure: Still relevant to understanding the structure, function and dynamics of biological membranes after more than 40 years. *Biochimica et Biophysica Acta (BBA) - Biomembranes*, 1838 (6):1451–1466, June 2014. ISSN 0005-2736. doi: 10.1016/j.bbamem.2013.10.019.

[95] Erdinc Sezgin, Ilya Levental, Satyajit Mayor, and Christian Eggeling. The mystery of membrane organization: Composition, regulation and roles of lipid rafts. *Nature Reviews Molecular Cell Biology*, 18(6):361–374, June 2017. ISSN 1471-0080. doi: 10.1038/nrm.2017.16.

[96] Paul Mueller, Donald O. Rudin, H. Ti Tien, and William C. Wescott. Reconstitution of Cell Membrane Structure in vitro and its Transformation into an Excitable System. *Nature*, 194(4832):979–980, June 1962. ISSN 1476-4687. doi: 10.1038/194979a0.

[97] Morgan Chabanon, Jeanne C. Stachowiak, and Padmini Rangamani. Systems biology of cellular membranes: A convergence with biophysics. *Wiley interdisciplinary reviews. Systems biology and medicine*, 9(5):10.1002/wsbm.1386, September 2017. ISSN 1939-5094. doi: 10.1002/wsbm.1386.

[98] Alessandra Luchini and Giuseppe Vitiello. Mimicking the Mammalian Plasma Membrane: An Overview of Lipid Membrane Models for Biophysical Studies. *Biomimetics*, 6(1):3, March 2021. ISSN 2313-7673. doi: 10.3390/biomimetics6010003.

[99] Heiko Keller, Remigiusz Worch, and Petra Schwille. Model Membrane Systems. In Mark A. Williams and Tina Daviter, editors, *Protein-Ligand Interactions: Methods and Applications*, pages 417–438. Humana Press, Totowa, NJ, 2013. ISBN 978-1-62703-398-5. doi: 10.1007/978-1-62703-398-5_15.

[100] Thibaut J. Lagny and Patricia Bassereau. Bioinspired membrane-based systems for a physical approach of cell organization and dynamics: Usefulness and limitations. *Interface Focus*, 5(4):20150038, August 2015. doi: 10.1098/rsfs.2015.0038.

[101] Dennis E. Discher and Adi Eisenberg. Polymer Vesicles. *Science*, 297(5583):967–973, August 2002. doi: 10.1126/science.1074972.

[102] Xin Huang, Mei Li, David C. Green, David S. Williams, Avinash J. Patil, and Stephen Mann. Interfacial assembly of protein–polymer nano-conjugates into stimulus-responsive biomimetic protocells. *Nature Communications*, 4(1):2239, July 2013. ISSN 2041-1723. doi: 10.1038/ncomms3239.

[103] Virgil Percec, Daniela A. Wilson, Pawaret Leowanawat, Christopher J. Wilson, Andrew D. Hughes, Mark S. Kaucher, Daniel A. Hammer, Dalia H. Levine, Anthony J. Kim, Frank S. Bates, Kevin P. Davis, Timothy P. Lodge, Michael L. Klein, Russell H. DeVane, Emad Aqad, Brad M. Rosen, Andreea O. Argintaru, Monika J. Sienkowska, Kari Rissanen, Sami Nummelin, and Jarmo Ropponen. Self-Assembly of Janus Dendrimers into Uniform Dendrimersomes and Other Complex Architectures. *Science*, 328(5981):1009–1014, May 2010. doi: 10.1126/science.1185547.

[104] Shukun Tang, Zahra Davoudi, Guangtian Wang, Zihao Xu, Tanzeel Rehman, Aleksander Prominski, Bozhi Tian, Kaitlin M. Bratlie, Haisheng Peng, and Qun Wang. Soft materials as biological and artificial membranes. *Chemical Society Reviews*, 50 (22):12679–12701, November 2021. ISSN 1460-4744. doi: 10.1039/D1CS00029B.

[105] Aleksander Czogalla, Michał Grzybek, Walis Jones, and Ünal Coskun. Validity and applicability of membrane model systems for studying interactions of peripheral membrane proteins with lipids. *Biochimica et Biophysica Acta (BBA) - Molecular and Cell Biology of Lipids*, 1841(8):1049–1059, August 2014. ISSN 1388-1981. doi: 10.1016/j.bbalip.2013.12.012.

[106] Christina G. Siontorou, Georgia-Paraskevi Nikoleli, Dimitrios P. Nikolelis, and Stefanos K. Karapetis. Artificial Lipid Membranes: Past, Present, and Future. *Membranes*, 7(3):38, September 2017. ISSN 2077-0375. doi: 10.3390/membranes7030038.

[107] A A Brian and H M McConnell. Allogeneic stimulation of cytotoxic T cells by supported planar membranes. *Proceedings of the National Academy of Sciences*, 81 (19):6159–6163, October 1984. doi: 10.1073/pnas.81.19.6159.

[108] Ralf P. Richter, Rémi Bérat, and Alain R. Brisson. Formation of Solid-Supported Lipid Bilayers: An Integrated View. *Langmuir*, 22(8):3497–3505, April 2006. ISSN 0743-7463, 1520-5827. doi: 10.1021/la052687c.

[109] Wan-Chen Lin, Cheng-Han Yu, Sara Triffo, and Jay T. Groves. Supported Membrane Formation, Characterization, Functionalization, and Patterning for Application in

Biological Science and Technology. *Current Protocols in Chemical Biology*, 2(4): 235–269, 2010. ISSN 2160-4762. doi: 10.1002/9780470559277.ch100131.

[110] Ralf P. Richter, Nicolas Maury, and Alain R. Brisson. On the Effect of the Solid Support on the Interleaflet Distribution of Lipids in Supported Lipid Bilayers. *Langmuir*, 21(1):299–304, January 2005. ISSN 0743-7463. doi: 10.1021/la0478402.

[111] Martín Eduardo Villanueva, Laure Bar, and Patricia Losada-Pérez. Surface nanoroughness impacts the formation and stability of supported lipid bilayers. *Colloids and Surfaces A: Physicochemical and Engineering Aspects*, 682:132943, February 2024. ISSN 0927-7757. doi: 10.1016/j.colsurfa.2023.132943.

[112] Motomu Tanaka and Erich Sackmann. Polymer-supported membranes as models of the cell surface. *Nature*, 437(7059):656–663, September 2005. ISSN 1476-4687. doi: 10.1038/nature04164.

[113] Samuel Rebaud, Ofelia Maniti, and Agnès P. Girard-Egrot. Tethered bilayer lipid membranes (tBLMs): Interest and applications for biological membrane investigations. *Biochimie*, 107:135–142, December 2014. ISSN 0300-9084. doi: 10.1016/j.biochi.2014.06.021.

[114] Harvey T. McMahon and Jennifer L. Gallop. Membrane curvature and mechanisms of dynamic cell membrane remodelling. *Nature*, 438(7068):590–596, December 2005. ISSN 1476-4687. doi: 10.1038/nature04396.

[115] Harvey T. McMahon and Emmanuel Boucrot. Membrane curvature at a glance. *Journal of Cell Science*, 128(6):1065–1070, March 2015. ISSN 0021-9533. doi: 10.1242/jcs.114454.

[116] Lukas Wettmann, Mike Bonny, and Karsten Kruse. Effects of geometry and topography on Min-protein dynamics. *PLOS ONE*, 13(8):e0203050, August 2018. ISSN 1932-6203. doi: 10.1371/journal.pone.0203050.

[117] Ryosuke Mizuta, Fumihito Inoue, Yoshihiro Sasaki, Shin-ichi Sawada, and Kazunari Akiyoshi. A Facile Method to Coat Nanoparticles with Lipid Bilayer Membrane: Hybrid Silica Nanoparticles Disguised as Biomembrane Vesicles by Particle Penetration of Concentrated Lipid Layers. *Small*, 19(12):2206153, 2023. ISSN 1613-6829. doi: 10.1002/smll.202206153.

[118] Jan Vavra, Ivan Rehor, Torsten Rendler, Mona Jani, Jan Bednar, Michael M. Baksh, Andrea Zappe, Joerg Wrachtrup, and Petr Cigler. Supported Lipid Bilayers on Fluorescent Nanodiamonds: A Structurally Defined and Versatile Coating for Bioapplications. *Advanced Functional Materials*, 28(45):1803406, 2018. ISSN 1616-3028. doi: 10.1002/adfm.201803406.

[119] Kate Stokes, Kieran Clark, David Odetade, Mike Hardy, and Pola Goldberg Oppenheimer. Advances in lithographic techniques for precision nanostructure fabrication in biomedical applications. *Discover Nano*, 18(1):153, December 2023. ISSN 2731-9229. doi: 10.1186/s11671-023-03938-x.

[120] Fridtjof Brauns, Grzegorz Pawlik, Jacob Halatek, Jacob Kerssemakers, Erwin Frey, and Cees Dekker. Bulk-surface coupling identifies the mechanistic connection between Min-protein patterns in vivo and in vitro. *Nature Communications*, 12(1):3312, June 2021. ISSN 2041-1723. doi: 10.1038/s41467-021-23412-5.

[121] Katja Zieske and Petra Schwille. Reconstitution of Pole-to-Pole Oscillations of Min Proteins in Microengineered Polydimethylsiloxane Compartments. *Angewandte Chemie International Edition*, 52(1):459–462, 2013. ISSN 1521-3773. doi: 10.1002/anie.201207078.

[122] Yaron Caspi and Cees Dekker. Mapping out Min protein patterns in fully confined fluidic chambers. *eLife*, 5:e19271, November 2016. ISSN 2050-084X. doi: 10.7554/eLife.19271.

[123] Katja Zieske and Petra Schwille. Reconstitution of self-organizing protein gradients as spatial cues in cell-free systems. *eLife*, 3:e03949, October 2014. ISSN 2050-084X. doi: 10.7554/eLife.03949.

[124] Hiromune Eto, Naoki Soga, Henri G. Franquelim, Philipp Glock, Alena Khmelinskaia, Lei Kai, Michael Heymann, Hiroyuki Noji, and Petra Schwille. Design of Sealable Custom-Shaped Cell Mimicries Based on Self-Assembled Monolayers on CYTOP Polymer. *ACS Applied Materials & Interfaces*, 11(24):21372–21380, June 2019. ISSN 1944-8244. doi: 10.1021/acsami.9b05073.

[125] Senthil Arumugam, Grzegorz Chwastek, Elisabeth Fischer-Friedrich, Carina Ehrig, Ingolf Mönch, and Petra Schwille. Surface Topology Engineering of Membranes for the Mechanical Investigation of the Tubulin Homologue FtsZ. *Angewandte Chemie International Edition*, 51(47):11858–11862, 2012. ISSN 1521-3773. doi: 10.1002/anie.201204332.

[126] Katja Zieske, Jakob Schweizer, and Petra Schwille. Surface topology assisted alignment of Min protein waves. *FEBS Letters*, 588(15):2545–2549, 2014. ISSN 1873-3468. doi: 10.1016/j.febslet.2014.06.026.

[127] Alexandre Beber, Cyntia Taveneau, Manuela Nania, Feng-Ching Tsai, Aurelie Di Cicco, Patricia Bassereau, Daniel Lévy, João T. Cabral, Hervé Isambert, Stéphanie Mangenot, and Aurélie Bertin. Membrane reshaping by micrometric curvature sensitive septin filaments. *Nature Communications*, 10(1):420, January 2019. ISSN 2041-1723. doi: 10.1038/s41467-019-08344-5.

[128] Melissa Rinaldin, Sebastiaan L. D. Ten Haaf, Ernst J. Vegter, Casper Van Der Wel, Piermarco Fonda, Luca Giomi, and Daniela J. Kraft. Lipid membranes supported by polydimethylsiloxane substrates with designed geometry. *Soft Matter*, 20(37): 7379–7386, 2024. ISSN 1744-683X, 1744-6848. doi: 10.1039/D4SM00380B.

[129] Paulo Jorge Bártolo. Stereolithographic Processes. In Paulo Jorge Bártolo, editor, *Stereolithography: Materials, Processes and Applications*, pages 1–36. Springer US, Boston, MA, 2011. ISBN 978-0-387-92904-0. doi: 10.1007/978-0-387-92904-0_1.

[130] Christopher Barner-Kowollik, Martin Bastmeyer, Eva Blasco, Guillaume Delaittre, Patrick Müller, Benjamin Richter, and Martin Wegener. 3D Laser Micro- and Nanoprinting: Challenges for Chemistry. *Angewandte Chemie International Edition*, 56(50):15828–15845, 2017. ISSN 1521-3773. doi: 10.1002/anie.201704695.

[131] Miłosz Pawlicki, Hazel A. Collins, Robert G. Denning, and Harry L. Anderson. Two-Photon Absorption and the Design of Two-Photon Dyes. *Angewandte Chemie International Edition*, 48(18):3244–3266, 2009. ISSN 1521-3773. doi: 10.1002/anie.200805257.

[132] V. Harinarayana and Y. C. Shin. Two-photon lithography for three-dimensional fabrication in micro/nanoscale regime: A comprehensive review. *Optics & Laser Technology*, 142:107180, October 2021. ISSN 0030-3992. doi: 10.1016/j.optlastec.2021.107180.

[133] Enrico Domenico Lemma, Barbara Spagnolo, Massimo De Vittorio, and Ferruccio Pisanello. Studying Cell Mechanobiology in 3D: The Two-Photon Lithography Approach. *Trends in Biotechnology*, 37(4):358–372, April 2019. ISSN 0167-7799, 1879-3096. doi: 10.1016/j.tibtech.2018.09.008.

[134] R. Houbertz, L. Fröhlich, M. Popall, U. Streppel, P. Dannberg, A. Bräuer, J. Serbin, and B.n. Chichkov. Inorganic–Organic Hybrid Polymers for Information Technology: From Planar Technology to 3D Nanostructures. *Advanced Engineering Materials*, 5 (8):551–555, 2003. ISSN 1527-2648. doi: 10.1002/adem.200310096.

[135] Hiromune Eto, Henri G. Franquelim, Michael Heymann, and Petra Schwille. Membrane-coated 3D architectures for bottom-up synthetic biology. *Soft Matter*, page 10.1039.D1SM00112D, 2021. ISSN 1744-683X, 1744-6848. doi: 10.1039/D1SM00112D.

[136] Franziska Klein, Thomas Striebel, Joachim Fischer, Zhongxiang Jiang, Clemens M. Franz, Georg von Freymann, Martin Wegener, and Martin Bastmeyer. Elastic Fully Three-dimensional Microstructure Scaffolds for Cell Force Measurements. *Advanced Materials*, 22(8):868–871, 2010. ISSN 1521-4095. doi: 10.1002/adma.200902515.

[137] Haiyang Jia, Johannes Flommersfeld, Michael Heymann, Sven K. Vogel, Henri G. Franquelim, David B. Brückner, Hiromune Eto, Chase P. Broedersz, and Petra

Schwille. 3D printed protein-based robotic structures actuated by molecular motor assemblies. *Nature Materials*, 21(6):703–709, June 2022. ISSN 1476-4660. doi: 10.1038/s41563-022-01258-6.

[138] A. D. Bangham, M. M. Standish, and J. C. Watkins. Diffusion of univalent ions across the lamellae of swollen phospholipids. *Journal of Molecular Biology*, 13(1): 238–IN27, August 1965. ISSN 0022-2836. doi: 10.1016/S0022-2836(65)80093-6.

[139] Emeline Rideau, Rumiana Dimova, Petra Schwille, Frederik R. Wurm, and Katharina Landfester. Liposomes and polymersomes: A comparative review towards cell mimicking. *Chemical Society Reviews*, 47(23):8572–8610, November 2018. ISSN 1460-4744. doi: 10.1039/C8CS00162F.

[140] Abolfazl Akbarzadeh, Rogaie Rezaei-Sadabady, Soodabeh Davaran, Sang Woo Joo, Nosratollah Zarghami, Younes Hanifehpour, Mohammad Samiei, Mohammad Kouhi, and Kazem Nejati-Koshki. Liposome: Classification, preparation, and applications. *Nanoscale Research Letters*, 8(1):102, February 2013. ISSN 1556-276X. doi: 10.1186/1556-276X-8-102.

[141] Theresa M. Allen and Pieter R. Cullis. Liposomal drug delivery systems: From concept to clinical applications. *Advanced Drug Delivery Reviews*, 65(1):36–48, January 2013. ISSN 0169-409X. doi: 10.1016/j.addr.2012.09.037.

[142] Thomas Litschel and Petra Schwille. Protein Reconstitution Inside Giant Unilamellar Vesicles. *Annual Review of Biophysics*, 50(1):null, 2021. doi: 10.1146/annurev-biophys-100620-114132.

[143] Shunshi Kohyama, Adrián Merino-Salomón, and Petra Schwille. In vitro assembly, positioning and contraction of a division ring in minimal cells. *Nature Communications*, 13(1):6098, October 2022. ISSN 2041-1723. doi: 10.1038/s41467-022-33679-x.

[144] Samsuzzoha Mondal, Karthik B. Narayan, Imania Powers, Samuel Botterbusch, and Tobias Baumgart. Endophilin recruitment drives membrane curvature generation through coincidence detection of GPCR loop interactions and negative lipid charge. *Journal of Biological Chemistry*, 296:100140, January 2021. ISSN 0021-9258. doi: 10.1074/jbc.RA120.016118.

[145] Yasuyuki Inaoka and Masahito Yamazaki. Vesicle Fission of Giant Unilamellar Vesicles of Liquid-Ordered-Phase Membranes Induced by Amphiphiles with a Single Long Hydrocarbon Chain. *Langmuir*, 23(2):720–728, January 2007. ISSN 0743-7463. doi: 10.1021/la062078k.

[146] Nicoletta Kahya, Dag Scherfeld, Kirsten Bacia, and Petra Schwille. Lipid domain formation and dynamics in giant unilamellar vesicles explored by fluorescence correlation spectroscopy. *Journal of Structural Biology*, 147(1):77–89, July 2004. ISSN 1047-8477. doi: 10.1016/j.jsb.2003.09.021.

[147] Rumiana Dimova, Said Aranda, Natalya Bezlyepkina, Vesselin Nikolov, Karin A. Riske, and Reinhard Lipowsky. A practical guide to giant vesicles. Probing the membrane nanoregime via optical microscopy. *Journal of Physics. Condensed Matter: An Institute of Physics Journal*, 18(28):S1151–1176, July 2006. ISSN 0953-8984. doi: 10.1088/0953-8984/18/28/S04.

[148] Vikram Kjøller Bhatia, Nikos S. Hatzakis, and Dimitrios Stamou. A unifying mechanism accounts for sensing of membrane curvature by BAR domains, amphipathic helices and membrane-anchored proteins. *Seminars in Cell & Developmental Biology*, 21(4):381–390, June 2010. ISSN 1084-9521. doi: 10.1016/j.semcdb.2009.12.004.

[149] Andrew Callan-Jones and Patricia Bassereau. Curvature-driven membrane lipid and protein distribution. *Current Opinion in Solid State and Materials Science*, 17(4): 143–150, August 2013. ISSN 1359-0286. doi: 10.1016/j.cossms.2013.08.004.

[150] John P. Reeves and Robert M. Dowben. Formation and properties of thin-walled phospholipid vesicles. *Journal of Cellular Physiology*, 73(1):49–60, 1969. ISSN 1097-4652. doi: 10.1002/jcp.1040730108.

[151] Miglena I. Angelova and Dimiter S. Dimitrov. Liposome electroformation. *Faraday Discussions of the Chemical Society*, 81(0):303–311, January 1986. ISSN 0301-7249. doi: 10.1039/DC9868100303.

[152] Hammad A. Faizi, Annie Tsui, Rumiana Dimova, and Petia M. Vlahovska. Bending Rigidity, Capacitance, and Shear Viscosity of Giant Vesicle Membranes Prepared by Spontaneous Swelling, Electroformation, Gel-Assisted, and Phase Transfer Methods: A Comparative Study. *Langmuir*, 38(34):10548–10557, August 2022. ISSN 0743-7463. doi: 10.1021/acs.langmuir.2c01402.

[153] Philippe Méléard, Luis A. Bagatolli, and Tanja Pott. Giant unilamellar vesicle electroformation from lipid mixtures to native membranes under physiological conditions. *Methods in Enzymology*, 465:161–176, 2009. ISSN 1557-7988. doi: 10.1016/S0076-6879(09)65009-6.

[154] Kévin Carvalho, Laurence Ramos, Christian Roy, and Catherine Picart. Giant Unilamellar Vesicles Containing Phosphatidylinositol(4,5)bisphosphate: Characterization and Functionality. *Biophysical Journal*, 95(9):4348–4360, November 2008. ISSN 0006-3495. doi: 10.1529/biophysj.107.126912.

[155] Ida Louise Jørgensen, Gerdi Christine Kemmer, and Thomas Günther Pomorski. Membrane protein reconstitution into giant unilamellar vesicles: A review on current techniques. *European Biophysics Journal*, 46(2):103–119, March 2017. ISSN 1432-1017. doi: 10.1007/s00249-016-1155-9.

[156] Sophie Pautot, Barbara J. Frisken, and D. A. Weitz. Production of Unilamellar Vesicles Using an Inverted Emulsion. *Langmuir*, 19(7):2870–2879, April 2003. ISSN 0743-7463. doi: 10.1021/la026100v.

[157] Peter Walde, Katia Cosentino, Helen Engel, and Pasquale Stano. Giant Vesicles: Preparations and Applications. *ChemBioChem*, 11(7):848–865, 2010. ISSN 1439-7633. doi: 10.1002/cbic.201000010.

[158] Yiting Zhang, Haruto Obuchi, and Taro Toyota. A Practical Guide to Preparation and Applications of Giant Unilamellar Vesicles Formed via Centrifugation of Water-in-Oil Emulsion Droplets. *Membranes*, 13(4):440, April 2023. ISSN 2077-0375. doi: 10.3390/membranes13040440.

[159] Kazuya Nishimura, Hiroaki Suzuki, Taro Toyota, and Tetsuya Yomo. Size control of giant unilamellar vesicles prepared from inverted emulsion droplets. *Journal of Colloid and Interface Science*, 376(1):119–125, June 2012. ISSN 0021-9797. doi: 10.1016/j.jcis.2012.02.029.

[160] Sandro Matosevic and Brian M. Paegel. Layer-by-layer cell membrane assembly. *Nature Chemistry*, 5(11):958–963, November 2013. ISSN 1755-4349. doi: 10.1038/nchem.1765.

[161] Jeanne C. Stachowiak, David L. Richmond, Thomas H. Li, Françoise Brochard-Wyart, and Daniel A. Fletcher. Inkjet formation of unilamellar lipid vesicles for cell-like encapsulation. *Lab on a Chip*, 9(14):2003–2009, July 2009. ISSN 1473-0189. doi: 10.1039/B904984C.

[162] Manouk Abkarian, Etienne Loiseau, and Gladys Massiera. Continuous droplet interface crossing encapsulation (cDICE) for high throughput monodisperse vesicle design. *Soft Matter*, 7(10):4610–4614, May 2011. ISSN 1744-6848. doi: 10.1039/C1SM05239J.

[163] David L. Richmond, Eva M. Schmid, Sascha Martens, Jeanne C. Stachowiak, Nicole Liska, and Daniel A. Fletcher. Forming giant vesicles with controlled membrane composition, asymmetry, and contents. *Proceedings of the National Academy of Sciences*, 108(23):9431–9436, June 2011. doi: 10.1073/pnas.1016410108.

[164] Nicholas A Wright and Richard Poulsom. Omnis cellula e cellula revisited: Cell biology as the foundation of pathology. *The Journal of Pathology*, 226(2):145–147, 2012. ISSN 1096-9896. doi: 10.1002/path.3030.

[165] Clare L Kirkpatrick and Patrick H Viollier. New(s) to the (Z-)ring. *Current Opinion in Microbiology*, 14(6):691–697, December 2011. ISSN 1369-5274. doi: 10.1016/j.mib.2011.09.011.

[166] Thomas D Pollard. Mechanics of cytokinesis in eukaryotes. *Current Opinion in Cell Biology*, 22(1):50–56, February 2010. ISSN 0955-0674. doi: 10.1016/j.ceb.2009.11.010.

[167] Alireza Mashaghi and Cees Dekker. Systems and synthetic biology approaches to cell division. *Systems and Synthetic Biology*, 8(3):173–178, September 2014. ISSN 1872-5325. doi: 10.1007/s11693-014-9132-z.

[168] Mu-Yueh Chang, Hirotaka Ariyama, Wilhelm T. S. Huck, and Nan-Nan Deng. Division in synthetic cells. *Chemical Society Reviews*, 52(10):3307–3325, May 2023. ISSN 1460-4744. doi: 10.1039/D2CS00985D.

[169] Yannik Dreher, Kevin Jahnke, Elizaveta Bobkova, Joachim P. Spatz, and Kerstin Göpfrich. Division and Regrowth of Phase-Separated Giant Unilamellar Vesicles. *Angewandte Chemie International Edition*, 60(19):10661–10669, 2021. ISSN 1521-3773. doi: 10.1002/anie.202014174.

[170] Takehiro Jimbo, Yuka Sakuma, Naohito Urakami, Primož Ziherl, and Masayuki Imai. Role of Inverse-Cone-Shape Lipids in Temperature-Controlled Self-Reproduction of Binary Vesicles. *Biophysical Journal*, 110(7):1551–1562, April 2016. ISSN 0006-3495. doi: 10.1016/j.bpj.2016.02.028.

[171] Ylenia Miele, Zsófia Medveczky, Gábor Holló, Borbála Tegze, Imre Derényi, Zoltán Hórvölgyi, Emiliano Altamura, István Lagzi, and Federico Rossi. Self-division of giant vesicles driven by an internal enzymatic reaction. *Chemical Science*, 11(12): 3228–3235, March 2020. ISSN 2041-6539. doi: 10.1039/C9SC05195C.

[172] Yan Yu, Julie A. Vroman, Sung Chul Bae, and Steve Granick. Vesicle budding induced by a pore-forming peptide. *Journal of the American Chemical Society*, 132 (1):195–201, January 2010. ISSN 1520-5126. doi: 10.1021/ja9059014.

[173] Ting F. Zhu, Katarzyna Adamala, Na Zhang, and Jack W. Szostak. Photochemically driven redox chemistry induces protocell membrane pearling and division. *Proceedings of the National Academy of Sciences*, 109(25):9828–9832, June 2012. doi: 10.1073/pnas.1203212109.

[174] Ana Isabel Rico, Marcin Krupka, and Miguel Vicente. In the Beginning, *Escherichia coli* Assembled the Proto-ring: An Initial Phase of Division*. *Journal of Biological Chemistry*, 288(29):20830–20836, July 2013. ISSN 0021-9258. doi: 10.1074/jbc.R113.479519.

[175] Tanneke den Blaauwen, Leendert W Hamoen, and Petra Anne Levin. The divisome at 25: The road ahead. *Current Opinion in Microbiology*, 36:85–94, April 2017. ISSN 1369-5274. doi: 10.1016/j.mib.2017.01.007.

[176] Petra Anne Levin and Anuradha Janakiraman. Localization, Assembly, and Activation of the Escherichia coli Cell Division Machinery. *EcoSal Plus*, 9(2):eESP00222021, December 2021. ISSN 2324-6200. doi: 10.1128/ecosalplus.ESP-0022-2021.

[177] Mohamed Attaibi and Tanneke den Blaauwen. An Updated Model of the Divisome: Regulation of the Septal Peptidoglycan Synthesis Machinery by the Divisome. *International Journal of Molecular Sciences*, 23(7):3537, March 2022. ISSN 1422-0067. doi: 10.3390/ijms23073537.

[178] Carla Coltharp and Jie Xiao. Beyond force generation: Why is a dynamic ring of FtsZ polymers essential for bacterial cytokinesis? *BioEssays : news and reviews in molecular, cellular and developmental biology*, 39(1):1–11, January 2017. ISSN 0265-9247. doi: 10.1002/bies.201600179.

[179] Masaki Osawa and Harold P. Erickson. Liposome division by a simple bacterial division machinery. *Proceedings of the National Academy of Sciences*, 110(27):11000–11004, July 2013. doi: 10.1073/pnas.1222254110.

[180] Ryan McQuillen and Jie Xiao. Insights into the Structure, Function, and Dynamics of the Bacterial Cytokinetic FtsZ-Ring. *Annual Review of Biophysics*, 49(1):309–341, May 2020. ISSN 1936-122X, 1936-1238. doi: 10.1146/annurev-biophys-121219-081703.

[181] Harold P. Erickson, David E. Anderson, and Masaki Osawa. FtsZ in bacterial cytokinesis: Cytoskeleton and force generator all in one. *Microbiology and molecular biology reviews: MMBR*, 74(4):504–528, December 2010. ISSN 1098-5557. doi: 10.1128/MMBR.00021-10.

[182] Senthil Arumugam, Grzegorz Chwastek, Elisabeth Fischer-Friedrich, Carina Ehrig, Ingolf Mönch, and Petra Schwille. Surface Topology Engineering of Membranes for the Mechanical Investigation of the Tubulin Homologue FtsZ. *Angewandte Chemie International Edition*, 51(47):11858–11862, 2012. ISSN 1521-3773. doi: 10.1002/anie.201204332.

[183] Lucia Baldauf, Lennard van Buren, Federico Fanalista, and Gijsje Hendrika Koenderink. Actomyosin-Driven Division of a Synthetic Cell. *ACS Synthetic Biology*, 11 (10):3120–3133, October 2022. doi: 10.1021/acssynbio.2c00287.

[184] J. E. Heuser and M. W. Kirschner. Filament organization revealed in platinum replicas of freeze-dried cytoskeletons. *The Journal of Cell Biology*, 86(1):212–234, July 1980. ISSN 0021-9525. doi: 10.1083/jcb.86.1.212.

[185] D. Bray and J. G. White. Cortical Flow in Animal Cells. *Science*, 239(4842):883–888, February 1988. doi: 10.1126/science.3277283.

[186] Tim Hohmann and Faramarz Dehghani. The Cytoskeleton—A Complex Interacting Meshwork. *Cells*, 8(4):362, April 2019. ISSN 2073-4409. doi: 10.3390/cells8040362.

[187] W. Kabsch, H. G. Mannherz, D. Suck, E. F. Pai, and K. C. Holmes. Atomic structure of the actin:DNase I complex. *Nature*, 347(6288):37–44, September 1990. ISSN 0028-0836. doi: 10.1038/347037a0.

[188] Thomas D. Pollard. Actin and Actin-Binding Proteins. *Cold Spring Harbor Perspectives in Biology*, 8(8):a018226, August 2016. ISSN 1943-0264. doi: 10.1101/cshperspect.a018226.

[189] Benjamin J Perrin and James M Ervasti. The Actin Gene Family: Function Follows Isoform. *Cytoskeleton (Hoboken, N.j.)*, 67(10):630–634, October 2010. ISSN 1949-3584. doi: 10.1002/cm.20475.

[190] Anna S Kashina. Regulation of actin isoforms in cellular and developmental processes. *Seminars in cell & developmental biology*, 102:113–121, June 2020. ISSN 1084-9521. doi: 10.1016/j.semcdb.2019.12.003.

[191] H. E. Huxley. ELECTRON MICROSCOPE STUDIES ON THE STRUCTURE OF NATURAL AND SYNTHETIC PROTEIN FILAMENTS FROM STRIATED MUSCLE. *Journal of Molecular Biology*, 7:281–308, September 1963. ISSN 0022-2836. doi: 10.1016/s0022-2836(63)80008-x.

[192] A. Wegner. Head to tail polymerization of actin. *Journal of Molecular Biology*, 108 (1):139–150, November 1976. ISSN 0022-2836. doi: 10.1016/s0022-2836(76)80100-3.

[193] Pekka Lappalainen, Tommi Kotila, Antoine Jégou, and Guillaume Romet-Lemonne. Biochemical and mechanical regulation of actin dynamics. *Nature Reviews Molecular Cell Biology*, 23(12):836–852, December 2022. ISSN 1471-0080. doi: 10.1038/s41580-022-00508-4.

[194] W. A. Engelhardt and M. N. Ljubimowa. Myosine and Adenosinetriphosphatase. *Nature*, 144(3650):668–669, October 1939. ISSN 1476-4687. doi: 10.1038/144668b0.

[195] Thomas A. Masters, John Kendrick-Jones, and Folma Buss. Myosins: Domain Organisation, Motor Properties, Physiological Roles and Cellular Functions. In Brigitte M. Jockusch, editor, *The Actin Cytoskeleton*, pages 77–122. Springer International Publishing, Cham, 2017. ISBN 978-3-319-46371-1. doi: 10.1007/164_2016_29.

[196] I. Mabuchi and M. Okuno. The effect of myosin antibody on the division of starfish blastomeres. *The Journal of Cell Biology*, 74(1):251–263, July 1977. ISSN 0021-9525. doi: 10.1083/jcb.74.1.251.

[197] James R. Sellers and Sarah M. Heissler. Nonmuscle myosin-2 isoforms. *Current Biology*, 29(8):R275–R278, April 2019. ISSN 0960-9822. doi: 10.1016/j.cub.2019.03.022.

[198] Natalya G Dulyaninova and Anne R Bresnick. The heavy chain has its day. *Bioarchitecture*, 3(4):77–85, 2013. ISSN 1949-0992. doi: 10.4161/bioa.26133.

[199] Thomas D. Pollard. Myosins in Cytokinesis. In Lynne M. Coluccio, editor, *Myosins: A Superfamily of Molecular Motors*, pages 233–244. Springer International Publishing, Cham, 2020. ISBN 978-3-030-38062-5. doi: 10.1007/978-3-030-38062-5_11.

[200] A. F. Huxley and R. Niedergerke. Structural Changes in Muscle During Contraction: Interference Microscopy of Living Muscle Fibres. *Nature*, 173(4412):971–973, May 1954. ISSN 1476-4687. doi: 10.1038/173971a0.

[201] Fumio Matsumura. Regulation of myosin II during cytokinesis in higher eukaryotes. *Trends in Cell Biology*, 15(7):371–377, July 2005. ISSN 0962-8924. doi: 10.1016/j.tcb.2005.05.004.

[202] Thomas D. Pollard and Jian-Qiu Wu. Understanding cytokinesis: Lessons from fission yeast. *Nature Reviews. Molecular Cell Biology*, 11(2):149–155, February 2010. ISSN 1471-0080. doi: 10.1038/nrm2834.

[203] Thomas D. Pollard and Ben O'Shaughnessy. Molecular Mechanism of Cytokinesis. *Annual Review of Biochemistry*, 88(Volume 88, 2019):661–689, June 2019. ISSN 0066-4154, 1545-4509. doi: 10.1146/annurev-biochem-062917-012530.

[204] Tim Hohmann and Faramarz Dehghani. The Cytoskeleton—A Complex Interacting Meshwork. *Cells*, 8(4):362, April 2019. ISSN 2073-4409. doi: 10.3390/cells8040362.

[205] Thomas H. Cheffings, Nigel J. Burroughs, and Mohan K. Balasubramanian. Actomyosin Ring Formation and Tension Generation in Eukaryotic Cytokinesis. *Current Biology*, 26(15):R719–R737, August 2016. ISSN 0960-9822. doi: 10.1016/j.cub.2016.06.071.

[206] Yinan Liu and Douglas Robinson. Recent advances in cytokinesis: Understanding the molecular underpinnings. *F1000Research*, 7:F1000 Faculty Rev–1849, November 2018. ISSN 2046-1402. doi: 10.12688/f1000research.16502.1.

[207] R. Rappaport. *Cytokinesis in Animal Cells*. Developmental and Cell Biology Series. Cambridge University Press, Cambridge, 1996. ISBN 978-0-521-01936-1. doi: 10.1017/CBO9780511529764.

[208] Angika Basant and Michael Glotzer. Spatiotemporal Regulation of RhoA during Cytokinesis. *Current Biology*, 28(9):R570–R580, May 2018. ISSN 0960-9822. doi: 10.1016/j.cub.2018.03.045.

[209] Mian Zhou and Yu-Li Wang. Distinct Pathways for the Early Recruitment of Myosin II and Actin to the Cytokinetic Furrow. *Molecular Biology of the Cell*, 19(1):318–326, January 2008. ISSN 1059-1524. doi: 10.1091/mbc.e07-08-0783.

[210] Benjamin A. Wolfe, Tohru Takaki, Mark Petronczki, and Michael Glotzer. Polo-Like Kinase 1 Directs Assembly of the HsCyk-4 RhoGAP/Ect2 RhoGEF Complex to Initiate Cleavage Furrow Formation. *PLOS Biology*, 7(5):e1000110, May 2009. ISSN 1545-7885. doi: 10.1371/journal.pbio.1000110.

[211] William M. Bement, Hélène A. Benink, and George von Dassow. A microtubule-dependent zone of active RhoA during cleavage plane specification. *The Journal of Cell Biology*, 170(1):91–101, July 2005. ISSN 0021-9525. doi: 10.1083/jcb.200501131.

[212] Tomohito Higashi, Tomoyuki Ikeda, Ryutaro Shirakawa, Hirokazu Kondo, Mitsunori Kawato, Masahito Horiguchi, Tomohiko Okuda, Katsuya Okawa, Shuya Fukai, Osamu Nureki, Toru Kita, and Hisanori Horiuchi. Biochemical Characterization of the Rho GTPase-regulated Actin Assembly by Diaphanous-related Formins, mDia1 and Daam1, in Platelets*. *Journal of Biological Chemistry*, 283(13):8746–8755, March 2008. ISSN 0021-9258. doi: 10.1074/jbc.M707839200.

[213] Hidetaka Kosako, Toshimichi Yoshida, Fumio Matsumura, Toshimasa Ishizaki, Shuh Narumiya, and Masaki Inagaki. Rho-kinase/ROCK is involved in cytokinesis through the phosphorylation of myosin light chain and not ezrin/radixin/moesin proteins at the cleavage furrow. *Oncogene*, 19(52):6059–6064, December 2000. ISSN 1476-5594. doi: 10.1038/sj.onc.1203987.

[214] Rebecca A. Green, Ewa Paluch, and Karen Oegema. Cytokinesis in Animal Cells. *Annual Review of Cell and Developmental Biology*, 28(1):29–58, November 2012. ISSN 1081-0706, 1530-8995. doi: 10.1146/annurev-cellbio-101011-155718.

[215] Amel Kechad, Silvana Jananji, Yvonne Ruella, and Gilles R. X. Hickson. Anillin Acts as a Bifunctional Linker Coordinating Midbody Ring Biogenesis during Cytokinesis. *Current Biology*, 22(3):197–203, February 2012. ISSN 0960-9822. doi: 10.1016/j.cub.2011.11.062.

[216] Nour El Amine, Amel Kechad, Silvana Jananji, and Gilles R.X. Hickson. Opposing actions of septins and Sticky on Anillin promote the transition from contractile to midbody ring. *The Journal of Cell Biology*, 203(3):487–504, November 2013. ISSN 0021-9525. doi: 10.1083/jcb.201305053.

[217] P. Maupin and T. D. Pollard. Arrangement of actin filaments and myosin-like filaments in the contractile ring and of actin-like filaments in the mitotic spindle of dividing HeLa cells. *Journal of Ultrastructure and Molecular Structure Research*, 94 (1):92–103, January 1986. ISSN 0889-1605. doi: 10.1016/0889-1605(86)90055-8.

[218] Caroline Laplante, Fang Huang, Irene R. Tebbs, Joerg Bewersdorf, and Thomas D. Pollard. Molecular organization of cytokinesis nodes and contractile rings by super-resolution fluorescence microscopy of live fission yeast. *Proceedings of the National Academy of Sciences of the United States of America*, 113(40):E5876–E5885, October 2016. ISSN 1091-6490. doi: 10.1073/pnas.1608252113.

[219] Sathish Thiyagarajan, Shuyuan Wang, and Ben O'Shaughnessy. A node organization in the actomyosin contractile ring generates tension and aids stability. *Molecular Biology of the Cell*, 28(23):3286–3297, November 2017. ISSN 1059-1524, 1939-4586. doi: 10.1091/mbc.e17-06-0386.

[220] Martin Lenz, Todd Thoresen, Margaret L. Gardel, and Aaron R. Dinner. Contractile Units in Disordered Actomyosin Bundles Arise from F-Actin Buckling. *Physical Review Letters*, 108(23):238107, June 2012. doi: 10.1103/PhysRevLett.108.238107.

[221] Dimitrios Vavylonis, Jian-Qiu Wu, Steven Hao, Ben O'Shaughnessy, and Thomas D. Pollard. Assembly Mechanism of the Contractile Ring for Cytokinesis by Fission Yeast. *Science*, 319(5859):97–100, January 2008. doi: 10.1126/science.1151086.

[222] John H. Henson, Gabriela Reyes, Nina T. Lo, Karina Herrera, Quenelle W. McKim, Hannah Y. Herzon, Maritriny Galvez-Ceron, Alexandra E. Hershey, Rachael S. Kim, and Charles B. Shuster. Cytokinetic contractile ring structural progression in an early embryo: Positioning of scaffolding proteins, recruitment of α-actinin, and effects of myosin II inhibition. *Frontiers in Cell and Developmental Biology*, 12, September 2024. ISSN 2296-634X. doi: 10.3389/fcell.2024.1483345.

[223] John H. Henson, Casey E. Ditzler, Aphnie Germain, Patrick M. Irwin, Eric T. Vogt, Shucheng Yang, Xufeng Wu, and Charles B. Shuster. The ultrastructural organization of actin and myosin II filaments in the contractile ring: New support for an old model of cytokinesis. *Molecular Biology of the Cell*, 28(5):613–623, March 2017. ISSN 1059-1524. doi: 10.1091/mbc.e16-06-0466.

[224] T E Schroeder. Dynamics of the contractile ring. *Society of General Physiologists series*, 30:305–334, January 1975. ISSN 0094-7733.

[225] Tomoko Kamasaki, Masako Osumi, and Issei Mabuchi. Three-dimensional arrangement of F-actin in the contractile ring of fission yeast. *Journal of Cell Biology*, 178 (5):765–771, August 2007. ISSN 0021-9525. doi: 10.1083/jcb.200612018.

[226] Ana Carvalho, Arshad Desai, and Karen Oegema. Structural Memory in the Contractile Ring Makes the Duration of Cytokinesis Independent of Cell Size. *Cell*, 137 (5):926–937, May 2009. ISSN 0092-8674. doi: 10.1016/j.cell.2009.03.021.

[227] Aidan M. Fenix, Nilay Taneja, Carmen A. Buttler, John Lewis, Schuyler B. Van Engelenburg, Ryoma Ohi, and Dylan T. Burnette. Expansion and concatenation of nonmuscle myosin IIA filaments drive cellular contractile system formation during interphase and mitosis. *Molecular Biology of the Cell*, 27(9):1465–1478, May 2016. ISSN 1059-1524. doi: 10.1091/mbc.E15-10-0725.

[228] Jackie C. Cheng, Andrew L. Miller, and Sarah E. Webb. Organization and function of microfilaments during late epiboly in zebrafish embryos. *Developmental Dynamics*, 231(2):313–323, 2004. ISSN 1097-0177. doi: 10.1002/dvdy.20144.

[229] Mathias Köppen, Beatriz García Fernández, Lara Carvalho, Antonio Jacinto, and Carl-Philipp Heisenberg. Coordinated cell-shape changes control epithelial movement in zebrafish and Drosophila. *Development*, 133(14):2671–2681, July 2006. ISSN 0950-1991. doi: 10.1242/dev.02439.

[230] Damien Laporte, Ran Zhao, and Jian-Qiu Wu. Mechanisms of contractile-ring assembly in fission yeast and beyond. *Seminars in Cell & Developmental Biology*, 21 (9):892–898, December 2010. ISSN 1084-9521. doi: 10.1016/j.semcdb.2010.08.004.

[231] Ben O'Shaughnessy and Sathish Thiyagarajan. Mechanisms of contractile ring tension production and constriction. *Biophysical Reviews*, 10(6):1667–1681, December 2018. ISSN 1867-2469. doi: 10.1007/s12551-018-0476-6.

[232] Matthew R. Stachowiak, Caroline Laplante, Harvey F. Chin, Boris Guirao, Erdem Karatekin, Thomas D. Pollard, and Ben O'Shaughnessy. Mechanism of Cytokinetic Contractile Ring Constriction in Fission Yeast. *Developmental Cell*, 29(5):547–561, June 2014. ISSN 1534-5807. doi: 10.1016/j.devcel.2014.04.021.

[233] Alexander Zumdieck, Karsten Kruse, Henrik Bringmann, Anthony A. Hyman, and Frank Jülicher. Stress Generation and Filament Turnover during Actin Ring Constriction. *PLOS ONE*, 2(8):e696, August 2007. ISSN 1932-6203. doi: 10.1371/journal.pone.0000696.

[234] Cornelia Schwayer, Mateusz Sikora, Jana Slováková, Roland Kardos, and Carl-Philipp Heisenberg. Actin Rings of Power. *Developmental Cell*, 37(6):493–506, June 2016. ISSN 1534-5807. doi: 10.1016/j.devcel.2016.05.024.

[235] Amel Kechad, Silvana Jananji, Yvonne Ruella, and Gilles R. X. Hickson. Anillin acts as a bifunctional linker coordinating midbody ring biogenesis during cytokinesis. *Current biology: CB*, 22(3):197–203, February 2012. ISSN 1879-0445. doi: 10.1016/j.cub.2011.11.062.

[236] James H. Hurley and Phyllis I. Hanson. Membrane budding and scission by the ESCRT machinery: It's all in the neck. *Nature Reviews. Molecular Cell Biology*, 11 (8):556–566, August 2010. ISSN 1471-0080. doi: 10.1038/nrm2937.

[237] William M. Henne, Nicholas J. Buchkovich, and Scott D. Emr. The ESCRT Pathway. *Developmental Cell*, 21(1):77–91, July 2011. ISSN 1534-5807. doi: 10.1016/j.devcel.2011.05.015.

[238] J D Cortese, B Schwab, C Frieden, and E L Elson. Actin polymerization induces a shape change in actin-containing vesicles. *Proceedings of the National Academy of Sciences of the United States of America*, 86(15):5773–5777, August 1989. ISSN 0027-8424.

[239] H Miyata and H Hotani. Morphological changes in liposomes caused by polymerization of encapsulated actin and spontaneous formation of actin bundles. *Proceedings of the National Academy of Sciences*, 89(23):11547–11551, December 1992. doi: 10.1073/pnas.89.23.11547.

[240] E. Helfer, S. Harlepp, L. Bourdieu, J. Robert, F. C. MacKintosh, and D. Chatenay. Microrheology of Biopolymer-Membrane Complexes. *Physical Review Letters*, 85(2): 457–460, July 2000. doi: 10.1103/PhysRevLett.85.457.

[241] Allen P. Liu and Daniel A. Fletcher. Actin Polymerization Serves as a Membrane Domain Switch in Model Lipid Bilayers. *Biophysical Journal*, 91(11):4064–4070, December 2006. ISSN 0006-3495. doi: 10.1529/biophysj.106.090852.

[242] Fabina Binth Kandiyoth and Alphée Michelot. Reconstitution of actin-based cellular processes: Why encapsulation changes the rules. *European Journal of Cell Biology*, 102(4):151368, December 2023. ISSN 0171-9335. doi: 10.1016/j.ejcb.2023.151368.

[243] Anders Aufderhorst-Roberts and Margarita Staykova. Scratching beyond the surface — minimal actin assemblies as tools to elucidate mechanical reinforcement and shape change. *Emerging Topics in Life Sciences*, 6(6):583–592, December 2022. ISSN 2397-8554. doi: 10.1042/ETLS20220052.

[244] Laurent Limozin and Erich Sackmann. Polymorphism of Cross-Linked Actin Networks in Giant Vesicles. *Physical Review Letters*, 89(16):168103, September 2002. doi: 10.1103/PhysRevLett.89.168103.

[245] Makoto Honda, Kingo Takiguchi, Satoshi Ishikawa, and Hirokazu Hotani. Morphogenesis of liposomes encapsulating actin depends on the type of actin-crosslinking1. *Journal of Molecular Biology*, 287(2):293–300, March 1999. ISSN 0022-2836. doi: 10.1006/jmbi.1999.2592.

[246] Brooke E. Waechtler, Rajan Jayasankar, Emma P. Morin, and Douglas N. Robinson. Benefits and challenges of reconstituting the actin cortex. *Cytoskeleton*, 81(12):843–863, 2024. ISSN 1949-3592. doi: 10.1002/cm.21855.

[247] Léa-Laetitia Pontani, Jasper van der Gucht, Guillaume Salbreux, Julien Heuvingh, Jean-François Joanny, and Cécile Sykes. Reconstitution of an Actin Cortex Inside a Liposome. *Biophysical Journal*, 96(1):192–198, January 2009. ISSN 0006-3495. doi: 10.1016/j.bpj.2008.09.029.

[248] Feng-Ching Tsai and Gijsje Hendrika Koenderink. Shape control of lipid bilayer membranes by confined actin bundles. *Soft Matter*, 11(45):8834–8847, November 2015. ISSN 1744-6848. doi: 10.1039/C5SM01583A.

[249] Katharina Dürre, Felix C. Keber, Philip Bleicher, Fridtjof Brauns, Christian J. Cyron, Jan Faix, and Andreas R. Bausch. Capping protein-controlled actin polymerization shapes lipid membranes. *Nature Communications*, 9(1):1630, April 2018. ISSN 2041-1723. doi: 10.1038/s41467-018-03918-1.

[250] Etienne Loiseau, Jochen A. M. Schneider, Felix C. Keber, Carina Pelzl, Gladys Massiera, Guillaume Salbreux, and Andreas R. Bausch. Shape remodeling and blebbing of active cytoskeletal vesicles. *Science Advances*, 2(4):e1500465, April 2016. doi: 10.1126/sciadv.1500465.

[251] Kevin Carvalho, Joël Lemière, Fahima Faqir, John Manzi, Laurent Blanchoin, Julie Plastino, Timo Betz, and Cécile Sykes. Actin polymerization or myosin contraction: Two ways to build up cortical tension for symmetry breaking. *Philosophical Transactions of the Royal Society B: Biological Sciences*, 368(1629):20130005, November 2013. doi: 10.1098/rstb.2013.0005.

[252] Feng-Ching Tsai, Björn Stuhrmann, and Gijsje H. Koenderink. Encapsulation of Active Cytoskeletal Protein Networks in Cell-Sized Liposomes. *Langmuir*, 27(16): 10061–10071, August 2011. ISSN 0743-7463. doi: 10.1021/la201604z.

[253] Kevin Carvalho, Feng-Ching Tsai, Edouard Lees, Raphaël Voituriez, Gijsje H. Koenderink, and Cecile Sykes. Cell-sized liposomes reveal how actomyosin cortical tension drives shape change. *Proceedings of the National Academy of Sciences*, 110(41): 16456–16461, October 2013. doi: 10.1073/pnas.1221524110.

[254] Nadab H. Wubshet, Yashar Bashirzadeh, and Allen P. Liu. Fascin-induced actin protrusions are suppressed by dendritic networks in giant unilamellar vesicles. *Molecular Biology of the Cell*, 32(18):1634–1640, August 2021. ISSN 1059-1524. doi: 10.1091/mbc.E21-02-0080.

[255] Rogério Lopes dos Santos and Clément Campillo. Studying actin-induced cell shape changes using Giant Unilamellar Vesicles and reconstituted actin networks. *Biochemical Society Transactions*, 50(5):1527, October 2022. doi: 10.1042/BST20220900.

[256] Martin Lenz. Geometrical Origins of Contractility in Disordered Actomyosin Networks. *Physical Review X*, 4(4):041002, October 2014. doi: 10.1103/PhysRevX.4.041002.

[257] Thomas H. Cheffings, Nigel J. Burroughs, and Mohan K. Balasubramanian. Actin turnover ensures uniform tension distribution during cytokinetic actomyosin ring contraction. *Molecular Biology of the Cell*, 30(8):933–941, April 2019. ISSN 1059-1524. doi: 10.1091/mbc.E18-08-0511.

[258] Siddharth Deshpande and Thomas Pfohl. Real-Time Dynamics of Emerging Actin Networks in Cell-Mimicking Compartments. *PLOS ONE*, 10(3):e0116521, March 2015. ISSN 1932-6203. doi: 10.1371/journal.pone.0116521.

[259] Yashar Bashirzadeh and Allen P. Liu. Encapsulation of the cytoskeleton: Towards mimicking the mechanics of a cell. *Soft Matter*, 15(42):8425–8436, October 2019. ISSN 1744-6848. doi: 10.1039/C9SM01669D.

[260] Mireille M. A. E. Claessens, Mark Bathe, Erwin Frey, and Andreas R. Bausch. Actin-binding proteins sensitively mediate F-actin bundle stiffness. *Nature Materials*, 5(9): 748–753, September 2006. ISSN 1476-4660. doi: 10.1038/nmat1718.

[261] Hajer Ennomani, Gaëlle Letort, Christophe Guérin, Jean-Louis Martiel, Wenxiang Cao, François Nédélec, Enrique M. De La Cruz, Manuel Théry, and Laurent Blanchoin. Architecture and Connectivity Govern Actin Network Contractility. *Current Biology*, 26(5):616–626, March 2016. ISSN 0960-9822. doi: 10.1016/j.cub.2015.12.069.

[262] Yashar Bashirzadeh, Steven A. Redford, Chatipat Lorpaiboon, Alessandro Groaz, Hossein Moghimianavval, Thomas Litschel, Petra Schwille, Glen M. Hocky, Aaron R. Dinner, and Allen P. Liu. Actin crosslinker competition and sorting drive emergent GUV size-dependent actin network architecture. *Communications Biology*, 4(1):1–11, September 2021. ISSN 2399-3642. doi: 10.1038/s42003-021-02653-6.

[263] Yashar Bashirzadeh, Hossein Moghimianavval, and Allen P. Liu. Encapsulated actomyosin patterns drive cell-like membrane shape changes. *iScience*, 25(5):104236, April 2022. ISSN 2589-0042. doi: 10.1016/j.isci.2022.104236.

[264] Makito Miyazaki, Masataka Chiba, Hiroki Eguchi, Takashi Ohki, and Shin'ichi Ishiwata. Cell-sized spherical confinement induces the spontaneous formation of contractile actomyosin rings in vitro. *Nature Cell Biology*, 17(4):480–489, April 2015. ISSN 1476-4679. doi: 10.1038/ncb3142.

[265] M. M. a. E. Claessens, R. Tharmann, K. Kroy, and A. R. Bausch. Microstructure and viscoelasticity of confined semiflexible polymer networks. *Nature Physics*, 2(3): 186–189, March 2006. ISSN 1745-2481. doi: 10.1038/nphys241.

[266] Greg Morrison and D. Thirumalai. Semiflexible chains in confined spaces. *Physical Review E*, 79(1):011924, January 2009. doi: 10.1103/PhysRevE.79.011924.

[267] Thomas Litschel, Charlotte F. Kelley, Danielle Holz, Maral Adeli Koudehi, Sven K. Vogel, Laura Burbaum, Naoko Mizuno, Dimitrios Vavylonis, and Petra Schwille. Reconstitution of contractile actomyosin rings in vesicles. *Nature Communications*, 12, April 2021. ISSN 2041-1723. doi: 10.1038/s41467-021-22422-7.

[268] Manos Mavrakis, Yannick Azou-Gros, Feng-Ching Tsai, José Alvarado, Aurélie Bertin, Francois Iv, Alla Kress, Sophie Brasselet, Gijsje H. Koenderink, and Thomas Lecuit. Septins promote F-actin ring formation by crosslinking actin filaments into curved bundles. *Nature Cell Biology*, 16(4):322–334, April 2014. ISSN 1476-4679. doi: 10.1038/ncb2921.

[269] Ondřej Kučera, Valerie Siahaan, Daniel Janda, Sietske H. Dijkstra, Eliška Pilátová, Eva Zatecka, Stefan Diez, Marcus Braun, and Zdenek Lansky. Anillin propels myosin-independent constriction of actin rings. *Nature Communications*, 12(1):4595, July 2021. ISSN 2041-1723. doi: 10.1038/s41467-021-24474-1.

[270] Kristina A. Ganzinger, Adrián Merino-Salomón, Daniela A. García-Soriano, A. Nelson Butterfield, Thomas Litschel, Frank Siedler, and Petra Schwille. FtsZ Reorganization Facilitates Deformation of Giant Vesicles in Microfluidic Traps. *Angewandte Chemie International Edition*, 59(48):21372–21376, 2020. ISSN 1521-3773. doi: 10.1002/anie.202001928.

[271] Ryota Sakamoto and Michael P. Murrell. Mechanical power is maximized during contractile ring-like formation in a biomimetic dividing cell model. *Nature Communications*, 15(1):9731, November 2024. ISSN 2041-1723. doi: 10.1038/s41467-024-53228-y.

[272] Henri G. Franquelim, Alena Khmelinskaia, Jean-Philippe Sobczak, Hendrik Dietz, and Petra Schwille. Membrane sculpting by curved DNA origami scaffolds. *Nature Communications*, 9(1):811, February 2018. ISSN 2041-1723. doi: 10.1038/s41467-018-03198-9.

[273] Sisi Fan, Shuo Wang, Longjiang Ding, Thomas Speck, Hao Yan, Stephan Nussberger, and Na Liu. Morphology remodelling and membrane channel formation in synthetic cells via reconfigurable DNA nanorafts. *Nature Materials*, 24(2):278–286, February 2025. ISSN 1476-4660. doi: 10.1038/s41563-024-02075-9.

[274] Shiva Razavi, Felix Wong, Bedri Abubaker-Sharif, Hideaki T. Matsubayashi, Hideki Nakamura, Nhung Thi Hong Nguyen, Douglas N. Robinson, Baoyu Chen, Pablo A. Iglesias, and Takanari Inoue. Synthetic control of actin polymerization and symmetry breaking in active protocells. *Science Advances*, 10(24):eadk9731, June 2024. doi: 10.1126/sciadv.adk9731.

[275] Eric Karsenti. Self-organization in cell biology: A brief history. *Nature Reviews Molecular Cell Biology*, 9(3):255–262, March 2008. ISSN 1471-0080. doi: 10.1038/nrm2357.

[276] Tom Misteli. The concept of self-organization in cellular architecture. *Journal of Cell Biology*, 155(2):181–186, October 2001. ISSN 0021-9525. doi: 10.1083/jcb.200108110.

[277] Roland Wedlich-Söldner and Timo Betz. Self-organization: The fundament of cell biology. *Philosophical Transactions of the Royal Society B: Biological Sciences*, 373 (1747):20170103, April 2018. doi: 10.1098/rstb.2017.0103.

[278] Leif Dehmelt and Philippe Bastiaens. Self-Organization in Cells. In Hildegard Meyer-Ortmanns and Stefan Thurner, editors, *Principles of Evolution: From the Planck*

Epoch to Complex Multicellular Life, pages 219–238. Springer, Berlin, Heidelberg, 2011. ISBN 978-3-642-18137-5. doi: 10.1007/978-3-642-18137-5_9.

[279] Scott Camazine, Jean-Louis Deneubourg, Nigel R. Franks, James Sneyd, Guy Theraulaz, and Eric Bonabeau. *Self-Organization in Biological Systems*. Princeton University Press, May 2020. ISBN 978-0-691-21292-0. doi: 10.1515/9780691212920.

[280] Alan Mathison Turing. The chemical basis of morphogenesis. *Philosophical Transactions of the Royal Society of London. Series B, Biological Sciences*, 237(641):37–72, August 1952. doi: 10.1098/rstb.1952.0012.

[281] Shigeru Kondo and Takashi Miura. Reaction-Diffusion Model as a Framework for Understanding Biological Pattern Formation. *Science*, 329(5999):1616–1620, September 2010. doi: 10.1126/science.1179047.

[282] J. Halatek, F. Brauns, and E. Frey. Self-organization principles of intracellular pattern formation. *Philosophical Transactions of the Royal Society B: Biological Sciences*, 373(1747):20170107, May 2018. ISSN 0962-8436, 1471-2970. doi: 10.1098/rstb.2017.0107.

[283] Shigeru Kondo. An updated kernel-based Turing model for studying the mechanisms of biological pattern formation. *Journal of Theoretical Biology*, 414:120–127, February 2017. ISSN 0022-5193. doi: 10.1016/j.jtbi.2016.11.003.

[284] Amit N. Landge, Benjamin M. Jordan, Xavier Diego, and Patrick Müller. Pattern formation mechanisms of self-organizing reaction-diffusion systems. *Developmental Biology*, 460(1):2–11, April 2020. ISSN 0012-1606. doi: 10.1016/j.ydbio.2019.10.031.

[285] Sean T. Vittadello, Thomas Leyshon, David Schnoerr, and Michael P. H. Stumpf. Turing pattern design principles and their robustness. *Philosophical Transactions of the Royal Society A: Mathematical, Physical and Engineering Sciences*, 379(2213): 20200272, November 2021. doi: 10.1098/rsta.2020.0272.

[286] A. N. Zaikin and A. M. Zhabotinsky. Concentration Wave Propagation in Two-dimensional Liquid-phase Self-oscillating System. *Nature*, 225(5232):535–537, February 1970. ISSN 1476-4687. doi: 10.1038/225535b0.

[287] Nathan Tompkins, Ning Li, Camille Girabawe, Michael Heymann, G. Bard Ermentrout, Irving R. Epstein, and Seth Fraden. Testing Turing's theory of morphogenesis in chemical cells. *Proceedings of the National Academy of Sciences of the United States of America*, 111(12):4397–4402, March 2014. ISSN 0027-8424. doi: 10.1073/pnas.1322005111.

[288] A. Gierer and H. Meinhardt. A theory of biological pattern formation. *Kybernetik*, 12(1):30–39, December 1972. ISSN 1432-0770. doi: 10.1007/BF00289234.

[289] Hans Meinhardt and Alfred Gierer. Pattern formation by local self-activation and lateral inhibition. *BioEssays*, 22(8):753–760, 2000. ISSN 1521-1878. doi: 10.1002/1521-1878(200008)22:8<753::AID-BIES9>3.0.CO;2-Z.

[290] J. Raspopovic, L. Marcon, L. Russo, and J. Sharpe. Digit patterning is controlled by a Bmp-Sox9-Wnt Turing network modulated by morphogen gradients. *Science*, 345(6196):566–570, August 2014. doi: 10.1126/science.1252960.

[291] Stuart A. Newman. The Turing mechanism in vertebrate limb patterning. *Nature Reviews Molecular Cell Biology*, 8(6):1–1, June 2007. ISSN 1471-0080. doi: 10.1038/nrm1830-c1.

[292] Mostafa Bendahmane, Elmahdi Erraji, and Fahd Karami. A 3D reaction–diffusion system describing calcium dynamics in cardiac cell. *Mathematical Modelling of Natural Phenomena*, 14(2):205, 2019. ISSN 0973-5348, 1760-6101. doi: 10.1051/mmnp/2018064.

[293] Siowling Soh, Marta Byrska, Kristiana Kandere-Grzybowska, and Bartosz A. Grzybowski. Reaction -Diffusion Systems in Intracellular Molecular Transport and Control. *Angewandte Chemie (International ed. in English)*, 49(25):4170–4198, June 2010. ISSN 1433-7851. doi: 10.1002/anie.200905513.

[294] Douglas I. Johnson. Cdc42: An Essential Rho-Type GTPase Controlling Eukaryotic Cell Polarity. *Microbiology and Molecular Biology Reviews*, 63(1):54–105, March 1999. doi: 10.1128/mmbr.63.1.54-105.1999.

[295] Lukasz Kozubowski, Koji Saito, Jayme M. Johnson, Audrey S. Howell, Trevin R. Zyla, and Daniel J. Lew. Symmetry-Breaking Polarization Driven by a Cdc42p GEF-PAK Complex. *Current Biology*, 18(22):1719–1726, November 2008. ISSN 0960-9822. doi: 10.1016/j.cub.2008.09.060.

[296] Andrew B. Goryachev and Alexandra V. Pokhilko. Dynamics of Cdc42 network embodies a Turing-type mechanism of yeast cell polarity. *FEBS Letters*, 582(10): 1437–1443, April 2008. ISSN 0014-5793. doi: 10.1016/j.febslet.2008.03.029.

[297] Jaan Männik and Matthew W. Bailey. Spatial coordination between chromosomes and cell division proteins in Escherichia coli. *Frontiers in Microbiology*, 6, April 2015. ISSN 1664-302X. doi: 10.3389/fmicb.2015.00306.

[298] Matthew W. Bailey, Paola Bisicchia, Boyd T. Warren, David J. Sherratt, and Jaan Männik. Evidence for Divisome Localization Mechanisms Independent of the Min System and SlmA in Escherichia coli. *PLOS Genetics*, 10(8):e1004504, August 2014. ISSN 1553-7404. doi: 10.1371/journal.pgen.1004504.

[299] Hongbaek Cho, Heather R. McManus, Simon L. Dove, and Thomas G. Bernhardt. Nucleoid occlusion factor SlmA is a DNA-activated FtsZ polymerization antagonist.

Proceedings of the National Academy of Sciences, 108(9):3773–3778, March 2011. doi: 10.1073/pnas.1018674108.

[300] H. I. Adler, W. D. Fisher, A. Cohen, and Alice A. Hardigree. MINIATURE escherichia coli CELLS DEFICIENT IN DNA*. *Proceedings of the National Academy of Sciences*, 57(2):321–326, February 1967. doi: 10.1073/pnas.57.2.321.

[301] E Davie, K Sydnor, and L I Rothfield. Genetic basis of minicell formation in Escherichia coli K-12. *Journal of Bacteriology*, 158(3):1202–1203, June 1984. doi: 10.1128/jb.158.3.1202-1203.1984.

[302] Piet A. J. de Boer, Robin E. Crossley, and Lawrence I. Rothfield. A division inhibitor and a topological specificity factor coded for by the minicell locus determine proper placement of the division septum in E. coli. *Cell*, 56(4):641–649, February 1989. ISSN 0092-8674. doi: 10.1016/0092-8674(89)90586-2.

[303] David M. Raskin and Piet A. J. de Boer. Rapid pole-to-pole oscillation of a protein required for directing division to the middle of Escherichia coli. *Proceedings of the National Academy of Sciences*, 96(9):4971–4976, April 1999. doi: 10.1073/pnas.96.9.4971.

[304] Detlef D Leipe, Yuri I Wolf, Eugene V Koonin, and L Aravind. Classification and evolution of P-loop GTPases and related ATPases1. *Journal of Molecular Biology*, 317(1):41–72, March 2002. ISSN 0022-2836. doi: 10.1006/jmbi.2001.5378.

[305] Beatrice Ramm, Tamara Heermann, and Petra Schwille. The E. coli MinCDE system in the regulation of protein patterns and gradients. *Cellular and Molecular Life Sciences*, 76(21):4245–4273, 2019. ISSN 1420-682X. doi: 10.1007/s00018-019-03218-x.

[306] Ikuko Hayashi, Takuji Oyama, and Kosuke Morikawa. Structural and functional studies of MinD ATPase: Implications for the molecular recognition of the bacterial cell division apparatus. *The EMBO Journal*, 20(8):1819–1828, April 2001. ISSN 0261-4189. doi: 10.1093/emboj/20.8.1819.

[307] Tim H. Szeto, Susan L. Rowland, Lawrence I. Rothfield, and Glenn F. King. Membrane localization of MinD is mediated by a C-terminal motif that is conserved across eubacteria, archaea, and chloroplasts. *Proceedings of the National Academy of Sciences*, 99(24):15693–15698, November 2002. doi: 10.1073/pnas.232590599.

[308] Tim H. Szeto, Susan L. Rowland, Cheryl L. Habrukowich, and Glenn F. King. The MinD Membrane Targeting Sequence Is a Transplantable Lipid-binding Helix*. *Journal of Biological Chemistry*, 278(41):40050–40056, October 2003. ISSN 0021-9258. doi: 10.1074/jbc.M306876200.

[309] Zonglin Hu, Edward P. Gogol, and Joe Lutkenhaus. Dynamic assembly of MinD on phospholipid vesicles regulated by ATP and MinE. *Proceedings of the National Academy of Sciences*, 99(10):6761–6766, May 2002. doi: 10.1073/pnas.102059099.

[310] Laura L. Lackner, David M. Raskin, and Piet A. J. de Boer. ATP-Dependent Interactions between Escherichia coli Min Proteins and the Phospholipid Membrane In Vitro. *Journal of Bacteriology*, 185(3):735–749, February 2003. doi: 10.1128/jb.185.3.735-749.2003.

[311] Atsushi Miyagi, Beatrice Ramm, Petra Schwille, and Simon Scheuring. High-Speed Atomic Force Microscopy Reveals the Inner Workings of the MinDE Protein Oscillator. *Nano Letters*, 18(1):288–296, January 2018. ISSN 1530-6984. doi: 10.1021/acs.nanolett.7b04128.

[312] Jacob Halatek and Erwin Frey. Highly Canalized MinD Transfer and MinE Sequestration Explain the Origin of Robust MinCDE-Protein Dynamics. *Cell Reports*, 1 (6):741–752, June 2012. ISSN 2211-1247. doi: 10.1016/j.celrep.2012.04.005.

[313] Zonglin Hu and Joe Lutkenhaus. Topological Regulation of Cell Division in *E. coli*. *Molecular Cell*, 7(6):1337–1343, June 2001. ISSN 1097-2765. doi: 10.1016/S1097-2765(01)00273-8.

[314] Fabai Wu, Bas G. C. van Schie, Juan E. Keymer, and Cees Dekker. Symmetry and scale orient Min protein patterns in shaped bacterial sculptures. *Nature Nanotechnology*, 10(8):719–726, August 2015. ISSN 1748-3395. doi: 10.1038/nnano.2015.126.

[315] Cheng-Wei Hsieh, Ti-Yu Lin, Hsin-Mei Lai, Chu-Chi Lin, Ting-Sung Hsieh, and Yu-Ling Shih. Direct MinE–membrane interaction contributes to the proper localization of MinDE in E. coli. *Molecular Microbiology*, 75(2):499–512, January 2010. ISSN 0950-382X. doi: 10.1111/j.1365-2958.2009.07006.x.

[316] Glenn F. King, Yu-Ling Shih, Mark W. Maciejewski, Naresh P. S. Bains, Borlan Pan, Susan L. Rowland, Gregory P. Mullen, and Lawrence I. Rothfield. Structural basis for the topological specificity function of MinE. *Nature Structural Biology*, 7 (11):1013–1017, November 2000. ISSN 1545-9985. doi: 10.1038/80917.

[317] Kyung-Tae Park, Wei Wu, Kevin P. Battaile, Scott Lovell, Todd Holyoak, and Joe Lutkenhaus. The Min Oscillator Uses MinD-Dependent Conformational Changes in MinE to Spatially Regulate Cytokinesis. *Cell*, 146(3):396–407, August 2011. ISSN 0092-8674. doi: 10.1016/j.cell.2011.06.042.

[318] Kyung-Tae Park, Wei Wu, Scott Lovell, and Joe Lutkenhaus. Mechanism of the asymmetric activation of the MinD ATPase by MinE. *Molecular Microbiology*, 85 (2):271–281, July 2012. ISSN 1365-2958. doi: 10.1111/j.1365-2958.2012.08110.x.

[319] Martin Loose, Elisabeth Fischer-Friedrich, Christoph Herold, Karsten Kruse, and Petra Schwille. Min protein patterns emerge from rapid rebinding and membrane interaction of MinE. *Nature Structural & Molecular Biology*, 18(5):577–583, May 2011. ISSN 1545-9985. doi: 10.1038/nsmb.2037.

[320] Z. Hu, A. Mukherjee, S. Pichoff, and J. Lutkenhaus. The MinC component of the division site selection system in Escherichia coli interacts with FtsZ to prevent polymerization. *Proceedings of the National Academy of Sciences of the United States of America*, 96(26):14819–14824, 1999. doi: 10.1073/pnas.96.26.14819.

[321] Alex Dajkovic, Ganhui Lan, Sean X. Sun, Denis Wirtz, and Joe Lutkenhaus. MinC Spatially Controls Bacterial Cytokinesis by Antagonizing the Scaffolding Function of FtsZ. *Current Biology*, 18(4):235–244, February 2008. ISSN 0960-9822. doi: 10.1016/j.cub.2008.01.042.

[322] Huaijin Zhou and Joe Lutkenhaus. The Switch I and II Regions of MinD Are Required for Binding and Activating MinC. *Journal of Bacteriology*, 186(5):1546–1555, March 2004. doi: 10.1128/jb.186.5.1546-1555.2004.

[323] Wei Wu, Kyung-Tae Park, Todd Holyoak, and Joe Lutkenhaus. Determination of the structure of the MinD–ATP complex reveals the orientation of MinD on the membrane and the relative location of the binding sites for MinE and MinC. *Molecular Microbiology*, 79(6):1515–1528, 2011. ISSN 1365-2958. doi: 10.1111/j.1365-2958.2010.07536.x.

[324] Z. Hu and J. Lutkenhaus. Topological regulation of cell division in Escherichia coli involves rapid pole to pole oscillation of the division inhibitor MinC under the control of MinD and MinE. *Molecular Microbiology*, 34(1):82–90, 1999. doi: 10.1046/j.1365-2958.1999.01575.x.

[325] David M. Raskin and Piet A. J. de Boer. MinDE-Dependent Pole-to-Pole Oscillation of Division Inhibitor MinC in Escherichia coli. *Journal of Bacteriology*, 181(20):6419–6424, October 1999. doi: 10.1128/jb.181.20.6419-6424.1999.

[326] Saud H. Ayed, Adam D. Cloutier, Laura J. McLeod, Alexander C. Y. Foo, Adam M. Damry, and Natalie K. Goto. Dissecting the role of conformational change and membrane binding by the bacterial cell division regulator MinE in the stimulation of MinD ATPase activity. *Journal of Biological Chemistry*, 292(50):20732–20743, December 2017. ISSN 0021-9258. doi: 10.1074/jbc.M117.805945.

[327] B. Di Ventura and V. Sourjik. Self-organized partitioning of dynamically localized proteins in bacterial cell division. *Molecular Systems Biology*, 7, 2011. doi: 10.1038/msb.2010.111.

[328] Martin Loose, Elisabeth Fischer-Friedrich, Jonas Ries, Karsten Kruse, and Petra Schwille. Spatial Regulators for Bacterial Cell Division Self-Organize into Surface Waves in Vitro. *Science*, 320(5877):789–792, May 2008. doi: 10.1126/science.1154413.

[329] Anthony G. Vecchiarelli, Min Li, Michiyo Mizuuchi, and Kiyoshi Mizuuchi. Differential affinities of MinD and MinE to anionic phospholipid influence Min patterning dynamics in vitro. *Molecular Microbiology*, 93(3):453–463, 2014. ISSN 1365-2958. doi: 10.1111/mmi.12669.

[330] Ariadna Martos, Zdenek Petrasek, and Petra Schwille. Propagation of MinCDE waves on free-standing membranes. *Environmental Microbiology*, 15(12):3319–3326, 2013. ISSN 1462-2920. doi: 10.1111/1462-2920.12295.

[331] Anthony G. Vecchiarelli, Min Li, Michiyo Mizuuchi, Ling Chin Hwang, Yeonee Seol, Keir C. Neuman, and Kiyoshi Mizuuchi. Membrane-bound MinDE complex acts as a toggle switch that drives Min oscillation coupled to cytoplasmic depletion of MinD. *Proceedings of the National Academy of Sciences*, 113(11):E1479–E1488, March 2016. doi: 10.1073/pnas.1600644113.

[332] Ariadna Martos, Mercedes Jiménez, Germán Rivas, and Petra Schwille. Towards a bottom-up reconstitution of bacterial cell division. *Trends in Cell Biology*, 22(12): 634–643, December 2012. ISSN 0962-8924. doi: 10.1016/j.tcb.2012.09.003.

[333] Philipp Glock, Beatrice Ramm, Tamara Heermann, Simon Kretschmer, Jakob Schweizer, Jonas Mücksch, Gökberk Alagöz, and Petra Schwille. Stationary Patterns in a Two-Protein Reaction-Diffusion System. *ACS Synthetic Biology*, 8(1): 148–157, January 2019. doi: 10.1021/acssynbio.8b00415.

[334] Beatrice Ramm, Andriy Goychuk, Alena Khmelinskaia, Philipp Blumhardt, Hiromune Eto, Kristina A. Ganzinger, Erwin Frey, and Petra Schwille. A diffusiophoretic mechanism for ATP-driven transport without motor proteins. *Nature Physics*, 17(7): 850–858, July 2021. ISSN 1745-2481. doi: 10.1038/s41567-021-01213-3.

[335] Jakob Schweizer, Martin Loose, Mike Bonny, Karsten Kruse, Ingolf Mönch, and Petra Schwille. Geometry sensing by self-organized protein patterns. *Proceedings of the National Academy of Sciences*, 109(38):15283–15288, September 2012. doi: 10.1073/pnas.1206953109.

[336] Laeschkir Würthner, Fridtjof Brauns, Grzegorz Pawlik, Jacob Halatek, Jacob Kerssemakers, Cees Dekker, and Erwin Frey. Bridging scales in a multiscale pattern-forming system. *Proceedings of the National Academy of Sciences*, 119(33):e2206888119, August 2022. doi: 10.1073/pnas.2206888119.

[337] Tom Burkart, Manon C. Wigbers, Laeschkir Würthner, and Erwin Frey. Control of protein-based pattern formation via guiding cues. *Nature Reviews Physics*, 4(8): 511–527, August 2022. ISSN 2522-5820. doi: 10.1038/s42254-022-00461-3.

[338] Thomas Litschel, Beatrice Ramm, Roel Maas, Michael Heymann, and Petra Schwille. Beating Vesicles: Encapsulated Protein Oscillations Cause Dynamic Membrane Deformations. *Angewandte Chemie (International Ed. in English)*, 57(50):16286–16290, December 2018. ISSN 1433-7851. doi: 10.1002/anie.201808750.

[339] Elisa Godino, Jonás Noguera López, David Foschepoth, Céline Cleij, Anne Doerr, Clara Ferrer Castellà, and Christophe Danelon. De novo synthesized Min proteins drive oscillatory liposome deformation and regulate FtsA-FtsZ cytoskeletal patterns. *Nature Communications*, 10(1):4969, October 2019. ISSN 2041-1723. doi: 10.1038/s41467-019-12932-w.

[340] Beatrice Ramm, Philipp Glock, Jonas Mücksch, Philipp Blumhardt, Daniela A. García-Soriano, Michael Heymann, and Petra Schwille. The MinDE system is a generic spatial cue for membrane protein distribution in vitro. *Nature Communications*, 9, September 2018. ISSN 2041-1723. doi: 10.1038/s41467-018-06310-1.

[341] B. V. Derjaguin, S. S. Dukhin, and A. A. Korotkova. Diffusiophoresis in electrolyte solutions and its role in the Mechanism of the formation of films from caoutchouc latexes by the ionic deposition method. *Progress in Surface Science*, 43(1):153–158, May 1993. ISSN 0079-6816. doi: 10.1016/0079-6816(93)90024-P.

[342] Nicola De Franceschi, Weria Pezeshkian, Alessio Fragasso, Bart M. H. Bruininks, Sean Tsai, Siewert J. Marrink, and Cees Dekker. Synthetic Membrane Shaper for Controlled Liposome Deformation. *ACS Nano*, 17(2):966–978, January 2023. ISSN 1936-0851. doi: 10.1021/acsnano.2c06125.

[343] María Reverte-López, Svetozar Gavrilovic, Adrián Merino-Salomón, Hiromune Eto, Ana Yagüe Relimpio, Germán Rivas, and Petra Schwille. Protein-Based Patterning to Spatially Functionalize Biomimetic Membranes. *Small Methods*, 7(12):2300173, 2023. ISSN 2366-9608. doi: 10.1002/smtd.202300173.

[344] María Reverte-López, Nishu Kanwa, Yusuf Qutbuddin, Viktoriia Belousova, Marion Jasnin, and Petra Schwille. Self-organized spatial targeting of contractile actomyosin rings for synthetic cell division. *Nature Communications*, 15(1):10415, November 2024. ISSN 2041-1723. doi: 10.1038/s41467-024-54807-9.

[345] Tamara Heermann, Henri G. Franquelim, Philipp Glock, Leon Harrington, and Petra Schwille. Probing Biomolecular Interactions by a Pattern-Forming Peptide–Conjugate Sensor. *Bioconjugate Chemistry*, 32(1):172–181, January 2021. ISSN 1043-1802. doi: 10.1021/acs.bioconjchem.0c00596.

[346] Tanja K. Claus, Benjamin Richter, Vincent Hahn, Alexander Welle, Sven Kayser, Martin Wegener, Martin Bastmeyer, Guillaume Delaittre, and Christopher Barner-Kowollik. Simultaneous Dual Encoding of Three-Dimensional Structures by Light-Induced Modular Ligation. *Angewandte Chemie International Edition*, 55(11):3817–3822, 2016. ISSN 1521-3773. doi: 10.1002/anie.201509937.

[347] Hakan Ceylan, Immihan Ceren Yasa, and Metin Sitti. 3D Chemical Patterning of Micromaterials for Encoded Functionality. *Advanced Materials*, 29(9):1605072, 2017. ISSN 1521-4095. doi: 10.1002/adma.201605072.

[348] Xiangzhao Ai, Shuyan Wang, Yaou Duan, Qiangzhe Zhang, Maggie S. Chen, Weiwei Gao, and Liangfang Zhang. Emerging Approaches to Functionalizing Cell Membrane-Coated Nanoparticles. *Biochemistry*, 60(13):941–955, April 2021. ISSN 0006-2960. doi: 10.1021/acs.biochem.0c00343.

[349] Alexander S. Cheung, David K. Y. Zhang, Sandeep T. Koshy, and David J. Mooney. Scaffolds that mimic antigen-presenting cells enable ex vivo expansion of primary T cells. *Nature Biotechnology*, 36(2):160–169, February 2018. ISSN 1546-1696. doi: 10.1038/nbt.4047.

[350] Svetozar Gavrilović, Gereon Andreas Brüggenthies, Johann Moritz Weck, Amelie Heuer-Jungemann, and Petra Schwille. Protein-Assisted Large-Scale Assembly and Differential Patterning of DNA Origami Lattices. *Small*, page 2309680, 2024. ISSN 1613-6829. doi: 10.1002/smll.202309680.

[351] Benjamin M. Alessio and Ankur Gupta. Diffusiophoresis-enhanced Turing patterns. *Science Advances*, 9(45):eadj2457, November 2023. doi: 10.1126/sciadv.adj2457.

[352] Shunshi Kohyama, Natsuhiko Yoshinaga, Miho Yanagisawa, Kei Fujiwara, and Nobuhide Doi. Cell-sized confinement controls generation and stability of a protein wave for spatiotemporal regulation in cells. *eLife*, 8:e44591, July 2019. ISSN 2050-084X. doi: 10.7554/eLife.44591.

[353] Nicola De Franceschi, Roman Barth, Sabrina Meindlhumer, Alessio Fragasso, and Cees Dekker. Dynamin A as a one-component division machinery for synthetic cells. *Nature Nanotechnology*, 19(1):70–76, January 2024. ISSN 1748-3395. doi: 10.1038/s41565-023-01510-3.

[354] Kevin Jahnke, Vanessa Huth, Ulrike Mersdorf, Na Liu, and Kerstin Göpfrich. Bottom-Up Assembly of Synthetic Cells with a DNA Cytoskeleton. *ACS Nano*, 16(5):7233–7241, May 2022. ISSN 1936-0851. doi: 10.1021/acsnano.1c10703.

[355] Margaret L. Daly, Kengo Nishi, Stephen J. Klawa, Kameryn Y. Hinton, Yuan Gao, and Ronit Freeman. Designer peptide–DNA cytoskeletons regulate the function of synthetic cells. *Nature Chemistry*, 16(8):1229–1239, August 2024. ISSN 1755-4349. doi: 10.1038/s41557-024-01509-w.

[356] Pengfei Zhan, Kevin Jahnke, Na Liu, and Kerstin Göpfrich. Functional DNA-based cytoskeletons for synthetic cells. *Nature Chemistry*, 14(8):958–963, August 2022. ISSN 1755-4349. doi: 10.1038/s41557-022-00945-w.

[357] Sebastian Novosedlik, Felix Reichel, Thijs van Veldhuisen, Yudong Li, Hanglong Wu, Henk Janssen, Jochen Guck, and Jan van Hest. Cytoskeleton-functionalized synthetic cells with life-like mechanical features and regulated membrane dynamicity. *Nature Chemistry*, pages 1–9, January 2025. ISSN 1755-4349. doi: 10.1038/s41557-024-01697-5.

[358] Eugenia Schneider, Jakob Schweizer, and Michael Mangold. Bringing the parts together: Steps towards an in-silico protocell. *IFAC-PapersOnLine*, 49(26):20–25, January 2016. ISSN 2405-8963. doi: 10.1016/j.ifacol.2016.12.097.

[359] Jinho Park, Myeongsang Lee, Briana Lee, Nicholas Castaneda, Laurene Tetard, and Ellen Hyeran Kang. Crowding tunes the organization and mechanics of actin bundles formed by crosslinking proteins. *FEBS Letters*, 595(1):26–40, 2021. ISSN 1873-3468. doi: 10.1002/1873-3468.13949.

[360] Jaan Männik, Fabai Wu, Felix J. H. Hol, Paola Bisicchia, David J. Sherratt, Juan E. Keymer, and Cees Dekker. Robustness and accuracy of cell division in Escherichia coli in diverse cell shapes. *Proceedings of the National Academy of Sciences*, 109(18): 6957–6962, May 2012. doi: 10.1073/pnas.1120854109.

[361] Meifang Fu, Henri G. Franquelim, Simon Kretschmer, and Petra Schwille. Non-Equilibrium Large-Scale Membrane Transformations Driven by MinDE Biochemical Reaction Cycles. *Angewandte Chemie International Edition*, 60(12):6496–6502, 2021. ISSN 1521-3773. doi: 10.1002/anie.202015184.

[362] Jeanne C. Stachowiak, Eva M. Schmid, Christopher J. Ryan, Hyoung Sook Ann, Darryl Y. Sasaki, Michael B. Sherman, Phillip L. Geissler, Daniel A. Fletcher, and Carl C. Hayden. Membrane bending by protein–protein crowding. *Nature Cell Biology*, 14(9):944–949, September 2012. ISSN 1476-4679. doi: 10.1038/ncb2561.

[363] David J. Busch, Justin R. Houser, Carl C. Hayden, Michael B. Sherman, Eileen M. Lafer, and Jeanne C. Stachowiak. Intrinsically disordered proteins drive membrane curvature. *Nature Communications*, 6(1):7875, July 2015. ISSN 2041-1723. doi: 10.1038/ncomms8875.

[364] Tom Burkart, Benedikt J. Müller, and Erwin Frey. Dimensionality reduction in bulk-boundary reaction-diffusion systems. *Physical Review E*, 110(3):034412, September 2024. doi: 10.1103/PhysRevE.110.034412.

[365] Laeschkir Würthner, Andriy Goychuk, and Erwin Frey. Geometry-induced patterns through mechanochemical coupling. *Physical Review E*, 108(1):014404, July 2023. doi: 10.1103/PhysRevE.108.014404.

[366] D. E. Harris and D. M. Warshaw. Smooth and skeletal muscle myosin both exhibit low duty cycles at zero load in vitro. *The Journal of Biological Chemistry*, 268(20): 14764–14768, July 1993. ISSN 0021-9258.

[367] Samantha Stam, Jon Alberts, Margaret L. Gardel, and Edwin Munro. Isoforms Confer Characteristic Force Generation and Mechanosensation by Myosin II Filaments. *Biophysical Journal*, 108(8):1997–2006, April 2015. ISSN 0006-3495. doi: 10.1016/j.bpj.2015.03.030.

[368] Mihály Kovács, Kavitha Thirumurugan, Peter J. Knight, and James R. Sellers. Load-dependent mechanism of nonmuscle myosin 2. *Proceedings of the National Academy of Sciences*, 104(24):9994–9999, June 2007. doi: 10.1073/pnas.0701181104.

[369] Sarah M. Heissler and Dietmar J. Manstein. Nonmuscle myosin-2: Mix and match. *Cellular and Molecular Life Sciences: CMLS*, 70(1):1–21, May 2012. ISSN 1420-682X. doi: 10.1007/s00018-012-1002-9.

[370] Rui Gong, Matthew J. Reynolds, Keith R. Carney, Keith Hamilton, Tamara C. Bidone, and Gregory M. Alushin. Fascin structural plasticity mediates flexible actin bundle construction. *Nature Structural & Molecular Biology*, pages 1–13, January 2025. ISSN 1545-9985. doi: 10.1038/s41594-024-01477-2.

[371] Ryota Sakamoto and Michael P. Murrell. F-actin architecture determines the conversion of chemical energy into mechanical work. *Nature Communications*, 15(1):3444, April 2024. ISSN 2041-1723. doi: 10.1038/s41467-024-47593-x.

[372] M. L. Gardel, J. H. Shin, F. C. MacKintosh, L. Mahadevan, P. Matsudaira, and D. A. Weitz. Elastic Behavior of Cross-Linked and Bundled Actin Networks. *Science*, 304 (5675):1301–1305, May 2004. doi: 10.1126/science.1095087.

[373] Hideyo Takatsuki, Elina Bengtsson, and Alf Månsson. Persistence length of fascin-cross-linked actin filament bundles in solution and the in vitro motility assay. *Biochimica et Biophysica Acta (BBA) - General Subjects*, 1840(6):1933–1942, June 2014. ISSN 0304-4165. doi: 10.1016/j.bbagen.2014.01.012.

[374] Kimberly L. Weirich, Samantha Stam, Edwin Munro, and Margaret L. Gardel. Actin bundle architecture and mechanics regulate myosin II force generation. *Biophysical Journal*, 120(10):1957–1970, May 2021. ISSN 0006-3495, 1542-0086. doi: 10.1016/j.bpj.2021.03.026.

[375] Feng-Ching Tsai, Gwendal Guérin, Julien Pernier, and Patricia Bassereau. Actin-membrane linkers: Insights from synthetic reconstituted systems. *European Journal of Cell Biology*, 103(2):151402, June 2024. ISSN 0171-9335. doi: 10.1016/j.ejcb.2024.151402.

[376] Kyohei Matsuda, Mitsuhiro Sugawa, Masahiko Yamagishi, Noriyuki Kodera, and Junichiro Yajima. Visualizing dynamic actin cross-linking processes driven by the actin-binding protein anillin. *FEBS Letters*, 594(8):1237–1247, 2020. ISSN 1873-3468. doi: 10.1002/1873-3468.13720.

[377] Alisa J. Piekny and Michael Glotzer. Anillin Is a Scaffold Protein That Links RhoA, Actin, and Myosin during Cytokinesis. *Current Biology*, 18(1):30–36, January 2008. ISSN 0960-9822. doi: 10.1016/j.cub.2007.11.068.

[378] Pier Paolo D'Avino. How to scaffold the contractile ring for a safe cytokinesis – lessons from Anillin-related proteins. *Journal of Cell Science*, 122(8):1071–1079, April 2009. ISSN 0021-9533. doi: 10.1242/jcs.034785.

[379] O. Sandre, L. Moreaux, and F. Brochard-Wyart. Dynamics of transient pores in stretched vesicles. *Proceedings of the National Academy of Sciences of the United States of America*, 96(19):10591–10596, September 1999. ISSN 0027-8424. doi: 10.1073/pnas.96.19.10591.

[380] Rafael B. Lira, Fernanda S. C. Leomil, Renan J. Melo, Karin A. Riske, and Rumiana Dimova. To Close or to Collapse: The Role of Charges on Membrane Stability upon Pore Formation. *Advanced Science*, 8(11):2004068, 2021. ISSN 2198-3844. doi: 10.1002/advs.202004068.

[381] Md. Masum Billah, Marzuk Ahmed, Md. Zahidul Islam, and Masahito Yamazaki. Processes and mechanisms underlying burst of giant unilamellar vesicles induced by antimicrobial peptides and compounds. *Biochimica et Biophysica Acta (BBA) - Biomembranes*, 1866(5):184330, June 2024. ISSN 0005-2736. doi: 10.1016/j.bbamem.2024.184330.

[382] Mikhail Lebedev, Fung-Yi Chan, Anna Lochner, Jennifer Bellessem, Daniel S. Osório, Elisabeth Rackles, Tamara Mikeladze-Dvali, Ana Xavier Carvalho, and Esther Zanin. Anillin forms linear structures and facilitates furrow ingression after septin and formin depletion. *Cell Reports*, 42(9):113076, September 2023. ISSN 2211-1247. doi: 10.1016/j.celrep.2023.113076.

[383] Yu-Ling Shih, Ling-Ting Huang, Yu-Ming Tu, Bo-Fan Lee, Yu-Chiuan Bau, Chia Yee Hong, Hsiao-lin Lee, Yan-Ping Shih, Min-Feng Hsu, Jui-Szu Chen, Zheng-Xin Lu, and Ling Chao. Active Transport of Membrane Components by Dynamic Min Protein Waves. *Biophysical Journal*, 116(3):215a, February 2019. ISSN 00063495. doi: 10.1016/j.bpj.2018.11.1189.

[384] Beatrice Ramm. *Self-organization and molecular transport by a biological reaction-diffusion system.* Text.PhDThesis, Ludwig-Maximilians-Universität München, February 2020.

[385] Sumie Eto, Rumie Matsumura, Yasuhiro Shimane, Mai Fujimi, Samuel Berhanu, Takeshi Kasama, and Yutetsu Kuruma. Phospholipid synthesis inside phospholipid membrane vesicles. *Communications Biology*, 5(1):1–11, September 2022. ISSN 2399-3642. doi: 10.1038/s42003-022-03999-1.

Appendix

I Appendix to Section 3.1

Supplementary Information for Publication P1 with Supplementary Figures and descriptions of Supplementary Videos.

small methods

Supporting Information

for *Small Methods*, DOI 10.1002/smtd.202300173

Protein-Based Patterning to Spatially Functionalize Biomimetic Membranes

*María Reverte-López, Svetozar Gavrilovic, Adrián Merino-Salomón, Hiromune Eto, Ana Yagüe Relimpio, Germán Rivas and Petra Schwille**

Supporting Information

Protein-based Patterning to Spatially Functionalize Biomimetic Membranes

*María Reverte-López[§], Svetozar Gavrilovic[§], Adrián Merino-Salomón[§], Hiromune Eto, Ana Yagüe Relimpio, Germán Rivas and Petra Schwille**

Supplementary Video S1. Timelapse of a microswimmer-like structure showing dynamic positioning of FtsZ-mCherry-mts filaments on their surface by wave-type MinDE patterns.

Supplementary Video S2. 360º view of the Z-projections performed on a confocal stack depicting FtsZ-mCherry-mts patterning induced by the MinDE system.

Supplementary Video S3. 360º view of the Z-projections performed on a confocal stack depicting FtsZ-mCherry-mts patterning induced by the MinDE system.

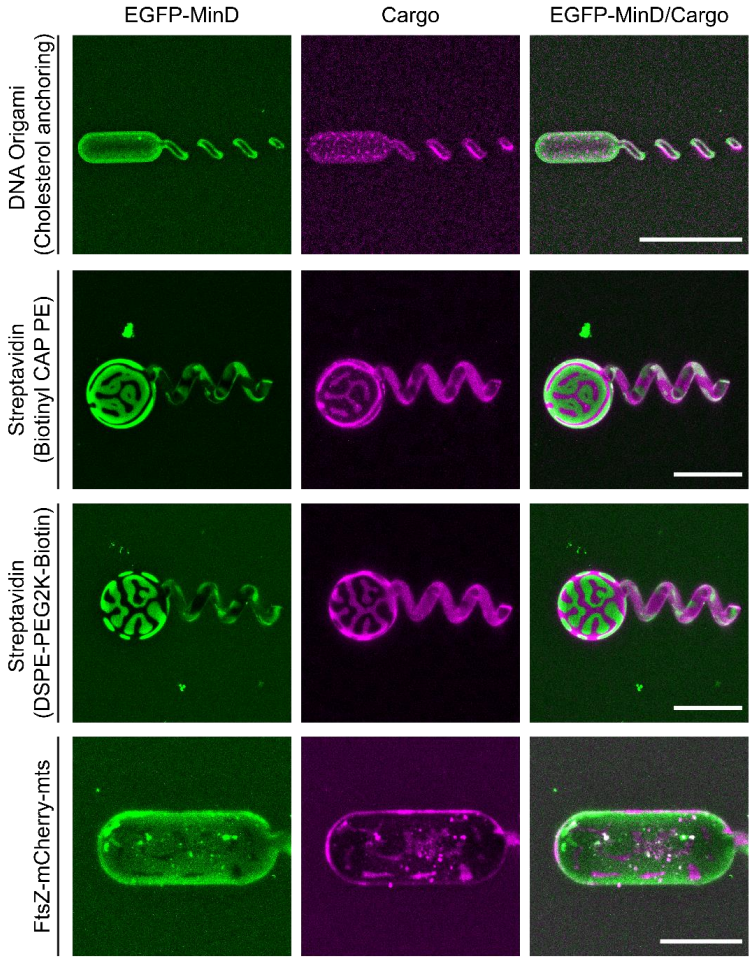

Figure S1. MinDE-driven patterning of cargo molecules on 3D microstructures. Patterning is possible irrespective of the shape of the microswimmer-like structures printed. Scale bars are 50 µm for DNA origami, streptavidin bound to Biotinyl-Cap-PE and streptavidin bound to PEG2K-Biotin. For FtsZ-mCherry-mts scale bar is 20 µm.

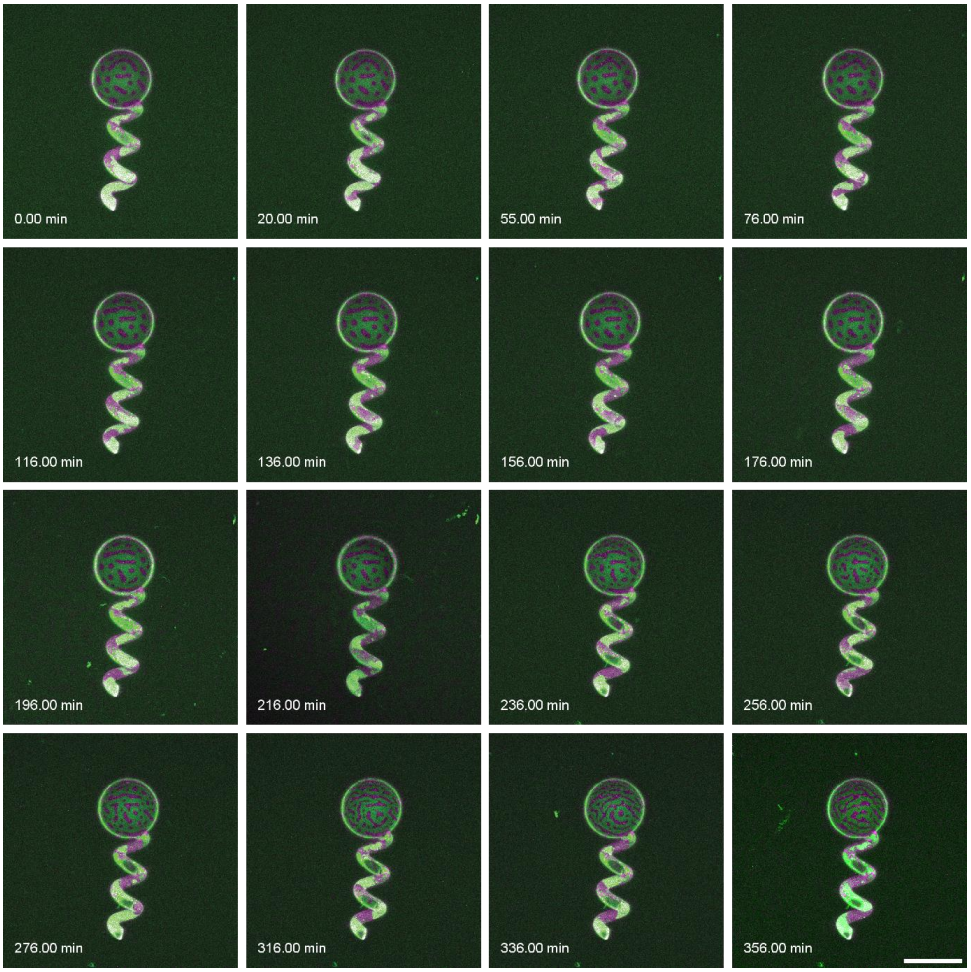

Figure S2. Time tracking of Biotinyl-Cap-PE bound Atto655-streptavidin (magenta) patterning by MinDE proteins (green) on a 3D printed microswimmer-like structure. Z-Projections of confocal images depicting the patterning of a microswimmer structure over 6 hours. After 15 minutes where Min patterns settle into a labyrinth configuration (timepoint 0.00 min), the microswimmer head retains this characteristic Turing pattern with only subtle changes in MinE minima like spots fusing or MinD maxima changing position at the tail. Owing to the initially added ATP concentration, and the fact that the system was not replenished of this nucleotide during timelapse acquisition, ATP depletion affects MinDE dynamics and shape changes occur after 5 hours (last row of timepoints shown). However, MinDE patterning retains its labyrinthic type. Scale bar is 50 µm.

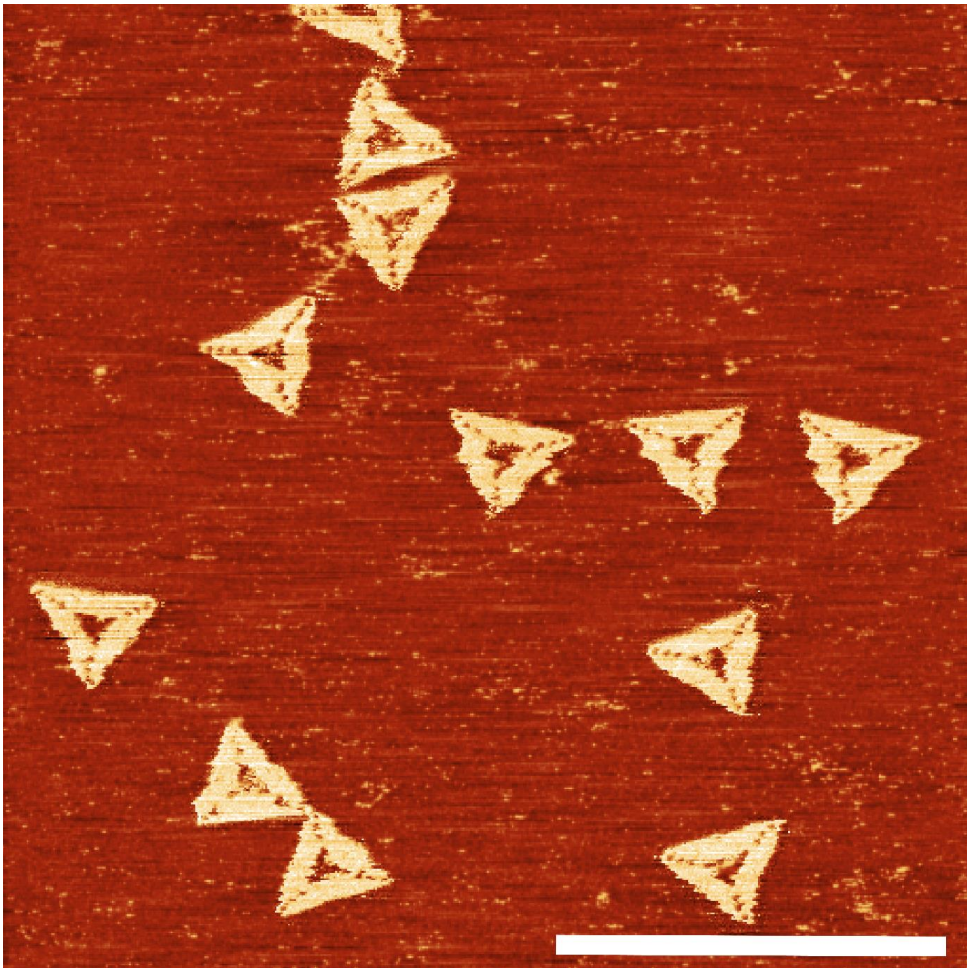

Figure S3. AFM image of the DNA origami structure (Rothemund triangle) used as cargo. Scale bar is 400 nm.

II Appendix to Section 3.2

Supplementary Information for Publication P2 with Supplementary Figures and descriptions of Supplementary Videos.

Supplementary information for

Self-organized spatial targeting of contractile actomyosin rings for synthetic cell division

María Reverte-López[1], Nishu Kanwa[1], Yusuf Qutbuddin[1], Viktoriia Belousova[1], Marion Jasnin[2], Petra Schwille[1*]

[1]*Department of Cellular and Molecular Biophysics, Max Planck Institute of Biochemistry, Martinsried, D-82152, Germany*

[2]*Helmholtz Pioneer Campus, Helmholtz Munich, Neuherberg, D-85764*, *Germany; Department of Chemistry, Technical University of Munich, Garching,* D-85748, *Germany*

[*]Corresponding author: schwille@biochem.mpg.de

Supplementary Figures

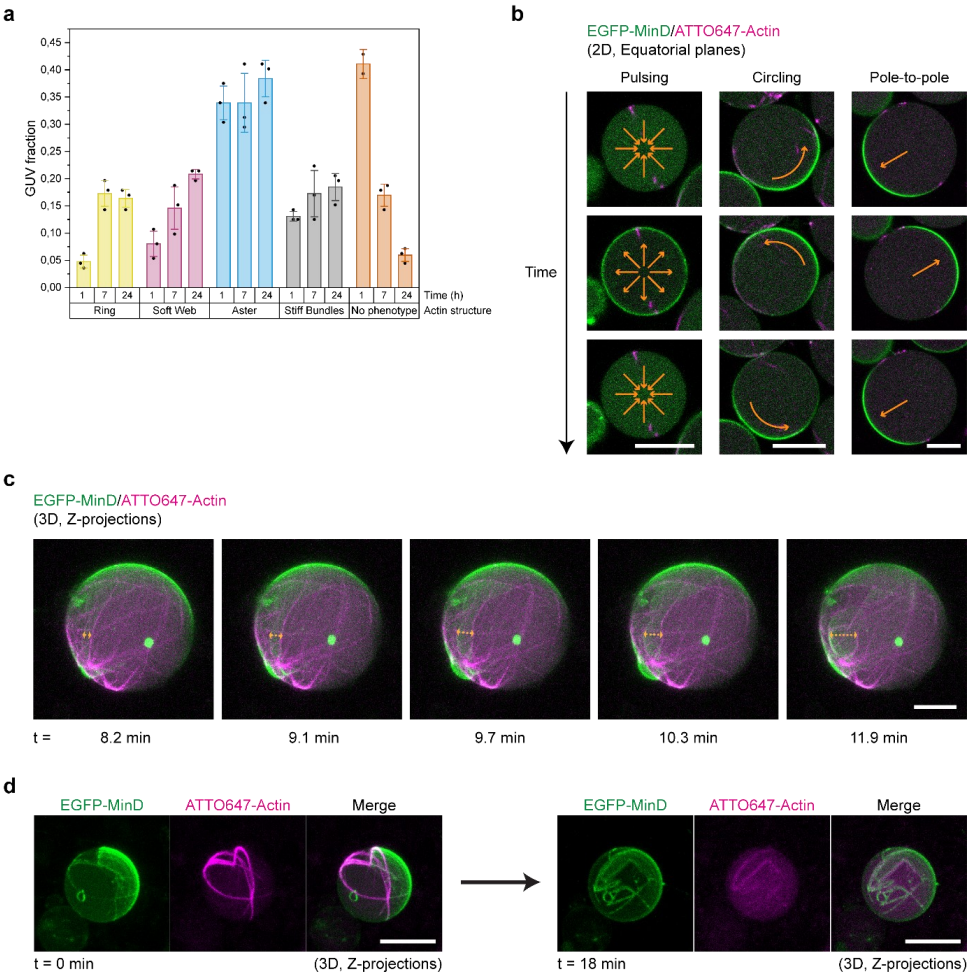

Supplementary Fig. 1 MinDE dynamic oscillations spatiotemporally re-arrange actomyosin bundles via diffusiophoresis. a Bar graph showing the frequencies of actin structures observed inside GUVs at three different timepoints after vesicle production. Inner solution mix: 2.4 µM actin, 0.6 µM fascin (fascin/actin molar ratio = 0.25), 0.05 µM myosin II, 50 g/L Ficoll70, 3 µM MinD, 3 µM MinE and 5 mM ATP. Experiments performed n = 3, total number of GUVs (< 25 µm) analyzed per experiment = 336, number of GUVs analyzed per timepoint = 112. Data shown as mean values with individual data points for each independent experiment. Error bars represent the standard deviation of the 3 experimental runs. **b** 2D confocal images of the three main types of dynamic Min oscillations (pulsing, circling and

pole-to-pole) when the MinDE system is co-reconstituted with actomyosin structures inside vesicles. Orange arrows are meant to represent the direction and dynamic behaviour of the MinDE oscillations. Scale bars: 10 µm. **c** Time-lapse 3D confocal projections of the diffusiophoretic rearrangement of bundles on the vesicle membrane. The chaotic and incremental MinDE binding to areas of the membrane delimited by actomyosin bundles allows the diffusiophoretic transport of neutravidin-bound actin which, in this example, results in the bundles of the soft web being pulled apart (orange dotted arrows). Vesicle inner content: 4 mM actin, 2 mM fascin, 0.05 µM myosin II, 50 g/L Ficoll70, 3 µM MinD, 3 µM MinE and 5 mM ATP. Scale bar: 10 µm. **d** 3D projections of confocal time series showing the collapse of an actomyosin network inside a vesicle induced by the MinDE system. Scale bars: 10 µm. Source data are provided as a Source Data file.

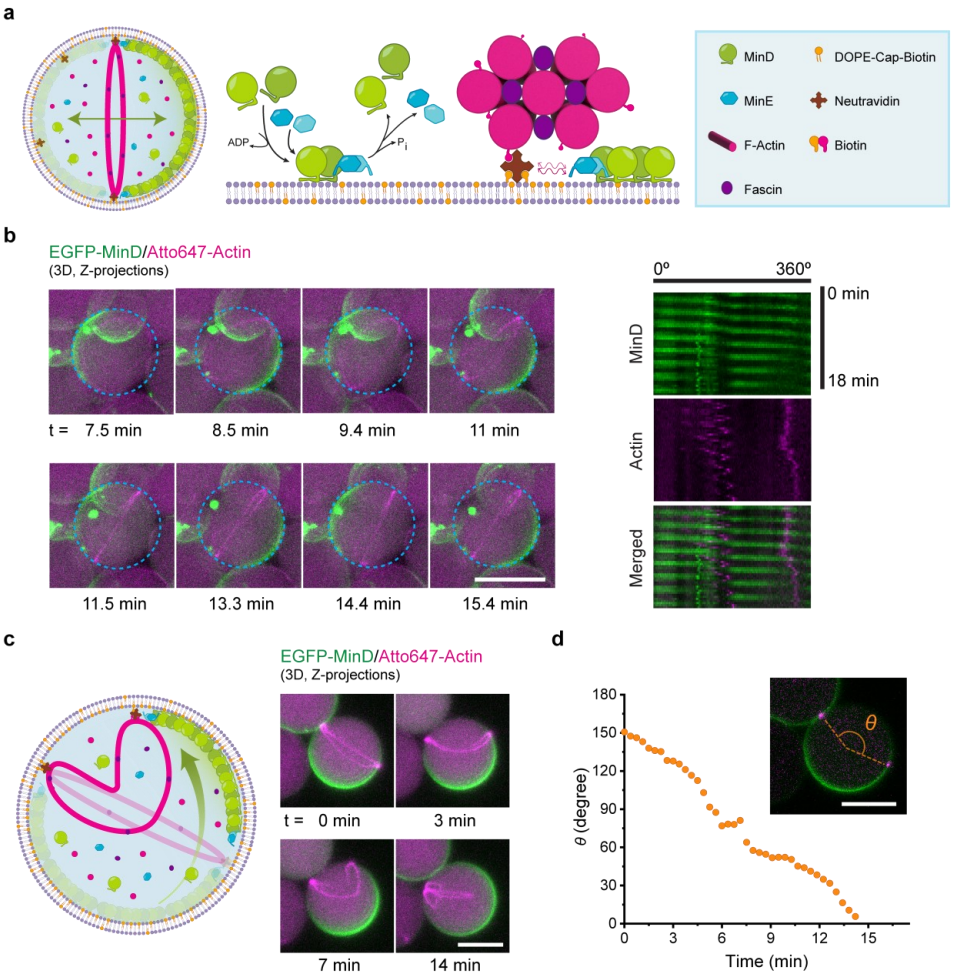

Supplementary Fig. 2 MinDE-driven positioning and buckling of fascin-bundled actin rings inside vesicles. a Schematic illustration of the proteins and molecules employed in encapsulation experiments for sections b and c and the diffusiophoretic effect between actin-fascin bundles and Min proteins at the membrane. **b** 3D projections of confocal time series showing the positioning of a fascin-bundled actin ring by Min proteins. The MinDE pole-to-pole oscillation at the membrane re-orients the ring and locates it perpendicular to the MinDE pattern. Kymographs generated at the GUV equator (blue dotted circle) depict the MinDE-driven change in ring orientation. Vesicle inner content: 1.5 mM actin, 0.3 mM fascin, 10 g/L Ficoll70, 3.2 µM MinD, 1.6 µM MinE and 5 mM ATP. Scale bar: 20 µm. **c** Schematic illustration and 3D projections over time of a vesicle containing an actin ring being folded by the circling oscillation of Min proteins. The MinD protein flux at the rear end of the ring causes

the translocation of one of the ring's endpoints towards its diametrically opposite side. Scale bar: 10 µm. **d** Time course analysis of the angle (θ) between the two endpoints of the ring in section c. After 15 minutes, the counterclockwise MinDE circling pattern co-localizes both endpoints and the ring adopts a folded conformation. Scale bar: 10 µm. Source data are provided as a Source Data file.

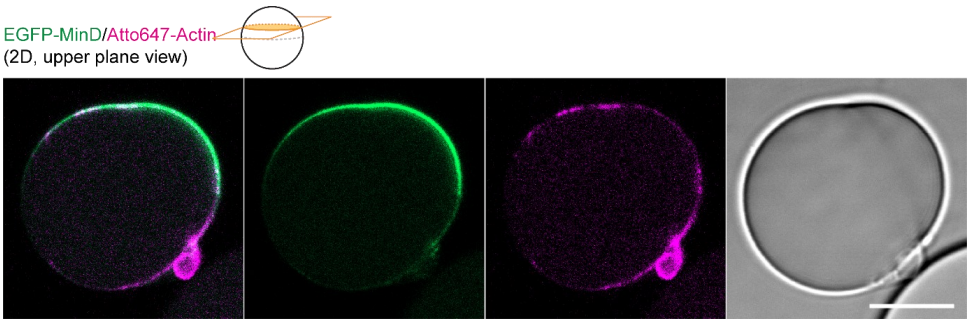

Supplementary Fig. 3 Membrane out-bud formed on a vesicle with a positioned actomyosin soft web. 2D confocal cross-sections from an upper plane of the vesicle in Fig. 3 showing an outward bud attached to the vesicle membrane. Inner solution mix: 2.4 µM actin, 0.6 µM fascin (fascin/actin molar ratio = 0.25), 0.05 µM myosin II, 50 g/L Ficoll70, 3 µM MinD, 3 µM MinE and 5 mM ATP. Scale bar: 10µm.

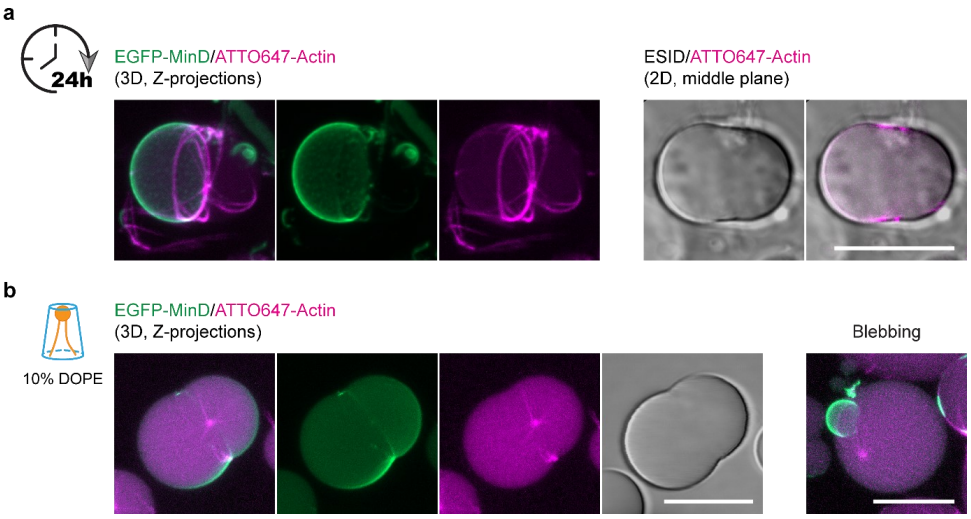

Supplementary Fig. 4 Equatorial deformation and blebbing of vesicles under different experimental conditions. a Confocal images taken 24 hours after encapsulation of a GUV presenting a static MinDE binding to the membrane and a network of actomyosin bundles tightly bound to its furrowed equator (aspect ratio = 0.75). Encapsulating conditions: 2.4 µM actin, 0.6 µM fascin, 0.05 µM myosin II, 50 g/L Ficoll70, 3 µM MinD, 3 µM MinE and 5 mM ATP. Scale bar: 20 µm. **b** Confocal images of two GUVs with a membrane composition consisting of 60% POPC, 30% POPG and 10% DOPE. The deformations and blebbing observed in the presence of this inverse-cone shaped lipid serves as a proof of concept for the addition of other curvature-inducing elements towards contraction enhancement. Inner GUV content as specified in a. Scale bars: 20 µm.

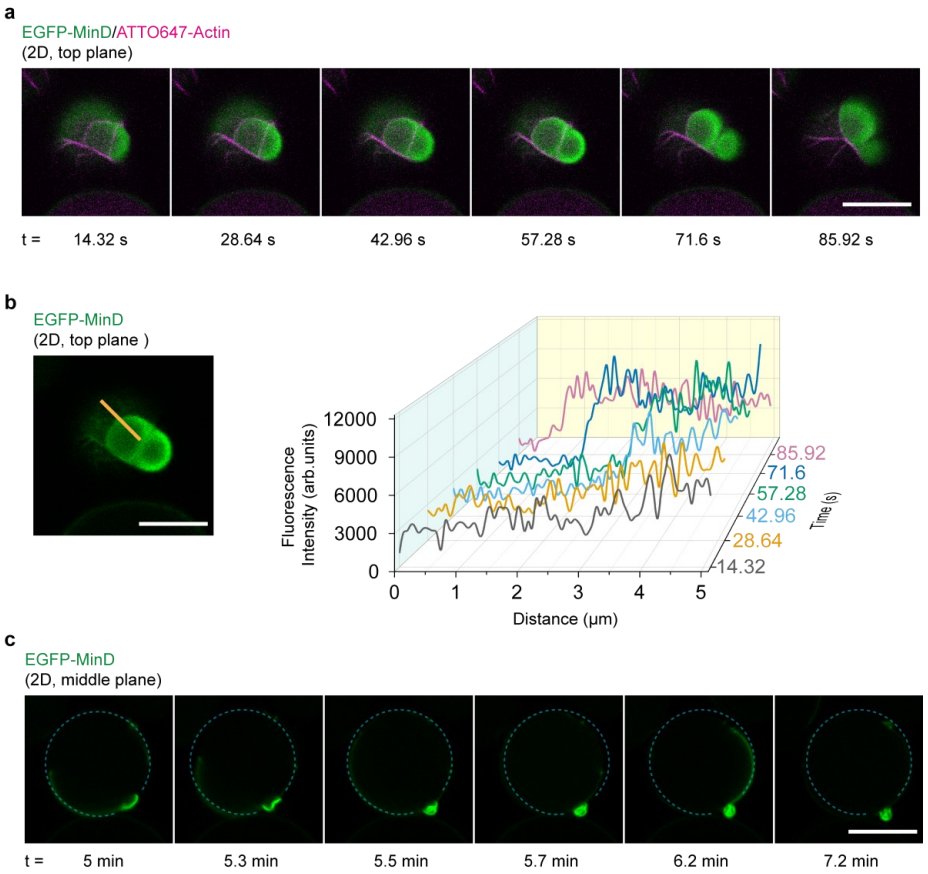

Supplementary Fig. 5 MinDE-induced membrane deformations in vesicles containing reconstituted actomyosin architectures. a Time evolution of bleb initiation on one the forming blebs depicted in Fig. 3. Confocal images of the GUV top plane show how, as Min proteins start binding and accumulating on two regions delimited by actomyosin bundles, outward membrane protrusions form. Encapsulating conditions as specified in Fig. 3. Scale bar: 10 µm. **b** 3D waterfall plot shows the EGFP-MinD fluorescence intensity of a line (orange) drawn over the GUV in section a at six different time points. As the bleb grows with time, the EGFP-MinD fluorescence intensity at the inside of the area delimited by actomyosin bundles increases. Simultaneously, the line section that falls outside of the actomyosin-delimited compartment shows a gradual decline in EGFP-MinD fluorescence intensity over time. Scale bar: 10 µm. **c** Confocal cross-section images at different time points of the vesicle in section a and b which show the formation of a membrane out-bud after blebbing. The outline of the vesicle is depicted as a blue dashed circle. Scale bar: 10 µm. Source data are provided as a Source Data file.

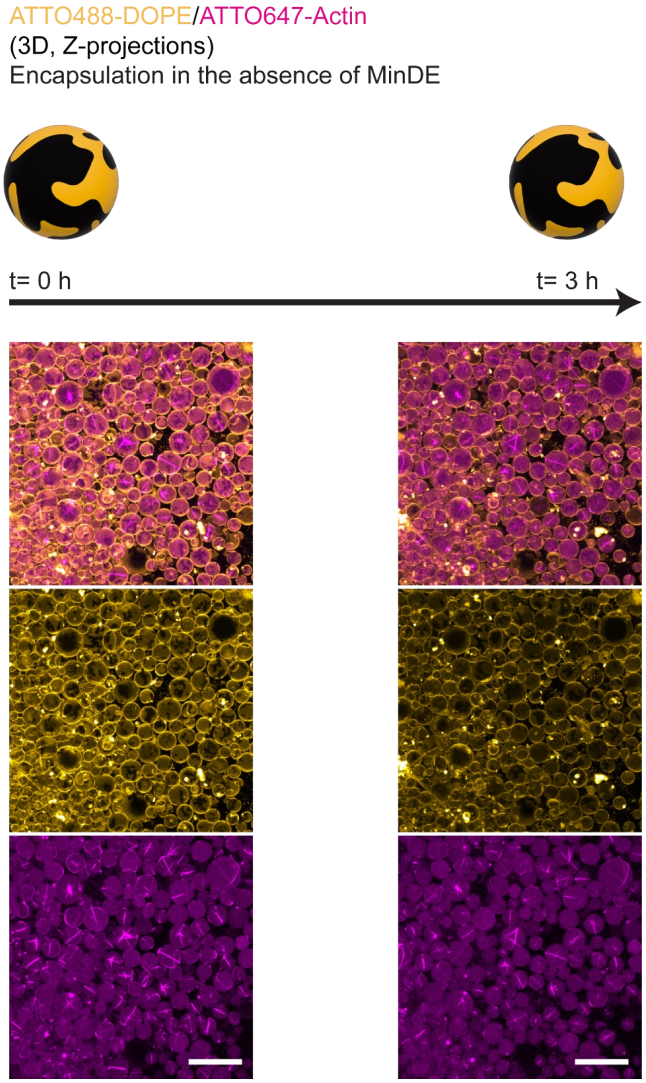

Supplementary Fig. 6 Phase-separated vesicles retain their spherical phenotype in the absence of MinDE proteins. 3D projections of confocal images taken from a three-hour timelapse acquired right after encapsulation. Phase-separated vesicles containing actomyosin networks remain spherical over time and no membrane deformations are observed on the population. Inner encapsulation mix: 2.4 µM actin, 0.6 µM fascin (fascin/actin molar ratio = 0.25), 0.05 µM myosin, 20 g/L Ficoll70 and 5 mM ATP. Encapsulation experiments performed n = 3. Scale bars: 50 µm.

Description of Supplementary Movies

Note: all movies were generated from Z-stack fluorescence time series by 3D Standard Deviation Z-Projections. The actin channel is depicted in magenta, the MinD channel in green and the brightfield (ESID) channel in greyscale.

File Name: Supplementary Movie 1

Description: MinDE-driven reorganization and positioning of actomyosin bundles at mid-cell. By exploiting the diffusiophoretic transport induced by MinDE proteins, membrane-bound actomyosin bundles are positioned at the equatorial plane of the vesicle, perpendicular to the MinDE pole-to-pole oscillations. Inner content of the vesicle: 2.4 μM actin, 0.6 μM fascin (fascin/actin molar ratio = 0.25), 0.05 μM myosin II, 50 g/L Ficoll70, 3 μM MinD, 3 μM MinE and 5 mM ATP. Timestamp indicates hh:mm:ss. Scale bar: 10 μm.

File Name: Supplementary Movie 2

Description: Constriction of a vesicle at mid-cell by a positioned actomyosin ring. Min pole-to-pole oscillations position an actomyosin ring at the equatorial plane of the vesicle which induces the constriction of the membrane. Stable localization of the ring by Min proteins allows the vesicle to maintain an ellipsoidal shape. Inner content of the vesicle: 4 μM actin, 2 μM fascin (fascin/actin molar ratio = 0.5), 0.05 μM myosin II, 50 g/L Ficoll70, 3 μM MinD, 3 μM MinE and 5 mM ATP. Timestamp indicates hh:mm:ss. Scale bar: 10 μm.

File Name: Supplementary Movie 3

Description: Deformation of a vesicle by a positioned actomyosin soft web. Min pole-to-pole oscillations position the bundles of an actomyosin soft web perpendicular to the Min pattern axis. The strongly anchored actomyosin bundles induce the deformation of the vesicle membrane, breaking GUV spherical symmetry. The membrane out-bud was already present when confocal acquisition started. Inner content of the vesicle: 2.4 μM actin, 0.6 μM fascin, 0.05 μM myosin II, 50 g/L Ficoll70, 3 μM MinD, 3 μM MinE and 5 mM ATP. Timestamp indicates hh:mm:ss. Scale bar: 10 μm.

File Name: Supplementary Movie 4

Description: Deformation of a vesicle by a peripheral actomyosin ring. Vesicle exhibiting Min oscillations which ultimately degenerate to slow circling waves. The constriction of non-positioned actomyosin bundles on one side of the vesicle yields its asymmetric dumbbell shape. Inner content of the vesicle: 4 µM actin, 2 µM fascin, 0.05 µM myosin II, 20 g/L Ficoll70, 3 µM MinD, 3 µM MinE and 5 mM ATP. Timestamp indicates hh:mm:ss. Scale bar: 10 µm.

File Name: Supplementary Movie 5

Description: MinDE-induced blebbing in a vesicle containing a reconstituted actomyosin soft web. MinDE chaotic oscillations on the vesicle membrane induce the deformation of areas delimited by lipid-anchored actomyosin bundles into outward bleb protrusions. The dynamicity of MinDE oscillations is responsible for the growth and retraction of the observed deformations at different areas of the vesicle. Inner content of the vesicle: 2.4 µM actin, 0.6 µM fascin, 0.05 µM myosin II, 50 g/L Ficoll70, 3 µM MinD, 3 µM MinE and 5 mM ATP. Timestamp indicates hh:mm:ss. Scale bar: 10 µm.

File Name: Supplementary Movie 6

Description: MinDE chaotic oscillations on actomyosin networks can generate outward membrane protrusions of different sizes. Example of a vesicle which, over the course of 15 minutes, shows several dynamic membrane deformations of varying scale. Inner content of the vesicle: 4 µM actin, 2 µM fascin, 0.05 µM myosin II, 50 g/L Ficoll70, 3 µM MinD, 3 µM MinE and 5 mM ATP. Timestamp indicates hh:mm:ss. Scale bar: 10 µm.

File Name: Supplementary Movie 7

Description: MinDE-induced bleb deformations on a phase-separated vesicles containing an actomyosin network. Dynamic MinDE oscillations on Ld domains can reorganize membrane-anchored actomyosin bundles, deform Ld domains into outward bleb-like protrusion and remodel the vesicle's domains. As oscillations progress and actomyosin bundles fold, it is possible to observe the maneuvering and splitting of domains. Inner encapsulation

mix: 2.4 µM actin, 0.6 µM fascin, 0.05 µM myosin II, 20 g/L Ficoll70, 3 µM MinD, 3 µM MinE and 5 mM ATP. Timestamp indicates hh:mm:ss. Scale bar: 10 µm.

File Name: Supplementary Movie 8

Description: Phase-separated vesicles retain their spherical phenotype in the absence of MinDE proteins. Control experiment over 3 hours show that phase-separated vesicles containing actomyosin assemblies, but without Min proteins, maintain their spherical shape and no membrane deformations arise. Inner content of the vesicle**:** 2.4 µM actin, 0.6 µM fascin, 0.05 µM myosin, 20 g/L Ficoll70 and 5 mM ATP Timestamp indicates hh:mm:ss. Scale bar: 20 µm.

III Appendix to Section 4.1

Supplementary figures and data

MinDE-free patterned microswimmers for their implementation in downstream experimental techniques

Experiments performed in collaboration with Svetozar Gavrilovic showed that, while MinDE proteins spatiotemporally control membrane-bound DNA origami, crosslinking of this cargo is possible via polyT oligonucleotides. After washing the chamber with Min buffer, Min proteins are removed from the microswimmer membrane, leaving an immobile lattice of DNA origami stably anchored to the membrane according to the anti-correlated MinDE pattern. Microswimmers can now be incorporated into different buffer and experimental conditions for subsequent purposes.

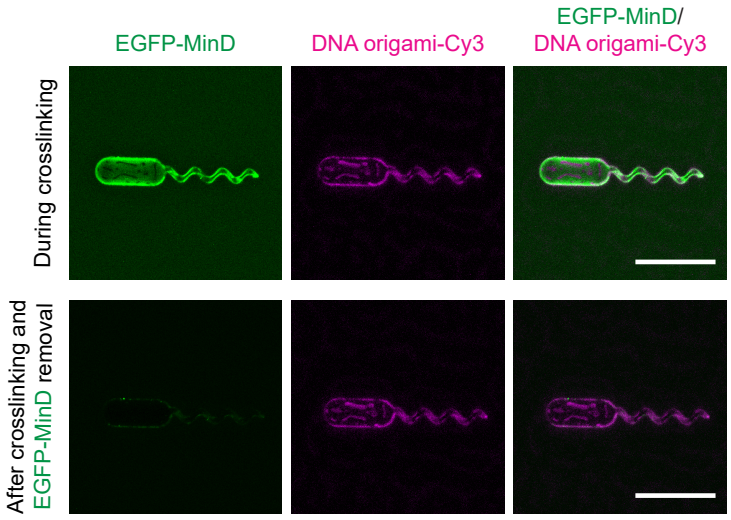

Figure III.1. Patterned and crosslinked DNA origami on microswimmer structures after MinDE removal. 3D projections of confocal images showing a microswimmer structure with crosslinked DNA origami on its surface. After MinDE-driven patterning of DNA origami on the SLB-coated structure, this cargo, equipped with eighteen staples containing poly-adenine overhangs (six per triangle side), was crosslinked via sticky-end hybridization by the addition of polyT linker oligonucleotides to preserve the achieved patterning (top row). After a 20-minute incubation to ensure adequate DNA crosslinking, MinDE proteins were removed from the chamber by buffer washing, and DNA origami positioning on the microswimmer was tracked over time. After more than 24 hours, the patterned DNA origami was confirmed to remain immobile on the surface of the microswimmer (bottom row). Scale bar is 50 μm.

Membrane geometry effects on MinDE patterning of cargo molecules

To further ascertain the effect of surface curvature and topology on MinDE patterns with our 3D-printing tools at hand, I show here additional microstructures with two distinct micron-scale topographies. One is a 12 μm tall stepped pyramid containing 6 consecutively smaller steps (CAD design kindly provided by Dr. Hiromune Eto, Figure III.2a), while the other is a 3D sinusoidal model which can be described as the 360° revolution of a damped oscillation function (Figure III.2b).

In general, while performing MinDE *in vitro* reconstitution experiments on both microstructures, as well as microswimmers, I did not observe a change in the Min pattern phase diagram for Ormocomp surfaces (see Figure 1c in publication P1). Without any adjustment in MinD-MinE ratios, Turing patterns like spots or labyrinths developed in accordance with the previously curated phase diagram. In this regard, when pyramid structures were patterned by a MinDE labyrinth configuration, MinE minima (occupied by streptavidin in the form of elongated paths), aligned both parallel and perpendicular to the pyramid and generated non-disrupted patterns on both the horizontal and vertical surfaces of the echelons and their junctions. The scale and distribution of these right-angled corners did not induce visible effects in either labyrinth or in spot patterns, and diffusiophoretic transport was not disturbed. This might be due to the size scale of the microstructure and the high bulk-volume of the chamber in relation to its overall surface.

Interestingly, when MinDE formed labyrinth patterns on curved surfaces with varying depth and widths (Figure III.2b), MinDE patterns showed atypical features. MinE minima at concave (negatively curved) regions aligned parallel and in a circumferential fashion to the grooves of the microstructure (orange arrows and dotted circles). Furthermore, the width and height of the grooves seemed to have an effect on the distribution of elongated MinE minima. The deeper and wider the concave region, the more likely the minima were to arrange in a circumferential-like path—an effect that is reminiscent of the Min wavefront alignment to grooves with similar scale [126].

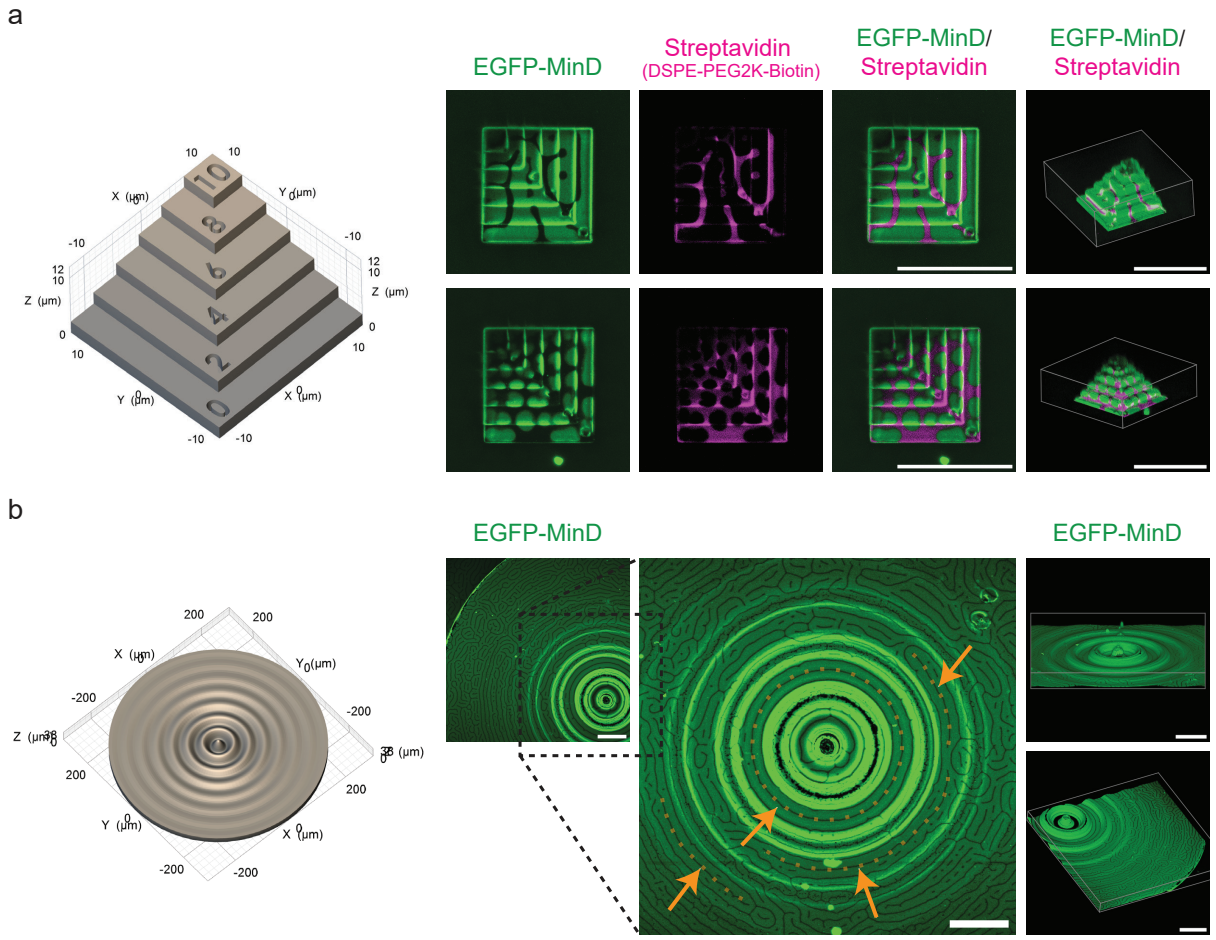

Figure III.2. MinDE patterning study on different 3D-printed geometrical shapes and curved Ormocomp surfaces. a) 3D-printed stepped pyramid containing six consecutively smaller square steps. Its surface was coated with an SLB following the same membrane preparation protocol as for microswimmers, and cargo patterning was performed via MinDE positioning of DNA origami. 3D projections of confocal z-stack images show two different Turing patterns, labyrinth and spots, generated on their surface with no discernable disturbances at straight-angled regions. Last column corresponds to the 3D representation of the microstructures obtained by 3D rendering of the z-stacks acquired. b) 3D-printed microgrooves designed by revolving 360° the damped oscillator function $y(x) = e^{(-0.12x)} \cos(1 + 1.5x)$ $-5 \leq x \leq 25$, and scaling this geometry 10 times in all coordinate axes. 3D projections of confocal images demonstrate that MinE minima at concave regions (negative curvature) align parallel to the circumferential path of the grooves (orange arrows and dotted lines). 3D rendering of the microstructure at different angles show complete MinD coverage (rightmost column). Scale bars are 50 μm.

IV Appendix to Section 4.5.1

Supplementary figures and data

Reconstitution of anillo-actin rings and networks in GUVs

To test whether the encapsulation of anillin and actin yields rings similar to those observed in solution by Kučera *et al.*, I employed the inverted emulsion method as described in publication P2 to generate GUVs containing both proteins. Similarly to previous strategies for actomyosin ring assembly, I anchored actin to the inner leaflet of the vesicles by employing biotinylated lipids. As crowding agents, 50 g/L Ficoll70 and 10 g/L BSA were incorporated to the inner solution mix with salt, $MgCl_2$, and ATP concentrations matching those used in publication P2 (50 mM KCl, 10 mM Tris-HCl, 5 mM $MgCl_2$, and 5mM ATP). The encapsulation of anillin and actin under these conditions at three different molar ratios (1 μM Anillin/2.4 μM Actin, 0.4 M/M; 2 μM Anillin/2.4 μM Actin, 0.8 M/M; and 4 μM Anillin/2.4 μM Actin, 1.6 M/M) yielded three distinct anillo-actin phenotypes consistently observed in all experimental conditions tested: asters, soft bundle networks, and single anillo-actin rings (Figure 4.1).

Membrane deformation and vesicle bursting induced by anillo-actin networks

To investigate the evolution of these anillo-actin architectures within GUVs over time, I performed time-lapse confocal imagining of the obtained vesicles. Interestingly, at anillin/actin molar ratios above 0.4 M/M, a high number of vesicles lost their contrast in the brightfield channel and began bursting 20 minutes after vesicle production, continuing over the course of 2 hours (Figure IV.1a). As a result, the inner vesicle contents were rapidly released into the outer solution. Closer inspection of the anillo-actin structures over time revealed the folding and creasing of anillo-actin rings and networks as they deformed to maximize their overlap (Figure IV.1b). To rule out possible imaging artefacts, I performed control experiments without laser exposure (control data not shown). I first imaged vesicles containing anillo-actin networks to confirm successful encapsulation, and then kept them protected from light during a two-hour incubation period. Subsequent confocal microscopy confirmed that, even without laser exposure, the number of vesicles in the chamber substantially decreased and anillo-actin structures appeared floating in the outer solution, indicating past vesicle bursting.

Co-reconstitution of MinDE oscillations and anillo-actin structures

To achieve spatiotemporal control over anillo-actin bundles at the membrane and position them at the equator, I performed encapsulation experiments to co-reconstitute MinDE oscillations with anillo-actin structures inside GUVs. I tested the standard Min encapsula-

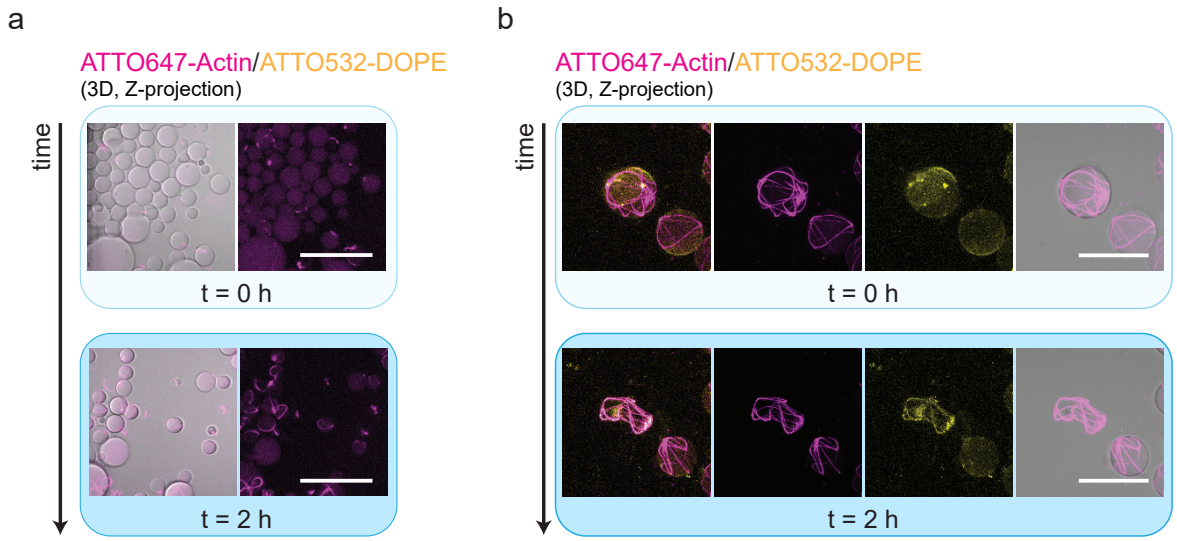

Figure IV.1. Vesicle bursting induced by the contraction and collapse of anillo-actin structures. a) 3D projections of time-lapse confocal images show vesicles encapsulating anillo-actin structures undergoing bursting. After 2 hours, anillin-driven contractile forces result in membrane rupture and release of vesicle contents into the outer solution. GUV inner solution mix: 4 μM Anillin/2.4 μM Actin (1.6 M/M), 0.01 g/L Neutravidin, 4% OptiPrep, 50 g/L Ficoll70, 10 g/L BSA and 5 mM ATP. b) 3D projections of time-lapse confocal images depicting the folding and collapse of anillo-actin structures inside two GUVs (lipid membrane labelled in yellow). After two hours, one of the vesicles (left) bursts, and the anillo-actin structure remains floating in the outer buffer solution. GUV inner solution mix as specified in (a). Scale bars are 50 μm.

tion concentrations (3 μM MinD, 3 μM MinE) with three anillin/actin molar ratios: 2 μM Anillin/2.4 μM Actin (0.8 M/M); 3 μM Anillin/3 μM Actin (1 M/M); and 4 μM Anillin/2.4 μM Actin (1.6 M/M). At higher anillin/actin molar ratios (1 and 1.6 M/M), which continued yielding GUV bursting, only very few vesicles exhibited MinDE oscillations capable of positioning anillo-actin bundles. In the majority of GUVs, Min proteins were unable to transport the biotin-anchored anillo-actin bundles, which assembled mostly as an immobile soft network. In one instance, however, I captured a vesicle with an anillo-actin ring significantly deforming the GUV at mid-cell while Min proteins oscillated in a pole-to-pole pattern at the lateral sides of the vesicle (Figure 4.2).

Nevertheless, across all anillin/actin molar ratios tested, substantial membrane deformations were observed in vesicles containing non-positioned anillo-actin networks (Figure 4.3 and Figure IV.2). As the networks contracted over the span of several hours, the anillo-actin bundles pinched the vesicle membranes, inducing equatorial furrowing. Ultimately, the vesicles, taking a symmetrical two-lobed shape, returned to their spherical form after complete network contraction due to the bundles "slipping" away from the membrane equator.

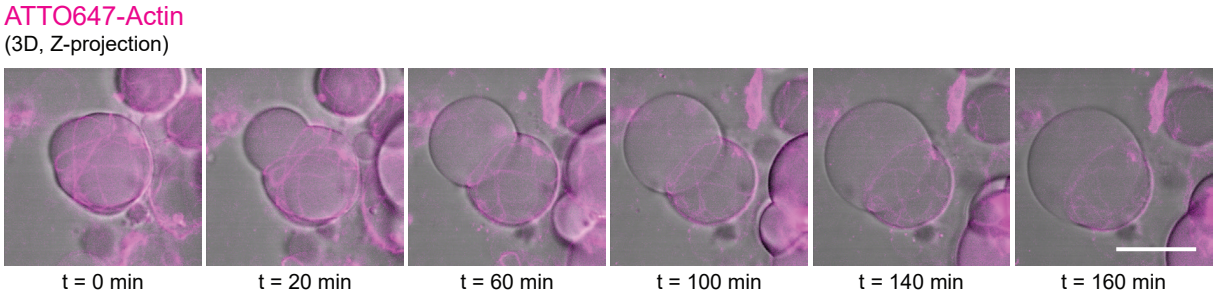

Figure IV.2. Time-lapse tracking of GUV deformations induced by contractile anillo-actin networks. 3D projections of a confocal z-stack show a vesicle deforming due to the contraction of an anillo-actin network (the equatorial plane from the brightfield channel is superimposed onto the 3D projection of the fluorescence confocal stack). After almost 3 hours, the vesicle returns to its spherical shape. GUV inner solution mix: 4 μM Anillin/2.4 μM Actin (1.6 M/M), 3 μM MinD, 3 μM MinE, 0.01 g/L Neutravidin, 4% OptiPrep, 50 g/L Ficoll70, 10 g/L BSA, and 5mM ATP. Scale bar is 20 μm.

Study of anillin-PIP3 interaction via *in vitro* encapsulation assays

To ascertain the feasibility of binding anillo-actin structures to PIP3-containing vesicle membranes, I encapsulated anillin at three different concentrations inside GUVs containing 5% PIP3. To study the interaction of the PH domain of anillin with the vesicle membrane, I acquired confocal microscopy images and evaluated qualitatively the GFP-anillin fluorescence intensity at the membrane (Figure IV.3a). At low concentrations of anillin (0.5 μM), a well-defined fluorescence halo tracing the lipid membrane was observed in many of the vesicles. Increasing the concentration of anillin yielded membrane binding; however, fluorescence intensity at the GUV membrane decreased compared to samples at 0.5 μM anillin. Lastly, when I encapsulated 4 μM anillin inside vesicles, large globular structures reminiscent of protein aggregates localized at the membrane, while the lumen of GUVs exhibited a higher fluorescence signal relative to the other two anillin concentrations tested.

PIP3-mediated membrane binding of anillo-actin structures

To prevent vesicle bursting due to anillo-actin contractile forces, the biotin-neutravidin anchoring strategy was subsequently discarded. To decrease the effective forces and membrane footprint of the bundles, as well as to render these structures diffusive on the membrane, I then turned to PIP3 as an alternative membrane-binding approach. Incorporating 5% of PIP3 into POPC vesicles, the goal was to utilize PIP3-mediated specific interactions with anillin (confirmed by experiments in Figure IV.3a) to bind actin bundles to the vesicle inner leaflet.

Therefore, to test whether anillo-actin structures bind the membrane of PIP3-containing vesicles, I performed additional *in vitro* encapsulation experiments. At a 2:1 anillin/actin

molar ratio, vesicles exhibited anillo-actin phenotypes similar to those obtained with biotinylated membranes. Importantly, rings and soft bundle networks appeared curved and bound to the membrane. To investigate the effect of these PIP3-bound anillo-actin networks on the vesicles, I then performed time-lapse confocal imaging of GUV samples. After approximately 3 hours, anillo-actin structures exhibited contractility and induced membrane transformations in the form of blebs and tubes (Figure IV.3b, yellow and blue arrows, respectively). Employing time-lapse confocal imaging, I confirmed that the membrane blebs and tube retracted and changed shape as the anillo-actin network contracted. In addition, changes in anillo-actin network topology yielded a visible change in the surface area and size of the vesicle.

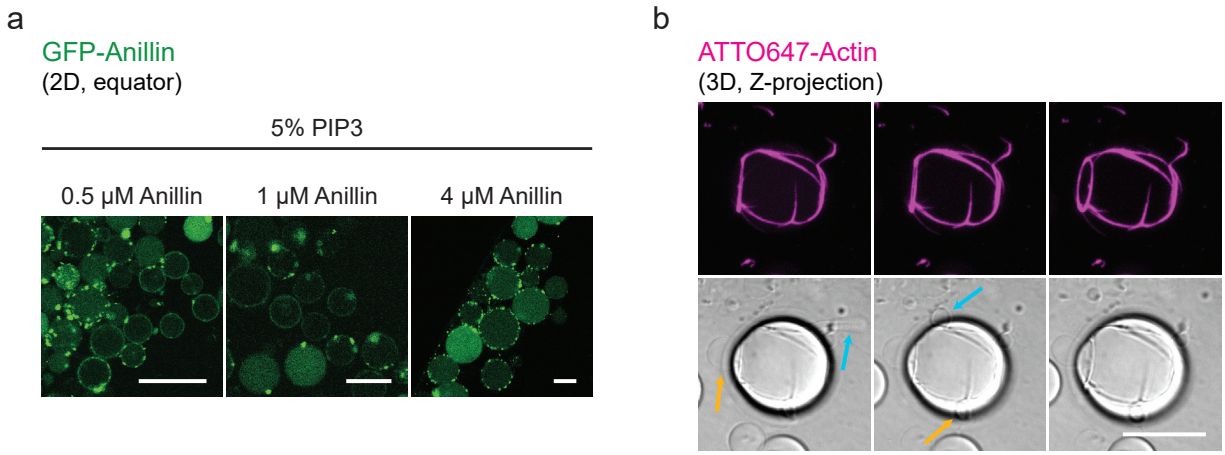

Figure IV.3. Encapsulation of membrane-bound anillo-actin structures with PIP3. a) 2D confocal images showing the encapsulation of Anillin (0.5 μM, 1 μM, and 4μM) inside POPC vesicles containing 5% PIP3. Enhanced membrane binding is observed at 0.5 μM Anillin. At 4 μM, anillin aggregates form at the membrane. GUV inner solution mix: Anillin (50% labelled with GFP-Anillin), 50 g/L Ficoll70, 10 g/L BSA, and 5mM ATP. GFP-anillin was kindly provided by the Lansky & Braun Lab. b) 3D projections of a confocal z-stack depicting an anillo-actin network bound to a vesicle via PIP3 lipids. The tension built by the anillo-actin network generates a membrane tube (blue arrow) and several outward blebs (yellow arrows). As the sliding of f-actin filaments progresses, the network topology changes, and the membrane deformations observed evolve (e.g., membrane tube retracts into a bleb). A visible increase in surface area of the vesicle is also observed. GUV inner mix: 4 μM Anillin/2 μM Actin (2 M/M), 50 g/L Ficoll70, 10 g/L BSA and 5mM ATP. Scale bars are 20 μm.

Supplementary methods

Anillin purification

Homo sapiens pEGFP-Anillin (GeneBank accession number: BC070066) plasmid was purchased from Addgene (Addgene Number #68027). The anillin gene was PCR-amplified (for primers used, see details below) and cloned into the pCoofy41 vector (Addgene plasmid #55184) containing a C-terminal 6xHis-tag to obtain pCoofy41_Anillin_chis plasmid.

The protein was expressed in SF9 insect cells. The insect cells were harvested after 4 days by centrifugation at 300×g for 10 min at 4 °C in an Avanti J-26S ultracentrifuge (JLA-9.1000 rotor, Beckman Coulter). The cell pellet was resuspended in 5 mL ice-cold phosphate buffered saline (PBS) and stored at −80 °C for further use. For cell lysis, the insect cells were disrupted by sonication in 30 mL ice-cold Lysis buffer (50 mM Tris-HCl pH 7.5, 500 mM NaCl, 1 mM TCEP) supplemented with 10 mM imidazole and Protease Inhibitor Cocktail (cOmplete, EDTA free, Roche), and centrifuged at 20,000×g for 60 min at 4 °C in the Avanti J-26S ultracentrifuge (JA-25.50 rotor, Beckman Coulter). The cleared cell lysate was loaded on 1 mL lysis buffer-equilibrated Ni-NTA resin (Ni-NTA Agarose, Qiagen) at 4 °C. The Ni-NTA column was washed with high-salt buffer (50 mM Tris-HCl pH 7.5, 1000 mM NaCl, 1 mM TCEP), followed by low-salt buffer (50 mM Tris-HCl pH 7.5, 50 mM NaCl, 1 mM TCEP) and the protein was eluted in elution buffer (50 mM Tris-HCl pH 7.5, 50 mM NaCl, 250 mM Imidazole, 1 mM TCEP). The fractions containing Anillin-chis were pooled, concentrated using an Amicon ultracentrifuge filter, and loaded onto a HiLoad 16/600 Superdex 200pg size exclusion column (Cytiva 28-9893-35) in storage buffer (50 mM Tris-HCl pH 7.5, 300 mM KCl, 5% Glycerol, 1 mM TCEP). Protein-containing fractions were pooled, concentrated, and flash-frozen in liquid nitrogen. Protein concentration was measured using Nanodrop Spectrophotometer (ThermoFisher).

Primer information

Primer: pCoofy41_Anillin_chis

Template Vector: pCoofy41

p41_chis_FW: CATCATCATCATCACCACTGACGCCATTAACCTGATGTTCTGG
pC41_Anilin_chis_RV: GTAAACGGATCCATGGTGGCGGGCCCCTGGAACAGAAC

Template Insert: Anillin

Anillin_chis_RV: CAGTGGTGATGATGATGATGAGGCTTTCCAATAGGTTTGTAGC
Anillin_chis_FW: AAGTTCTGTTCCAGGGGCCCGCCACCATGGATCCGTTTACGGAGAAACT

Proteins and crowding agents

Actin (α-actin skeletal muscle, rabbit), ATTO647-Actin (α-actin skeletal muscle, rabbit) and Biotin-Actin (α-actin skeletal muscle, rabbit) were purchased from HYPERMOL (Germany). GFP-Anillin was a kind gift from the Lansky & Braun Lab. Stock solutions of the purchased proteins were prepared by following the handling instructions of the manufacturer. A stock solution of neutravidin (Thermo Fisher Scientific Inc., Massachusetts, USA) was prepared by dissolving the protein in water according to the reconstitution instructions. MinE-His, His-MinD and His-EGFP-MinD were purified as described elsewhere [328]. Stock solutions of the crowding agents BSA (Sigma-Aldrich, St. Louis, USA), Ficoll70 (Sigma-Aldrich, St. Louis, USA), and 60% Iodixanol (OptiPrepTM) were prepared as previously reported [344].

GUV production

Lipids were purchased from Avanti Polar Lipids (USA). Vesicles were produced in 96 well-plates by the inverted emulsion method as previously described [344]. Lipid mixes employed consisted either of POPC:POPG:Biotinyl CAP PE in a 7.9:2:0.1 molar ratio or POPC:PIP3 in a 9.5:0.5 molar ratio. To label the membrane, 0.05% ATTO532-DOPE was added to the lipid mix. For vesicles containing biotinylated lipids, the actin mix comprised: 86% unlabelled g-actin, 10% ATTO647-actin, and 4% biotinylated actin. For vesicles with PIP3, the actin mix consisted of: 90% unlabelled g-actin and 10% ATTO647-actin. When Min proteins were included in the inner solution mix, MinD consisted of 70% His-MinD and 30% His-EGDP-MinD. All inner solution mixes for GUV production were prepared in a final buffer concentration (reaction buffer) of 50 mM KCl, 10 mM Tris-HCl, and 5 mM $MgCl_2$.

Fluorescence microscopy

Imaging of vesicles was performed on a LSM800 confocal laser-scanning microscope using a C-Apochromat 40×/1.2NA water-immersion objective (Carl Zeiss, Germany). Fluorophores were excited using diode-pumped solid-state lasers: 488 nm (EGFP-MinD, GFP-Anillin, ATTO532-DOPE), and 640 nm (ATTO647-Actin).

Acknowledgements

This will be long but I don't think I'd like to apologise for that. I have three pages to capture more than 4 years of my life with the Schwillies and that is truly, truly difficult. The sun might not have shone much through the windows of the membrane lab, but I found a distinct type of happiness and warmth in your jokes, the meetings in the kitchen around terrible coffee, your kindness and support, the shared chocolate, your brilliant scientific advice and assistance, and the many more aspects that have made this journey worth the stress and worries.

To start, I'd like to thank my supervisor Prof. Petra Schwille. Thank you for all the inspiring ideas and opportunities you have given me. Your constant support was akin to when an adult teaches a kid to ride a bike, steering the handlebars when needed and always at the back, paying attention and adjusting the direction when needed. I spent this journey in an amazing place with incredible resources and surrounded by the best people and that's all thanks to you.

I'd also like to thank Prof. Heinrich Leonhardt, for taking over the role of faculty supervisor and providing thoughtful guidance and scientific advice over the years. For his input on the project's evolution and his helpful ideas, I also thank Prof. Ralf Jungmann.

The starting round of thanks to collaborators and co-authors starts with Marion Jasnin. Marion, thanks for your unconditional support when I most needed it and all the brilliant advice, your help was vital in many ways. I also thank Prof. Erwin Frey, together with Ivan Maryshev, Henrik Weyer and Jan Willeke, for instrumental discussions which helped me understand and appreciate the beauty behind complex physics principles. To the enclave in Madrid, this once lost master's student would like to greatly thank Prof. Germán Rivas, for always being the connection link, the kind mentor, and the genie of extraordinary opportunities. Germán, I hope one day I can return your endless support. Thanks also to Gianfranco, my ribosomal buddy, for the fun in the lab whenever you paid us a visit.

For their help around the lab and for their unstoppable support bringing tidiness, coffee bags, and light-hearted conversations, I would like to say many thanks to Kerstin, Michaela, Bea, Claudia, Thomas, Helge, Marion, Sigi and Sandra. A big thank you to Katharina, for being the master behind the annoyingly tricky purification of anillin, and also to Frank

for sharing with me his knowledge on microfabrication and for always assisting with the SEM imaging when printing jobs proved difficult. I'd also like to thank Silke and Ines for their advice and work that greatly helped me deal with the bureaucracy monster living at the MPIB.

The round of thanks to PhD students and postdocs starts with the alumni first. Big thanks to Hiro, the 2PP mentor who showed a mini master's me everything I know about printing. Without his time and patience those microswimmers would not exist. I'd also like to thank the boardgame master Adrián, who shared his priceless advice that helped me survive life in Munich and the hardships accompanying the encapsulation of proteins. Thanks a lot to Henri, who, even in Leipzig, still made sure to give the best input and ideas to solve the darkest Min mysteries. And thanks also to Thomas, who made sure to give me a quick masterclass on actin right before leaving. The postdoc privilege compels me to start with the gum thief, aka Nishu. Thanks a lot for your contagious optimism, for bringing your magic hands to this lab, and for doing your thing with those demixed blebbing vesicles. I'd also like to thank the supreme dessert-sharer Kareem, for helping me with his encyclopedic knowledge on the synbio literature, his microfab-related advice, and for his never ending stash of dad-jokes. Thanks a lot to the creative chef Zexi, for answering my stupid questions about lipids and for her patience with the development of our flubby pet. To my gossip queen Anastasija, thank you for understanding and sharing my struggles with vesicle production and your mood-lifting C1-level Spanish conversations. Thanks a lot to the best burek maker Aleksandra, for sharing your precious protein knowledge with me and always bringing your contagious smile with you. Thanks a lot to the best Tokyo guide Shunshi, for sharing his endless knowledge about Mins and for the seed he once planted about the co-reconstitution of Mins and actin. Without him, that would have never materialized into a paper. I'd also like to thank Beza's dad, Adam, thanks a lot for sharing your scientific knowledge and experience and for great quality time around food, movies and moonshine vodka.

To the PhDs, the smaller gears of this lab... a bit worn at the edges, but always up and down working on booking our entire catalogue of microscopes, complaining about the coffee machine (you all got an espresso now!), and blaming Munich's summer humidity for the low GUV yields, thank you from deep down my dust-covered heart. Sveto, thank you for being my battle companion and for sharing your "yang"-type of science which (most of the times, eh!) complemented my "yin"-like ways. For your constant chocolate offers, support and patience, thanks always. Thanks also to the supernice Schwillie director of photography, aka Yusuf. Thanks for always answering my dumb questions about membranes and physics in general. Thanks to my officemate, Ringberg roommate Vika. For the many laughs in that strangely warm office, for assisting with your PURE hands when it was most needed during those revisions, and for having a few brain cells always at the same frequency as mine. Thanks to Béla, the best protein designer the Schwille lab has grown. Thank you for always being open to my questions and for putting a smile on my face with your support. Thanks also to the best volleyball player and polyglot of the lab, aka Henry. Thank you for

always asking the right questions, sharing your endless protein knowledge, and bringing the best advice to any project. I'd also like to thank the private microscope expert of the lab, Jan. Thank you for always helping me get the best images and answering my dumb questions. To the new Schwillie rookies full of energy and enthusiasm: An, Marco, Nastasja, Andrey and the rest. Thanks for all your amazing Min-related doubts which made me question my knowledge almost every bloody time. Thanks also to Philipp, the new coffee master. Thanks for taking that big responsibility off the shoulders of this bleary-eyed PhD.

I would also like to thank all of my lifelong friends scattered all over Munich, Madrid, Denmark, and Switzerland, for listening attentively to my senseless complaints, for taking me to (unannounced) hikes and beautiful places so I could touch some grass, for lots of good conversations around pear-risottos and Spanish omelettes, for those meet-ups during Christmas every year, and for sharing their precious advice and time.

Pardon the Spanish but of course, con mucha ilusión doy las gracias a la extensa familia Reverte y los buenos López, por vuestros ánimos y apoyo todos estos años. Y finalmente, con muchísimo orgullo y los ojillos un poco vidriosos, doy las gracias a mis padres Fernando y Lourdes, quienes han trabajado incansablemente para dármelo todo y más. Gracias por vuestro apoyo incondicional, por haberme hecho la que soy hoy y por participar conmigo de todo este trayecto. Vuestra niña ya está muy grande pero con ella también el amor que os tiene.

fin

Curriculum Vitae

Education

2022– present	**PhD student** in Biology at Ludwig-Maximilians-Universität München
2021– present	PhD student at International Max Planck Research School for Molecules of Life (IMPRS-ML)
2018-20	**M.Sc** in Molecular and Cellular Biology at Menéndez Pelayo International University
2014-18	**B.Sc.** in Biomedical Engineering, University Carlos III of Madrid.

Research Experience

2020– present **Research Scientist**
Max Planck Institute of Biochemistry, Martinsried, Germany
Research Group: Cellular and Molecular Biophysics
Mentor: Prof. Dr. Petra Schwille
Thesis title: Modular engineering of self-division in synthetic cells

2019–2020 **Research Assistant**
Margarita Salas Biological Research Center (CIB-CSIC), Madrid (Spain)
Research Group: Systems Biochemistry of Bacterial Division
Mentor: Prof. Dr. Germán Rivas Caballero
Master's thesis title: Development of a synthetic cytoplasm to study protein interactions in bacterial division

2017–2018 **Undergraduate Research Trainee**
Center for Molecular Biology Severo Ochoa (CBMSO), Madrid (Spain)
Research Group: Department of Genome Dynamics and Function
Mentor: Dr. Santiago Ramón-Maiques
Bachelor's thesis title: Structural and functional studies on CAD: the anti-tumoral target protein leading the de novo biosynthesis of pyrimidines

Research Publications

2024 **M. Reverte-López**, N. Kanwa, Y. Qutbuddin, V. Belousova, M. Jasnin, and P. Schwille. Self-organized spatial targeting of contractile actomyosin rings for synthetic cell division. Nature Communications, 15(1):10415, Nov. 2024.

2023 **M. Reverte-López**, S. Gavrilovic, A. Merino-Salomón, H. Eto, A. Yagüe Relimpio, G. Rivas, and P. Schwille. Protein-Based Patterning to Spatially Functionalize Biomimetic Membranes. Small Methods, 7(12):2300173, June 2023.

2023 M. Fu, T. Burkart, I. Maryshev, H. G. Franquelim, A. Merino-Salomón, **M. Reverte-López**, E. Frey, and P. Schwille. Mechanochemical feedback loop drives persistent motion of liposomes. Nature Physics, 19(8):1211–1218, Aug. 2023.

2023 A. Kaufmann, M. Vigogne, T. A. Neuendorf, **M. Reverte-López**, G. Rivas, and J. Thiele. Studying Nucleoid-Associated Protein–DNA Interactions Using Polymer Microgels as Synthetic Mimics. ACS Synthetic Biology, 12(12):3695–3703, Dec. 2023.

2018 F. del Caño-Ochoa, A. Grande-García, **M. Reverte-López**, M. D'Abramo, and S. Ramón-Maiques. Characterization of the catalytic flexible loop in the dihydroorotase domain of the human multi-enzymatic protein CAD. Journal of Biological Chemistry, 293(49):18903–18913, Dec. 2018.

Academic Achievements and Awards

2023 Best Poster Award at SynCell Conference, Minnesota (USA)
2023 Design selected as official cover for the journal Small Methods
2022 2nd Best Talk Award at IMPRS-ML Seminar